

Contents

ASM Sc. J.
Volume 4(1), 2010

RESEARCH ARTICLES

- Ex-vivo* Differentiation of Stem Cells from Human
Extracted Deciduous Teeth into Bone Forming Cells** 1
S.N. Fazliah, S. Jaafar, S. Shamsuddin, Z. Zainudin,
A.B. Hilmi, A.R. Razila and S.F. Abdullah
- Ion Beam Elemental Analysis of Doped SiO₂ Optical Fibre and Its
Thermoluminescence Response When Irradiated with Protons** 15
A.T. Ramli, S. Hashim, D.A. Bradley, H. Wagiran, M. Webb and C. Jeynes
- Data Cognitive Complexity: A New Measure** 22
J.K. Chhabra, R.S. Bhatia and V.P. Singh
- Methane Adsorption Characteristics of Copper Oxide
Modified NaY Zeolite Adsorbents** 29
K.S.N. Kamarudin, Y.Y. Chieng, H. Hamdan and H. Mat
- Influence of CO₂ Flux on the Properties of Carbonate Apatite
Synthesized by Solid State Reaction** 41
K. Jamuna, K. Noorsal, F.A. Zakaria and Z.H. Hussin
- Communication Systems Melioration by Employing Fast Frequency
Hopping Spread Spectrum with Low-density Parity-check Codes** 48
A. Yahya, O. Sidek and M.F.M. Salleh
- Ionic Conductivity and Morphological Studies of Plasticized
Poly(methyl methacrylate) Polymer Electrolyte Films** 55
Z. Osman, L. Othman, K.B. Md Isa, A. Ahmad and N. Kamarulzaman

Continued on the inside of the back cover.

ISSN 1823-6782



ASM JOURNAL

Science

In Pursuit of Excellence in Science

Vol. 4, No. 1, June 2010 • ISSN : 1823-6782

ASM Science Journal 4(1) 2010





Price (2 Issues)

Malaysia: RM100 (*Individual*)
RM200 (*Institution*)

Other Countries: USD50 (*Individual*)
USD100 (*Institution*)





ASM Science

JOURNAL

INTERNATIONAL ADVISORY BOARD

Ahmed Zewail (Nobel Laureate)
Richard R. Ernst (Nobel Laureate)
John Sheppard Mackenzie
M.S. Swaminathan

EDITORIAL BOARD

Editor-in-Chief/Chairman: Md. Ikram Mohd Said

Abdul Latiff Mohamad
Chia Swee Ping
Ibrahim Komoo
Lam Sai Kit
Lee Chnoong Kheng
Looi Lai Meng
Mashkuri Yaacob
Mazlan Othman
Mohd Ali Hashim
Francis Ng
Radin Umar Radin Sohadi

Cover:

Figure on the right is the High Voltage Engineering Europe 2.0 MV Medium Current Plus Tandetron™ accelerator providing 2.5 MeV protons which is situated in Surrey Ion Beam Centre. It is taken from *Figure 1(a)* of the article *Ion Beam Elemental Analysis of Doped SiO₂ Optical Fibre and Its Thermoluminescence Response When Irradiated with Proton*—research work undertaken by scientists from the University of Technology Malaysia and the University of Surrey, Guildford, U.K. (pp. 15–21).

Figure on the top left of the cover shows skeletons of simulated flood from an article which describes characterization of skeletons of simulated droughts and flood of water bodies (*Figure 5*, pp. 68). Subsequent designs shown below are from *Figures 6 and 4* of the first research article of this issue—*Ex-vivo Differentiation of Stem Cells from Human Extracted Deciduous Teeth into Bone Forming Cells* which describes the isolation of mesenchymal stem cells derived from extracted deciduous teeth and differentiate them into osteoblast and identifies the molecular characterization of the differentiated cells by using reverse transcriptase PCR (RT-PCR) analysis.



© Academy of Sciences Malaysia

All rights reserved. No part of this publication may be reproduced in any form or by any means without permission in writing from the Academy of Sciences Malaysia

The Editorial Board, in accepting contributions for publications, accepts no responsibility for the views expressed by authors

Published by the Academy of Sciences Malaysia



The Academy of Sciences Malaysia (ASM)

The Academy of Sciences Malaysia (ASM) was established, under the *Academy of Sciences Act 1994* which came into force on 1 February 1995, with the ultimate aim to pursue excellence in science. Thus the mission enshrined is to pursue, encourage and enhance excellence in the field of science, engineering and technology for the development of the nation and the benefit of mankind.

The functions of the Academy are as follows:

- To promote and foster the development of science, engineering and technology
- To provide a forum for the interchange of ideas among scientists, engineers and technologists
- To promote national awareness, understanding and appreciation of the role of science, engineering and technology in human progress
- To promote creativity among scientists, engineers and technologists
- To promote national self-reliance in the field of science, engineering and technology
- To act as a forum for maintaining awareness on the part of the Government of the significance of the role of science, engineering and technology in the development process of the nation and for bringing national development needs to the attention of the scientists, engineers and technologists
- To analyse particular national problems and identify where science, engineering and technology can contribute to their solution and accordingly to make recommendations to the Government
- To keep in touch with developments in science, engineering and technology and identify those developments which are relevant to national needs to bring such developments to the attention of the Government
- To prepare reports, papers or other documents relating to the national science, engineering and technology policy and make the necessary recommendations to the Government
- To initiate and sponsor multi-disciplinary studies related to and necessary for the better understanding of the social and economic implications of science, engineering and technology
- To encourage research and development and education and training of the appropriate scientific, engineering and technical man power

- To establish and maintain relations between the Academy and overseas bodies having the same or almost similar objectives in science, engineering and technology as the Academy
- To advise on matters related to science, engineering and technology as may be requested by the Government from time to time; and
- To carry out such other actions that are consistent with the *1994 Academy of Sciences Act* as may be required in order to facilitate the advancement of science, engineering and technology in Malaysia, and the well being and status of the Academy.

The Academy is governed by a Council. Various Working Committees and Task Forces are charged with developing strategies, plans and programmes in line with the Academy's objectives and functions.

The functions of the Council are:

- To formulate policy relating to the functions of the Academy
- To administer the affairs of the Academy
- To appoint such officers or servants of the Academy as are necessary for the due administration of the Academy
- To supervise and control its officers and servants
- To administer the Fund; and
- To convene general meetings of the Academy to decide on matters which under this Act are required to be decided by the Academy.

The Academy has Fellows and Honorary Fellows. The Fellows comprise Foundation Fellows and Elected Fellows. The Academy Fellows are selected from the ranks of eminent Malaysian scientists, engineers and technocrats in the fields of medical sciences, engineering sciences, biological sciences, mathematical and physical sciences, chemical sciences, information technology and science and technology development and industry.

The Future

Creativity and innovation are recognised the world over as the key measure of the competitiveness of a nation. Within the context of K-Economy and the framework of National Innovation System (NIS), ASM will continue to spearhead efforts that will take innovation and creativity to new heights in the fields of sciences, engineering and technology and work towards making Malaysia an intellectual force to be reckoned with.

Contents

ASM Sc. J.
Volume 4(1), 2010

RESEARCH ARTICLES

- Ex-vivo* Differentiation of Stem Cells from Human
Extracted Deciduous Teeth into Bone Forming Cells** 1
S.N. Fazliah, S. Jaafar, S. Shamsuddin, Z. Zainudin,
A.B. Hilmi, A.R. Razila and S.F. Abdullah
- Ion Beam Elemental Analysis of Doped SiO₂ Optical Fibre and Its
Thermoluminescence Response When Irradiated with Protons** 15
A.T. Ramli, S. Hashim, D.A. Bradley, H. Wagiran, M. Webb and C. Jeynes
- Data Cognitive Complexity: A New Measure** 22
J.K. Chhabra, R.S. Bhatia and V.P. Singh
- Methane Adsorption Characteristics of Copper Oxide
Modified NaY Zeolite Adsorbents** 29
K.S.N. Kamarudin, Y.Y. Chieng, H. Hamdan and H. Mat
- Influence of CO₂ Flux on the Properties of Carbonate Apatite
Synthesized by Solid State Reaction** 41
K. Jamuna, K. Noorsal, F.A. Zakaria and Z.H. Hussin
- Communication Systems Melioration by Employing Fast Frequency
Hopping Spread Spectrum with Low-density Parity-check Codes** 48
A. Yahya, O. Sidek and M.F.M. Salleh
- Ionic Conductivity and Morphological Studies of Plasticized
Poly(methyl methacrylate) Polymer Electrolyte Films** 55
Z. Osman, L. Othman, K.B. Md Isa, A. Ahmad and N. Kamarulzaman
- Characterization of Skeletons of Simulated Drought and
Flood of Water Bodies** 62
S. Dinesh
- Effects of Nitrate, Phosphate, Temperature and Light-dark Cycle on
Algal Growth Potential of *Chlorococcum* sp. from Reeve Hill, Antarctica** 74
D. Masdialily, W.O.W. Maznah, M. Faradina and M. Mashhor
- Effects of Temperature on the Photosynthetic Parameters of
Antarctic Benthic Microalgal Community** 81
S. Salleh, A. McMinn, M. Mohammad, Z. Yasin and S.H.A. Tan



ANNOUNCEMENTS

Mahathir Science Award 2011 (Invitation for Nomination)	89
22nd Pacific Science Congress	90
Malaysian Science and Technology Congress 2010	92
ASM Publications	93



Ex-vivo Differentiation of Stem Cells from Human Extracted Deciduous Teeth into Bone Forming Cells

S.N. Fazliah^{1*}, S. Jaafar¹, S. Shamsuddin², Z. Zainudin², A.B. Hilmi¹, A.R. Razila¹ and S.F. Abdullah¹

Stem cells from human extracted deciduous teeth (SHED) have the ability to multiply much faster and double their population in culture at a greater rate, indicating that it may be in a more immature state than other type of adult stem cells. Mesenchymal stem cells (MSC) from human primary molars were isolated and cultured in media supplemented with 20% fetal bovine serum. The MSCs were confirmed using CD 105 and CD 166 and the identification of the osteoblast cells were done using reverse transcriptase polymerase chain reaction (RT-PCR) analysis. Differentiated osteoblast cells (DOC) were characterized by alkaline phosphatase and von Kossa staining followed by immunocytochemistry staining using osteocalcin and osteonectin antibodies. Further validation of SHED was done by RT-PCR to detect the presence of insulin-like growth factor 2 (IGF-2) and discoidin domain tyrosine kinase-2 (DDTK-2) transcripts, while the presence of Runx-2 mRNA was used to characterize DOC. The results showed that SHED was found positive for CD 105 and CD 166 and could differentiate into osteoblast, bone forming cells. The findings revealed the presence of distinct MSC population which had the capability to generate living human cells that could be a possible source for tissue engineering in the future.

Key words: human dental pulp, stem cells; extracted deciduous teeth, mesenchymal stem cells, von Kossa staining, alkaline phosphatase

Stem cells are primal cells, common to all multi-cellular organisms, that retain the ability to renew themselves through cell division (self-renewal) and can differentiate into a wide range of specialized cell types (pluripotential). A population of putative post-natal stem cells in human dental pulp, dental pulp stem cells (DPSCs) have been identified. The most striking feature of DPSCs is their ability to regenerate a dentin-pulp-like complex that is composed of mineralized matrix with tubules lined with odontoblasts and fibrous tissue containing blood vessels in an arrangement similar to the dentin-pulp complex found in normal human teeth (Gronthos *et al.* 2000). Previous studies have demonstrated that, like osteoblasts, pulp cells express bone markers such as bone sialoprotein, alkaline phosphatase, type I collagen, and osteocalcin (Gronthos *et al.* 2000; Shiba *et al.* 1998). Their differentiation is regulated by various potent regulators of bone formation, including members of the TGF β superfamily and cytokines (Gronthos *et al.* 2000; Buchaille *et al.* 2000). The similarity of the gene expression profiles between DPSCs and precursors of osteoblasts, bone marrow stromal stem cells (BMSSCs) has been reported (Onishi *et al.* 1999). Recently, stem cells and the dental pulp have shown to have potential roles in dentine regeneration and repair (Sonoyama *et al.* 2006). The objectives of this study were to isolate mesenchymal stem cells (MSCs) derived from extracted

deciduous teeth and differentiate them into osteoblast and to identify the molecular characterization of the differentiated cells by using reverse transcriptase PCR analysis.

MATERIALS AND METHODS

Tooth Sampling

The teeth were obtained from patients aged between 4 to 7 years old attending dental clinics or undergoing dental surgery. Prior to the tooth collection, the Ethical Committee and the Internal Review Board of Universiti Sains Malaysia had approved this study and all samples were obtained under approved guidelines. The sample size calculation using PS software (Dupont & Plummer 1997) was based on comparing two means (Insulin-like growth factor 2 and Discoidin domain tyrosine kinase) from DPSCs, in order to detect the difference of 1 unit (IGF-2) with 80% power and alpha of 0.05. Eleven teeth were needed in this study [SD was estimated as 0.8, the ratio between 2 factors was 1:1 ($m=1$)] (Shi *et al.* 2001). About 11 deciduous teeth were extracted from children aged 4–5 years under sterile surgical procedure. Only teeth either free from cavities and caries or with minor decay were selected. Three teeth fractured during sectioning leaving 8 teeth to be processed and used

¹School of Dental Sciences, Universiti Sains Malaysia, 16150 Kubang Kerian, Kelantan, Malaysia

²School of Health Sciences, Universiti Sains Malaysia, 16150 Kubang Kerian Kelantan, Malaysia

*Corresponding author (e-mail: fazliah@amdi.usm.edu.my)

in this study. After the extraction procedure, the tooth was immediately washed with normal saline and placed into a container containing Hank's Balance Salt Solution (HBSS) (to preserve the tissues from degradation), supplemented with 1% (v/v) Penicillin-Streptomycin (antibiotic) (Gibco™, Invitrogen, USA), 5% (v/v) Fetal Bovine Serum (FBS) (protein supplement) (Gibco™, Invitrogen, USA), Fungizone (antifungal) (BioWhittaker™, Cambrex, USA) and Gentamycin (antibacterial) (Gibco™, Invitrogen, China).

Dissection of Tissue and Cell Culture

Within 24 hours, the tooth was cut at the enamel-cementum junction (CEJ) using a hard tissue material cutter (Exakt 300, Exakt Apparatebau GMBH & Co. KG, Germany). The sectioned tooth was then briefly immersed in 75% (v/v) ethanol (Merck, Germany) followed by immersion in Dubecco's Phosphate Buffered Saline (DPBS) (Gibco™, Invitrogen, USA) and placed in a beaker containing DPBS (Gibco™, Invitrogen, USA), treated with Penicillin-Streptomycin (Gibco™, Invitrogen, USA) before extraction of the dental pulp in a class II safety biocabinet (Delta Series, Labconco, USA).

Sterile tissue forceps and medium size barb roaches were used when extracting the dental pulp tissue which was later transferred into 15 ml tubes containing PBS and penicillin-streptomycin and centrifuged at 1200 r.p.m. (Hettichzentrifugen, Germany) for 5 min. The supernatant was discarded and the tissues were digested using digestive solution containing 3 mg/ml of Collagenase Type 1 (Gibco™, Invitrogen, Germany) and 4 mg/ml of Dispase (Gibco™, Invitrogen, Germany) in a humidified atmosphere at 37°C with 5% CO₂ incubator (Thermo Forma, USA) for 1 h. A 70 µm cell strainer was used to disaggregate the digested and undigested pulp tissue. The digested tissue were put into 50 ml tubes and centrifuged (Hettichzentrifugen, Germany) at 2000 r.p.m. for 5 min. The supernatant was discarded and then 1 ml culture medium was added into the tube, the residue was resuspended and then poured into T-25 culture flasks (Nunc, Denmark).

To propagate the pulp cells, 4 ml of culture medium were added into the flask. Culture medium containing alpha Modified Eagle's Medium (α MEM) (BioWhittaker™, Cambrex, USA) supplemented with 20% (v/v) FCS (Gibco), 100 mM L-ascorbic acid 2-phosphate (Stem cell Technologies, Canada), 200 mM L-glutamine (Gibco™, Invitrogen, Japan) and 5000 units/ml penicillin/streptomycin (Gibco™, Invitrogen, Germany) was added and then it was incubated in a humidified atmosphere at 37°C with 5% CO₂ (Thermo Forma, USA). After 24 hours, non-adherent cells were removed. The adherent cells were washed vigorously twice with PBS to remove adherent debris. Subsequently, fresh complete medium was added.

The medium was replaced every 3 to 4 days. Observations were made at day 0, 1, 5 and 15.

Characterization of SHED by Immunocytochemistry

Immunostaining was performed by biotin-streptavidin-horseradish peroxidase (HRP) complexed antibodies to detect primary antibodies. SHED early passages and hMSC (human Mesenchymal Stem Cells) (Cambrex, USA) were placed in 4-well chamber slides (Nunc, Denmark) with density of 4×10^4 cells per well. After two days of culture in growth medium, the cells were fixed in absolute cold methanol (Merck, Germany) at 0°C for 20 min. A blocking reagent (Dakocytomation, USA) was added and the cells were incubated with primary antibodies overnight. Mouse monoclonal anti-human endoglin (CD105) (Chemicon, USA) with dilution 1:25 was added to the positive control of hMSC and SHED. Similarly, mouse monoclonal antihuman CD166 (DakoCytomation, USA) with dilution 1:50 was added to the positive control of hMSC and SHED. Meanwhile for the negative control, SHED were incubated with rabbit immunoglobulin fraction (normal) with dilution 1:25 (DakoCytomation, Denmark). For the negative control, SHED were incubated with rabbit immunoglobulin fraction (normal) with dilution 1:50 (DakoCytomation, Denmark). The primary antibodies were detected by immunoperoxidase diaminobenzidine (DAB) secondary detection system (Dakocytomation, USA).

Characterization of SHED by RT-PCR

Reverse Transcriptase-PCR (RT-PCR) was used to identify and quantify the specific mRNA of cells. SHED early passages and hMSC (Cambrex, USA) were cultured using growth medium in T-75 flask and harvested after the cells were 100% confluent. Total cellular RNA was isolated as according to the manufacturer's instructions. Amplification of gene performed by one step RT-PCR and mastermix were prepared according to the recommendations by the manufacturer (RNeasy®, Qiagen, Germany). The PCR products were separated by gel electrophoresis using 1.5% agarose gel (1st Base, Malaysia) at 150 volt for 35 minutes (Elite 300, Wealtec, USA). The bands of stained gel (Sybr® Green, Applied Biosystem, USA) were visualized by ultraviolet illumination (UV trasilluminator, Wealtec, USA) and images were captured using AlphaEaseFC™ (Alpha Innotech, USA).

As a stem cell marker, genes that were used to characterize SHED were insulin-like growth factor-2 (IGF-2) and discoidin domain tyrosine kinase-2 (DDTK-2) while glyceraldehyde-3-phosphate dehydrogenase (GAPDH) was used as a housekeeping gene. The sequences of the primers used for RT-PCR are shown in *Table 1*. Total cellular RNA isolated from hMSC (Cambrex, USA) was also used as the positive control for cell type; for the negative control, a blank was used.

Table 1. Sequences of RT-PCR primers for analysis of differentiation specific gene expression.

Genes	Primer sequences	Size (bp)
Housekeeping gene GAPDH	Sense: 5'-cccatcaccatcttcagga-3' Antisense: 5'-cccatcaccatcttcagga-3'	631
SHED specific gene IGF-2	Sense: 5'-ctctccgtgtcttctctcc-3' Antisense: 5'-cgggccagatgtgtacttt-3'	196
DDTK-2	Sense: 5'-caagaacagccctattcca-3' Antisense: 5'-caagaacagccctattcca-3'	231
Bone specific genes Runx-2	Sense: 5'-atgcttcattcgctcacaaac-3' Antisense: 5'-ccaaaagaagtttctgcatgg-3'	294

Differentiation of SHED into Osteoblasts

SHED can be differentiated into osteoblasts using osteogenic medium (Jaiswal *et al.* 1997). To induce osteogenesis, medium was prepared by supplementing alpha modification Eagle's medium (BioWhittaker™, Cambrex, USA) with 20% (v/v) FBS (Gibco, USA), 10 nM Dexamethasone (Sigma Aldrich, Germany), 0.2 mM L-ascorbic acid 2-phosphate (Stem cell Technologies, Canada), 200 mM L-glutamine (Gibco, Japan), pretreated with 5000 units/ml penicillin/streptomycin (Gibco, Japan) and 3.5 mM β -Glycerophosphate (Sigma Aldrich, Germany). Once the MSC approximately reached a confluent of 80% to 90%, osteogenic medium was added and the cells were incubated in a humidified atmosphere at 37 °C with 5% CO₂. The medium was changed every 3 to 4 days. Observations were made at day 7, 14 and 21.

Characterization of Differentiated Osteoblast Cells from SHED Using Alkaline Phosphatase Staining

Alkaline phosphatase (ALP) activity of cells was evaluated by alkaline phosphatase staining. ALP activity staining could be visualized stained red after being exposed to the incubation medium. The cultures were assessed by this technique on day 7, 14 and 21 of induction. The SHED early passages, hMSC (Cambrex, USA) and osteoblast cells (Cambrex, USA) were seeded in 6-well plates (Nunc, Denmark) at a density of 4×10^4 cells per well. Osteogenic medium was added to the osteoblast cells, the positive control hMSC and SHED after the cells were 80%–90% confluent. For the negative control, the SHED were cultured in growth medium. The cultures were fixed in cold methanol (Merck, Germany) for 20 min. Incubating medium containing 0.2 M Tris EDTA solution (Sigma Aldrich, Switzerland), 0.1 M hydrochloric acid (HCL) (Merck, Germany), distilled water, 4% (v/v) new fuchsin (Sigma Aldrich, Germany), 4% (w/v) sodium nitrate (Sigma Aldrich, Germany) and naphthol phosphate (Sigma Aldrich, Germany) was added for 15 min. For background staining, hematoxylin was used and the cells were mounted (R&M Chemicals, UK). The

ALP staining results were analyzed by an image analyzer (Zeiss, Germany) with images captured by a digital camera (Nikon E 4500, Japan).

Characterization of Differentiated Osteoblast Cells from SHED Using Von Kossa Staining

Von Kossa staining enabled the demonstration of the deposits of calcium or calcium salt which were stained black after being treated with silver nitrate. The cells were assessed by this technique on day 7, 14 and 21 of induction. The SHED early passages, hMSC (Cambrex, USA) and osteoblast cells (Cambrex, USA) were seeded in 6-well plates (Nunc, Denmark) at a density of 4×10^4 cells per well. Osteogenic medium was added to the osteoblast cells, the positive control hMSC and SHED after the cells were 80%–90% confluent. For the negative control, the SHED were cultured in growth medium. The cultures were fixed in cold methanol (Merck, Germany) for 20 min, covered with 5% (w/v) silver nitrate (Sigma Aldrich, Germany) solution and kept under a 100–600 watt light for 1 h and then counterstained with 1% (w/v) neutral red (Merck, Germany). After washing, the slides were dried and mounted (R&M Chemicals, UK). Mounting the slides prolonged the viewing time of the sample. The Von Kossa staining results were analyzed by an image analyzer (Zeiss, Germany) with images captured by a digital camera (Nikon E 4500, Japan).

Characterization of Differentiated Osteoblast Cells from SHED using Immunocytochemical Analysis

For differentiated osteoblast characterization, immunostaining was performed by biotin-streptavidin – horseradish peroxidase (HRP) complexed antibodies to detect primary antibodies. The cultures were assessed by this technique on day 7, 14 and 21 of induction. Seeding at 4×10^4 SHED early passages, hMSC (Cambrex, USA) and osteoblast cells (Cambrex, USA) were placed in 4-well chamber slides (Nunc, Denmark). After the cells were 80%–90% confluent, osteogenic medium was added to all cultures.

The cells were fixed in absolute cold methanol at 0°C for 20 min. Blocking reagent (Dakocytomation, USA) was added and all cells were incubated with primary antibodies overnight. The rabbit polyclonal anti-human osteonectin (Chemicon, USA) at a dilution of 1:500 was added to the osteoblast cells, the positive control of induced hMSC and induced SHED. Meanwhile, for the negative control, induced SHEDs were incubated with rabbit immunoglobulin fraction (normal) (DakoCytomation, Denmark) at a dilution of 1:500. Similarly, mouse monoclonal anti-human osteocalcin (Zymed Laboratories, USA) at a dilution of 1:500 was added to the osteoblast cells, the positive control of induced hMSC and induced SHED. Meanwhile, for the negative control, induced SHED were incubated with rabbit immunoglobulin fraction (normal) (DakoCytomation, Denmark) at a dilution of 1:500. The primary antibodies were identified by immunoperoxidase DAB secondary detection system (Dakocytomation, USA).

Characterization of Differentiated Osteoblast Cells from SHED Using RT-PCR

For differentiated osteoblast characterization, osteoblast cells (Cambrex, USA), SHED and Hela cells (Cambrex, USA) were grown in T-75 flasks (Nunc, Denmark) using growth medium. Osteogenic medium was added to the osteoblasts and SHED after the cells were 80%–90% confluent. The cultures were harvested at day 7, 14 and 21 and then were kept in RNA stabilization solution (RNAlater, Ambion, USA) before the extraction of RNA.

For RNA extraction, total cellular RNA was isolated by Prefect RNA™ Eukaryotic, Mini (Eppendorf, Germany) according to the manufacturer's instructions. The purity of total cellular RNA was evaluated by measuring the absorbance at 260nm (A_{260}) and 280nm (A_{280}) using a

spectrophotometer (Biophotometer, Eppendorf, Germany). Absorbance reading at A_{260} measured the RNA concentration and it had to be greater than 0.15 to be significant. The integrity of total RNA for differentiated osteoblast cells was assessed by 1% (w/v) agarose gel electrophoresis at 100 Volt for 60 min. The 28 S and 18 S bands were seen at 5000 bp and 3000 bp RNA ladder (New England Biolabs, UK).

Amplification of target gene was performed by one step RT-PCR and the mastermix was prepared according to the recommendations by the manufacturer (RNeasy®, Qiagen, Germany). The PCR products were separated by gel electrophoresis using 1.5% (w/v) agarose gel (1st Base, Malaysia) at 150 Volt for 35 min (Elite 300, Wealtec, USA). The bands of stained gel (Sybr® Green, Applied Biosystem, USA) were visualized by ultraviolet illumination (UV trasilluminator, Wealtec, USA) and the images were captured using AlphaEaseFC™ (Alpha Innotech, USA). The mRNA expression of Runx-2 was used as the biomarker for differentiated osteoblast cells and GAPDH was used as the housekeeping gene (Table 1). Sequencing was done by sending the samples to 1st Base (Malaysia) to verify each of the amplified genes.

RESULTS

Adherent cells grown on culture flasks displayed the typical morphology of SHED. These attached cells were dental pulp stem cells as the culture medium promoted prompt proliferation only to SHED. The colonies were seen to arise from single cells and contained both spindle shaped cells and large flat cells, they became colonies and later the primary cultures were grown to a confluence of between 80% to 100% before being trypsinized and then passaged into T-75 flasks for further applications (Figure 1).

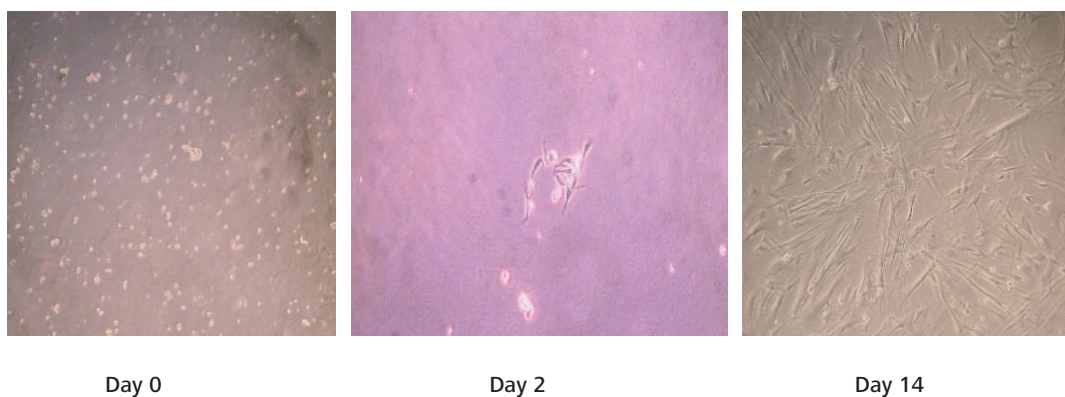


Figure 1. On day 0, the digested dental pulp including fibroblast, mesenchymal cells and macrophages were seen floating inside the flask at this early stage. On day 2, small rounded and a spindle shaped cell was seen attached to the flask and at day 14, the spindle-shaped cells have become 80% confluent ($\times 40$).

Immunophenotyping and Genotypic Characterizations of SHED

The characterization of SHED by immunocytochemistry using CD166 and CD105 showed that SHED was positive for both antibodies against human antigen CD105 and CD 166 (Figure 2). The characterization of SHED by RT-PCR analysis showed that expressions of DDTK-2 and IGF-2 were revealed on SHED (Figure 3).

Phenotypic and Genotypic Characterizations of Differentiated Osteoblast Cells from SHED

Differentiation of SHED into osteoblast showed that on day 7 the cells remained in spindle shape as SHED. The morphology of these cells had changed to cuboidal or polygonal on day 14 and finally mineralization was observed on day 21 (Figure 4).

For the characterization of differentiated osteoblast cells from SHED, the ALP activity as marker for early osteogenic differentiation showed it was strongly expressed on day 7 as compared to day 21 for differentiated osteoblast cells (DOC), induced hMSC and osteoblast cells. Non-differentiated osteoblast cells (non-DOC) showed no red stain (Figure 5).

Von Kossa staining was used as a marker for late osteogenic differentiation. Mineralization was observed when calcium phosphate deposits were demonstrated in black stained by Von Kossa assay which were obviously observed on day 21 in DOC. However, mineralization was not found on non-DOC (Figure 6).

The characterization of differentiated osteoblast cells using osteonectin (ON) showed that after an overnight incubation, ON expression was demonstrated in a brownish colour. The ON expression on DOC, positive control of hMSC and osteoblast cells were strongly expressed on day 7 and 14 as compared to day 21 where the ON expression had decreased. No ON expression was detected on negative control (Figure 7).

Osteocalcin (OC) was used as a marker for late osteogenesis and its expression was assessed on days 7, 14, and 21 for each cell type. After overnight incubation, OC expression was demonstrated as a brownish colour. The OC expression on DOC, positive control hMSC and osteoblast cells were strongly expressed on day 21 as compared to day 7 where the expression was low. No OC expression was detected on control negative (Figure 8).

Characterization of differentiated osteoblast cells by RT-PCR analysis using Runx-2 mRNA as marker showed that the test had revealed mRNA expression of GAPDH as a housekeeping gene and Runx-2 on DOC (Figures 9–10).

DISCUSSION

Stem cell could be obtained from tooth components such as permanent tooth pulp (Laino *et al.* 2006; Shi *et al.* 2001), periodontal ligament (Shi *et al.* 2001) and exfoliated deciduous tooth (Miura *et al.* 2003). The utilization of SHED had advantages besides its availability and quality for research. Less ethical and devotional issues have arisen subsequent to using SHED in research rather than embryonic stem cells or other adult stem cells, the usage of which proved controversial and the cells could actually also promote nerve cell survival (Nosrat *et al.* 2004). Some researchers had shown the potential of injecting dental pulp-derived MSC into brain cells as a possible cell-based therapy for neurodegenerative diseases such as Parkinson's and treatment for spinal cord injuries (Nosrat *et al.* 2004) while others have shown that stem cells from permanent tooth have the ability to produce dentin or pulp-like complex (Gronthos *et al.* 2000). Hence, research on stem cells from tooth would in turn benefit clinicians and health policy makers for treating neurological and tooth disease and implementing genetic modification of stem cells to produce therapeutic agents.

The dissection of a tooth must be done within 24 h to avoid prolonged exposure to the transport medium which might be infected by bacteria and fungi during tooth collection. Moreover, the tooth itself actually could have conferred the contamination. The extraction of dental pulp tissue from a sectioned tooth had to be done immediately after dissection to maintain the vitality of the tissue.

The molar and incisor deciduous teeth in this study were collected from very young children with the aim of yielding a very highly proliferative cell population that would be vigorously ready to differentiate. The most important factor to consider was whether the proliferation and differentiation of undifferentiated MSC reduced with age. Umbilical cord blood (UCB) has been claimed as an excellent alternative source of MSC because the cells contained in UCB can be considered as "very young" (Lee *et al.* 2004) and it had been demonstrated that the number and the differentiating potential of bone marrow mesenchymal cells decreased with age (D'Ippolito *et al.* 1999). Others had claimed that the MSC differentiation capacity to osteoblasts and adipocytes was maintained irrespective to donor age (Justesen *et al.* 2002). That study had demonstrated the outstanding source of MSC from deciduous teeth considering the availability and quality of research, and the avoidance of the ethical and devotional issues. In fact, in older pulp from permanent teeth, the number of undifferentiated mesenchymal cells might diminish, which might also reduce the regenerative potential of the pulp (Hargreaves & Goodies 2002).

The proliferation of cells demonstrated that the adherent cells obtained from SHED had a durable, self renewing capability and under an osteogenic medium, they were

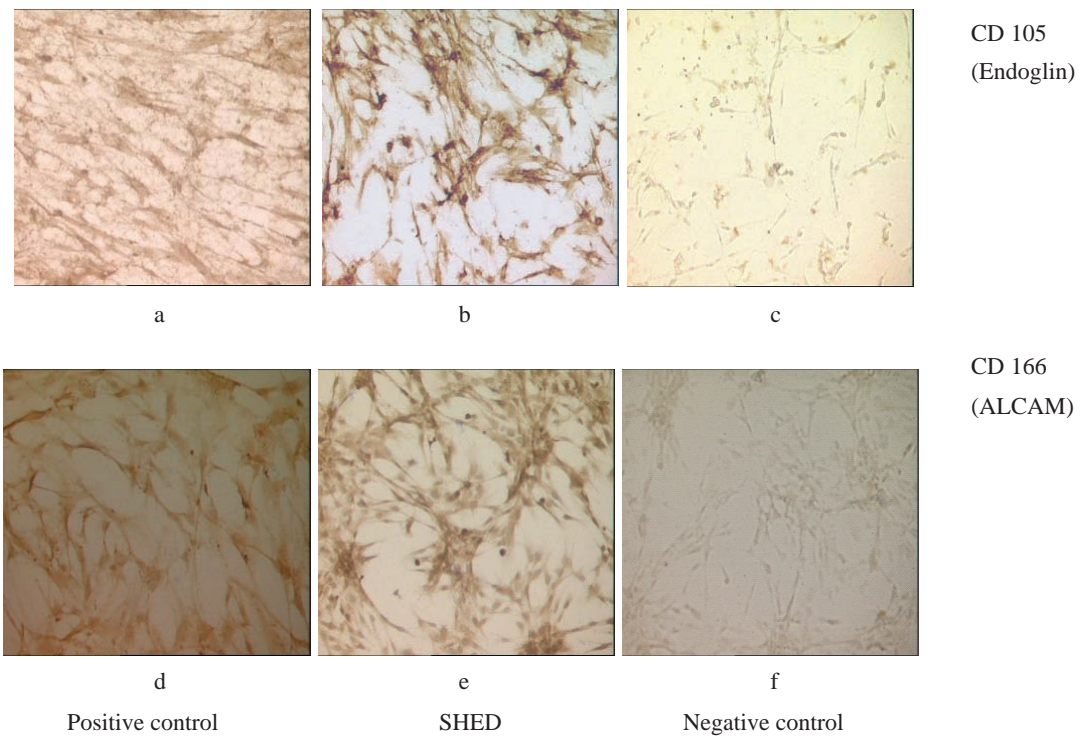
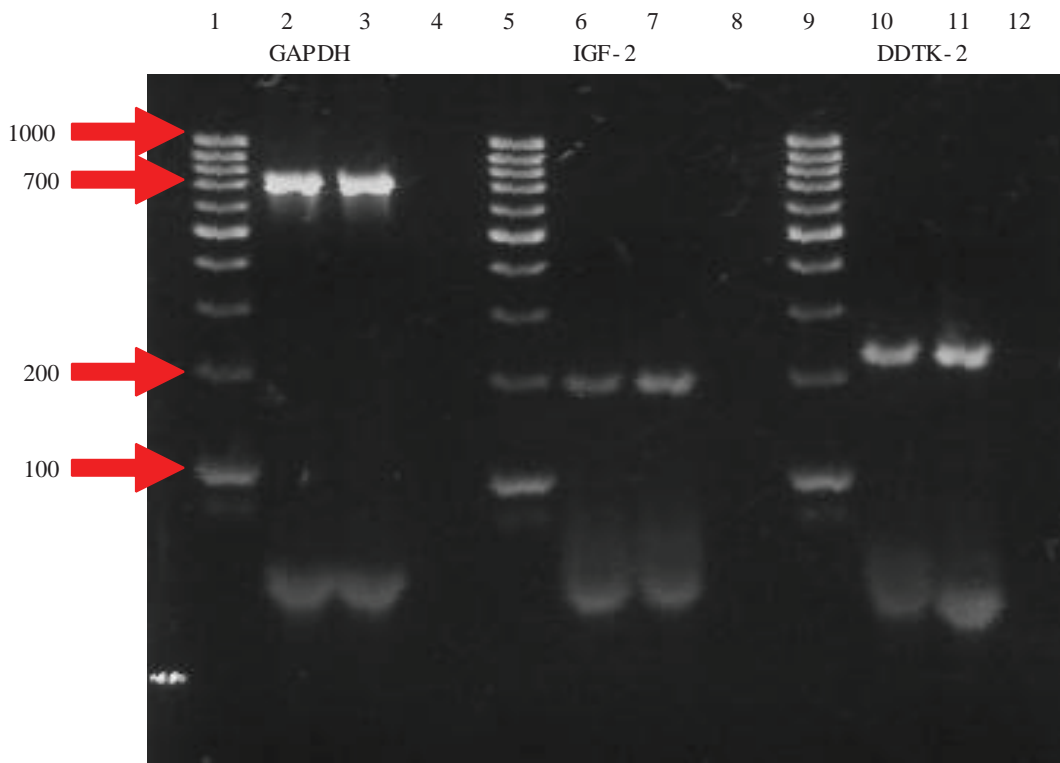


Figure 2. SHED (b, e) was found positive for both CD 105 and CD 166, which was consistent with findings for human bone marrow mesenchymal stem cells(a, d). No expression was detected on the negative control cells (c, f) ($\times 40$).



Lane 1,5, 9 = 100 bp ladder; Lane 2,6,10 = SHED; Lane 4,8,12 = No cells; Lane 3,7,11 = hMSC

Figure 3. The characterization of stem cells using IGF-2 and DDTK-2. The mRNA levels of each gene were amplified at 196 bp and 231 bp. PCR products were separated on 1.5% (w/v) agarose gel at 150 volt for 35 min.



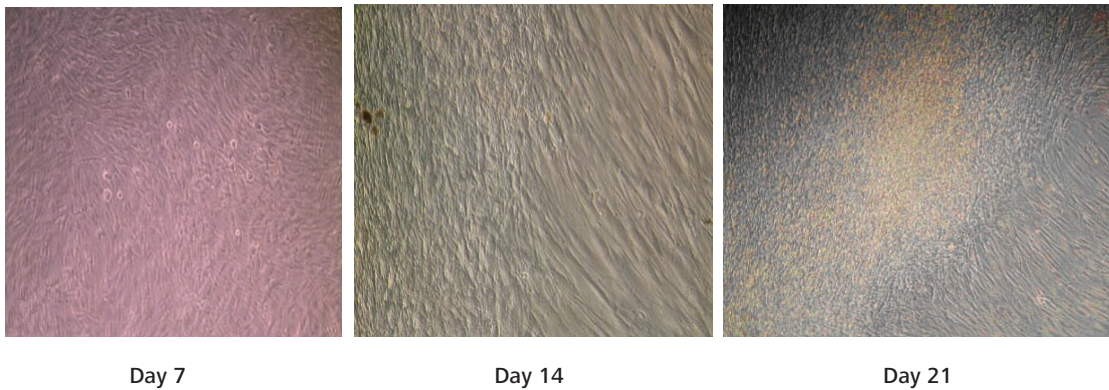


Figure 4. The differentiated cells remain in spindle shape as SHED on day 7 but the morphology of these cells changed to cuboidal or polygonal on day 14 and finally mineralization was observed on day 21 ($\times 40$).



Figure 5. Characterization of differentiated osteoblast cells by ALP staining viewed at $\times 100$. Sites of ALP activity was demonstrated by the red stain. ALP activity was higher at day 7 and gradually decreased.

able to differentiate into bone-forming osteoblast. This was proven in our results by ALP and von Kossa staining. This characterization capability of MSC had been observed in human placenta (Fukuchi *et al.* 2004) and in human bone marrow and permanent teeth (Gronthos *et al.* 2000). MSC derived from dental pulp exhibited a higher proliferation rate as compared to MSC derived from bone marrow *in vitro* (Gronthos *et al.* 2000). MSC, as with other progenitor cells, grew in three phases with an initial lag phase (3 to 4 days) followed by rapid expansion and then a subsequent stationary phase (Bruder *et al.* 1997; Colter *et al.* 2001). This study demonstrated that single cells on day 1 became colonies on day 5 and then 80% to 100% confluence was

rapidly achieved between day 21 to 28 (Figure 1). The stationary phase which is depletion of growth, was not determined because in our study, only early culture of cells from third to sixth passages had been selected for differentiation since proliferation was reduced with old cells.

MSC initially consisted of three colonies: spindle shape cells (Bruder *et al.* 1997; Colter *et al.* 2001; Lee *et al.* 2005); large flat cells (Bruder *et al.* 1997; Colter *et al.* 2001) and small round cells (Colter *et al.* 2001). Our results (Figure 1) demonstrated that during day 0, single round cells were clearly seen. The cells changed their morphology to spindle

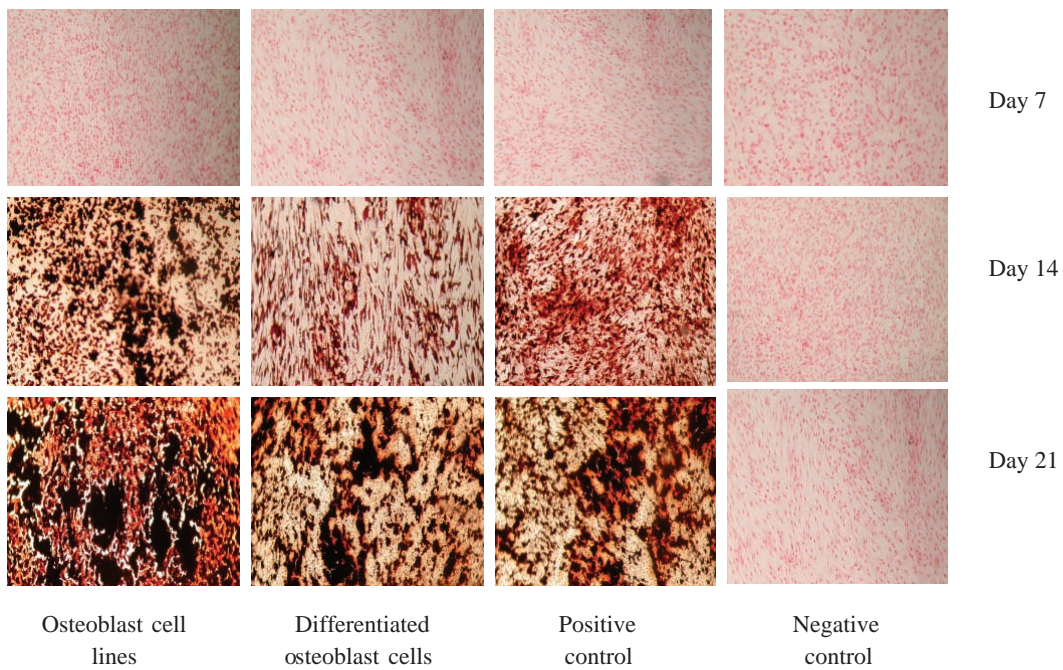


Figure 6. Characterization of differentiated osteoblast cells by von Kossa staining viewed at $\times 100$. Calcium deposits were seen by black deposit accumulation on day 21.

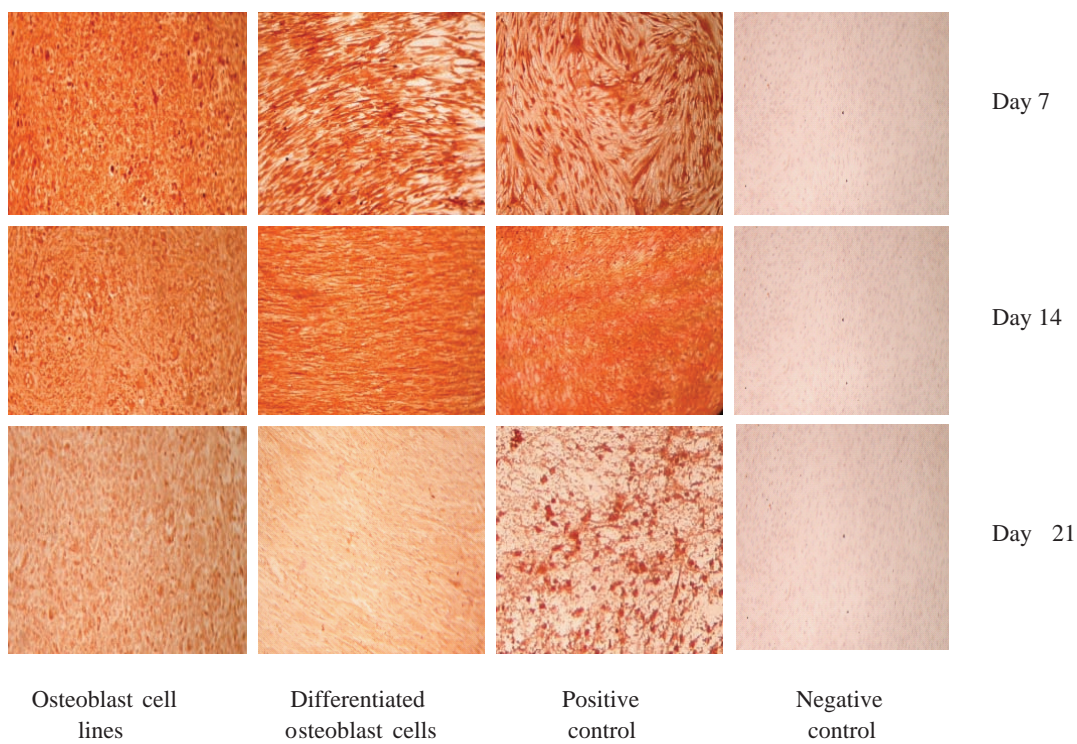


Figure 7. Characterization of differentiated osteoblast cells by immunocytochemistry staining using ON antibody viewed at $\times 100$. The ON expression was demonstrated in brown. The ON was expressed strongly in differentiated osteoblast at day 7 and 14 (darker intensity showed increased expression).

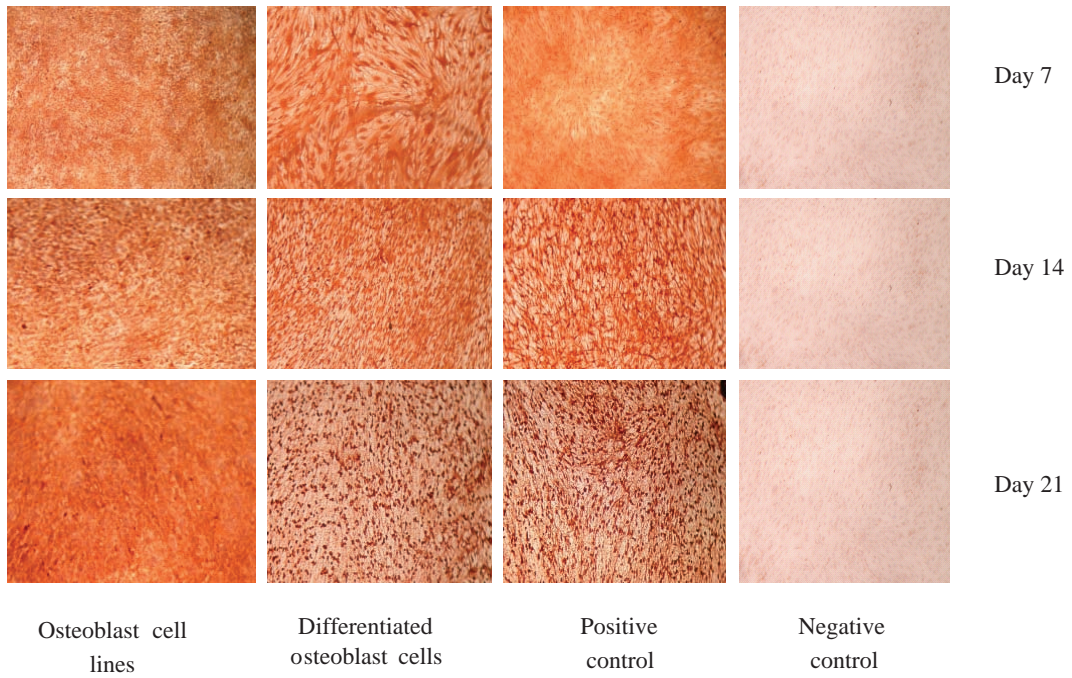
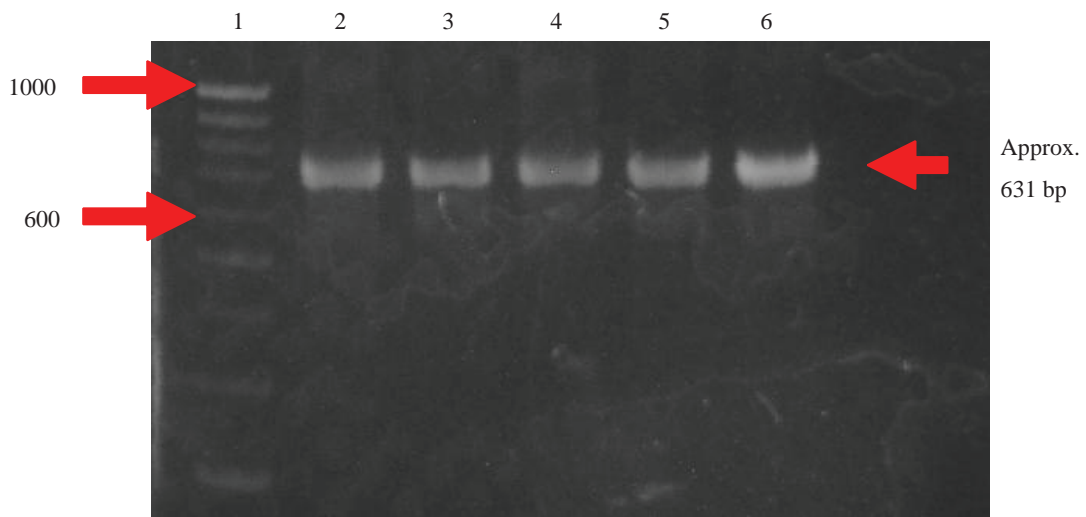
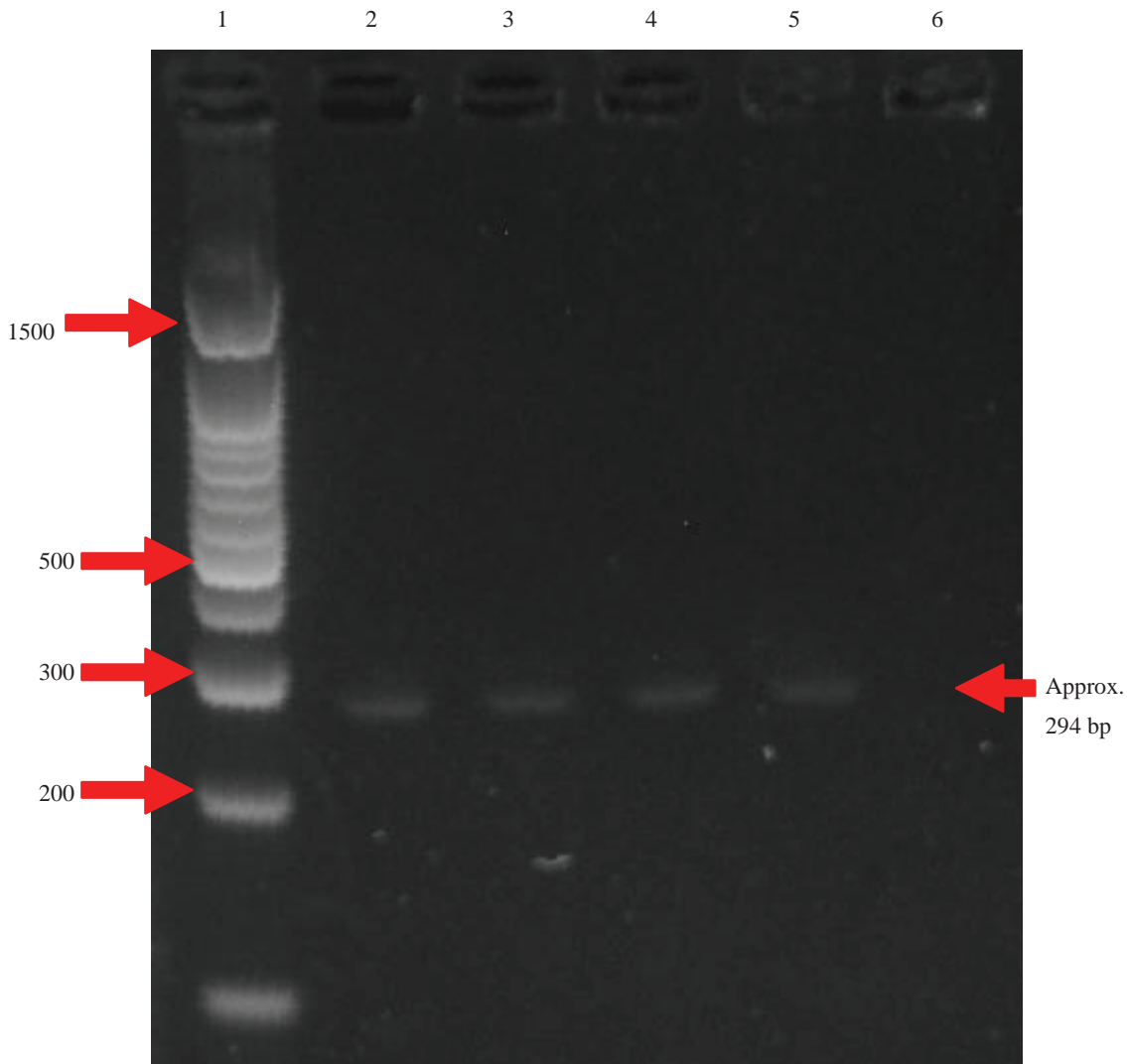


Figure 8. Characterization of differentiated osteoblast cells by immunocytochemistry staining using OC antibody viewed at $\times 100$. The OC expression was demonstrated in brown. OC was expressed strongly in differentiated osteoblast at day 21 (darker intensity showed increased expression).



Lane 1 = 100 bp ladder; Lane 2 = Osteoblast cells ; Lane 3 = DOC day 7; Lane 4 = DOC day 14; Lane 5 = DOC day 21; Lane 6 = Cervical cancer cells

Figure 9. RT-PCR analysis of GAPDH. As a house keeping gene, GAPDH was clearly detected on osteoblast cell, Hela cells and all time frames of DOC cultures at 631 bp. PCR products were separated on 1.5% (w/v) agarose gel at 150 volt for 35 min.



Lane 1 = 100 bp ladder; Lane 2 = Osteoblast cells; Lane 3 = DOC day 7; Lane 4 = DOC day 14; Lane 5 = DOC day 21; Lane 6 = Cervical cancer cells

Figure 10. RT-PCR analysis of Runx-2. As an osteoblast transcription factor, Runx-2 transcript migrated at 294 bp. PCR products were separated on 1.5% (w/v) agarose gel at 150 volt for 35 min.

shape on day 1 and large flat cells were clearly seen on day 5. Only spindle shape and large flat cell morphology could be seen once the cells had confluent. Similar morphology can be observed in human MSC isolated from bone marrow (Colter *et al.* 2001).

Phenotypic and genotypic characterizations of dental pulp stem cells and differentiated osteoblast cells were demonstrated by cytochemical staining, immunocytochemistry and RT-PCR analysis. Immunocytochemistry had many advantages over other biochemical tests. It was specific, sensitive, flexible and cost-effective. The interpretation of other histological staining patterns such as Florescence *in-situ* hybridization (FISH) was a

highly skilled task requiring a great deal of experience combined with intuition and deduction. Using immunological reagents however, the particular characteristic of a different protein could be highlighted as it appeared distinct, different proteins were regarded as different antigen. The presence of any antigen could be determined by an antibody reagent which was specific for that antigen. Antibody titre and dilutions as well as incubation time, and temperature were tightly interwoven with their effect on the quality of immunocytochemical staining.

The ability to isolate pure and intact RNA is essential in the study of gene expression and transcription. That is the

reason that we used 100% cells confluent for SHED and differentiated osteoblast cells before the cells underwent RT-PCR analysis in this study. The difficulty in isolating RNA is that ribonucleases (RNase) are ubiquitous, very stable and function under a variety of conditions which would be unstable for most other enzymes. All protocol for RNA isolation use RNase inhibitors or methods that can cause cells to be disrupted and become inactive RNase simultaneously. The successful isolation of intact RNA requires effective disruption of cells, denaturation of nucleoprotein complexes, inactivation of RNase activity and removal of contaminating DNA and proteins.

Total RNA isolated from SHED and differentiated osteoblast cells has firstly to be reversed transcribed into complementary DNA. The process from RNA to DNA is called reverse transcription. RT-PCR can be performed to detect even a single RNA molecule. PCR has rapidly become one of the most widely used techniques in molecular biology and for various good reasons. It is a rapid, inexpensive and simple means of producing more than 10 million copies of a target DNA sequence.

To characterize cell surface markers, the cluster of differentiation prefix CD was used to identify specific cell membrane molecules expressed on cells. During the proliferation and differentiation process, many T cells expressed T-cell receptors (TCR) with antigen recognition sites that bind self-antigens. Antigenic surface markers of our SHED had been detected by immunocytochemistry using CD166 and CD105. MSC was isolated from bone marrow and characterized using another MSC surface marker including SH2, SH3, CD29, CD71, CD106, CD124, CD44 and CD90 antibodies (Pittenger *et al.* 1999). In our study, SHED was found positive for both antibodies against human antigen, CD105 and CD166. Both of these antibodies strongly reacted with an antigen present on MSC and non-hematopoietic progenitor cells. Immunophenotypes of MSC found in umbilical cord blood (Lee *et al.* 2005) and dental papilla (Ikeda *et al.* 2006) showed that cultured cells from them were strongly positive for CD105 and CD166.

CD166 is a human activated leukocyte cell adhesion molecule (ALCAM). The distribution of cell adhesion molecules and substrate adhesion molecules as potential control factors in tooth development has been a subject of increasing interest (Garant 2003). CD166 is a component of the Ig superfamily and is expressed on activated T cells, B cells, thymic epithelial cells, fibroblast, keratinocytes and neurons. CD166 has been identified as a receptor for 100 kD ALCAM. The monoclonal CD166 antibody was shown to be reactive with an ALCAM antigen present on undifferentiated mesenchymal cells, which disappeared once the cells embarked upon the osteogenic pathway and began to express cell surface alkaline phosphatase (Bruder *et al.* 1997).

CD105 is an epitope present on the transforming growth factor-beta receptor endoglin. Endoglin is a transmembrane glycoprotein expressed by vascular endothelial cells. It functions as an ancillary receptor influencing binding of the transforming growth factor beta (TGF- β) family ligands to signaling receptors. CD105 is a component of the TGF- β receptor system and can bind TGF- β 1 and TGF- β 2. CD105 is highly expressed by vascular endothelial cells (Garant 2003).

MSC expressed several transcripts for various growth factors and genes indicated to be enriched in stem cells. The profile of gene expressions in MSC have been identified with their important contribution of extracellular matrixes, adhesion molecules, cell motility, TGF- β signaling, growth factor receptors, DNA repair, protein folding and ubiquitination as part of transcriptomes (Silva *et al.* 2003). The transcripts of insulin-like growth factor-2 gene (IGF-2) and discoidin domain tyrosine kinase 2 gene (DDTK-2) were demonstrated to be present by RT-PCR in the isolated SHED. We therefore found that RT-PCR analysis revealed the presence of DDTK-2 mRNA and IGF-2 mRNA. It has been reported that IGF-2 and DDTK-2 were highly expressed in the dental pulp stem cell as compared to Collagen Type I α -2 mRNA which also is coded for growth factors (Shi *et al.* 2001).

Human growth hormone (HGH) known as somatotropin is a major polypeptide hormone that consists of 191 amino acids. It is secreted by the anterior lobe of the pituitary gland and promotes the growth of healthy new cells by stimulating the release of IGF-1 and IGF-2, which influences the metabolism of proteins, carbohydrates and lipids and is known as the hormone of youth.

IGF-2 also known as somatomedin, is an important growth factor of HGH. It is a mitogen for many cell types and an important modulator of muscle growth and differentiation, essential for maintaining organs such as the brain/nervous system, liver and kidneys. IGF-2 has been used to establish pluripotent cell lines (Takahashi *et al.* 1995) and maintain undifferentiated stem cells from the inner cell mass in culture (NewMan-Smith *et al.* 1995; Takahashi *et al.* 1995). IGF-2 stimulated growth and/or differentiation and inhibited apoptosis for certain cell types including hematopoietic progenitors (Zhang & Lodish 2004).

A signaling molecule, Discoidin Domain Tyrosine Kinase 2 gene (DDTK-2) has been identified in connective tissues. DDTK-2 is binded to various collagen proteins as their activating ligands and is involved in the regulation of cell growth, differentiation, metabolism and proliferation. DDTK-2 is a tyrosine receptor expressed in mesenchymal tissues (Vogel 1999). The cell rich zone of dental pulp tissue has a high density of MSC. Injured odontoblasts are replaced by MSC that migrate from the cell rich zone onto

the dentin inner surface of teeth (Hargreaves & Goodies 2002). Teeth and bone are specialized hard tissue which closely resemble each other. Bone density is maintained by a dynamic balance of bone formation carried out by osteoblast and bone resorption by osteoclasts.

The mineralized components of teeth in addition to alveolar bone consist of dentin, enamel and cementum secreted by odontoblast, ameloblast and cementoblast respectively (Rani & MacDougall 2000).

Differentiation of mesenchymal cells into osteogenic lineage is accompanied by concomitant secretion of a complex extracellular matrix which comprised collagen, bone sialoprotein, various proteoglycans and other proteins that initiate the process of tissue mineralization to form calcified bone (Heng *et al.* 2004). This can be seen in five developmental stages such as mesenchymal stem cells, osteoprogenitor cells, preosteoblast, osteoblast and osteocytes. Osteogenesis is controlled by numerous extrinsic factors including hormones and growth factors, activated osteoblast specific signaling proteins and transcription factors. In our study, characterizations of differentiated osteoblast development which were in stage four were clearly observed by von Kossa staining, immunocytochemistry and RT-PCR. The osteocyte developmental stage could only be demonstrated *in vivo*.

Proliferation of osteoblastic cells involves the synthesis of a bone extracellular matrix and its accumulation and maturation is essential to the mineralization process. Once the mineralization has been achieved, it can contribute to the cease of proliferation (Owen *et al.* 1990; Stein & Lian, 1993; Stein & Stein 1995). This study had successfully demonstrated that SHED had undergone osteogenesis after being induced by the osteogenic medium for 21 days. Differentiation into osteoblast has provided novel therapeutic tools for the future of dentistry. In the field of dentistry, dental caries is a dynamic process that involves the demineralization and remineralization of tooth structure. Once the tooth structure is lost, there are no other material that can replace the enamel and dentin but the cavity can be filled with restorative material. Hopefully, by using the differentiated osteoblast from SHED, we can transplant the cells into the suitable recipient and allow for regeneration of new enamel and dentin. The cells can synthesize the matrix and later undergo mineralization in the coronal pulp. They may also stimulate the total closure of the pulp in the root canal (Goldberg & Smith 2004).

Hence, differentiated osteoblast cells could be used as bioactive agents to cure caries, oral cancer, correction of congenital defects and for the regeneration of teeth and tissues to restore oral functions.

Mineralization was detected by von Kossa staining with the accumulation of black deposit which was

calcium. Abdallah *et al.* (2006) has succeeded in isolating mesenchymal stem cells from human serum which have been shown to produce extracellular matrix that corresponds to the early stage of mineralization and, they have collected serum from young donors during the menstrual period in order to avoid large variations of sex hormones in the blood. Mineralization of our SHED was successfully demonstrated in Figure 4.

ALP is a membrane bound enzyme that is abundant in the early stage of bone formation (Dragoo *et al.* 2003). During the 7 days of induction with osteogenic medium (OM), the ALP activity was higher than with cultured cells on day 21. However, the bone marrow stem cells that had been cultured in osteogenic media on day 21 expressed maximal levels of ALP activity. This was because the behaviour of human bone cell cultures was in agreement with the model of osteoblastic differentiation. If osteoblastic differentiation was achieved, the formation of a mineralized matrix could contribute to the decrease in cell proliferation and increased ALP levels had been found to correlate with increase in bone formation (Coelho & Fernandes 2000). This study provided evidence that ALP activity of osteogenesis from human extracted deciduous teeth occurred earlier than ALP activity of osteogenesis from human bone marrow as mentioned previously (Coelho & Fernandes 2000) because on day 7, ALP activity in SHED was strongly expressed as compared to day 21. ALP activity was always associated with the production of any mineralized tissue, preferentially distributed along the apical surface and on cytoplasmic processes (Pintero *et al.* 1995).

The developmental sequence of bone consists of three phases, the proliferation with matrix secretion, matrix maturation and matrix mineralization. Each phase is characterized by the expression of different genes. The proliferation phase consists of cell multiplication, growth, maturation and the development of extracellular matrix. The second phase, matrix maturation is characterized by early osteogenic markers such as ALP, osteopontin (OP) and ON. The final stage of progenitor cell development into osteogenic lineage is matrix mineralization. Numerous markers which were specific to this stage had been used including von Kossa staining, bone sialoprotein and osteocalcin. Von Kossa staining is specific for calcified extra cellular matrix. These three phases were observed in stem cells derived from human fat (Dragoo *et al.* 2003).

The expressions of ON and OC have been demonstrated previously on bone marrow stem cells (BMSC) *in vitro* (Gronthos *et al.* 2000). They found that ON expressed strong staining while OC expressed weak staining in BMSCs' primary culture. These findings showed that ON is an early stage marker while OC is a late stage marker (Gronthos *et al.* 2000). Similarly, from our results, OC showed strong staining (highly expressed) when the cells changed into mineralized tissue.

Osteonectin has been proposed to have a role in the initiation of mineralization of bone matrix and is formed by cells which do not yet possess the morphologic phenotype of osteoblast and may be regarded as a differentiation marker of the osteoblastic lineage. It is a glycoprotein, has calcium-binding properties and is also known to be secreted protein, acidic and rich in cysteine. It is expressed by osteoprogenitor cells, osteoblast and newly formed osteocytes. Numerous cells of soft tissue, such as periodontal ligament, fibroblast and endothelial cells also produce ON. As a result of its ability to bind various collagens and substrate adhesion molecules, ON may have a generalized function in a calcium mediated organization of extracellular matrices (Young *et al.* 2003).

OC is a late bone marker secreted by osteoblast. There was a strong OC expression on day 21 as compared to day 7 (Figure 8). OC, also known as bone Gla protein, is a signal terminal for osteoblast differentiation. It is a vitamin K and vitamin D-dependent protein. In humans, OC gene was located on chromosome 1. OC is a low molecular weight protein containing three α -carboxylglutamic acids. The role of OC in bone mineralization was supported by the observation that osteocalcin mRNA was localized in osteoblast and simultaneously in the mineralized bone matrix. OC is localized over the mineralized portion of bone and in acellular cementum (McKee *et al.* 1992).

Miura *et al.* (2003) demonstrated the potential of exfoliated deciduous-derived MSC to differentiate into mineralized tissues and they found that the core binding factor alpha-1 (Cbfa-1), another name for Runx-2, was highly expressed in mineralized tissue (Miura *et al.* 2003). We also found that this gene was highly expressed in differentiated osteoblast cells (Figure 9).

Runx-2 serves as a master gene to turn on the expression of osteocalcin, osteopontin, bone sialoprotein and collagen synthesis. MSC differentiation into osteogenic cell line is preceded by the activation of the Runx-2 gene (Ducy *et al.* 1997).

In conclusion, our SHED cultures showed the presence of distinct mesenchymal cells that were highly proliferative and capable of differentiating into osteoblast and performing its appropriate functions. At the present time, concerned parents have already chosen to bank genetic material from umbilical cord blood to isolate and store living stem cells of their babies. Unfortunately, this choice was available only at the time of the child's birth. Now, people have a second chance by storing deciduous teeth stem cells. It provides a unique type of insurance, not only for the child but also for the entire family, at a reasonable cost compared to the storing of umbilical cord blood. Stem cell from teeth could be isolated and saved for future therapeutic treatment. Autologous banking could be done by collecting, processing and cryopreserving stem cells

obtained from deciduous teeth thus, acting as 'biological insurance'. Hopefully, our research group together with private expertise could establish, for the first time in Malaysia, a dental pulp stem cell bank.

ACKNOWLEDGEMENTS

We are indebted to the generous support from Academy of Sciences Malaysia for the Scientific Advancement Grant Allocation (SAGA) 304/PPSG/6153006.A118. We thank the staff and fellow researchers from the Craniofacial Laboratory, School of Dental Sciences for their assistance.

Date of submission: April 2008

Date of acceptance: December 2009

REFERENCES

- Abdallah, BM *et al.* 2006, 'Inhibition of osteoblast differentiation but not adipocyte differentiation of mesenchymal stem cells by sera obtained from aged females', *Bone*, vol. 39, no. 1, pp. 181–188.
- Bruder, S, Jaiswal, SP & Haynesworth, SE 1997, 'Growth kinetics, self-renewal, and the osteogenic potential of purified human mesenchymal stem cells during extensive subcultivation and following cryopreservation', *J. Cell Biochem.*, vol. 64, no. 3, pp. 278–294.
- Buchaille, R *et al.* 2000, 'Expression of the small leucine-rich proteoglycan osteoadherin/osteomodulin in human dental pulp and developing rat teeth', *Bone*, vol. 27, no. 2, pp. 265–270.
- Coelho, MJ & Fernandes, MH 2000, 'Human bone cell cultures in biocompatibility testing. Part II: Effect of ascorbic acid, beta-glycerophosphate and dexamethasone on osteoblastic differentiation', *Biomaterials*, vol. 21, no.11, pp. 1095–1102.
- Colter, DC, Sekiya, I & Prockop, DJ 2001, 'Identification of a subpopulation of rapidly self-renewing and multipotential adult stem cells in colonies of human marrow stromal cells', in *Proc Natl. Acad. Sci. USA*, vol. 98, no. 14, pp. 7841–7845.
- D'ippolito, G *et al.* 1999, 'Age-related osteogenic potential of mesenchymal stromal stem cells from human vertebral bone marrow', *J. Bone Miner. Res.*, vol. 14, no. 7, pp.1115–1122.
- Dragoo, JL *et al.* 2003, 'Bone induction by BMP-2 transduced stem cells derived from human fat', *J Orthop. Res.*, vol. 21, no. 4, pp. 622–629.
- Ducy, P *et al.* 1997, 'Osf2/Cbfa1: a transcriptional activator of osteoblast differentiation', *Cell*, vol. 89, no. 5, pp. 747–754.
- Fukuchi, Y *et al.* 2004, 'Human placenta-derived cells have mesenchymal stem/progenitor cell potential', *Stem Cells*, vol. 22, no. 5, pp. 649–658.
- Garant PR (eds) 2003, '*Oral cells and tissue*' Canada, 1st edn, Quintessence Publishing Co, Inc.

- Goldberg, M & Smith, AJ 2004, 'Cells and extracellular matrices of dentin and pulp: a biological basis for repair and tissue engineering', *Crit. Rev. Oral Biol. Med.*, vol. 15, no. 1, pp. 13–27.
- Gronthos, S *et al.* 2000, 'Postnatal human dental pulp stem cells (DPSCs *in vitro* and *in vivo*)', in *Proc. Natl. Acad. Sci.*, vol. 97, no. 25, pp. 13625–13630.
- Hargreaves, MK & Goodies, HE (eds) 2002, *Seltzer and Bender's dental pulp*, China, Quintessence Publishing Co, Inc, pp. 105, 248, 610.
- Heng, BC *et al.* 2004, 'Strategies for directing the differentiation of stem cells into the osteogenic lineage *in vitro*', *J Bone Miner. Res.*, vol. 19, no. 9, pp. 1379–1394.
- Ikeda, E *et al.* 2006, 'Osteogenic differentiation of human dental papilla mesenchymal cells', *Biochem. Biophys. Res. Commun.*, vol. 342, no. 4, pp. 1257–1262.
- Justesen, J *et al.* 2002, 'Maintenance of osteoblastic and adipocytic differentiation potential with age and osteoporosis in human marrow stromal cell cultures', *Calcif. Tissue Int.*, vol. 71, no. 1, pp. 36–44.
- Laino, G *et al.* 2006, 'In vitro bone production using stem cells derived from human dental pulp', *J. Craniofac. Surg.*, vol. 17, no. 3, pp. 511–515.
- Lee, MW *et al.* 2005, 'Isolation of mesenchymal stem cells from cryopreserved human umbilical cord blood', *Int. J. Hematol.*, vol. 81, no. 2, pp. 126–130.
- Lee, OK *et al.* 2004, 'Isolation of multipotent mesenchymal stem cells from umbilical cord blood', *Blood*, vol. 103, no. 5, pp. 1669–1675.
- McKee, MD, Glimcher, MJ & Nanci, A 1992, 'High-resolution immunolocalization of osteopontin and osteocalcin in bone and cartilage during endochondral ossification in the chicken tibia', *Anat. Rec.*, vol. 234, no. 4, pp. 479–492.
- Miura, M *et al.* 2003, 'SHED: Stem cells from human exfoliated deciduous teeth', in *Proc. Natl. Acad. Sci. USA*, vol. 100, no. 10, pp. 5807–5812.
- NewMan-Smith ED & Werb, Z 1995, 'Stem cell defects in parthenogenetic peri-implantation embryos', *Development*, vol. 121, no. 7, pp. 2069–2077.
- Nosrat IV, Smith CA, Mullally P *et al.* 2004 'Dental pulp cells provide neurotrophic support for dopaminergic neurons and differentiate into neurons *in vitro*; implications for tissue engineering and repair in the nervous system'. *Eur. J. Neurosci.*, vol. 19, no. 9, pp. 2388–2398.
- Onishi, T *et al.* 1999, 'Stimulation of proliferation and differentiation of dog dental pulp cells in serum-free culture medium by insulin-like growth factor', *Arch. Oral Biol.*, vol. 44, no. 3, pp. 361–371.
- Owen, TA *et al.* 1990, 'Progressive development of the rat osteoblast phenotype *in vitro*: reciprocal relationships in expression of genes associated with osteoblast proliferation and differentiation during formation of the bone extracellular matrix', *J. Cell Physiol.*, vol. 143, no. 3, pp. 420–430.
- Pinero, GJ 1995, 'Bone matrix proteins in osteogenesis and remodelling in the neonatal rat mandible as studied by immunolocalization of osteopontin, bone sialoprotein, alpha 2HS-glycoprotein and alkaline phosphatase', *Arch Oral Biol.*, vol. 40, no. 1, pp. 145–155.
- Pittenger, MF *et al.* 1999, 'Multilineage potential of adult human Mesenchymal stem cells', *Science*, vol. 284, no. 5411, pp. 143–147.
- Rani, CSS & MacDougall, M 2003, 'Dental cells express factors that regulate bone' resorption', *Mol. Cell Biol. Res. Commun.*, vol. 3, no. 1, pp. 145–152.
- Shi, S, Robey, PG & Gronthos, S 2001, 'Comparison of human dental pulp and bone marrow stromal stem cells by cDNA microarray analysis', *Bone*, vol. 29, no. 6, pp. 532–539.
- Shiba, H *et al.* 1998, 'Differential effects of various growth factors and cytokines on the syntheses of DNA, type I collagen, laminin, fibronectin, osteonectin/secreted protein, acidic and rich in cycteine (SPARC), and alkaline phosphatase by human pulp cells in culture', *J. Cell Physiol.*, vol. 174, no. 2, pp. 194–205.
- Silva, WA Jr, *et al.* 2003, 'The profile of gene expression of human marrow mesenchymal stem cells', *Stem Cells*, vol. 21, no. 6, pp. 661–669.
- Sonoyama, W, Liu, Y & Fang, D 2006, 'Mesenchymal stem cell-mediated functional tooth regeneration in swine', *PLoS ONE*, vol. 1, no. 1, pp. e79.
- Stein, GS 1995, 'Molecular mechanisms mediating control of cell cycle and cell growth', *Exp. Hematol.*, vol. 23, no. 10, pp. 1053–1061.
- Stein, GS & Lian, JB 1993, 'Molecular mechanisms mediating proliferation/differentiation interrelationships during progressive development of the osteoblast phenotype', *Endocr. Rev.*, vol. 14, no. 4, pp. 424–442.
- Takahashi, A *et al.* 1995, 'Synergistic effects of insulin-like growth factor II (IGF-II) with leukemia inhibiting factor (LIF) on establishment of rat pluripotential cell lines', *J. Vet. Med. Sci.*, vol. 57, no. 3, pp. 553–556.
- Vogel, W 1999, 'Discoidin domain receptors: structural relations and functional implications', *Faseb J.*, vol. 13, no. (suppl), pp. S77–S82.
- Young, M *et al.* (eds) 1993, *Molecular and cellular biology of the major noncollagenous protein in bone*, New York, Academic Press.

Ion Beam Elemental Analysis of Doped SiO₂ Optical Fibre and Its Thermoluminescence Response When Irradiated with Protons

A.T. Ramli^{1*}, S. Hashim¹, D.A. Bradley², H. Wagiran¹, M.Webb³ and C. Jaynes³

This research was focused on the thermoluminescence (TL) response of commercially produced single-mode telecommunication optical fibre manufactured by INOCORP (Canada). The fibres were either in the form of pure silica (SiO₂) or as SiO₂ doped with Ge or Al at concentrations appropriate for total internal reflection, as required for telecommunication purposes. Each of these INOCORP fibres had a core diameter of $125 \pm 0.1 \mu\text{m}$. It was noted that dopant concentration was not included among the data provided in the accompanying product data sheet. A particularly important parameter for obtaining the highest TL yield in this study was the dopant concentration of the SiO₂ fibre. The dopants tended to diffuse during the production of the optical fibre. To obtain this parameter, proton induced X-ray emission (PIXE) analysis was utilised. PIXE while having limited depth resolution could unambiguously identify elements and analyse trace elements with a detection limit approaching $\mu\text{g g}^{-1}$. For Al-doped fibres, dopant concentrations in the range of 0.98 – 2.93 mol% had been estimated, the equivalent range for Ge-doped fibres was 0.53 – 0.71 mol%. A linear dose response was observed following 2.5 MeV proton irradiation for Ge- and Al-doped fibres for up to 7 min exposure.

Key words: thermoluminescence; SiO₂ optical fibre; dopant; analysis; proton-induced X-ray emission; Ge; Al; Rutherford backscattering; elemental mapping

Radiation measurements for medical applications need to have a sensitive, robust and high spatial resolution system. The interest of the group was to develop and verify the performance of commercially produced doped SiO₂ optical fibre with the view of improving the thermoluminescence (TL) yield. The measurements were conducted after removing the plastic coating of the optical fibre to allow elemental analysis to be done using proton induced X-ray emission (PIXE) and Rutherford backscattering (RBS), technique on the core of the fibre.

Thermoluminescence has a well-established record as an effective basis for radiation dosimetry, especially in radiotherapy. In recent years, there has been interest in the use of particles such as protons, neutrons and alpha particles as well as heavy-ions and exotic ones such as pi-mesons. In the promising field of charged particle radiotherapy, there is potential for the use of protons for the treatment of tumours near critical structures. However in terms of current radiotherapeutic practice, the use of radiation types other than photons and electrons remain relatively small.

MATERIALS AND METHODS

Sample Preparation

In preparation for irradiation, the outer polymer coating of the optical fibre was removed by using a fibre stripper (Miller, USA) to allow investigation of the TL yield of the fibre core. Following removal of the outer cladding, the optical fibre was cleaned by means of a cotton cloth containing a small amount of methyl alcohol to completely remove any remaining polymer cladding. Subsequently, the fibre was cut into 0.5 cm long pieces using an optical fibre cleaver (Fujikura, Japan). The mass of each fibre, $0.20 \pm 0.02 \text{ mg}$, was measured using an electronic balance (PAG, Switzerland). Vacuum tweezers (Dymax 5, Surrey, UK) were used for handling and grouping of the TL materials.

Before making any irradiations and subsequent TL measurements, the fibres were annealed in an oven in order to standardise their sensitivity and thermal history. This also removed existing TL signals, established common TL sensitivity, and eliminated unstable low-temperature glow

¹Department of Physics, Universiti Teknologi Malaysia, 81310 Skudai, Johor, Malaysia

²Department of Physics, University of Surrey, Guildford, GU2 7XH, U.K.

³Surrey Ion Beam Centre, University of Surrey, Guildford, GU2 7XH, U.K.

*Corresponding author (e-mail: a_hma_d2003@yahoo.co.uk)

peaks. Annealing was performed with the fibres positioned in an oven set at 450°C for the period of 1 h. The fibres were retained in an alumina container during this time. To avoid thermal stress following the annealing cycle, the fibres were left inside the slowly cooling oven for a further 10 h to finally equilibrate at the temperature of 40°C.

Irradiation

The samples were made of either (a) pure SiO₂ or (b) SiO₂ doped with Al or (c) SiO₂ doped with Ge. The fibres were taped across the middle to the sample holders.

Using the microbeam line, 21 samples were irradiated with a 2.5 MeV proton beam. The range of exposure times was between a few seconds and 7 min. The monitored beam current was 40 pA.

For each irradiation, the beam was scanned across both the fibre and the sample holder. It was necessary to do this in order to locate the fibre without irradiating it first, and also to prevent charging. The RBS spectra corresponding only to the region of the fibres was selected, by using OM_DAQ software which utilized the Si map. The integrated area of the RBS spectrum was proportional to the charge delivered to the sample (assuming the samples had the same thickness). In this work, the integrated area was calculated for each fibre. It was proportional to the charge delivered to each fibre. Due to the difficulty in accessing the chamber

in which this work was carried out, the detector's solid angle was not known accurately and therefore an absolute determination of the charge has not been given.

TL Measurements

The optical fibre's TL yield was read out by using a Solaro TL reader (Vinten TLD, Reading, UK). A N₂ atmosphere was used to suppress spurious light signals from triboluminescence and to reduce oxidation of the heating element. During the readout the following parameters were used: preheat temperature of 160°C for 10 s; readout temperature of 300°C for 25 s and heating cycle rate of 25°C s⁻¹. Finally, an annealing temperature of 300°C was applied for 10 s to sweep out any residual signal. The TL yield obtained was then normalized to a unit mass of the particular TL medium.

Elemental Mapping

The University of Surrey hosted the Engineering and Physical Sciences Research Council (EPSRC) national ion beam facility. The microbeam facility was based on a 2.0 MV Tandatron™ accelerator (Figure 1). A review of the facilities offered by the Surrey ion beam centre was covered in detail by Simon *et al.* (2004).

In the present investigation, protons with an energy of 2.5 MeV were used. For the conducted PIXE and RBS

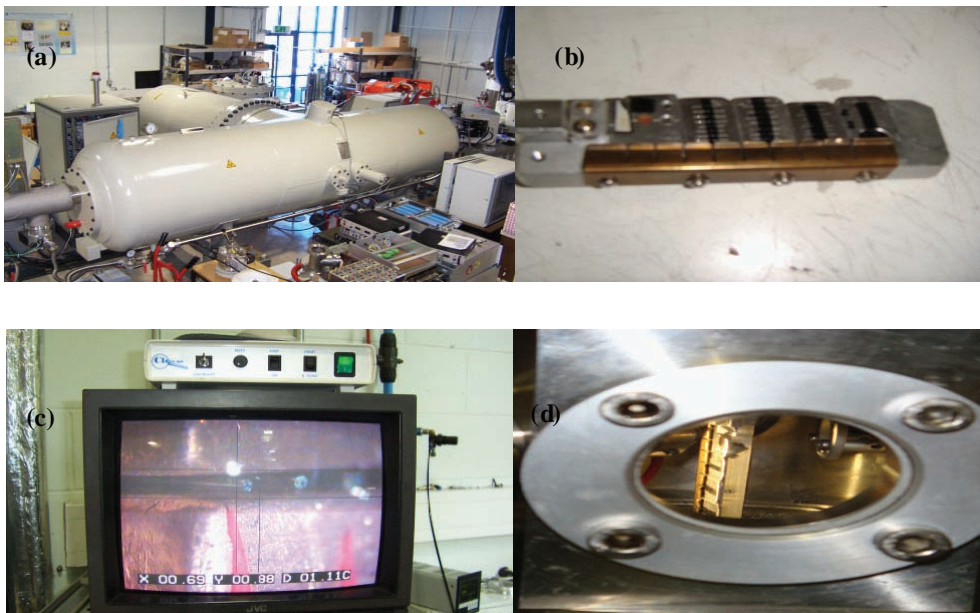


Figure 1. (a) The High Voltage Engineering Europe 2.0 MV Medium Current Plus Tandatron™ accelerator providing 2.5 MeV protons situated in Surrey Ion Beam Centre; (b) Four rows of doped optical fibres attached to an aluminium plate sample holder; (c) Magnified image of fibres on beam line as viewed using a microscope and a monitor display, showing two of the fibres ends on; (d) Samples of the optical fibres aligned to the sample position of the microbeam line, again showing the sample holder seen in (b) above being readied for proton irradiation.

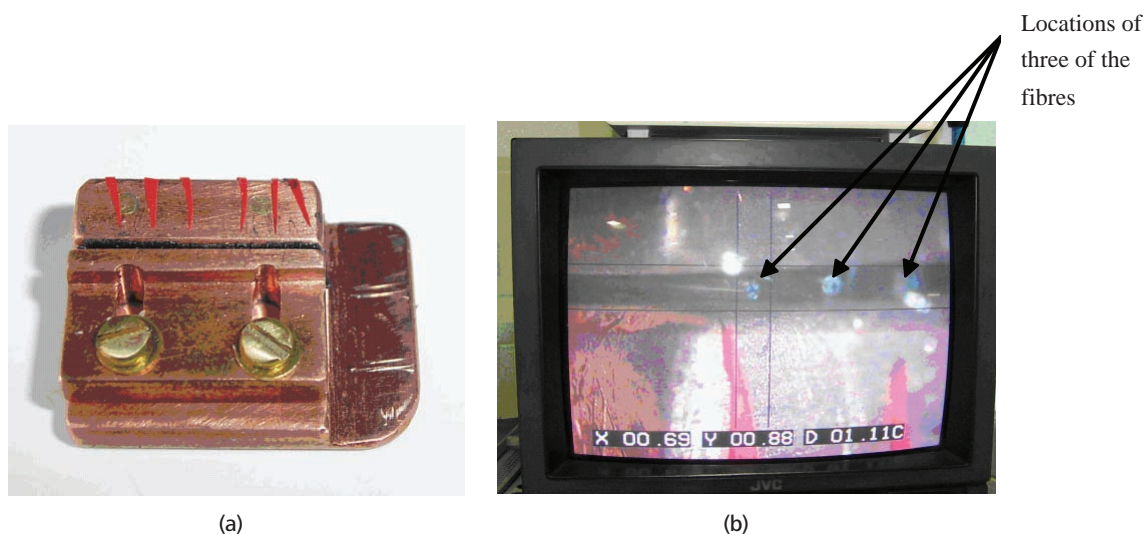


Figure 2. (a) The copper alignment block that acted as a drain for the beam current. It also allowed the use of Cu Rutherford Backscattering Spectrometry as a reference against which O₂ data could be compared. During proton irradiations for PIXE and RBS analysis, the optical fibres were sandwiched in a parallel orientation and held between two custom made copper blocks; (b) Sample positioning was carried out by using a video microscope in combination with an alignment laser to ensure that the sample was reproducibly positioned at the correct distance from the exit window. The sample was illuminated by using a fibre optic illuminator. The sample was mounted on a manual micrometer positioning stage with a total range of movement of 20 cm on each axis. Pointed markers were used for easy viewing and to make sure that the irradiation was performed on the correct fibres.

analysis, the scanning area was chosen to be 0.5×0.5 mm², with a spot size of 3×5 μm² and a beam current of ~ 70 pA. The scanning was done over the freshly cleaved cross-sectional areas of the optical fibre samples, producing a pixel-by-pixel map of the sample elemental composition (Figure 2).

The ion beam facility had two beam lines, a microbeam (in vacuum) line and a millibeam (in air) line, the latter allowed the study of wet samples. On each line, PIXE could be used to analyze a wide range of trace elements. The major advantage of the PIXE method was the possibility of simultaneous multi-elemental analysis, a shorter time for data collection and relatively easier sample preparation. In many cases, PIXE analysis might be considered to be non-destructive.

It is important to note here that the dopant distribution at the core and the inner cladding of a single-mode optical fibre determined the optical transmission properties of the fibre. If the fibre was exposed to high temperature for a period of time during its production, then the dopant distribution in the affected regions could have been altered due to dopant diffusion. Diffusion of germanium in silica optical fibre had been observed during splicing, manufacture of fused fibre coupler and fibre drawing (Lyytikäinen *et al.* 2004).

RESULTS

Determination of Dopant Concentration

Results from this investigation for samples of doped silica glass (with dopant concentrations from 0.01 mol % up to 33 mol %), produced using the sol-gel route were compared against previous studies. It was found from previous study by Yusoff *et al.* (2005), that the highest TL yield for Al and Ge doped fibres was at 4.0 mol% and 0.25 mol%, respectively.

Characteristic X-rays produced during the process of PIXE analysis provided information on the relative distribution of Ge, Al and Si concentrations. For O₂, use was made of RBS spectroscopy. It was noted that a significant proportion of the impinging protons backscattered from the atomic nuclei in the near surface (1 μm to 2 μm) of the sample. The backscattered energy of the proton was related to the mass of the target element from which the ion backscattered. Detection of the characteristic X-rays were obtained through the use of the PIXE detector. The detector was an e2v (e2v Technologies plc, Chelmsford, UK) with a Si(Li) 80 mm² crystal which was 2.7 mm thick, and equipped with a filter against soft X-rays. It had an energy resolution of 130 eV, a solid angle approximately 32 msr mounted at a backscattering angle of 45° to the

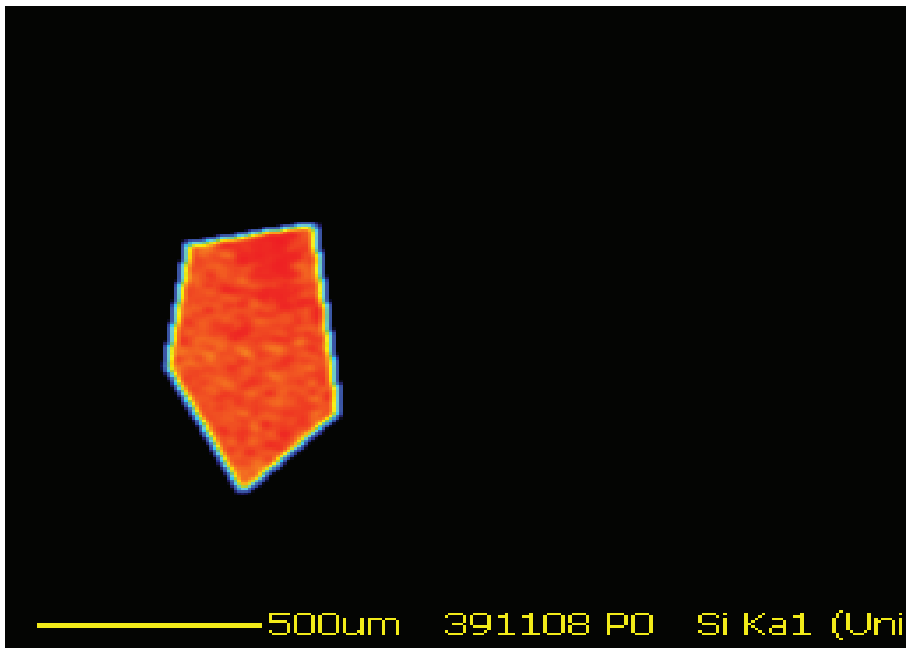


Figure 3. Selected area of the Pb glass sample for calibration of the PIXE and RBS detectors.

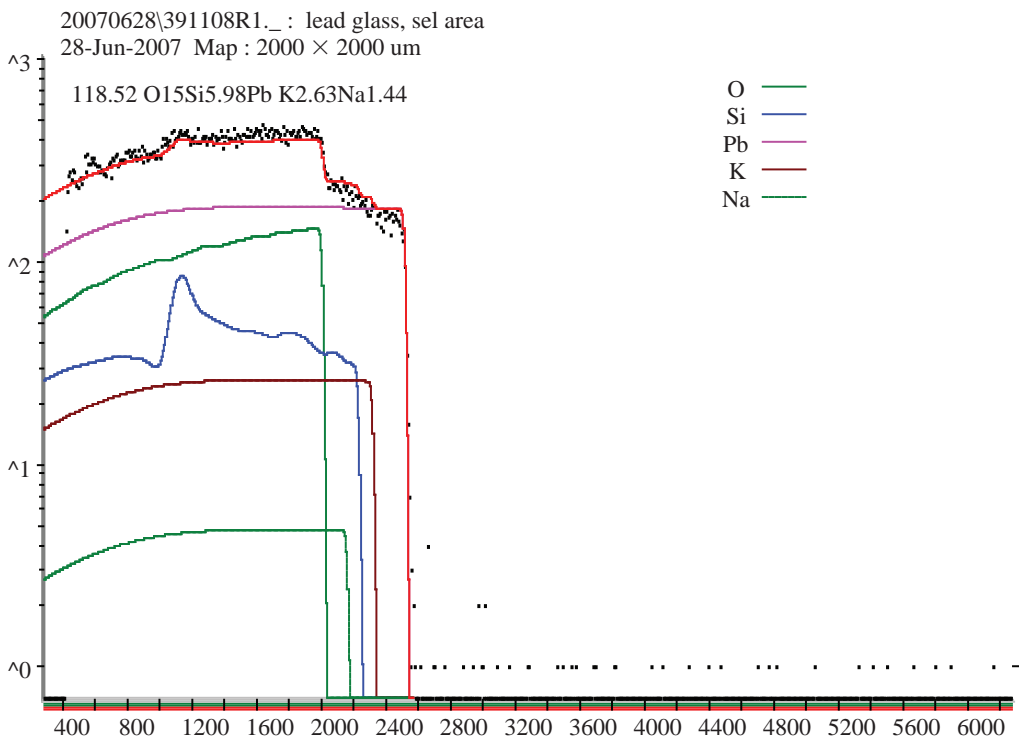


Figure 4. Fitted RBS spectrum for Pb glass calibration sample. The RBS spectrum determines the charge delivered and also the sample thickness. These parameters are used to obtain quantitative results from the PIXE data.



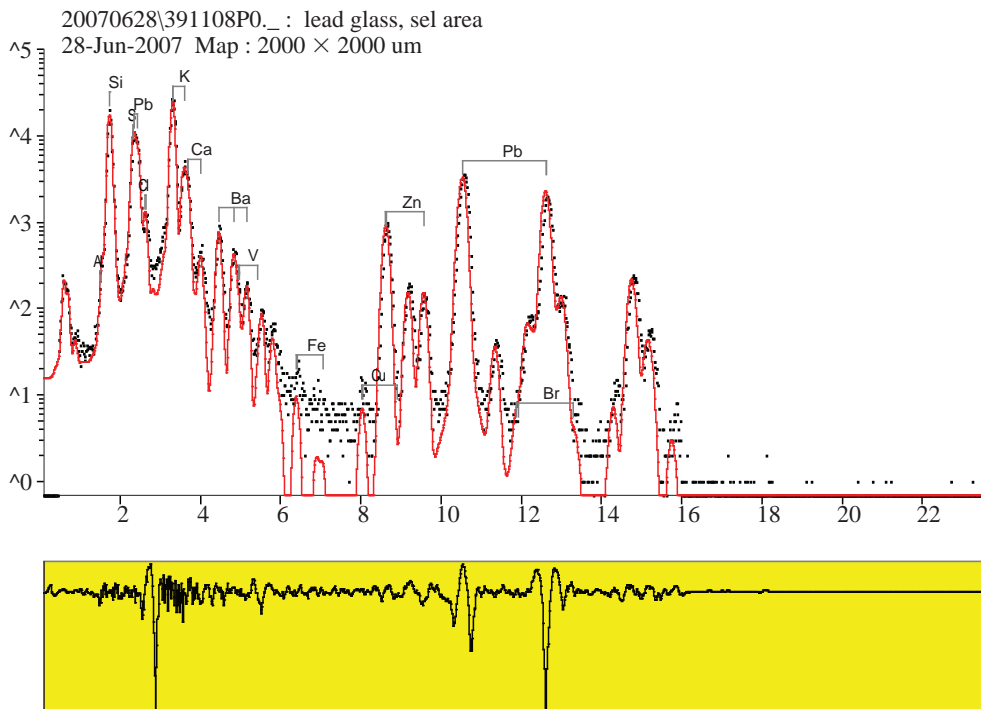


Figure 5. Fitted PIXE spectrum for Pb glass calibration sample. The detector distance has been adjusted, so that the relative quantities of each element in the spectrum match the known relative quantities. This gives the solid angle ratio between the two detectors in order to obtain quantitative information from the rest of the data.

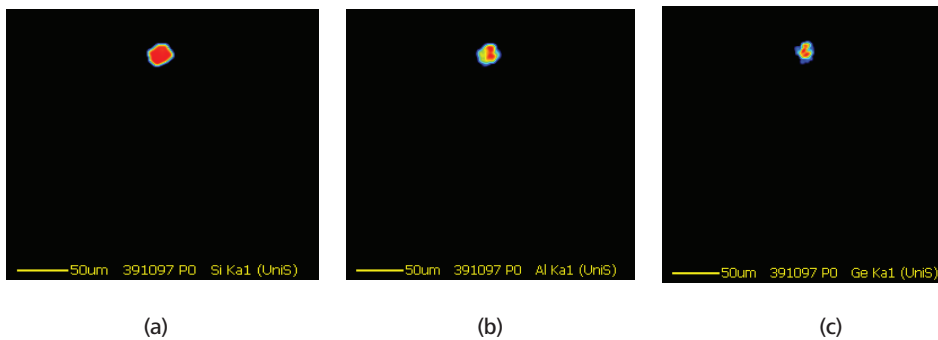


Figure 6. (a) In order to obtain quantitative results from these maps, it is necessary to use OM_DQA software to select the data from an area of interest, which encompass only the fibre; (b) Al dopant mapping; (c) Ge dopant mapping.

beam, a 6 μm Be window and a 130 μm Be filter. This crystal apparently has a 5 μm Si dead layer. For RBS, the backscattered protons were detected through the use of a silicon surface barrier detector, which was positioned at 155° scattering angle (above the beam at an angle of 25° to the beam) and provided an approximately 60 msr solid angle and an energy resolution of 17 keV.

The main uncertainties in the absolute quantification of PIXE elemental concentrations were the total deposited beam charge and the local matrix composition. The use of simultaneous RBS analysis could overcome this problem

by providing the ratio between the true charge and the measured charge (the ‘q factor’). After obtaining the ‘q factor’, the PIXE data could be normalized to provide an accuracy of 5% – 10% in most cases. Details of the acquisition system had been described by Grime and Dawson (1995) and Grime (1996).

In the present study, for Al-doped fibres, dopant concentrations in the range of 0.98 mol% – 2.93 mol% had been estimated, the equivalent range for Ge-doped fibres was 0.53 mol% – 0.71 mol%. PIXE and RBS analysis also detected the presence of other elements, including

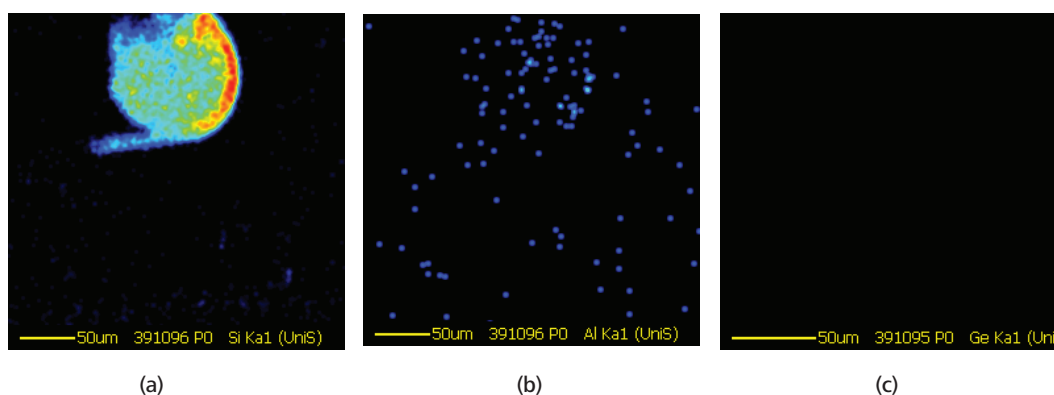


Figure 7. (a) 300 μm map of the cross section of the SiO₂ optical fibre; (b) The presence of Al dopant; (c) No Ge is seen on the map.

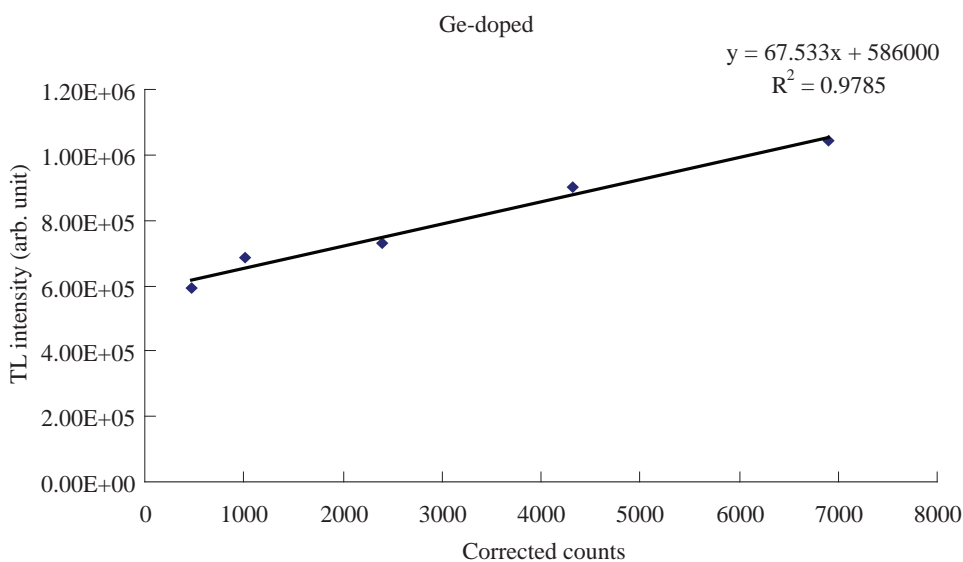


Figure 8. The TL response of Ge-doped fibres exposed to a 2.5 MeV proton beam with different exposure times. The investigation was carried out for 21 samples of optical fibre. Results are expressed in term of corrected counts.

P, Fe, Cl and Cu. However, the concentrations of these elements were relatively very small and could be considered to have negligible effects upon the TL yield of these fibres.

Proton Dose Response

Using the 2.5 MeV proton beam, 21 samples of optical fibre (each of length 0.5 cm) were irradiated for different exposure times. The TL measurements exhibit a linear

relationship with irradiation times of up to 7 min. The proton dose response is shown in Figure 8.

CONCLUSION

Use had been made of PIXE and RBS to map the relative presence of Al, Ge, Si and O. The commercially doped SiO₂ optical fibres showed a linear dose response to the 2.5 MeV proton beam.

Based on this study, it was the intention of this group to proceed with the development of Al and Ge-doped fibre with specific dopant concentrations that would provide the highest TL yield using the ion implantation technique.

ACKNOWLEDGEMENTS

We would like to thank the scientific and technical staff of the Surrey Ion Beam Centre for their help in carrying out elemental analysis and proton irradiations. This work was partially supported by the Academy of Sciences Malaysia and the Ministry of Higher Education Malaysia who provided research grants, and the Universiti Teknologi Malaysia who supported a research studentship.

Date of submission: September 2008

Date of acceptance: December 2009

REFERENCES

- Grime, GW & Dawson, M 1995, 'Recent developments in data acquisition and processing on the Oxford scanning proton microprobe', *Nuclear Instruments and Methods in Physics Research B*, vol. 104, pp. 107–113.
- Grime, GW 1996, 'The "Q factor" method: quantitative microPIXE analysis using RBS normalization', *Nuclear Instruments and Methods in Physics Research B.*, vol. 109/110, pp. 170–174.
- Lyytikäinen, K *et al.* 2004. 'Dopant diffusion during optical fibre drawing', *Optics Express*, vol. 12, pp. 972–977.
- Simon, A *et al.* 2004, 'The new Surrey ion beam analysis facility', *Nuclear Instruments and Methods in Physics Research B*, 219–220, 405–409.
- Yusoff, AL, Hugtenburg, RP & Bradley, DA 2005, 'Review of development of a silica-based thermoluminescence dosimeter', *Rad. Phys. Chem.*, vol. 74, pp. 459–481.

Data Cognitive Complexity: A New Measure

J.K. Chhabra^{1*}, R.S. Bhatia¹ and V.P. Singh¹

Every software has different dimensions of complexity. Some of these dimensions have attracted much attention from researchers and thus good progress has been reported in measuring aspects like control flow, data/information and operators/operands. On the other hand, the cognitive aspect of the complexity has not been explored much, although it has a strong influence on comprehension and maintenance of the software. The cognitive complexity measurement needs to take into consideration the working of the human memory and it's mind. Spatial distance is directly based on human memory's working and cognitive weights clearly indicate the human mind's involvement in understanding the control structures. This paper proposed a new measure of cognitive complexity based on both of these viewpoints. The proposed measure was an indicator of the cognitive efforts needed to realize the role of data members in the working of the software and it was also able to capture the different comprehension capabilities of different languages which the earlier existing measures had failed to do.

Key words: data spatial complexity; understandability; psychological complexity; cognitive weights; software metrics

The importance of measuring software complexity has been widely published and well accepted. There are different dimensions of software complexity. McCabe's cyclomatic complexity concentrated on control flow complexity (McCabe 1976) and Halstead's science measures were largely based on the size of the software (Halstead 1977). Similarly concept of live members and program weakness was used to measure design complexity (Conte *et al.* 1986; Aggarwal *et al.* 2002). Software complexity based on entropy was proposed by Harrison (1992) and Woodward *et al.* (1979) concentrated on program text's complexity. Cognitive complexity is another important aspect of complexity of software, but has gained relatively lesser attention from researchers.

In order to measure human efforts needed in comprehending software, the concept of cognitive complexity was initiated (Douce *et al.* 1999), where the concept of spatial complexity was also introduced which was based on the theory of working memory and was reported to affect understandability of the source code (Baddeley 1997). Spatial ability is a term that is used to refer to an individual's cognitive abilities relating to orientation, the location of objects in space, and the processing of location related visual information. Spatial ability has been correlated with the selection of problem solving strategy, and has played an important role in the formulation of an influential model of working memory (Douce *et al.* 1999). Program comprehension and software maintenance are considered to substantially use the programmers' spatial abilities and

the proper understanding of source code helps in effective debugging and maintenance of the software. This concept of spatial ability was further extended and strengthened by Shao and Wang (2003) in the form of code and data spatial complexity, and both of these measures were found to be strongly correlated with perfective maintenance activities (Chhabra *et al.* 2003).

Another measure of cognitive complexity was proposed by Shao and Wang as code functional size (CFS) in terms of cognitive weights (Shao & Wang 2003). This measure was based on the internal structure of the source code and assigned different weights to basic control structures (BCS) depending on their psychological complexity. This idea was further extended by also incorporating the effect of operators and operands (Mishra 2006a). Both of these proposed metrics were based on architectural aspect of genitive informatics.

Thus, two different dimensions of cognitive complexity have been identified by various researchers: spatial complexity and cognitive-weight-based complexity. Each of these two metrics is measuring a different cognitive aspect of the software. Spatial complexity is based on the theory of working memory and cognitive weights are based on the architectural structure of the source code. Spatial complexity treats all types of statements equally whether calls were sequential, iterative or recursive which is not acceptable from a cognitive viewpoint (Gold & Layzell 2005). Similarly cognitive weights do not consider at all

¹ Department of Computer Engineering, National Institute of Technology, Kurukshetra-136119 INDIA

*Corresponding author (e-mail: jitenderchhabra@rediffmail.com)

the individual's spatial abilities of orientation, location and processing of objects in the working memory. So none of these two metric is alone sufficient to measure the cognitive complexity in totality. Obviously it is desirable to have a new metric of cognitive complexity which should reflect spatial as well architectural complexity of the source code. This paper proposes a new metric named as data cognitive complexity (DCC) which combines both of these aspects into a single measure and thus is able to reveal both aspects of cognitive complexity.

Data Cognitive Complexity

The concept of the data spatial complexity (DSC) was introduced for the first time in the literature by Chhabra *et al.* (2003). This type of cognitive complexity was based on the spatial distance between the definition and use of various data members. The functionality of the software could be easily understood, if the programmer was able to comprehend the input and output. The processing was applied to input, and after many intermediate values, the final output gets generated. So in order to understand the full functionality of the software, all input, intermediate, and output values should be recognized. These values are represented through variables and constants in the software. So cognitive efforts needed to understand the software also depended on the variables and constants. Gold *et al.* pointed out that understanding the use of data also requires knowledge of control flow in which the data has been used (Gold & Layzell 2005). Hence the type of control structure in which the data members were used, should also be considered to measure comprehension. If a data member was used in a simple assignment statement, understanding its purpose was much easier than if it was used as a parameter in a recursive call.

Many researchers have already stressed the importance of considering the kind of control structure while computing the cognitive complexity (Shao & Wang 2003; Gold & Layzell 2003; Mishra 2006b). This architectural aspect of the complexity of the software could be easily reflected in cognitive complexity with help of weights of various types

of BCS. Shao and Wang (2003) identified the following cognitive weights for various control structures (Table 1).

The measures of cognitive complexity defined in Shao and Wang (2003); Mishra (2006a) and Mishra (2006b) considered only these weights which were reflection of architectural viewpoint and did not look into the spatial aspect at all. On the other hand, the importance of spatial distance towards cognitive complexity is well established and reported (Conte *et al.* 1986; Chhabra *et al.* 2003, Chhabra *et al.* 2004). Thus it is very pertinent to combine the impact of architectural as well as spatial aspects of the software to compute the cognitive complexity.

This paper proposes a new measure named as DCC which not only considers the spatial aspect, but also takes into consideration the architectural aspect of the software. To the best knowledge of the authors, no such attempt had been made in the literature to date to measure cognitive complexity based on both of these aspects. All of the previous work in the direction of cognitive complexity concentrated on only one of these two affecting parameters, either spatial complexity or architectural complexity. This paper was the first attempt towards covering both of these aspects and combining them so as to indicate a better cognitive complexity of the software. The weights of the BCS were combined along with the spatial distance between the definition and use of data members. All of the data members were used to store some input/output value or some intermediate values, which got processed many times to generate some final results. As the processing was carried out through various BCS, the purpose of a data member could be understood by tracking the different changes taking place on that member via various control statements. The type of control statement also influenced the comprehension of the change in a data member. For example, the changes to a data member inside iteration were obviously greater as compared to a simple sequential statement and thus more cognitive efforts were needed to understand the changes inside the iteration. Thus the cognitive weights of various types of BCS could be used to reflect that aspect in the complexity.

Table 1. Cognitive weights of various basic control structures.

Category	BCS	Weight
Sequence	Sequence	1
	Branch	2
Iteration	if then else	2
	case	3
	for – do	3
Embedded component	repeat – until	3
	while – do	3
	Function call	2
Concurrency	Recursion	3
	Parallel	4
	Interrupt	4

Every data member went through many transformations and at many times the current use of a data member was dependent on a previous change/use of the value of that member. Hence the spatial distance between two successive usages of a data member also affected the cognitive complexity. The data definition was hardly sufficient to understand the purpose of a data member. The purpose could be comprehended by observing the successive uses of that data member. The first use of a data member might depend on initialization (along with the definition), but its subsequent use was more correlated with its previous use. So the data cognitive complexity of any data member needed to be measured using the distance between its two successive uses. The greater the distance (in terms of lines of code) between the successive uses of the data members, the greater the cognitive effort required to understand the purpose of that data member. If a data member was successively used at very small intervals, the details about that data member remained in the working memory of the programmer, and thus he would be able to comprehend the use of that data member easily. On the other hand, if a data member was used after for instance 500 lines of its previous use, the programmer was very likely to have forgotten the details of that data member, and it would definitely take more effort to establish a connection between the current use of the data member and its previous use (Chhabra *et al.* 2003). The concept of the average span of a variable also endorsed the fact that the variable's use in a short span was an indication of lesser complexity (Conte *et al.* 1986; Aggarwal *et al.* 2002; Singh & Bhatia 1998).

We defined a new term Variable's Cognitive Complexity (VCC) of a data member (usually data members are stored as variables, hence the nomenclature) at particular use as:

$$VCC(dm, k) = W_k * distance(dm, k) \quad \dots 1$$

where, *dm* represents name of the data member and *k* represents line number of the use of that data member. *W_k* represents the cognitive weight of the BCS (Table 1), in which data member *dm* is used at line number *k*. The distance (*dm, k*) represents the absolute difference (in terms of lines of code) of the member *dm* between line number *k* and the line number of its previous use. If there was no previous use of the data member under consideration, then the distance was computed from the definition of that data member. If the data member was defined and used in the same source-code file, the distance could be calculated as above. At many times, software is written using multiple source-code files, then a data member may be defined in one file and used in some other file (e.g. external variables). In that case, the above definition of the distance would be incomplete. In that case, the distance was defined as follows:

$$\begin{aligned} \text{Distance} &= (\text{Distance of first use of the data member} \\ &\text{from top of current file}) \\ &+ (\text{Distance of definition of the data member from} \\ &\text{top of file containing definition}) \\ &+ (0.1 * (\text{total lines of code of remaining files}) / 2) \dots 2 \end{aligned}$$

The definition was based on the grounds explained by Chhabra *et al.* (2004) that in 90% of the cases, the programmer had an idea of the other file where the data member under consideration had been defined/used. For the remaining 10% of the cases, the programmer had to look into all of the remaining files. For those cases, we have taken the average distance of the remaining files and that had been multiplied by the worst-case probability i.e. 0.1, corresponding to the remaining 10 percent of cases.

Almost every member went through many processing changes to reach to a final value, hence the member's working could be understood by going through its changes through various control structures. Hence we define average variable's cognitive complexity (AVCC) of a data member as shown in Equation 3 below as an average of VCC values (as defined in Equation 1) of all uses of that member.

$$AVCC(dm) = \frac{\sum_{j=1}^p VCC(dm, k_j)}{p} \quad \dots 3$$

where *p* represented the count of uses of that data member and *k_j* represented the line number in which the *jth* use of the data member *dm* had been done.

Total DCC of the software was computed by averaging the AVCC (of Equation 3) of all data members:

$$\begin{aligned} DCC &= \frac{\sum_{i=1}^q AVCC(dm_i)}{q} \\ &= \frac{\sum_{i=1}^q \left(\frac{\sum_{j=1}^p AVCC(var_i, k_j)}{p} \right)}{q} \quad \dots 4 \end{aligned}$$

where *q* was the count of the data members in the software.

COMPUTATION OF DCC

In order to demonstrate the working of this metric, we took a program to compute the average length of several lines of text (Gottfried 2005).

```

1  #include<stdio.h>
2  int sum =0;
3  int lines = 0;
4  int linecount(void);
5  main()
6  {
7      int n;
8      float avg;
9      printf("Enter the text below");
10     while(( n = linecount()) > 0 ) {
11         sum += n;
12         ++lines;
13     }
14     avg = (float) sum / lines ;
15     printf("\nAverage number of characters per
        line: %5.2f", avg);
16 }
17 int linecount ( void )
18 {
19     char line [80] ;
20     int count = 0 ;
21     while (( line [count] = getchar() ) != '\n')
22         ++ count ;
23     return ( count );
24 }

```

This program used six variables namely sum, lines, n, avg, line and count. The value of AVCC was computed for each of these variables. For example, in order to compute the AVCC of n, we needed to go through all uses of variable n. Variable n was defined in line number 7 and its first use was at line number 10. Line number 10 was a while loop and had a cognitive weight W_k of 3, as per Table 1. Thus as per definition of VCC in Equation 1,

$$VCC(n, 10) = 3 * (10 - 7) = 3 * 3 = 9$$

Then, the next use of n was at line number 11, which was a sequential statement. Thus the weight W_k would be 1 and it's previous use was at line number 10. Hence

$$VCC(n, 11) = 1 * (11 - 10) = 1$$

As there was no other use of the variable n, the AVCC could be computed as per Equation 3:

$$AVCC(n) = (9 + 1) / 2 = 5.0$$

Similarly AVCC could be computed for each of the variables using Equation 3 and DCC could be computed as per Equation 4 by averaging AVCC of these six variables. The computed values are shown in Table 2.

COMPARISON OF DCC WITH DSC AND CFS

The CFS measure proposed by Shao and Wang (2003) had been computed by the authors (Wang & Shao 2003)

over three different language implementations for the same problem- in-between sum (IBS), in which they had reported that cognitive complexity was the same for the three languages. These results are contradictory to the earlier studies of many researchers where all of them had clearly mentioned that different languages had different levels and the language level had been reported to affect cognitive efforts of understanding (Halstead 1977; Singh 1995; Shen *et al.* 1983). Implementation in different languages of one algorithm could have same algorithmic complexity, but not cognitive complexity. The human comprehension level of the algorithm was definitely dependent on the type of language as well as the source code. Otherwise understanding the efforts of a complex program (e.g. linked list reversal) should be same for assembly language and Java, but obviously it was not so. Thus the cognitive efforts should not get measured as the same for different languages. Hence the CFS measure could not be accepted as a good cognitive measure, as it was not able to measure the language's effect on human mind's understandability. The CFS measure did not differentiate between cognitive complexity of the three different implementations in Pascal, C and Java language. Wang and Shao had shown these results to demonstrate the robustness of their metric (Wang & Shao 2003), but it was unacceptable to get the same value of comprehension capability for different languages. Hence the robustness concept was not applicable to the measurement of the cognitive aspect of complexity, although it might be acceptable from algorithmic complexity viewpoint. Thus the CFS measure needed to be modified. Similarly the DSC measure was also not appropriate for these three programs, due to lack of sufficient global data. Although DSC discriminated between different languages, it did not consider local members. The three implementations (Wang & Shao 2003), given in the three programs, were using some local members, each contributing significantly towards processing, and hence DSC was not able to compute any value for two of those implementations. The proposed DCC measure clearly reported different values for these three programs. Thus DCC was more suitable than both of the earlier proposed measures of cognitive complexity. Table 3 gives a comparison of these three metrics for all of the three implementations, shown in Figures 5, 6 and 7 of (Wang & Shao 2003, p. 72 & 73).

Table 2. AVCC Values for different variables.

Member	AVCC
sum	6.0
lines	5.5
n	5.0
avg	3.5
line	6.0
count	2.0
DCC	4.67

Table 3 clearly shows that CFS was the same for all three programs, DSC was zero for the first and third programs, as both had no global variables. On the other hand, the DCC value differed significantly for the three programs. The comparison would be clearly visible from the following graph.

Table 3. Comparison of three metrics.

	DCC	CFS	DSC
Program 1 (Figure 5)	8.88	9	0
Program 2 (Figure 6)	4.75	9	2.25
Program 3 (Figure 7)	6.2	9	0

From Figure 1, it could be easily noticed that the newly proposed metric was able to differentiate between the cognitive complexities of the three programs having different comprehension capabilities, which the other two metrics were not able to distinguish.

Another weakness of CFS was that it did not give any weightage to global/local intermediate variables used in the program. The proposed definition of CFS (Shao & Wang 2003, p. 1333) is :

$$CFS = (N_i + N_o) * W_c \quad \dots 5$$

where, N_i represents number of input, N_o represents number of output, and W_c is total weighted cognitive complexity of all BCS. The CFS computation was only dependent on the numbers of input and output. There was no impact of any other global, local, intermediate variable on its value. The

complexity of the code portion of the program would get some contribution through use of W_c , but the data part of the program got neglected, except for the input and output count. It had already been stressed (Chhabra *et al.* 2003, 2004) that data was also an integral part of the program's working and must be given its due importance especially while computing the cognitive complexity. The CFS metric was unaffected by the presence/absence of various data members. The value of DCC computed in Table 2 took into consideration the impact of all variables such as sum, count, lines, avg etc. but the CFS for that program would take into consideration only the n and line variables. Thus, DCC was a better reflector of the program's cognitive complexity than CFS. Moreover, the values of N_i and N_o used in computation of CFS were execution and interpretation dependent. For example, if we tried to compute the value of CFS for the program used in the section Computation of DCC, the value of N_i was dependent on the users' input given at the time of execution. A user might enter 30 lines each consisting of 50 letters during the first execution. In that case, should N_i be treated as 30 or $30 * 50 = 1500$? The paper (Shao & Wang 2003) was silent about this aspect. Even if it was assumed that each line would be treated as one input to count N_i , it became execution dependent. For example in the second execution of the program of the section Computation of DCC, if the user gave 3 lines as input, N_i changed to 3. The value of CFS as per Equation 5 for the first execution would be:

$$CFS = (30+1)*(3+3) = 186$$

For the second execution of the same program,

$$CFS = (3+1)*(3+3) = 24$$

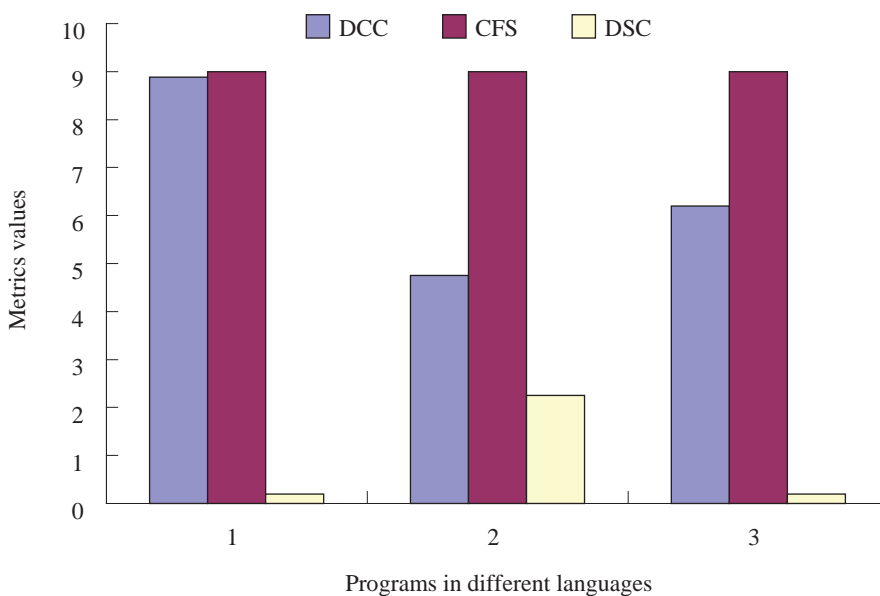


Figure 1. Comparison of three metrics for programs in different languages.

The value of CFS for the first execution was almost 8 times the second value. Now that behaviour of the CFS metric was quite unacceptable. The comprehension indicator (the purpose of cognitive complexity was to reflect comprehension) of the same program changed drastically depending on how much input were given dynamically, but it did not get affected by any number of global variables and intermediate results.

In order to display the inappropriateness of the CFS measure, let us consider two programs written for the following two situations:

P1: Read a number and print double of that number.

This program had one input and one output, and used Sequence only as BCS. So:

$$\text{CFS (P1)} = (1+1)*1=2$$

P2: Take input of an angle in degrees. Print the output y as:

$$y = \frac{\sin^{-1} [\cos(x) + \tan(x)]}{\tan^{-1} [\sin(x*2.5) - \cos(x/1.3)]}$$

where x is radian equivalent of the angle given.

Just as in case of P1, the program P2 also had one input and one output and the program could be implemented using sequence BCS (many sequential statements could be used one by one to compute intermediate values and then finally output y would get computed through another sequential statement). Note that functions such as \cos , \sin , \sin^{-1} could be always computed without any loop (many languages provided such functions directly to compute those values, otherwise those values could be approximated by using the initial 3–4 terms of their series formula). CFS for the program would be:

$$\text{CFS (P2)} = (1+1)*1=2$$

The CFS value for P1 as well as P2 came out to be same, although the difference of the complexity of the two programs was clearly evident. Now if we consider computation of the DCC metric for the two programs, the two values would differ significantly. The first program would not have any temporary or intermediate variables and program would be of 2–3 lines. So the DCC value for P1 would be quite small but the value of DCC for P2 would be much larger. The source code of program P2 would consist of many lines and would use many intermediate values. The increased number of lines would increase the spatial distance for many variables and the impact of all the intermediate values would also get considered in computing

DCC. So the DCC value of P2 would differ significantly from P1, although CFS did not. Hence DCC was clearly able to capture the cognitive complexity of programs in a much better way than CFS.

From the above discussions, it was clearly evident that the CFS measure took care of various control structures, but it was extremely poor in measuring the complexity of data members. Similarly, the DSC measure did not differentiate between various control structures at all, although the complexity of the nested ‘while’ loops was of much more than two sequential statements. The DCC metric was the one which removed the limitations of both the CFS and DSC measures. The DCC measure took into account the type of control structures, their impact on various data members as well as all the transformation steps involved in converting input to output, and thus was guaranteed to perform better than CFS and DSC.

FUTURE WORKS

The conceptual formulation of the proposed DCC measure was based on using the spatial as well as the architectural complexity of the software to compute cognitive efforts, and thus was expected to be better than any single measure. However, a more detailed empirical study was needed over software of varied sizes and its comparison with other cognitive measures is needed to be done, to judge its suitability.

CONCLUSION

This paper has proposed a new measure of cognitive complexity named as DCC, which was based on the combined effect of spatial complexity and cognitive weight of control structures. The theory of working on human memory towards the orientation and processing of data had been used to measure the spatial complexity of the data members and the contribution of architectural complexity towards cognitive efforts was computed by using the weight of various control structures processing the data members. While defining the metric, the possibility of developing software using multiple source code files had also been taken into consideration. The proposed measure had been shown to clearly capture the comprehension difference of the different languages and hence the measure was expected to be a good indicator of the cognitive efforts needed to understand the working of the software, and thus could become a useful tool for estimating the maintenance efforts of the software.

Date of submission: February 2009

Date of acceptance: December 2009

REFERENCES

- McCabe TJ 1976, 'A complexity Measure', in *IEEE Transactions on Software Engineering*, vol. SE-2, no. 4, pp. 308-319.
- Halstead MH 1977, *Elements of software science*, North Holland, New York.
- Conte SD, Dunsmore HE & Shen VY 1986, *Software engineering metrics and models*, Cummings Pub. Coi. Inc. USA.
- Aggarwal KK, Singh Y & Chhabra JK 2002, 'Computing program weakness using module coupling', *ACM SIGSOFT*, vol 27, no. 1, pp. 63-66.
- Harrison W 1992, 'An entropy based measure of software complexity', *IEEE Transactions on Software Engineering*, vol. 18, no. 11, pp. 1025-29.
- Woodward MR, Hennel MA & David A 1979, 'Measure of control flow complexity in program text', *IEEE Transactions on Software Engineering*, vol. SE-5, no. 1, pp. 45-50.
- Douce CR, Layzell PJ & Buckley J 1999, *Spatial measures of software complexity*, Technical Report, Information Technology Research Institute, University of Brighton, UK.
- Baddeley A 1997, *Human memory:theory and practice*, Revised Edition, Hove Psychology Press.
- Chhabra JK, Aggarwal KK & Singh Y 2003, Code and data spatial complexity: two important software understandability measures, *Information and Software Technology*, vol. 45, no. 8, pp. 539-546.
- Shao J & Wang J 2003, 'A new measure of software complexity based on cognitive weights', *Canadian Journal of Electrical & Computer Engineering*, vol. 28, no. 2, pp. 69-74.
- Mishra S 2006a, Modified cognitive complexity measure, in *Proceedings of 21st ISICIS'06 Lecture Notes in Computer Science*, 4263, pp.1050-59.
- Gold NE & Layzell PJ 2005, 'Spatial complexity metrics: an investigation of utility', *IEEE Transactions on Software Engineering*, vol. 3, no. 1, pp. 203-212.
- Mishra S 2006b, 'A Complexity measure based on cognitive weights', *International Journal of Theoretical and Applied Computer Science*, vol. 1, no. 1, pp. 1-10.
- Chhabra JK, Aggarwal KK & Singh Y 2004, 'Measurement of object oriented software spatial complexity', *Information and Software Technology*, vol. 46, no. 10, pp. 689-99.
- Singh Y & Bhatia P 1998, 'Module weakness: a new measure', *ACM SIGSOFT*, vol. 23, no. 5, pp. 81-82.
- Gottfried BS 2005, *Programming with C*, 2nd Edition, McGraw Hill.
- Wang Y & Shao J 2003, 'Measurement of the cognitive functional complexity of software', in *Proceedings of IEEE International Conference on Cognitive Informatics, ICCI'03*, 2003, pp. 67-74.
- Singh Y 1995, 'Metrics and design techniques for reliable software', PhD Thesis, Kurukshetra University, Kurukshetra.
- Shen VY, Conte SD & Dunsmore HE 1983, 'Software science revisited: a critical analysis of the theory and its empirical support', *IEEE Transactions on Software Engineering*, vol. SE-9, no. 2, pp. 155-165.

Methane Adsorption Characteristics of Copper Oxide Modified NaY Zeolite Adsorbents

K.S.N. Kamarudin^{1*}, Y.Y. Chieng¹, H. Hamdan² and H. Mat¹

Ordered microporous NaY zeolite and mesoporous copper oxide are high performance material as catalysts and adsorbents. The copper oxide-NaY zeolite modification in combination of their physicochemical properties could provide excellent opportunities for the creation of new gas adsorbents. In this study, modified NaY zeolite properties and methane adsorptive characteristics were investigated by dispersing copper oxide onto the NaY zeolite structure using the thermal dispersion method. The structures of the copper oxide modified zeolites were characterized by powder X-ray diffraction and Micromeritics ASAP 2000, while the methane adsorption characteristics were analyzed using a thermogravimetric analyzer. The results revealed that types of copper oxide, copper oxide loading concentration, calcination temperature and calcination time greatly affected the modified zeolite structure and gas methane adsorption characteristics.

Key words: NaY zeolite; modification; copper oxide; gas; thermal dispersion; methane adsorption; calcination temperature

In the last two decades, natural gas recovery using zeolite adsorbent for the separation of nitrogen and carbon dioxide from methane was becoming increasingly important (Chao 1990; Jayaraman *et al.* 2004; Cavenati *et al.* 2006; Delgado *et al.* 2007). The potential use of zeolite material for high energy density gas storage technology also requires such an adsorbent to have a high capacity and selectivity for methane (Nishimaya *et al.* 2001; Njikamp *et al.* 2001; Maurin *et al.* 2006; Ramirez-Cuesta & Mitchell, 2007). Among more than 150 types of synthetic zeolites, NaY zeolite with high surface area and regular cavity properties is an important material as catalyst for petrochemical application as well as a promising adsorbent to be employed in the gas adsorption and separation processes (Hasegawa *et al.* 2001; Mizukami *et al.* 2001; Harlick & Tezel 2004; Sultana *et al.* 2004; Salavati-Niasari 2008). In order to modify zeolite physicochemical properties to suit for a particular application, different types of metal oxide were used by dispersing them on the surface of zeolite (Alyea & Bhat 1995; Khouchaf *et al.* 1998; Dutta & Vaidyalingam 2003).

Metal oxide is an inorganic material having a unique structure which when dispersed on zeolite surfaces exhibits physicochemical properties that differ significantly from their bulk counterpart (Abdel-Fattah *et al.* 1997; Thoret *et al.* 1997; El-Shobaky *et al.* 1999; Ramirez-Cuesta & Mitchell 2007). In recent years, many applications for copper oxide in the field catalysis have been identified

(Delahay *et al.* 1998; Díaz & Lazo 2000; Turkey *et al.* 2001; Liu *et al.* 2004; Mediavilla *et al.* 2008). The bulk copper oxide also revealed attractive magnetic properties in nanoparticle technology as semiconductor, fuel cell, high temperature superconductor and sensor material (Ito *et al.* 1998; Chang *et al.* 2003; Cruccolini *et al.* 2004). In gas adsorption process, copper species or copper oxide compound has been dispersed on various types of porous support such as zeolite and mesoporous M41 materials for gaseous NO, CO, and N₂ adsorption (Szanyi & Paffett 1996; Sárkány 1997; Bordiga *et al.* 2001; Hadjiivanov *et al.* 2003). The surface area and stability of copper-based adsorbent has been improved. The addition of CuO and CuCl on dealuminated zeolite Y and activated carbon supported CuO also showed enhancement in the gas SO₂ adsorption capacity for industrial gas separation process (Deng & Lin 1997; Tseng & Wey 2004). The modified systems were generally exhibiting better adsorptive properties as compared to the host or the guest component itself. Moreover, highly efficient CuCl modified zeolite adsorbent prepared by thermal dispersion method that shows high selectivity for CO and ethylene has been widely commercialized (Xie *et al.* 1990).

Nevertheless, there is scarce literature available dealing with the methane adsorption characteristics of CuO modified NaY zeolite adsorbent. The influence of copper oxide on NaY physicochemical properties and methane adsorptive characteristics are still less understood.

¹ Faculty of Chemical and Natural Resources Engineering, Universiti Teknologi Malaysia, 81310 UTM Skudai, Johor, Malaysia

² Faculty of Science, Universiti Teknologi Malaysia, 81310 UTM Skudai, Johor, Malaysia

*Corresponding author (e-mail: sozana@fkkksa.utm.my)

Furthermore, the effects of experimental parameters on the gas adsorption properties are not straightforward. Consequently, this study was carried out to investigate the effects of experimental conditions on structural properties of copper oxide modified NaY and its relationship to CH₄ adsorption characteristics. The proper understanding of the corresponding conditions of modification would facilitate the development of novel methane adsorbents for specific applications.

EXPERIMENTAL

Copper oxide modified NaY zeolite adsorbents were prepared by the spontaneous thermal dispersion method. 2 g of NaY zeolite (CBV 100, Zeolyst Intl.) were mixed with powdered copper oxide (Merck), at a predetermined ratio corresponding up to 5 parts of copper oxide per unit cell NaY (290 μmol/g adsorbent). The resulting mixture was sieved to a particle size of 300 μm and calcined at elevated temperature with the heating rate of 10 K/min to 873.15 K for 24 h. The structural properties of copper oxide modified NaY zeolite were characterized by powder X-ray diffraction (XRD) with CuKα radiation ($\lambda = 1.5418 \text{ \AA}$) and 40 kV and 40 mA in the range of $2\theta = 2^\circ - 50^\circ$ at a scanning speed of 0.05 per second. Physical properties such as pore diameter, pore volume and micropore surface area were determined by nitrogen adsorption method using Micromeritics ASAP 2000 at 77 K.

Adsorption capacity of the modified adsorbents were measured using a Perkin-Elmer thermogravimetrics analyzer (TGA). In the adsorption process, the modified adsorbent was placed in a small sample cell, heated up to 673.15 K at a heating rate of 50°C/min and held at that temperature until there was no weight loss. Then, the temperature was lowered to 323.15 K and held at that temperature until the adsorption reached equilibrium. The weight change of the adsorbent was used to determine the adsorption performance of the materials.

RESULTS AND DISCUSSION

Effect of Copper Oxide Types

The first and second laws of thermodynamics could be used to explain that the dispersion of copper oxide into or onto the surfaces of zeolite was a spontaneous process that would gain in entropy. This was due to the fact that spontaneous dispersion was the decrease of free enthalpy of the whole system. Owing to that, the dispersion resulted in significant increase in entropy and formation of surface bonds comparable to the original bonds of the compounds. For a compound with not so high a melting point, its dispersion to a zeolite could be done by heating it at a suitable temperature well below its melting point (Xie &

Tang 1990). The dispersion could be verified by XRD, XPS, or EXAFS.

According to *ASTM D3906*, the crystallinity of samples which was denoted as relative intensity (I_{rel}) was determined by comparing the sum of the six reflection peaks ($\{331\}$, $\{511\}$, $\{440\}$, $\{533\}$, $\{642\}$, and $\{555\}$) of the treated samples with that of the NaY zeolite that taken as a reference (i.e. 100% crystalline at ambient temperature). The XRD spectrum (Figure 1) showed that the relative intensities of the modified NaY decreased, but unit cell parameter increased as compared to unloaded commercial NaY (Table 1). It was due to the contact between the NaY framework and the oxide particles within the pore of zeolite (Huang *et al.* 2004). The result also showed that the dispersion of copper oxide onto NaY zeolite slightly diminished the total surface area. The pore volume had been affected but the pore size almost remained constant, while the external surface areas of modified samples increased after the modification indicating the presence of Cu₂O and CuO which were dispersed on the external surface of the NaY support.

The crystalline phase of modified samples had decreased but the support had remained unchanged. In the process of calcination, 3-dimension bulk CuO was transformed into 2-dimension dispersed species on the surface of the NaY zeolite (Braun *et al.* 2000; Zhu *et al.* 2005a). That was the reason why no additional peaks that corresponded to the crystalline phase of bulk CuO ($2\theta = 35.54^\circ$ and 38.73°) has been formed outside the pore. However, XRD diagrams (Figure 1e) showed that Cu₂O was oxidized to some extent to form bulk CuO ($2\theta = 35.54^\circ$ and 38.73°) after the heat treatment (873.15 K). This was in conformity to the research reported by Zhu *et al.* (2005b). After the heat treatment at 873.15 K, a thin CuO layer which included some whiskers, was formed over the Cu₂O layer. Different types of copper oxide with different solid-state structure and particle size dispersed NaY zeolite showed different physical features after the modification. The physical properties such as the dynamic diameter of the copper oxide probably played a very important role in the dispersion phenomenon. The dissimilar chemical properties of copper oxide were responsible for the differences in their behaviour with the NaY zeolite.

The structural property modification using different types of copper oxide led to significant effects on its gas methane adsorptive characteristics. After copper oxide/NaY zeolite modification, CuO/NaY shows a more superior methane adsorption capacity ($13.43 \times 10^{-3} \text{ mol/g-adsorbent}$) than pure (unmodified) NaY, and Cu₂O/NaY (Figure 2). It was suggested that the CuO that was loaded into the NaY cages or coated on the external surface of NaY system during the thermal treatment, provided extra adsorption sites that were exposed to the adsorbates. The surface coating of two-dimensional copper oxide species onto NaY zeolite

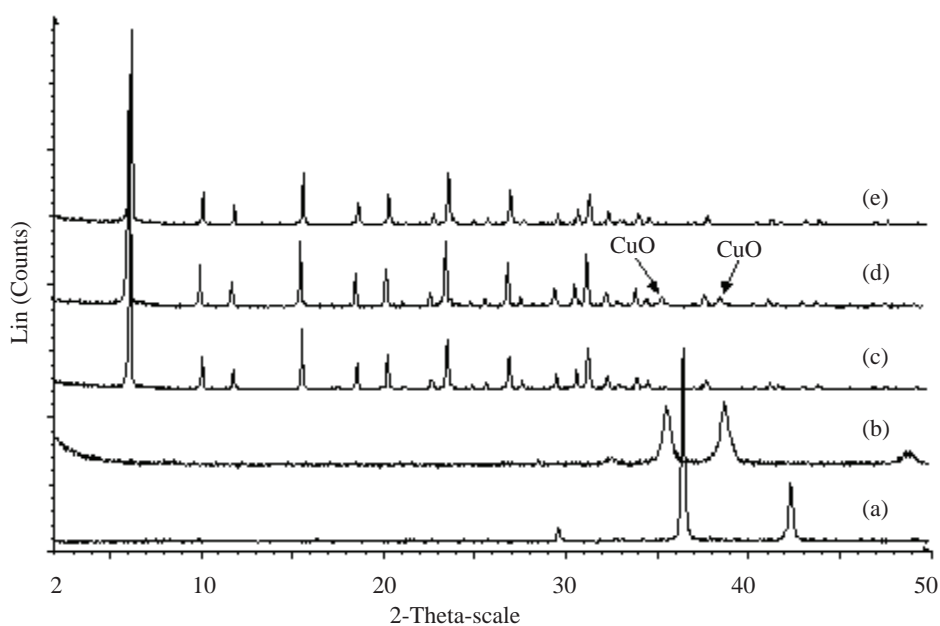


Figure 1. The XRD patterns of (a) Pure Cu_2O ; (b) Pure CuO ; (c) NaY ; (d) 5 $\text{Cu}_2\text{O}/\text{NaY}$ and (e) 5 CuO/NaY .

Table 1. Physical properties of copper oxide-modified zeolite NaY samples.

Sample	Micropore surface area (m^2/g)	External surface area (m^2/g)	Micropore volume ($\times 10^7 \text{ m}^3/\text{g}$)	Average pore diameter ($\times 10^9 \text{ m}$)	Unit cell parameter a_0 (\AA)	Relative intensity (I_{rel})
NaY	809.50	10.50	3.04	1.60	24.61	100.00
$\text{Cu}_2\text{O}/\text{NaY}$	784.73	13.05	2.93	1.58	24.63	91.82
CuO/NaY	773.69	21.00	2.88	1.61	24.63	96.43

might influence the surface reactivity of CuO with CH_4 gas. Meanwhile, Cu_2O covered by a thin layer of CuO with its different solid-state structure, electronegativity and physicochemical properties presented less ability and suitability for methane gas adsorption after the oxidation process. These results also indicated that the high surface area adsorbent would not necessarily result in a higher methane adsorption capacity. It depended on the structure and physical properties of the adsorbate and adsorbent after the modification as well as the extent of interaction of adsorbate with adsorbent surfaces.

Despite that, by employing the copper oxide- NaY zeolite modification, the gas adsorption kinetics could also be improved significantly. The linear parts of the initial gas uptake rates (Figure 2) indicated that the adsorption kinetics followed the similar trend as its CH_4 adsorption capacity. The high initial uptake rates resulted in significant improvement on the gas adsorption capacity. Copper oxide species dispersed on the zeolite external surfaces improved the interaction between the adsorbent with the

bulk adsorbates, while the copper oxide that dispersed into or was coated on the internal surface areas might have controlled led the pore size of adsorbent and affected the methane micropore diffusion into zeolite cavities.

Effect of Copper Oxide Loading

Figure 3 shows that the diffraction intensities decreased with the increase of CuO loading after CuO/NaY modification. No peaks corresponding to the crystalline phase of CuO were observed in modified samples with low CuO loadings ($<5 \text{ wt.}\%$ CuO/NaY). The disappearance of the XRD peaks assigned to CuO could be interpreted as well dispersed CuO on the surface of the support with the formation of a monolayer or sub-monolayer after the heat treatment (Xiao *et al.* 1998; Qian & Yan 2001). However, when the CuO loading was increased above its dispersion threshold value, the characteristics of crystalline CuO were clearly shown in the XRD spectrum. As the copper oxide loading concentration was increased, the XRD peaks intensities decreased regularly with lower crystallinity quality. The

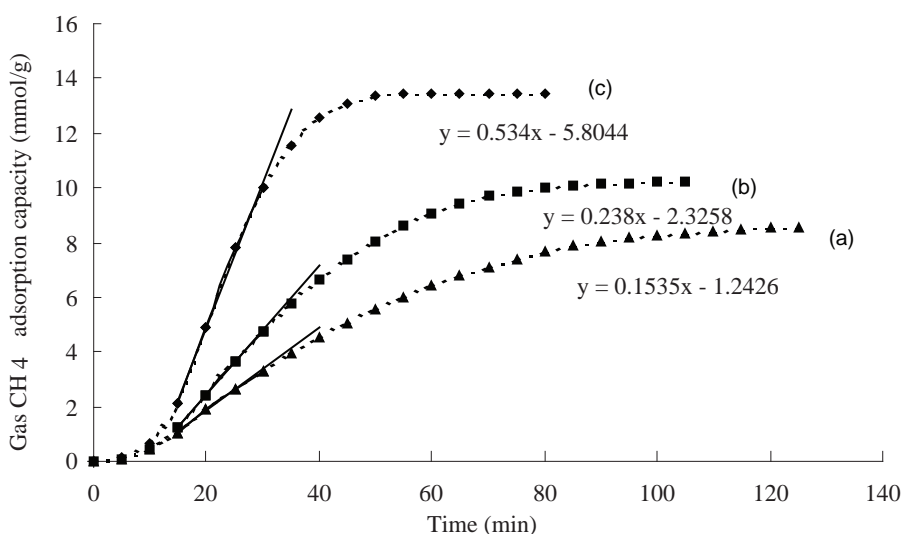


Figure 2. The adsorption curves of copper oxide modified NaY for CH₄ measured at 323.15 K and 138 kPa; (a) 5 Cu₂O/NaY; (b) NaY and (c) 5 CuO/NaY.

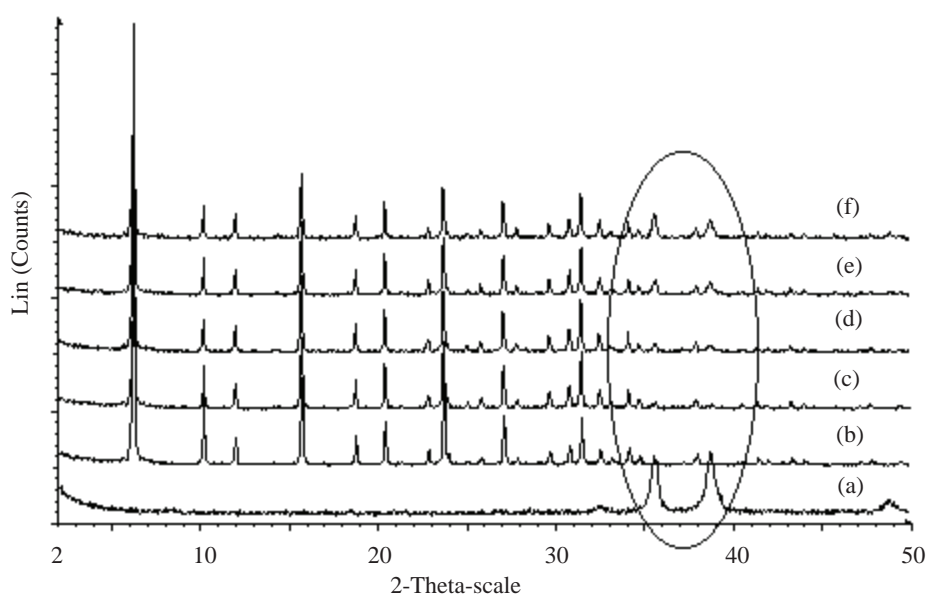


Figure 3. The XRD patterns of CuO/NaY samples: (a) CuO; (b) NaY; (c) 2.25 wt.% of CuO/NaY; (d) 5 wt.% of CuO/NaY; (e) 10 wt.% of CuO/NaY and (f) 15 wt.% of CuO/NaY.

large fractions of CuO agglomerated and were located on the external surface of the zeolite. The agglomeration phenomena could be estimated from the increase of average crystallite sizes estimated for CuO modified zeolite NaY particles by the Scherrer equation presented in Table 2 (Cullity 1978). As can be seen, the average crystallite sizes of the copper oxide particles below the dispersion capacity reacted with NaY zeolite after the heat treatment, and thus decreased the particle sizes after the modification.

Meanwhile, the particle size of the modified samples that were above 5 wt.% CuO increased with increasing copper oxide weight loadings.

Figure 4 shows the relationship of crystallinity and residual crystalline CuO (I_{rel}) with the total amount of CuO in CuO/NaY system (I_{CuO}/I_{rel}). When the CuO loading exceeded the dispersion capacity, the residual bulk CuO increased approximately linearly with the total amount of

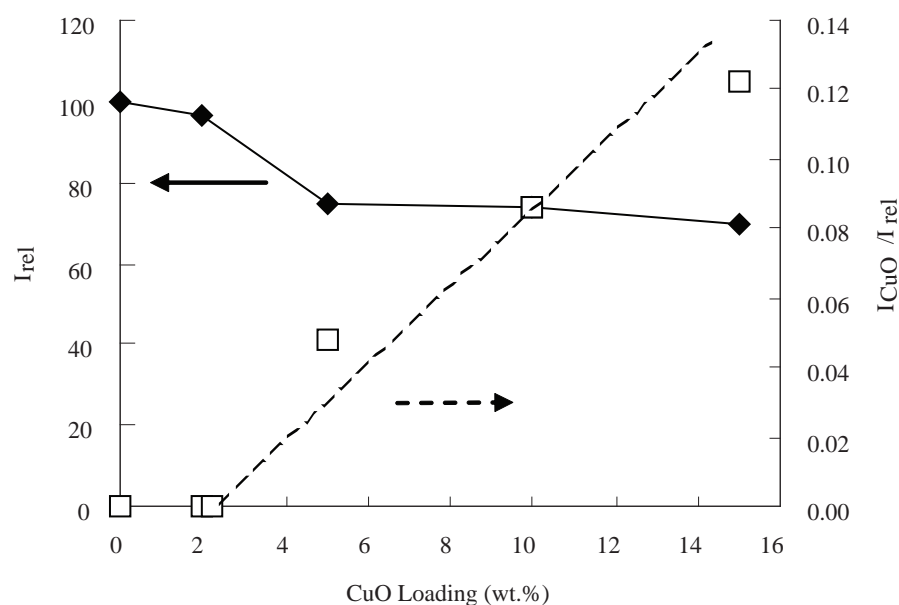


Figure 4. The influence of CuO loading concentration (wt.%) on the structure of modified samples.

Table 2. Effect of loading on structural characteristics of CuO modified NaY zeolite samples.

Samples	Loading (wt.%)	a_0 (Å)	Relative intensity (I_{rel})	Particle size (nm) ^a
NaY	–	24.61	100.00	68.69
CuO/NaY	2.00	24.62	96.02	53.13
CuO/NaY	2.25	24.62	96.43	54.27
CuO/NaY	5.00	24.68	86.45	68.68
CuO/NaY	10.00	24.68	84.32	68.69
CuO/NaY	15.00	24.68	70.15	79.35

^a Calculated based on Scherrer equation (Cullity 1978).

CuO in the samples. The intercept of the straight line plotted was assigned to the maximum dispersion capacity of the CuO that was spread out on NaY. Therefore, the amount of CuO in the adsorbent corresponded to 2.25 – 5 wt.%. CuO loading was approximately equivalent to complete the dispersion on the surface area of the zeolite NaY support. Apart from that, the loading concentration of copper oxide easily influenced the pore size of NaY zeolite system. The physical properties of the characterization results indicated that the BET specific surface area and micropore volume of the CuO modified NaY zeolite samples decreased with the increase in copper oxide loading concentration from 2.25 wt.% to 15 wt.% (Figure 5).

The influence of CuO loading concentration on the methane adsorption is shown in Figure 6. The NaY zeolite without CuO dispersion showed a CH₄ adsorption capacity of 8.4 mmol/g of adsorbent. When 2.0 wt.% of CuO was

loaded on NaY, the CH₄ adsorption capacity increased to 9.8 mmol/g of adsorbent. As the CuO loading was further increased, the adsorption capacities increased to higher values. The adsorption capacities finally increased to 13.4 mmol/g of adsorbent for the CuO loading of 2.25 wt.%, which was 60% higher than that of pure NaY. These results indicated that the loading of CuO which was up to 2.25 wt.% (maximum dispersion capacity) had probably modified the pore size of NaY zeolite to the degree, which was the most specific suitable pore size for methane adsorbate to interact and be adsorbed on the surfaces. However, on further increase of the CuO loading concentration, the CH₄ adsorption capacity dropped. It was suggested that when the CuO loading concentration was at 10 wt.% or above, bulk CuO formed agglomeration on the zeolite surface and thus blocked the pore windows, which restricted further diffusion of CH₄ gas to adsorb on the active adsorption sites of the zeolite internal surfaces.

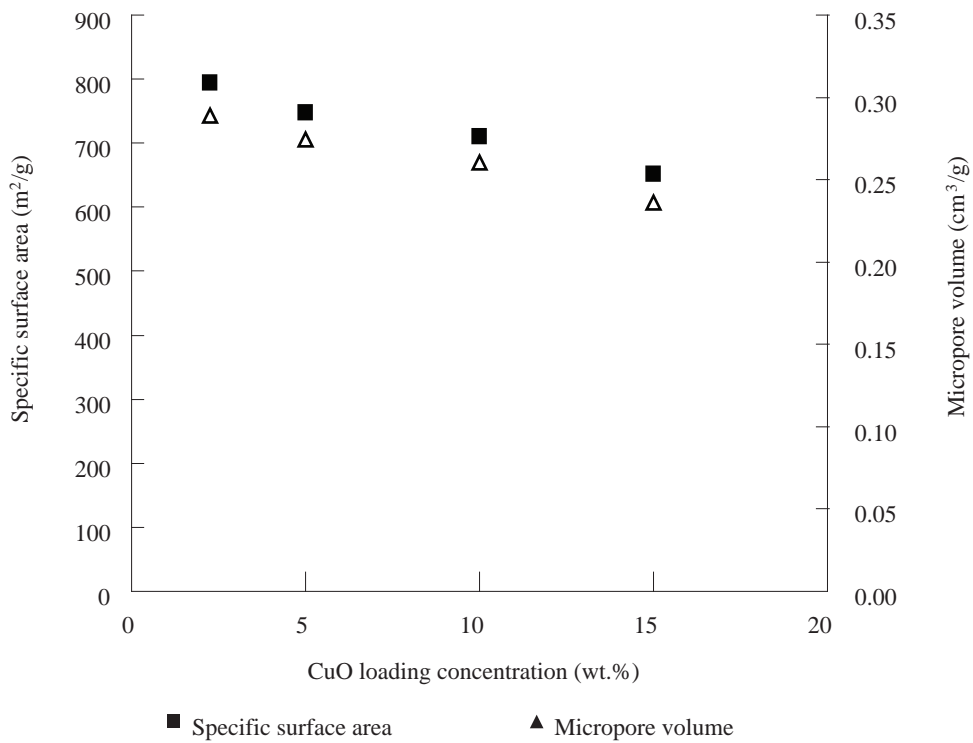


Figure 5. The effect of CuO loading concentration on NaY zeolite physical properties.

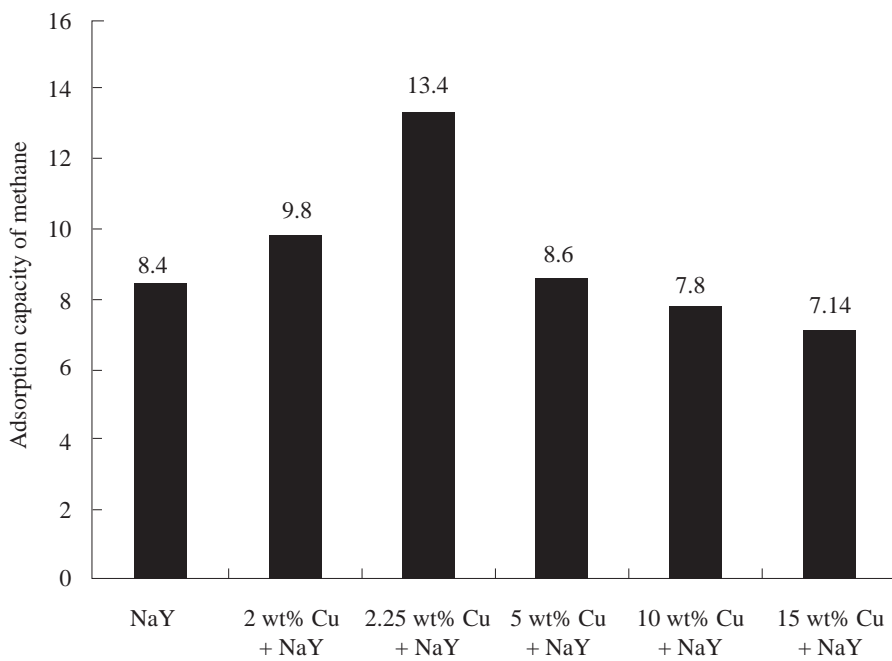


Figure 6. The effect of copper (II) oxide on methane adsorption characteristics.

Effect of Calcination Temperature

Calcination temperature was one of the most important parameters that affected the physicochemical properties of copper oxide modified zeolite and the adsorptive characteristics of methane. By varying the calcination temperature of CuO/NaY, the relative intensity of the modified sample was increased as compared to the physical mixture of copper (II) oxide and NaY zeolite at ambient temperature (Figure 7). NaY zeolite was thermally stable at 873.15 K for a 2.25 wt.% copper (II) oxide loading concentration with increasing crystallinity up to 96 %. The structure of CuO-NaY zeolite remained unchanged and thermally stable up to 973.15 K with a lower crystallinity as shown in the XRD diagrams and the relative intensity data (Table 3). At calcination temperatures of 773.15 K and below, the peaks of crystalline CuO were still present, but with reduced intensity as compared to the bulk CuO. The relative intensity of the modified sample increased significantly when the sample was heated to 873.15 K and no residual bulk crystalline CuO remained. Agglomerations of copper (II) oxide occurred on further increasing the calcination temperature up to 973.15 K, thus reducing the crystallinity of the samples (Figure 7 e). The structure of the modified sample collapsed when the heat treatment temperature rose to 1073.15 K (Figure 7 f).

Proper heat treatment processes modified to suitable calcination temperature did affect methane adsorption properties. Figure 8 shows the effect of calcination temperature on methane adsorption. Physical mixing of

CuO and NaY zeolite at 298.15 K gave CH₄ an adsorption capacity of 8.9 mmol/g of adsorbent. Thermal treatment at 773.15 K increased the adsorption capacity to 11.3 mmol/g of adsorbent. Further increasing the calcination temperature to 873.15 K, presented a maximum adsorption affinity of up to 13.4 mmol/g of adsorbent. These results indicated that a suitable calcination temperature (873.15 K) was utmostly critical to ensure the transformation of the entire three-dimensional bulk CuO to two-dimensional dispersed form. It was this two-dimensional copper oxide dispersed form that played the main role in the interaction with methane adsorbates. For a higher calcination temperature (973.15 K), methane adsorption capacity decreased to 8.8 mmol/g of adsorbent. High temperature caused the CuO dispersed species to migrate out to the external surfaces, forming agglomeration of bulk CuO that brought a decrease in methane adsorption. However, Figure 7 f shows that the structure of the modified sample collapsed during heat treatment at 1073.15 K and only 0.06 mmol of CH₄ was adsorbed per gram of adsorbent.

Effect of Calcination Time

As shown in Figure 9, after heating the mixture at 873.15 K for 12 h, some residual crystalline CuO still remained within the zeolite structure. These residuals totally vanished after the samples were calcined up to 24 h and longer. The longer calcination time resulted in the higher crystallinity of the modified NaY (Table 4). The results inferred that at temperature 873.15 K, the dispersion process was completed in about 24 h. However, for a longer calcination

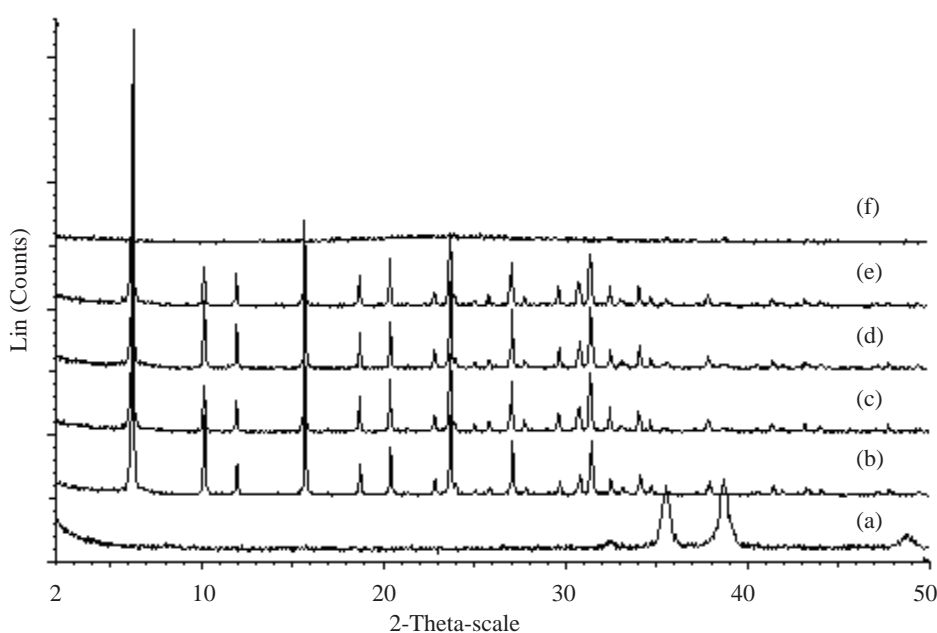


Figure 7. XRD patterns of 5 CuO/NaY samples after heat treatment: (a) CuO (298.15 K); (b) NaY (298.15 K); (c) 5 CuO/NaY (773.15 K); (d) 5 CuO/NaY (873.15 K); (e) 5 CuO/NaY (973.15 K) and (f) 5 CuO/NaY (1073.15 K).

Table 3. Effect of calcination temperature on structural characteristics of CuO modified NaY zeolite samples.

Samples	T (K)	a_0 (Å)	Relative intensity (I_{rel})	Particle size (nm) ^a
NaY	298.15	24.61	100.00	68.69
CuO/NaY	298.15	24.64	91.00	79.35
CuO/NaY	773.15	24.67	92.35	54.27
CuO/NaY	873.15	24.62	96.43	54.27
CuO/NaY	973.15	24.68	84.91	68.68
CuO/NaY	1073.15	Structure collapse		

^a Calculated based on Scherrer equation (Cullity 1978).

Table 4. Effect of calcination time on structural characteristics of CuO modified NaY zeolite samples.

Samples	Time (h)	a_0 (Å)	Relative intensity (I_{rel})	Particle size (nm) ^a
NaY	0	24.61	100.00	68.69
CuO/NaY	0	24.64	91.00	79.35
CuO/NaY	6	24.65	92.00	68.69
CuO/NaY	12	24.64	93.16	68.69
CuO/NaY	24	24.62	96.43	54.27
CuO/NaY	48	24.62	103.26	65.20

^a Calculated based on Scherrer equation (Cullity 1978).

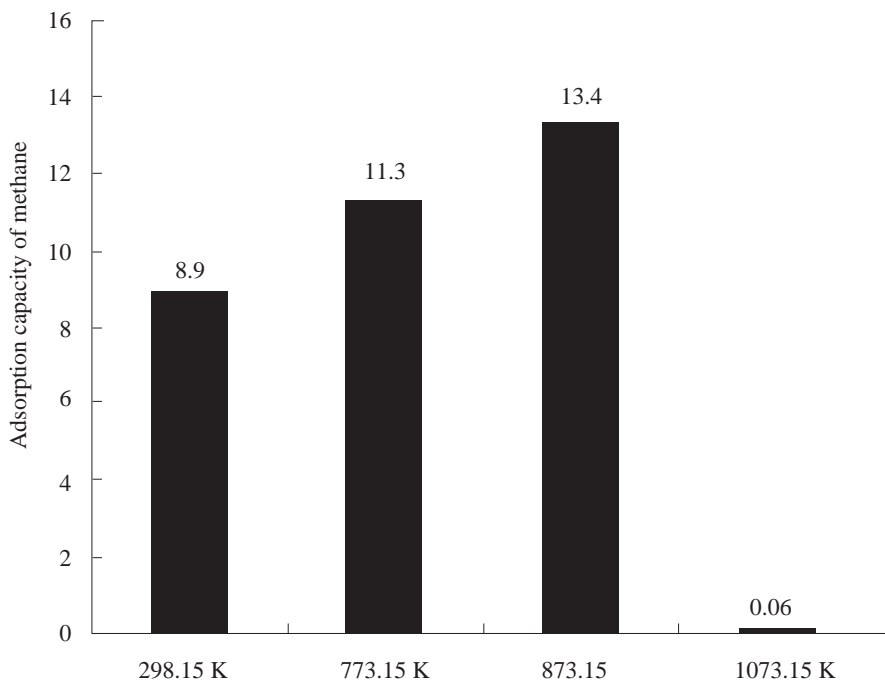


Figure 8. The effect of calcination temperature on methane adsorption capacity.

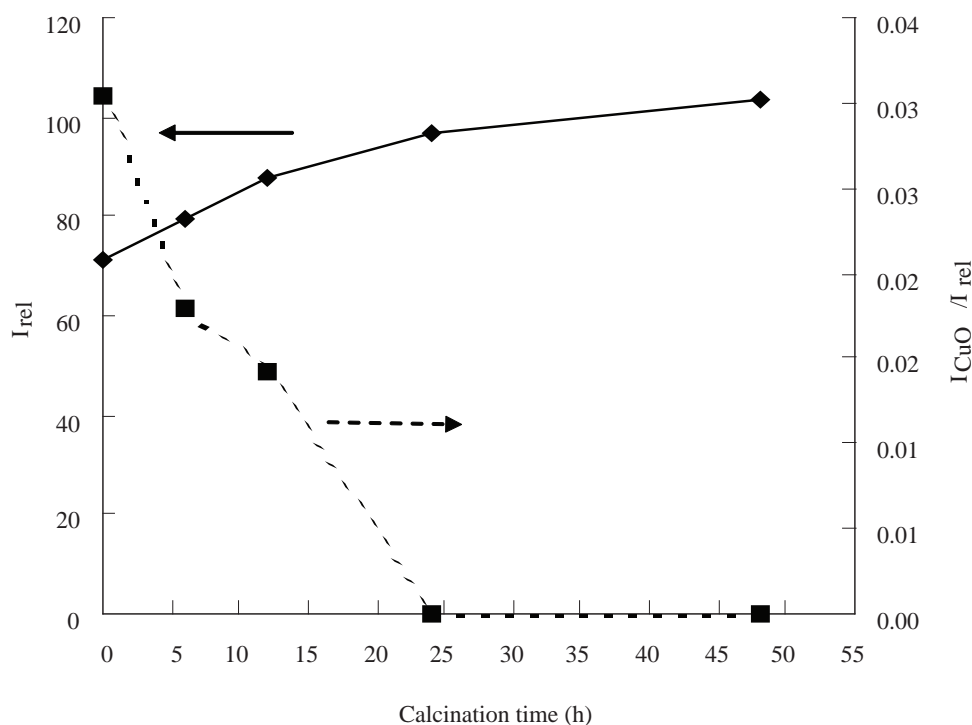


Figure 9. The influence of calcination time on the structure of modified samples.

Table 5. Effect of the duration of calcination on physical property characteristics.

Samples	Time (h)	BET surface area (m^2/g)	Micropore volume ($\times 10^7 m^3/g$)	Average pore diameter (\AA)
NaY	0	820.00	3.04	16.00
CuO/NaY	0	744.51	2.71	16.23
CuO/NaY	6	790.23	2.87	16.02
CuO/NaY	24	794.63	2.88	16.11
CuO/NaY	48	813.55	2.97	15.87

time, the particle size of the adsorbent formed was larger. The effect of calcination time on the physical properties of adsorbents is shown in Table 5.

The BET specific surface areas and micropore volumes increased simultaneously with the increase in calcination time. Meanwhile, the average pore diameter generally represented a declining trend. The increase in sample surface area and the decrease in pore size diameter were perhaps due to the proper dispersion of CuO into the internal surface of the zeolite matrix system. After heat treatment for 48 h, the particle size, surface area and micropore volume of the adsorbent increased which indicated the migration phenomena of some CuO out from the micropore of zeolite. As described by Dong *et al.*

(1997), after an optimum heat treatment process period for dispersing all the oxide species on the surface, further heat treatment would result in reversibility of the formation of bulk phase metal oxide and surface species metal oxide on zeolite surfaces. Hence, the satisfactory duration of heat treatment was very important for the proper dispersion of copper oxide on the zeolite surfaces.

Following the physical property changes, the duration of the calcination process would affect the adsorption capacity of methane (Figure 10). Six hours of calcination improved the CH_4 adsorption capacity to 10.1 mmol/g of adsorbent. Meanwhile, at 12 h and 24 h of calcination at 873.15 K, the dispersive temperature significantly kept enhancing the CH_4 adsorption performances to 12.9 mmol/g of adsorbent and

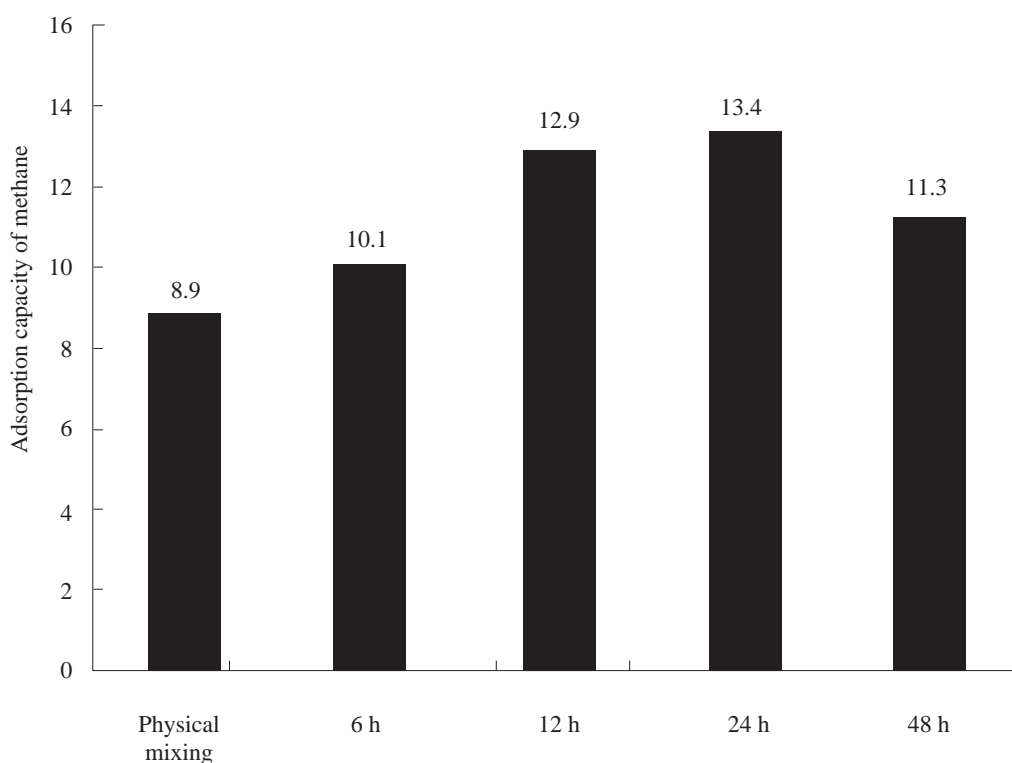


Figure 10. The effect of calcination time on methane adsorption capacity.

13.4 mmol/g of adsorbent, respectively. For heat treatment of more than 24 h, the CuO that dispersed onto the zeolite surfaces was described as in reversible form between the formation of bulk CuO and dispersed CuO species. Therefore, 48 hours of calcination not only increased the particle size of the adsorbent and the migration of some CuO out of the surface but also created a decrease in the methane adsorption capacity of up to 11.3 mmol/g of adsorbent.

CONCLUSION

The thermal dispersion of copper oxide onto/into the NaY zeolite surface was of importance to the development of a gas methane adsorbent. Copper oxide-NaY zeolite modification parameters such as types of copper oxide, copper oxide loading concentration, calcination temperature and duration of calcination treatment greatly influenced the physicochemical properties of NaY zeolite and its gas methane adsorptive characteristics. The results showed that at 2.25 wt.% of copper (II) oxide, the modified NaY zeolite that calcined at 873.15 K for 24 h showed the most promising results for methane adsorption capacity.

ACKNOWLEDGEMENTS

The authors wish to express their gratitude to the IRPA grant No. 74512 from the Ministry of Science, Technology and Innovation (MOSTI) Malaysia, and Universiti Teknologi Malaysia.

Date of submission: February 2009

Date of acceptance: December 2009

REFERENCES

- Abdel-Fattah, TM *et al.* 1997, 'Molecular catalyst design. synthesis, characterization and properties of zeolite NaY catalysts made with a tetranuclear copper (II) complex', *Catalysis Today*, vol. 33, pp. 313–322.
- Alyea, EC & Bhat, RN 1995, 'Methanol conversion to hydrocarbons over WO₃/HZSM-5 catalysts prepared by metal oxide vapor synthesis', *Zeolites*, vol. 15, pp. 318–323.
- Bordiga, S *et al.* 2001, 'Interaction of N₂, CO and NO with Cu-exchanged ETS-10: a compared FTIR study with other Cu-zeolites and with dispersed Cu₂O', *Catalysis Today*, vol. 70, pp. 91–105.

- Braun, S *et al.* 2000, 'Thermal spreading of MoO₃ onto silica supports', *Journal of Physical Chemistry B*, vol. 104, pp. 6584–6590.
- Cavenati, S, Grande, CA & Rodrigues AE 2006, 'Separation of CH₄/CO₂/N₂ mixtures by layered pressure swing adsorption for upgrade of natural gas', *Chemical Engineering Science* vol. 61, pp. 3893 – 3906.
- Chang, CL, Hsu, CC & Huang, TJ 2003, 'Cathode performance and oxygen-ion transport mechanism of copper oxide for solid-oxide fuel cells', *Journal of Solid State Electrochemica*, vol. 7, pp. 125–128.
- Chao, CC 1990, *Selective adsorption on magnesium-containing clinoptilolites*, U.S. Patent 4,964,889.
- Cruccolini, A, Narducci, R & Palombari, R 2004, 'Gas adsorption effects on surface conductivity of nonstoichiometric CuO', *Sensors and Actuators B*, vol. 98, pp. 227–232.
- Cullity, BD 1978, *Elements of X-ray diffraction*, United States of America, Addison-Wesley Publishing Company.
- Delahay, G *et al.* 1998, 'N₂O origin in NO reduction with NH₃ over copper zeolites' *Surface Chemistry and Catalysis*, vol. 1 pp. 229–235.
- Delgado JA *et al.* 2007, 'Carbon dioxide/methane separation by adsorption on sepiolite', *Journal of Natural Gas Chemistry*, vol. 16, pp. 235–243.
- Deng, SG & Lin, YS 1997, 'Microwave heating synthesis of supported sorbents', *Chemical Engineering Science*, vol. 52, pp. 1563–1575.
- Díaz, R & Lazo, MF 2000, 'Spectroscopic study of CuO/CoO catalysts supported by Si-Al-Y zeolite matrices prepared by two sol-gel methods', *Journal of Sol-Gel Science and Technology*, vol. 17, pp. 137–144.
- Dong, L, Chen, KD & Chen, Y 1997, 'Study of the interactions between MoO₃ and α -Fe₂O₃', *Journal of Solid State Chemistry*, vol. 129, pp. 30–36.
- Dutta, PK & Vaidyalingam, AS 2003, 'Zeolite-supported ruthenium oxide catalysts for photochemical reduction of water to hydrogen', *Microporous and Mesoporous Materials*, vol. 62, pp. 107–120.
- El-Shobaky, HG, Mokhtan, M & El-Shobaky, GA 1999, 'Physicochemical surface and catalytic properties of CuO-ZnO/Al₂O₃ system', *Applied Catalysis A: General*, vol. 180, pp. 335–344.
- Hadjiivanov, K *et al.* 2003 'Characterization of Cu/MCM-41 and Cu/MCM-48 mesoporous catalysts by FTIR spectroscopy of adsorbed CO', *Applied Catalysis A: General*, vol. 241, pp. 331–340.
- Harlick, PJE & Tezel, FH 2004, 'An experimental adsorbent screening study for CO₂ removal from N₂', *Microporous and Mesoporous Materials*, vol. 76, pp. 71–79.
- Hasegawa, Y *et al.* 2001, 'The separation of CO₂ using Y-type zeolite membranes ion-exchanged with alkali metal cations', *Separation and Purification Technology*, vol. 22–23, pp. 319–325.
- Huang, YJ *et al.* 2004, 'Speciation of copper in micropores', *Water, Air and Soil Pollution*, vol. 153, pp. 187–194.
- Ito, T *et al.* 1998, 'Single-crystal growth and characterization of Cu₂O and CuO' *Journal of Materials Science*, vol. 33, pp. 3555–3566.
- Jayaraman, A *et al.* 2004, 'Clinoptilolites for nitrogen/methane separation', *Chemical Engineering Science*, vol. 59, pp. 2407–2417.
- Khouchaf, L *et al.* 1998, 'Structural investigation of zinc oxide clustering in zeolite A and sodalite', *Microporous and Mesoporous Materials*, vol. 20, pp. 27–37.
- Liu, HD *et al.* 2004, 'Copper oxide modified NaY zeolite: Efficient catalysts for degrading N-nitrosopyrrolidine', in *Proceedings of the 14th International Zeolite Conference*, April 25–30, Cape Town, South Africa: Document Transformation Technologies, pp. 2527–2535.
- Mediavilla M *et al.* 2008, 'MIBK from acetone on Pd/H-[Ga] ZSM5 catalysts: Effect of metal loading', *Microporous and Mesoporous Materials*, vol. 116, pp. 627–632.
- Mizukami, K *et al.* 2001, 'Molecular dynamics calculations of CO₂/N₂ mixture through the NaY type zeolite membrane', *Journal of Membrane Science*, vol. 188, pp. 21–28.
- Nishimaya, N *et al.* 2001, 'Hyperstoichiometric hydrogen occlusion by palladium nanoparticles included in NaY zeolite', *Journal of Alloys and Compounds*, vol. 319, pp. 312–321.
- Njikamp, MG *et al.* 2001, 'Hydrogen storage using physisorption — materials demands', *Applied Physic A*, vol. 72, pp. 619–623.
- Qian, L & Yan, ZF 2001, 'Micropore modification of zeolites with transition-metal oxides', *Colloids and Surface A: Physico chemical and Engineering Aspects*, vol. 180, pp. 311–316.
- Ramirez-Cuesta AJ & Mitchell PCH 2007, 'Hydrogen adsorption in a copper ZSM5 zeolite. An inelastic neutron scattering study', *Catalysis Today*, vol. 120 pp. 368–373
- Salavati-Niasari M 2008, 'Template synthesis and characterization of host (nanopores of zeolite Y) /guest [Co(II)-tetraoxodithiatetraaza macrocyclic complexes] nanocomposite materials', *Polyhedron*, vol. 27, pp. 3207–3214.
- Sárkány, J 1997, 'FTIR study on the interaction of O₂ and CO with Cu⁺ ions in zeolite ZSM-5 formation and reactivity of superoxide', *Journal of Molecular Structure*, vol. 410–411, pp. 95–98.
- Sultana, A *et al.* 2004, 'Adsorptive separation of NO_x in presence of SO_x from gas mixtures simulating lean burn engine exhaust by pressure swing process on Na-Y zeolite', *Applied Catalysis B: Environmental*, vol. 48, pp. 65–76.
- Szanyi, J & Paffett, MT 1996, 'The adsorption of NO and reaction of NO with O₂ on H-, NaH-, CuH-, and Cu-ZSM-5: an *in situ* FTIR investigation', *Journal of Catalysis*, vol. 164, pp. 232–245.
- Thoret, J, Man, PP, & Fraissard, J 1997, 'Solid-solid interaction and reaction between antimony oxide, Sb₂O₃, and NaY or LaNaY zeolites. Comparison with V₂O₅ and MoO₃', *Zeolite*, vol. 18, pp. 152–161.
- Tseng, HH & Wey, MY 2004, 'Study of SO₂ adsorption and thermal regeneration over activated carbon-supported copper oxide catalysts', *Carbon*, vol. 42, pp. 2269–2278.

- Turky, AEMM, Radwan NRE & El-Shobaky, GA 2001, Surface and catalytic properties of CuO doped with MgO and Ag₂O', *Colloid and Surfaces A: Physicochemical and Engineering Aspects*, vol. 181, pp. 57–68.
- Xiao, FS *et al.* 1998, 'Dispersion of inorganic salts into zeolites and their pore modification', *Journal of Catalysis*, vol. 176, pp. 474–487.
- Xie, Y *et al.* 1990, *Adsorbents for used in the separation of carbon monoxide and/or unsaturated hydrocarbons from mixed gases*, U.S. Patent 4917711.
- Xie, YC & Tang, YQ 1990, 'Spontaneous monolayer dispersion of oxides and salts onto surfaces of supports: Application to heterogeneous catalysis', *Advances in Catalysis*, vol. 37, pp. 1–43.
- Zhu, HY *et al.* 2005a, 'Dispersion behaviors of molybdena on titania (rutile and/or anatase)', *Journal of Physical Chemistry B*, vol. 109, pp. 11720–11726.
- Zhu, Y, Mimura, K, & Isshiki, M 2005b, 'Influence of oxide grain morphology on formation of the CuO scale during oxidation of copper at 600–1000 °C', *Corrosion Science*, vol. 47, pp. 537–544.

Influence of CO₂ Flux on the Properties of Carbonate Apatite Synthesized by Solid State Reaction

K. Jamuna^{1*}, K. Noorsal¹, F.A. Zakaria¹ and Z.H. Hussin¹

Introducing CO₂ flux as the carbonate source had an effect on the carbonate content of carbonate apatite (CAp) synthesized by solid state reaction. The reactants were CaCO₃ and beta-tricalcium phosphate (β-TCP) and the heat treatment in air was performed at 1250°C followed by instant cooling in CO₂ flux for temperatures ranging from 800°C room temperature (RT). The influence of CO₂ flux at various temperature drop differences in the cooling process (1250°C RT, 1250°C–500°C, 1250°C–600°C, 1250°C–700°C, and 1250°C–800°C) was tested to optimize the carbonation degree and subsequent effects on the physical and mechanical properties of CAp. Thermally treated samples revealed an increasing degree of carbonation, achieving a maximum of 5.2 wt% at the highest (1250°C RT) and a minimum of 2.7 wt% at the lowest (1250°C–800°C) temperature drop differences, respectively. This showed that the carbonate content was correlated with the increase in exposure to CO₂ flux. However, consistent compressive strength, tensile strength, density and porosity were observed against increasing temperature drop differences which indicated that the degree of carbonation exerted no influence on the physical and mechanical properties of CAp. This method enabled the synthesis of solid state CAp simply by exposing calcium phosphate mixtures to CO₂ flux. It also allowed the control of carbonate content for desired medical applications.

Key words: carbonate apatite; solid state reaction; CO₂ flux; carbonate content; temperature differences; properties; physical; chemical; mechanical

The preparation of stoichiometric hydroxyapatite has been the most significantly targeted material for bone mineral substitute in recent decades but interest has now converged on the preparation of non-stoichiometric apatites which have closer chemical similarities with the inorganic phase of bone.

Non-stoichiometric apatites are quite easy to synthesise. However, their composition and crystal characteristics are more difficult to control, mainly because of the ability of the lattice to accept substitutes and vacancies. The most interesting of the non-stoichiometric apatites is CO₃²⁻-containing apatites which are close to bone mineral. Although bone mineral has a variable composition, diverse apatites mimicking the evolution of bone mineral in young and old animals can be prepared and their composition represented by a chemical formula analogous to that of bone mineral [Landi *et al.* 2004]. The main mineral constituent of bone tissue, biological apatite is always found with some carbonate in its structure [Barinov *et al.* 2006]. For example, in a recent review, the content of CO₂ which is present as carbonate in the organic fraction of enamel, dentine and bone was reported to be 3.0, 4.8, and 5.8 wt%, respectively [Fleet *et al.* 2003]. The overall carbonate content in bone mineral is about 4–8 wt% and it has been shown to vary depending on the age of the individual with an increase of

A-type in old bones. On the other hand, type B carbonate apatite is the most abundant species in the bones of young human beings [Landi *et al.* 2004].

Nevertheless, most researchers agree that based on various CAp preparation techniques, the carbonate ion can substitute for OH⁻ in the apatite channel (type A CAp) and for the phosphate ion (type B CAp) in order to mimic the inorganic phase of natural bone [Fleet *et al.* 2003]. The chemical formula of carbonate apatite is formally given by Ca_{10-x/2}[(PO₄)_{6-x}(CO₃)_x](OH)_{2-2y}(CO₃)_y on the basis of a simple charge neutrality [Suetsugu *et al.* 2000]. Thus, considering the above facts, significant attention was paid to the preparation of material most similar to the mineral composition of bones.

As a consequence, many investigations had been already carried out to prepare carbonate apatites [Landi *et al.* 2004; Krajewski *et al.* 2004] and most of them can be classified into two groups according to the processing method; one is wet [Landi *et al.* 2004] and the other is a solid state reaction [Verbeeck *et al.* 1995]. The benefits of the wet process are that the by-product is environmental friendly, e.g. water and the probability of contamination during processing was almost negligible. However, the setbacks are the composition of the resulting product is greatly affected

¹Advanced Materials Research Centre (AMREC), SIRIM Berhad, Lot 34, Jalan Hi-Tech 2/3, Kulim Hi-Tech Park, 09000 Kulim, Kedah, Malaysia

*Corresponding author (e-mail: jamuna@sirim.my)

by slight differences in the reaction parameters and even the time needed for obtaining CAP is too long depending on the reaction conditions. Poor reproducibility and high processing cost also set a barrier on the economical values needed for industrial scale production (Rhee 2002). Therefore, the solid state reaction is thought to be more suitable than the aforementioned as the capability to reproduce and lower the processing cost are extensively high, despite the risk of contamination during milling.

Studies have shown (Otsuka *et al.* 1994; Chaikina *et al.* 1997) that the calcium and phosphorus compounds used as the starting material in the solid state reaction process are anhydrous dicalcium phosphate (CaHPO_4), dicalcium phosphate dihydrate ($\text{CaHPO}_4 \cdot 2\text{H}_2\text{O}$), monocalcium phosphate monohydrate ($\text{Ca}(\text{H}_2\text{PO}_4)_2 \cdot \text{H}_2\text{O}$), calcium pyrophosphate ($\text{Ca}_2\text{P}_2\text{O}_7$), calcium carbonate (CaCO_3), calcium oxide (CaO), calcium hydroxide ($\text{Ca}(\text{OH})_2$), etc. From the above material, Fowler *et al.* (1974) has adopted a combination of calcium pyrophosphate and calcium carbonate to produce hydroxyapatite with a supply of water vapor as the source of the hydroxyl group. In contrast, Verbeeck *et al.* (1995) has reported a process that involves a combination of CaCO_3 , CaHPO_4 and KHCO_3 as the reactants; the three powders were homogenized by ball milling in an agate mortar, heat-treated with a supply of continuous CO_2 stream washed over 96% sulphuric acid for 60 h and then finally quenched in air to produce carbonate apatite. On the other hand, Roy *et al.* (1974) reported the solid state preparation of CAP, adopting β tri-calcium phosphate (β -TCP) and CaCO_3 as the precursors, where the powders reacted under CO_2 pressure at 850°C for 500 h. Thus, the methods and apparatus used in these processes are complicated and time consuming. In addition, no one have reported the effect of CO_2 flux during temperature drop unlike the continuous flow as reported by many (Landi *et al.* 2004; Verbeeck *et al.* 1995; Oliveira *et al.* 2001; Roy *et al.* 1974) in the heat-treatment of CAP prepared from solid state reactions at high temperatures.

In our investigation, a simple procedure to obtain pure CAP with varying amount of carbonate content was performed using a solid state reaction. In this single step heat-treatment, the reactants were exposed to CO_2 flux at various temperature drops and characterized to obtain the physical, chemical and mechanical properties.

The results were explained in terms of carbonation degree in the synthesized CAP obtained by CO_2 flux reaction at various temperature drop differences in the heat treatment process.

MATERIALS AND METHOD

Synthetic apatites with differing carbonate content were prepared by solid state reaction from calcium carbonate

(CaCO_3) and β -tricalcium phosphate powders ($\text{Ca}_3(\text{PO}_4)_2$) (both from Fluka) as the chemical precursors. These chemical precursors were mixed together so that the Ca/P mol ratio of the green calcium phosphate composition was 1.8. The calcium phosphate compositions were ball milled for 24 h to obtain a homogenous mixture of the chemical precursors in the initial stage of CAP synthesis. Cold isostatic press (CIP) was carried out at 30 000 p.s.i. (210 MPa) using a cold isostatic press (AIP CP360) on the ball milled calcium phosphate powder to obtain cylindrical shaped samples having a dimension of 10 mm (diameter) \times 15 mm (height). After CIP, the samples were cut into pellets using a knife and ground using silicon carbide abrasive paper with grit no. 600 to achieve sizes of 10 mm (dia) \times 4 mm (height) and 6 mm (dia) \times 12 mm (height) for tensile and compression testings, respectively.

In this study, a controlled atmospheric box furnace (Modutemp, KS77EVMGX, Australia) was used for firing the calcium phosphate pellets. The samples were placed randomly on a piece of flat alumina without any preferred sample position orientation and heated at $5^\circ\text{C}/\text{min}$ for up to 1250°C in air. Maintaining the temperature at 1250°C , the firing was continued for an hour in air. At the end point of 1 h firing at 1250°C , the temperature was set to decrease at $5^\circ\text{C}/\text{min}$ down to 30°C without turning off the furnace. At that point, as soon as the firing temperature dropped from 1250°C to 1249°C , 99.97% industrial grade CO_2 gas (9 l/min) was fluxed at different temperature drops separately in the ranges of 1249°C – 25°C , 1249°C – 500°C , 1249°C – 600°C , 1249°C – 700°C and 1249°C – 800°C whereby the reaction time was about 4 h 10 mins, 2 h 30 mins, 2 h 10 mins, 1 h 50 mins and 1 h 30 min, respectively. The gas flow was stopped immediately after the above drop points were reached and the samples left in air in the furnace until a temperature of 30°C was reached. In another experiment, CO_2 flux was exposed to the pellet samples throughout a complete heat-treatment cycle whereby the samples were heated from 30°C at $5^\circ\text{C}/\text{min}$ for up to 1250°C for an hour and annealed to 30°C . It was labeled as RT– 1250°C –RT; unlike the CO_2 flux exposure merely in the cooling process as for the aforementioned samples. The CO_2 flux throughout the cooling process was manually regulated in precision to avoid the CO_2 exposure on calcium phosphate samples beyond the desired temperature drop range.

The phases present on the surface of samples were identified using a X-ray diffractometer (XRD; Bruker, Advance D8, Germany) with Cu-K α radiation source at 1° incidence against surface and a scanning mode of $2^\circ/\text{min}$ with a step scanning rate of $0.02^\circ/10\text{s}$. The morphology of the samples, gold coated for 400 s using a sputter coater was also examined using a field-emission scanning electron microscope (FESEM; Leo 1525, Germany). The surface of the sample was scraped and mixed with KBr before made into thin pellets. A fourier transform infrared spectrum of the sample was obtained using a Nicolet MAGNA-IR

560 spectrometer E.S.P (FTIR; Nicolet, USA). In order to evaluate the Ca/P molar ratio of the samples, an inductively coupled plasma - mass spectrometric (ICP-MS) analysis was performed (Perkin Elmer Optima 2000DV). A carbon elemental analysis was performed by an automatic elemental analyzer (FISON Model EA 1108).

The diametral tensile strength and compressive strength of the samples were evaluated (Thomas *et al.* 1980; ASTM C 773–88), using an Universal Testing Machine INSTRON 5582 (UTM; Instron, USA) at a crosshead speed of 0.5 mm/min. A Helium Pycnometer (Micrometrics) with helium flow rate of 0.005 psig/min was used to determine the true density of the samples. However, bulk density and total porosity of the samples were measured according to *British Standard* EN623-2:1993 guidelines. On each sample, ten measurements were performed and the corresponding test results were reported as mean values.

RESULTS AND DISCUSSION

Figure 1 shows the results of XRD measurements on the samples which reacted with CO₂ flux at different temperature drop ranges to obtain CAP. The XRD patterns of all samples are very similar, except for the RT–1250°C–RT sample which showed the presence of secondary phase β -TCP in the major phase of carbonate apatite. It was presumed that this phenomenon was due to the decomposition of apatite at 1250°C. A similar phenomenon was reported by Roy

et al. 1974, in their investigation. Carbonate containing apatites which were prepared with excess of CO₂ were considered to represent maximum solid solutions under the experimental conditions. Thus, it was possible to assume that the excess of CO₂ flux had contributed to the maximum solid state reaction with the apatite, yielding decomposed carbonate apatite.

The recorded patterns for the samples which reacted with CO₂ flux at temperature drop from 1250°C to 800°C until RT were typical XRD patterns of carbonate apatite (Landi *et al.* 2004). On the other hand, mixtures of precursors consisting of β -TCP and CaCO₃ phases were detected to remain the same in both before and after ball milling treatments indicating that the formation of CAP solely by thermal treatment associated with CO₂ flux imposed on calcium phosphate samples.

In Figure 2, FTIR measurements on the samples which reacted with CO₂ flux at different temperature drop ranges to obtain CAP are shown. The profiles of all the samples were exactly the same and typical of CAP (Apfelbaum *et al.* 1992) except for the mixture of precursors exhibiting the broad stretching and bending mode of CO₃ ion at around 1500 cm⁻¹ due to the presence of CaCO₃. It implied that the carbonate apatite phase was only formed after heat treatment with CO₂ flux. This was in agreement with the distinctive measurement of infrared (IR) spectrum for heat treated samples showing bending modes of CO₃ ion at around 1550, 1460, 1420 and 875 cm⁻¹, respectively,

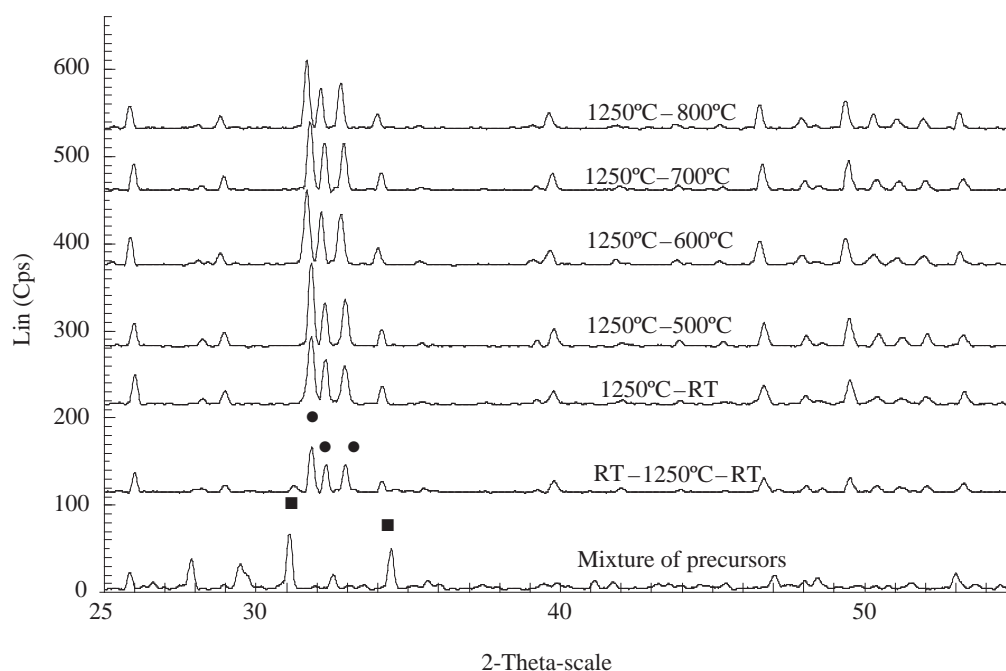


Figure 1. XRD patterns of samples reacted with CO₂ flux at different temperature drop ranges to obtain CAP. (■) β -TCP and (●) carbonate apatite.

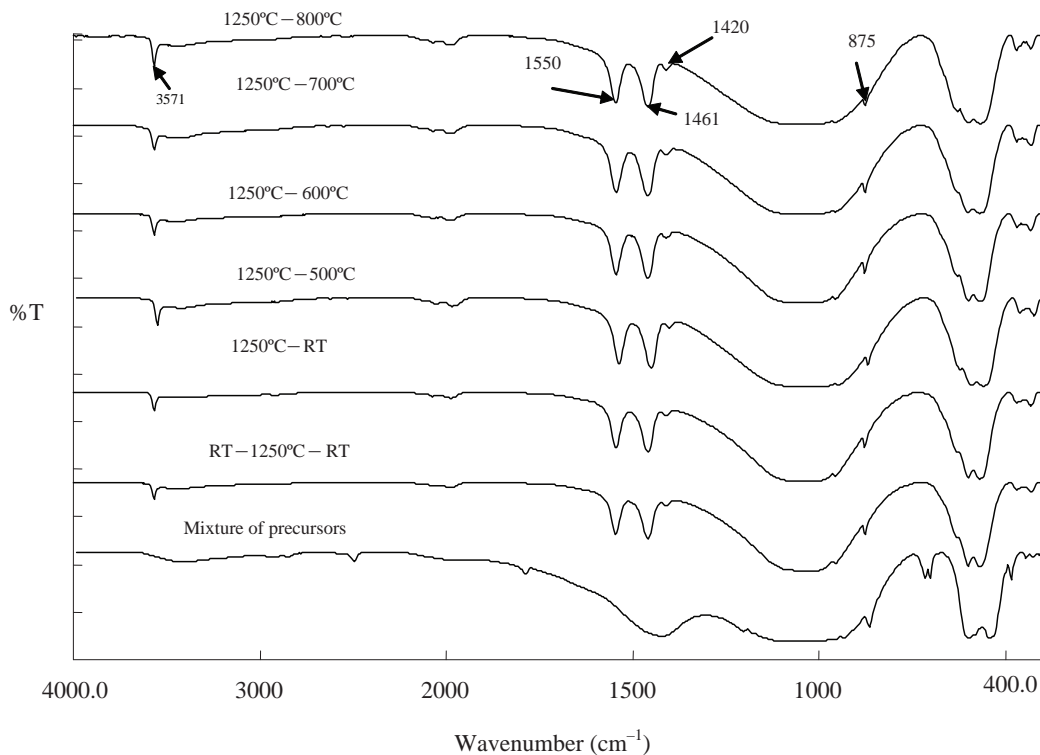


Figure 2. FTIR transmission spectra of samples which reacted with CO₂ flux at different temperature drop ranges to obtain CAP.

explaining CO₃ ion distribution at both anionic sites, the phosphate and hydroxyl indicating the formation of A+B type CAP (Apfelbaum *et al.* 1992). However, the inherence of OH ion bending mode at around 3570 cm⁻¹ showed that only partial substitution of the CO₃ ion had taken place at the OH⁻ site.

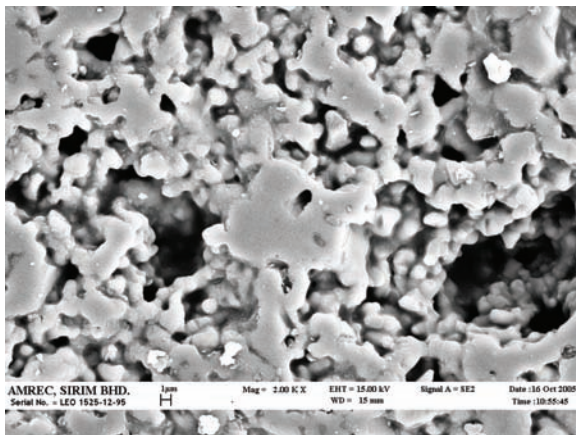
The microstructures of the CAP samples obtained from the CO₂ flux reaction in the complete cycle and cooling processes of the heat-treatment showed no differences in their surface morphology (Figures 3a and 3b). The micro morphology of the surface also showed a porous structure despite significant change in the carbonation degree. This was consistent with the similarities found on each sample surface for the various heat-treatment processes performed (Figures 3c–3f).

The calcium-based apatites showed no noticeable phase separations for the samples (Figure 3a) obtained from complete cycle (RT–1250°C–RT), even though the presence of separate phases of carbonate apatite and β – TCP were identified in XRD results (Figure 1).

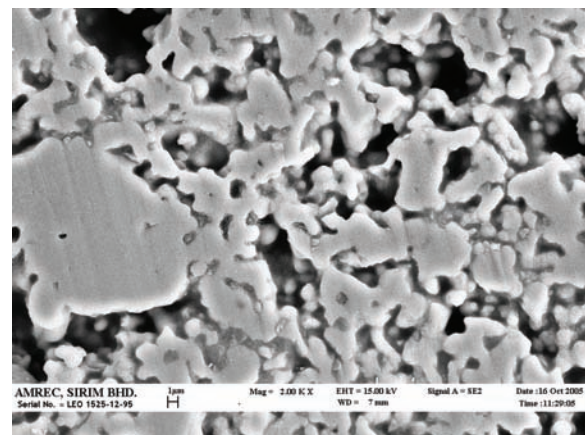
The results of calcium, phosphorus and carbon elemental analysis are reported in Table 1. Chemical analysis showed that the samples contained 2.74 wt% – 6.21 wt% of carbonate and their stoichiometry might possibly be comparable to Ca_{10-(x/2)}(PO₄)_{6-x}(CO₃)_x(OH)_{2-2y}(CO₃)_y with 0 < x < 3 and 0 < y < 1.

Furthermore, the observed carbonate degree was in the range of carbonate content reported to be found in enamel (3.0 wt%), dentine (4.8 wt%) and bone (5.8 wt%) (Fleet *et al.* 2003). Based on the tabulated carbon values, carbonation degree was significantly increasing for larger temperature drops. The increase of CO₂ adsorption in the apatite samples was conjectured to originate from the longer exposure to constant CO₂ flux due to larger temperature drops. The carbonation of samples reacted in CO₂ flux occurred in all the samples but the degree of occurrence was greater in RT–1250°C–RT (6.21wt% carbonate) although XRD analysis revealed the formation of decomposed secondary phase, β-TCP in the major CAP phase yielding impure CAP formation.

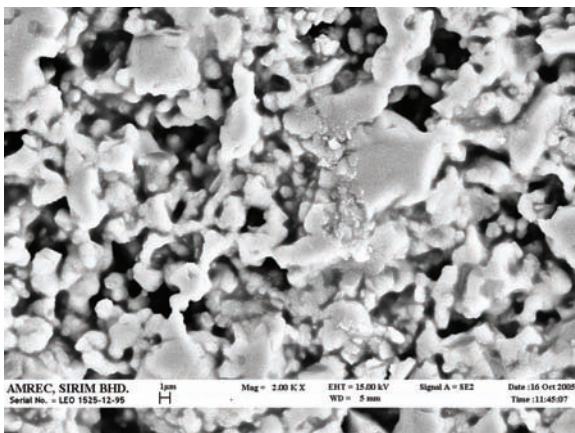
The experimental data for calcium and phosphorus were in agreement with the theoretical Ca/P molar ratio of 1.67 (type-A CAP) for samples treated in 1250°C–RT and 1250°C –500°C conditions though a slight variation was observed in the remaining heat treatments. Theoretically, based on the evaluated carbonate content (Table 1) and the above mentioned stoichiometry equation, the Ca/P molar ratio of all the samples measured between 1.670–1.678 which related to the maximum and minimum carbonation level of 2.74 wt% – 5.18 wt%, respectively. However, elemental analysis (Table 1) obtained from ICP evaluation revealed a variation in the Ca/P ratio showing values less than 1.67 and that needed further investigation. Moreover, there was a tendency for an increase in Ca/P molar ratio



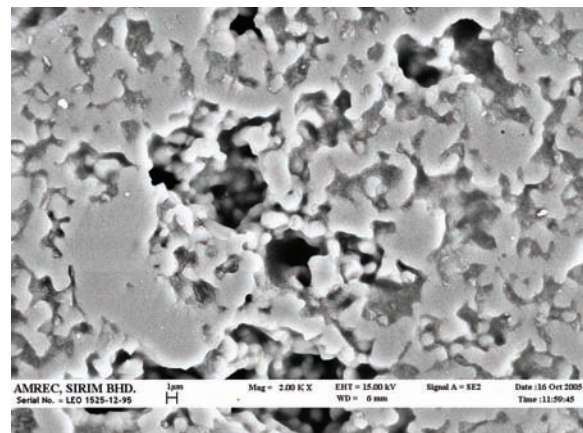
(a)



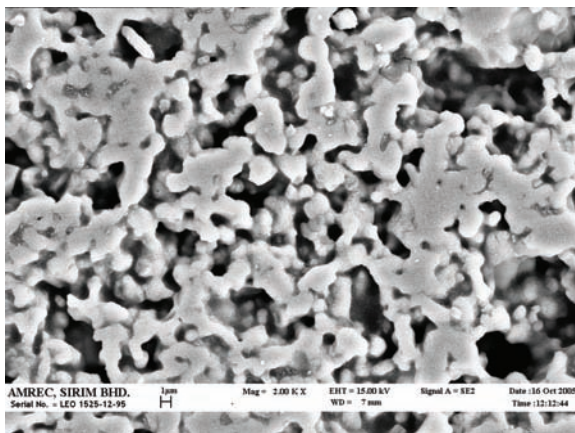
(b)



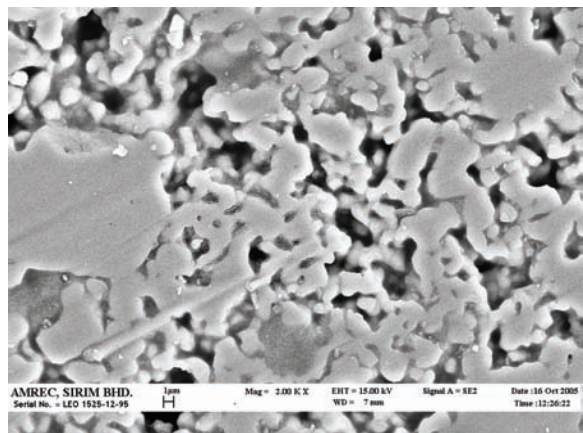
(c)



(d)



(e)



(f)

Figure 3. SEM micrographs of CaP samples obtained from CO₂ flux reaction in the (a) complete cycle (RT-1250°C-RT) and (b-f) cooling processes (1250°C-RT, 1250°C-500°C, 1250°C-600°C, 1250°C-700°C, 1250°C-800°C) of the heat-treatments, respectively.



Table 1. Chemical, physical and mechanical properties of CAp samples reacted with CO₂ flux at different temperature drop ranges.

Sample	CO ₃ ²⁻ content (wt%)	Ca/P molar ratio	True density (gcm ⁻³)	Total porosity (vol%)	Compressive strength (MPa)	Tensile strength (MPa)
RT–1250°C–RT	6.21 ± 0.17	1.617	3.10 ± 0.05	36.88 ± 1.26	27.39 ± 3.79	11.27 ± 1.54
1250°C–RT	5.18 ± 0.15	1.678	3.09 ± 0.03	39.39 ± 1.83	27.99 ± 8.13	8.90 ± 2.83
1250°C–500°C	4.03 ± 0.05	1.671	3.13 ± 0.04	36.81 ± 1.12	29.30 ± 5.24	8.06 ± 2.09
1250°C–600°C	3.53 ± 0.11	1.648	3.11 ± 0.04	39.49 ± 1.92	30.67 ± 4.91	8.08 ± 2.35
1250°C–700°C	3.05 ± 0.61	1.579	3.09 ± 0.01	38.66 ± 0.84	26.90 ± 3.18	9.38 ± 1.85
1250°C–800°C	2.74 ± 0.05	1.592	3.04 ± 0.02	39.30 ± 1.39	28.61 ± 4.06	8.94 ± 2.08

of more than 1.67 due to incorporation of CO₃ ions that substituted for PO₄ ions in the apatite lattice (Kontonasaki *et al.* 2002), as observed in FTIR measurements for a weak B-type substitution. However, that was not revealed in our elemental analysis results and needed further investigation.

In this work, calculated true density values were between 3.04 g/cm³ and 3.11 g/cm³ (Table 1), almost reaching the theoretical density of hydroxyapatite (HA) (3.156 g/cm³). The pycnometer determined that the total pore volume of the heat-treated CAp samples evaluated between 36.81 vol% – 39.49 vol% at different CO₂ flux conditions, which indicated the formation of micro porous CAp samples as evidenced in SEM micrographs (Figure 3). For bulk density measurement, a range of values between 1.86 g/cm³ and 1.97 g/cm³ were recorded. Furthermore, the insignificant changes of density and porosity measurements revealed that the CO₂ flux had a limited influence on the physical properties of CAp samples prepared using relevant chemical precursors and heat-treatment parameters.

Consistent with such results, both the compression and tensile testings showed fluctuating strengths comparable to the physical properties. The effect of different carbonation degrees of CAp prepared at various heat-treatments indicated the insignificant influence on both compressive (26.9 MPa – 30.7 MPa) and tensile (8.06 MPa – 11.27 MPa) strengths (Table 1). One possible factor that might help to explain the observed low and highly deviated statistical results for both strengths was the high internal porosity (~40 vol%) which was inherent in the synthesized samples. Morgan *et al.* 1997 has reported that the compressive strength of dense (porosity <5 vol%) carbonate apatite was 67 MPa which was 54% – 60% higher than the compressive strength of the investigated samples. Thus, it was possible to presume that the porosity in carbonate apatite relatively lowered the compressive strength of the material. Landi *et al.* (2004) also reported that the comparison of literature data about the mechanical resistance of apatite materials was difficult and often impossible due to the non-standardised testing procedures (variety of sintering temperatures, times and atmospheres were reported; inappropriate aspect ratios and small specimen dimensions

were sometimes used; sometimes the highest strength value from the best sample was selectively reported). Thus, the actual cause for the recorded low strengths needed further investigation.

CONCLUSION

Our study revealed that CO₂ flux had shown an influence on the carbonation degree of heat-treated CAp synthesized by solid state reaction in both complete cycle and cooling temperature drops but it did not show any significant influence on both physical and mechanical properties. The results also indicated that the complete formation of CAp with the highest carbonate content was relatively measured at 1250°C – RT. The observed 2.74 wt% – 5.18 wt% of carbonate content was in the reported range found in enamel, dentine and bone, thus providing a simple route to obtain the desired carbonate content suitable for medical applications. The density and porosity values showed that the solid state reaction performed in this study yielded CAp material with the maximum calculated true density of 3.11 g/cm³ and 40 vol% of pores, able to withstand 11.27 MPa of tension and 30.7 MPa of compression. Thus, the effect of internal porosity on the mechanical strength of CAp should be addressed in future studies.

ACKNOWLEDGEMENTS

The authors are grateful to the financial support received from Ministry of Science, Technology and Innovation through IRPA grants 09-01-01-0031 EA001.

Date of submission: August 2008

Date of acceptance: December 2009

REFERENCES

- Apfelbaum, F *et al.* 1992, 'An FTIR study of carbonate in synthetic apatites', *J. Inorg. Biochem.*, vol. 45, pp. 277–282.
- Barinov, SM *et al.* 2006, 'Carbonate loss from two magnesium-substituted carbonated apatites prepared by different

- synthesis techniques', *Mat. Res. Bull.*, vol. 41, pp. 485–494.
- Chaikina, M 1997, 'Mechanochemical synthesis of phosphates and apatites — new way of preparation of complex materials', *Phos. Res. Bull.*, vol. 7, pp. 35–8.
- Fleet, ME & Liu, X 2003, 'Carbonate apatite type A synthesized at high pressure: new space group (P3) and orientation of channel carbonate ion', *J. Sol. Sta. Chem.*, vol. 174, pp. 412–417.
- Fowler BO 1974, 'Infrared studies of apatites II. Preparation of normal and isotopically substituted calcium, strontium and barium hydroxyapatites and spectra-structure-composition correlations', *Inorg. Chem.*, vol. 13, pp. 207–14.
- Kontonasaki, E *et al.* 2002, 'Hydroxy carbonate apatite formation on particulate bioglass in vitro as a function of time', *Cryst. Res. Technol.*, vol. 37, pp. 1165–1171.
- Krajewski, A *et al.* 2004, 'Synthesis of carbonated hydroxyapatites: efficiency of the substitution and critical evaluation of analytical methods', *J. Mol. Struct.*, vol. 3, pp. 1–8.
- Landi, E *et al.* 2004, 'Influence of synthesis and sintering parameters on the characteristics of carbonate apatite', *Biomaterials*, vol. 25, pp. 1763–1770.
- Morgan, EF *et al.* 1997, 'Mechanical properties of carbonated apatite bone mineral substitute: strength, fracture and fatigue behaviour', *J. Mat. Sci.: Mat. In. Med.*, vol. 8, pp. 559–570.
- Oliveira, LMde, Rossi, AM & Lopes, RT 2001, 'Dose response of A-type carbonated apatites prepared under different conditions', *Rad. Phy. Chem.*, vol. 61, pp. 485–487.
- Otsuka, M *et al.* 1994, 'Mechanochemical synthesis of bioactive material: effect of environmental conditions on the phase transformation of calcium phosphates during grinding', *Bio-Med Mater. Eng.*, vol. 4, pp. 357–62.
- Rhee, SH 2002, 'Synthesis of hydroxyapatite via mechanochemical treatment', *Biomaterials*, vol. 23, pp. 1147–1152.
- Roy, DM, Eysel, W, & Dinger, D 1974, 'Hydrothermal synthesis of various carbonate containing calcium hydroxyapatites', *Mat. Res. Bull.*, vol. 9, pp. 35–40.
- Suetsugu, Y *et al.* 2000, 'Structure analysis of A-type carbonate apatite by a single-crystal X-ray diffraction method', *J. Sol. Sta. Chem.*, vol. 155, pp. 292–297.
- Verbeeck, RMH, Maeyer, EAP De, & Driessens, FCM 1995, 'Stoichiometry of potassium and carbonate containing apatites synthesized by solid state reactions', *Inorg. Chem.*, vol. 34, pp. 2084–2088.
- British Standard* 1993, 'Advanced technical ceramics – monolithic ceramics — general and textural properties, Part 2, Determination of density and porosity', *British Standard*, BS EN 623–2, 1993.
- American Standard Methods* 1988, 'Standard test method for compressive (crushing) strength of fired whiteware materials', *ASTM Standard*, C 773–88; 1988.

Communication Systems Melioration by Employing Fast Frequency Hopping Spread Spectrum with Low-density Parity-check Codes

A. Yahya*¹, O. Sidek² and M.F.M. Salleh³

Frequency hopping spread spectrum (FHSS) systems with partial band interference require appropriate compounding of spread spectrum modulation, error correcting code, diversity and decoding method to receive improved transmission signal. In this paper, a fast FHSS system with regular low-density parity-check codes was employed to cater some anti-jamming competence by using good waterfall and error floor performance. The performance evaluation of the previously mentioned system was conducted in the presence of partial band noise jamming. The best possible design of the system was achieved with the combination of diversity level $L=2$ with a probability rate of at 0.7 dB which showed the robustness of the system.

Key words: diversity level; fast frequency hopping spread spectrum; low-density parity-check; partial band noise jamming; transmission signal; simulation; error control coding; orthogonal code

Interference is a fussy problem in the fully crammed 2.4-GHz band, which is license free in most parts of the world. Industrial, scientific, and medical application programs exercise it, and microwave ovens are the crucial perpetrators when it involves interference. In order to edge the effects and essences of interference, frequency hopping spread spectrum (FHSS) techniques are being exercised by Bluetooth and Home radio frequency (RF). The core ability of FHSS is to cut down channel efficiency in support of lustiness and it is easier to enforce than the direct-sequence spread spectrum (DSSS) technique. Distinctive FHSS products inhabit a bandwidth of about 1 MHz and they accomplish higher power within each frequency band at any one time and consequently result in an enhanced instantaneous RF signal to noise ratio than other spread spectrum techniques (Don 2005).

FHSS systems with partial band interference require appropriate compounding of spread spectrum modulation, error correcting code, diversity and decoding method to receive improved transmission signals. An efficient and intelligent jammer usually reduces the efficiency and effectiveness of FHSS; nevertheless, this enhancement can be retained through the use of error control (EC) codes. Additionally, a jammed channel may not be stationary, thus channel state information which is usually called side information, can be employed to advance the performance of EC codes (Don 2005; Simon *et al.*1985; Levitt 1982).

It is recognized that diversity, chained with a forward error correcting code is the most reliable means of crossing the partial-band noise jammer in a FHSS communications system (Berlekamp1980). Great emphasis has been proposed to figure out effective methods of combining the diversity of transmissions. Once block coding with algebraic decoders is applied, then diversity transmissions can be combined and decisions executed on each of the received symbols before a received vector can be decoded.

In this paper, the application of a low-density parity-check (LDPC) code in a fast FHSS was measured and the performance of the LDPC coded system evaluated by using good waterfall and error floor execution. The simulation results signified that the LDPC coded schemes in the aforementioned system were carried out better than in the super orthogonal coded systems.

The error floor in turbo codes can be partially attributed the low-weight codewords in the code which is not ascertained since it is unapproachable to the simulation executed (Benedetto *et al.* 1996). Recent simulation of LDPC codes carried out on high speed hardware platforms indicates that LDPC codes exhibit error floors.

Recent research has indicated that the weight 2 bit nodes are authoritative in permitting good waterfall performance as well as raise the error floor for shorter block lengths,

¹School of Computer and Communication Engineering, University Malaysia Perlis, 02000 Kuala Perlis, Perlis, Malaysia

²Collaborative MicroElectronic Design Excellence Centre, Universiti Sains Malaysia, Engineering Campus, Malaysia, 14300 Nebong Tebal, Penang, Malaysia

³School of Electric and Electronics, Universiti Sains Malaysia, 14300 Nebong Tebal, Penang, Malaysia

*Corresponding author (e-mail: abidusm@gmail.com)

and irregular codes (Changyan *et al.* 1989). These nodes are arranged in a form of set and if there were any error, it compels the decoder not to decode the sequence correctly. The appropriate emplacement and confinement of the number of weight 2 nodes is the solution to enhance the performance of these codes for shorter block lengths.

Schremmer (2002) has investigated the pertinence of an irregular LDPC code at a rate $\frac{1}{2}$, having a block length of 1560 bits to a frequency hopped communications system with partial-band jamming. The decoder of the system is appropriate for a maximum of 60 iterations by employing coherent binary phase-shift keying.

In this paper, regular LDPC codes with a diversity order were employed with fast FHSS in a criterion error correction role to cater some anti-jamming competence which improved the quality of transmission signal. LDPC code possesses a low probability of decoding error, and has a simple instrumental algorithm to develop erasure information.

Various measures have been taken into account while considering coding for spread spectrum communications in the presence of partial band interference. The prime concern is whether the decoder experiences if the received signal has been jammed or not. Logically the decoder acknowledges and applies this side information in order to enhance the performance and equates the coding without the side information. An additional issue is interleaving.

If lower quality performance is expected hardware savings can be achieved by various means. This paper furnishes an analytical framework for assessing the performance of transmission signal using coded FHSS systems operating in the presence of jamming. The LDPC codes were employed as forward error control coding which covered each codeword of the orthogonal code as a single character in its large alphabet. Nevertheless, the LDPC as compared to other FEC coding had the noteworthy property that it was capable of correcting any character erasure.

FREQUENCY HOPPING SPREAD SPECTRUM

Frequency hopping is the most authentic and facile spread spectrum modulation to employ. Any radio comprising a digitally controlled frequency synthesizer can theoretically be converted to a frequency hopping radio. The addition of a Pseudonoise (PN) code generator is the core component of this conversion which selects the frequencies for transmission or reception. Most hopping systems use uniform frequency hopping over a band of frequencies. This is not essential, if both the transmitter and receiver of the system have determined in advance what are the frequencies to be skipped. Thus a frequency hopper of two meters could skip over commonly used repeater frequency

pairs. A frequency hopped system uses analog or digital carrier modulation by employing conventional narrow band radio techniques. Receiver de-hopping is accomplished by a synchronized PN code generator that drives the receiver's local oscillator frequency synthesizer (Dixon 1984; Simon *et al.* 2004).

FHSS splits the available frequency band into a series of subchannels. A transmitter hops from subchannel to subchannel, communicating short bursts of data on each channel for a predestinate period, adverted to as dwell time. The hopping sequence is apparently synchronized between transmitter and receiver to enable communications to occur. Federal Communications Commission regulations delineate sizing of the frequency band, the number of channels that can be employed, and the dwell time and power level of the transmitter.

A pseudorandom sequence is used to control the narrowband signal hops from one frequency to another in the FHSS. This results in a signal's dalliance at a predestinate frequency for a brisk period of time, resultantly in the possibility of interference from another signal source generating radiated power as a specific hop frequency is keyed in.

The effectuation of FHSS operating in the presence of partial band noise jamming and additive white Gaussian noise with one hop per signalling interval has already been examined (Simon *et al.* 1981; Chernbini & Milstein 1989; Su & Milstein 1989). Su and Milstein (1989) have proposed a system, based on the premise of synchronized time and phase, with the performance of a coherent FHSS system with quadrature modulations under the worst case of partial band noise jamming. The performance abjection due to fallible synchronization has been discussed by Chernbini and Milstein (1989), and Su and Milstein (1989). In order to rejuvenate the non-coherent demodulation and combination loss, a frequency diversity intrigue has been implemented for a phase-coherent FHSS system with partial band noise jamming (Lance & Kaleh 1998).

In the FHSS the receiver has bandwidth coped with data modulation, and accompanies the transmitter as it jumps around the band. If one of those jumps encounters a narrowband interferer, then the communications on that channel can be jammed. On the next jump, the narrowband interferer will be moved. This causes the receiver's electivity filters to eradicate the narrowband interferer, essentially independent of its power.

Applications of Frequency Hopping Spread Spectrum

FHSS is an executable option to direct sequence spread spectrum (DSSS) for protection against jamming and for code division multiple access (CDMA). In CDMA systems

established on FHSS, each pair of transmitter-receiver is assigned its own unique pseudorandom frequency hopped pattern. Excursus from this distinguishing feature, the transmitters and receivers, of all users may be indistinguishable, i.e. they have identical encoders, decoders, modulators and demodulators.

CDMA systems based on FHSS are especially generative for mobile users because the synchronization pre-requisites are not as rigorous as in DSSS systems. Additionally, frequency synthesis techniques and colligated hardware have been developed that make it possible to hop over bandwidth that are significantly wider, by one or more orders of magnitude, corresponding to those presently conceivable with DSSS signals. Therefore, larger processing gains are easily conceivable by FHSS which more than countervail the loss in operation congenital in noncoherent detection of frequency shift keying (FSK) modulated signals.

FHSS is very efficient against jamming signals. FHSS employing the FSK modulation system that implements coding, or merely repeats the information symbol on multiple hops, is very effective against a partial band jammer. As an aftermath, the jammer's threat is reduced to that of an equivalent broadband noise jammer whose transmitter power is spread across the channel bandwidth W .

OVERVEIW OF LOW DENSITY PARITY CHECK

LDPC codes are a category of linear codes which cater near capacity performance on a large collection of data transmission and storage channels whilst concurrently accommodating executable decoders. LDPC was invented by Gallager in early 1960 (Gallager 1960). LDPC codes are rendered with probabilistic encoding and decoding algorithms. Earlier, sparse random parity check matrices were being used which established promising distance properties (Gallager 1960).

LDPC codes are designated by a parity check H matrix comprising largely 0's and has a low density of 1's. More precisely, we can articulate that LDPC codes have very few 1's in each row and column with large minimum distances. Specifically, a (n, j, k) low-density code is a code of block length n and source block length k . The number of parity checks is delimited as: $m = n - k$. The parity check matrix weight (number of ones in each column or row) for LDPC codes can be either regular or irregular. LDPC is regular if the number of ones is constant in each column or row and gets irregular with a variable number of ones in each column or row.

A regular LDPC code is a linear block code whose parity-check matrix H constitutes exactly w_c 1's in each

column and exactly $w_r = w_c \binom{n}{m}$ 1's in each row, where $w_c m$ (equivalently, $w_c m$). The code rate $R = 1 - w_c/w_r$. Generally, irregular LDPC codes surpass regular LDPC codes.

Low density codes are not that much optimal in the fairly contrived sense of understating the probability of decoding error for a known block length, and it can be illustrated that the minimum rate being employed by them is bounded below channel capacity. Nevertheless, the simple decoding scheme innovation more than remunerates for these disadvantages.

LDPC codes have a congenital error detection capability, for instance one can merely check if the decoded sequence is an applicable code word by multiplying by the parity check matrix.

FORWARD ERROR CORRECTION CONTROL SYSTEM MODEL

The block diagram of fast FHSS with LDPC codes is shown in Figure 1 in which the LDPC encoder carried out in the similar way as any linear block code, by acknowledging its generation or parity check matrix. The frequency hopping patterns shaped by the receiver synthesizer and the transmitter were synchronized with each other, but counterbalanced by a fixed intermediate frequency which might be zero. The mixing function bumped off the frequency hopping pattern from the received signal. The mixer output was enforced to a band pass filter that expeled the double frequency components and power, that initiated outside the suitable frequency channel and brought forth the data modulated dehopped signal. The output of the dehopper was a sequence which comprised L diversity receptions for every n code symbol. Side information, considering the presence of interference, was distilled from the dehopper and demodulator. The L diversity receptions of a specified symbol were engaged along with the side information to form the decision statistic. A hard decision M -ary had to be prepared on the symbol, and this decision was coursed into the error-correction decoder. The probability of a bit error is represented by:

$$p = Q\left(\sqrt{\frac{2RE_b}{N_o}}\right) \quad \dots 1$$

where,

$R = k/n$ is the code rate.

The probability of decoding error was set by:

$$P_e(C) \leq \sum_{i=t+1}^n \binom{n}{i} p^i (1-p)^{n-i} \quad \dots 2$$

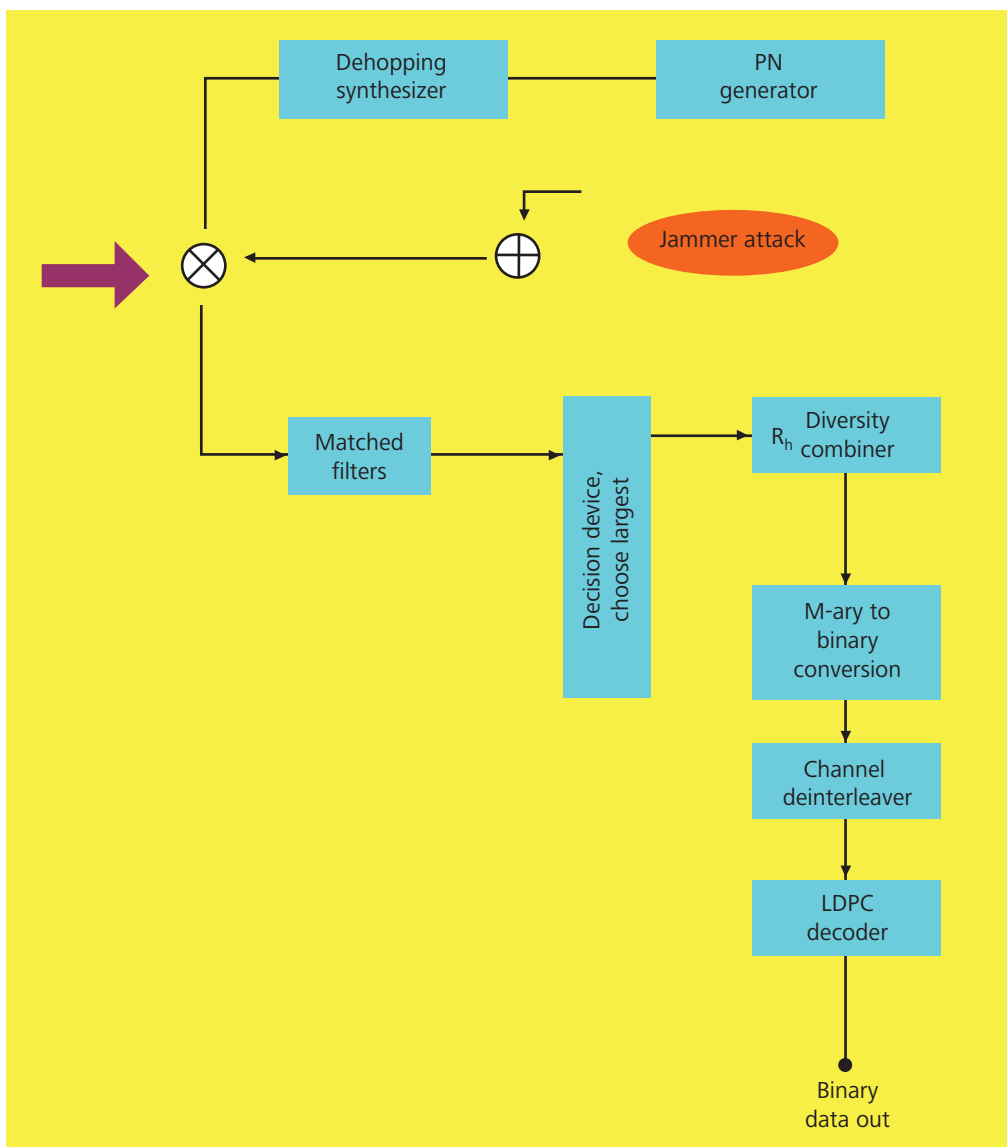
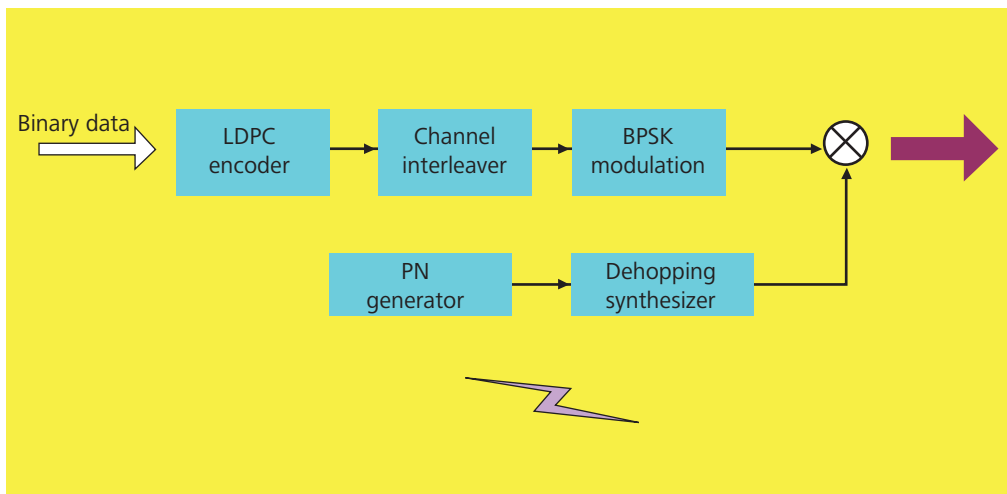


Figure 1. Block diagram of fast FHSS with LDPC encoder and decoder.

In this paper we accept that channel monitoring furnishes information about the state of the channel either in the presence or absence of jamming which could be exploited by the LDPC decoder to wipe out the symbols which were subject to heavy interference. In such cases the decoder sought to correct the erasures and the few errors that result of thermal noise with diversity technique. Once the number of erasure was larger than $e = n - k$, then the probability of error was set by:

$$P_{e,s;2} = \sum_{j=e+1}^n \binom{n}{j} \epsilon_s^j (1-\epsilon_s)^{n-j} \sum_{\substack{l_1+l_2=j \\ l_1 \leq j \\ l_2 \leq n-j}} \frac{l_1+l_2}{n} \binom{j}{l_1} p^{-l_1} (1-p)^{j-l_1} \binom{n-j}{l_2} P_o^{l_2} (1-P_o)^{n-j-l_2} \dots 3$$

In the aforementioned equation, p constituted the probability of error when there was partial band or multiple access interference and was established by:

$$p = \frac{\epsilon_1}{\epsilon_s} \left[1 - (1 - P_{J,o})^m \right] + \frac{\epsilon_2}{\epsilon_s} \left(1 - \frac{1}{M^m} \right) \dots 4$$

whereas ϵ_1 and ϵ_2 correspond to the probability of being jammed when not hit by the users and when hit by the users correspondingly.

RESULTS AND DISCUSSION

The coupling of diversity of order L with LDPC codes was examined in this paper. Most of the work was done on FHSS employing Reed Solomon coding since it was easy to keep up the phase coherence. Whilst employing fast frequency hopping it was inconceivable to perform differential detection within one hop. In this paper LDPC codes were employed in a criterion error correction role to cater some anti-jamming competence. The simulation results signified that the LDPC coded schemes in the aforementioned system were carried out better than the super orthogonal coded systems. The best possible design of the system with the combination of diversity and forward error correcting coding by employing binary phase shift keying was exploited in the system and their simulation results were illustrated in Figure 2. The channel coding code rate of $\frac{1}{2}$ was used for the 5120 block length data which was ready to confront any type of interference. A plot of probability of error as a function of E_b / N_J was shown in Figure 3 for $L=2$ when the system was under hostile partial band noise jamming. The proposed system coupled with LDPC showed better performance as compared to the system discussed by Tatsunami *et al.* (2006). The usance of hard decision decoding made the system more consistent as portrayed from the frequency response of the spread signal depicted in Figure 4. These results cater for information on the design of the robust system.

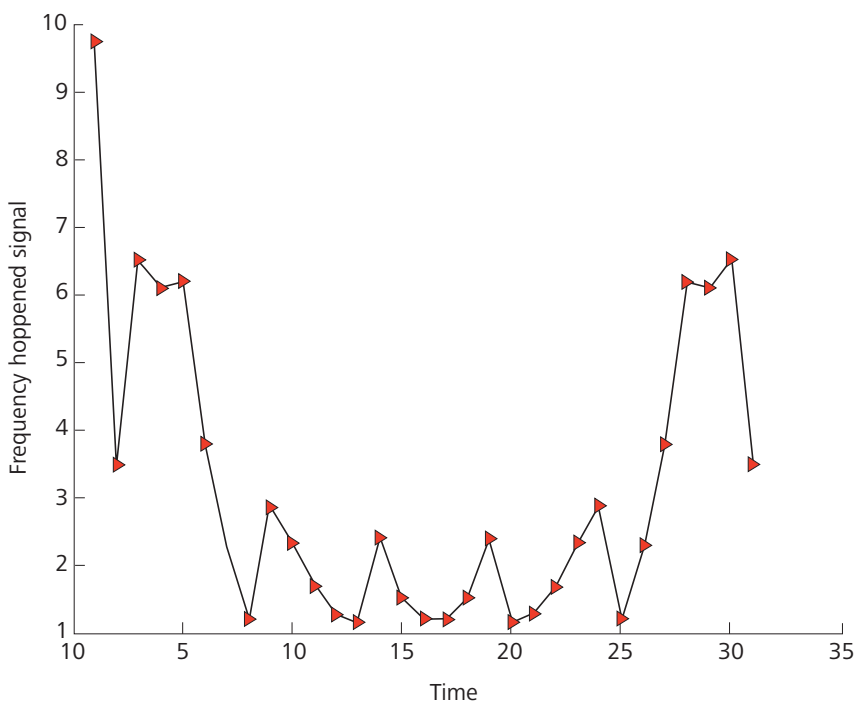


Figure 2. Fast frequency hopping spread spectrum using LDPC as a FEC.

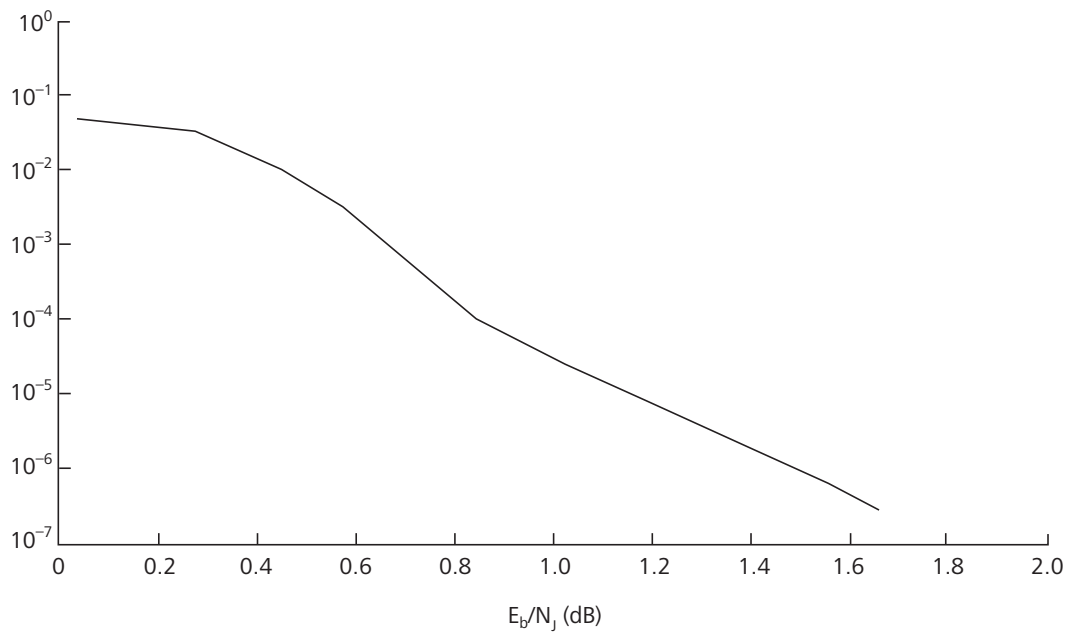


Figure 3. Probability of error for diversity level $L=2$.

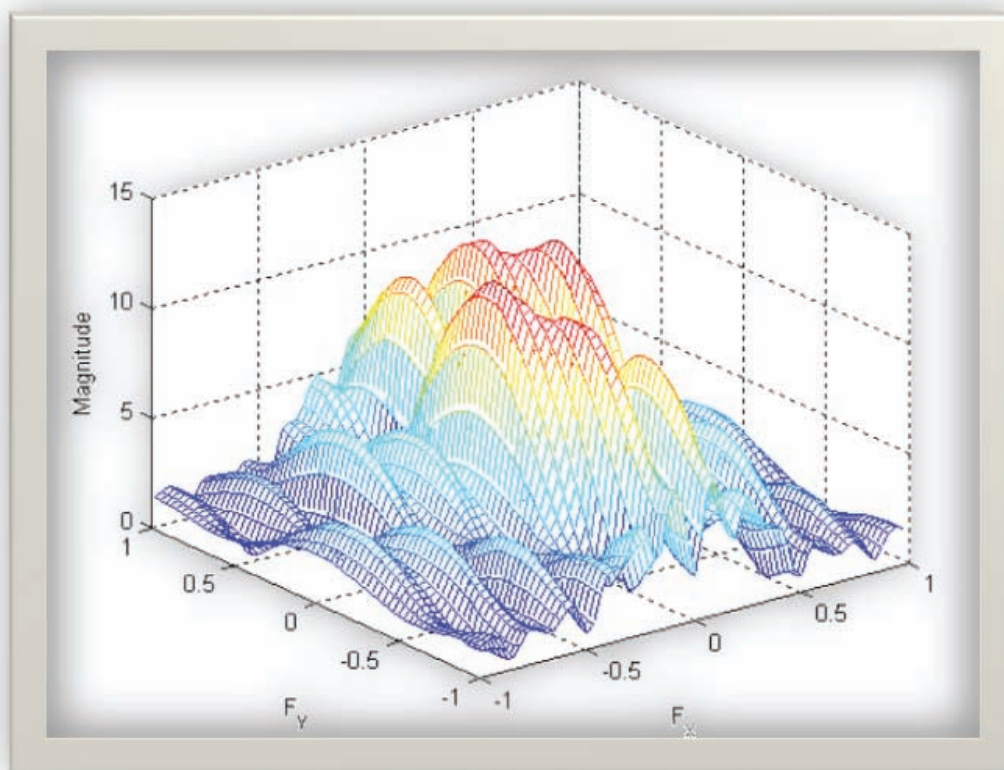


Figure 4. Frequency response of the spread signal.

CONCLUSION

Hardware savings can be accomplished by various means if low performance is tolerated. This paper offers an analytical framework for evaluating the performance of transmission signal utilizing coded fast FHSS systems functioning in the presence of partial band noise jamming. The regular LDPC codes were applied as forward error control coding which addressed each codeword of the orthogonal code as a single character in its large alphabet. The decreased computational complexity and inherent error checking ability of these codes could tender a high-quality substitute to Turbo Codes.

Date of submission: August 2008

Date of acceptance: December 2009

REFERENCES

- Benedetto, S & Montorsi, G 1996 'Unveiling turbo codes: some results on parallel concatenated coding schemes', *IEEE Trans. Inform. Theory*, vol. 42, pp. 409–428.
- Berlekamp, ER 1980, 'The technology of error correcting codes', in *Proc. IEEE.*, vol. 68, pp. 564–593.
- Chernbini, G & Milstein, LB 1989, 'Performance analysis of both hybrid and frequency-hopped phase coherent spread spectrum systems Part I: A hybrid DS/FH system', *IEEE Trans. Commun.*, vol. 37, pp. 600–611.
- Cherubini, G & Milstein, LB 1989, 'Performance analysis of both hybrid and frequency-hopped phase coherent spread spectrum systems Part 11: an FH system', *IEEE Trans. Commun.*, vol. 31, pp. 612–622.
- Changyan, D Proietti, D Telatar, E Richardson, T & Urbanke, R 'Finite-length analysis of low-density parity-check codes on the binary erasure channel', <<http://lthcwww.epfi.chj>>.
- Don, T 2005, *Principles of spread spectrum communication system*, Springer, New York.
- Dixon, RC 1984, *Spread spectrum systems*, John Wiley & Sons, Inc. Gallager, RG 1962, 'Low-density parity-check codes', *IEEE Transactions on Information Theory*, vol. 8 no. 1, pp. 21–28.
- Lance, E & Kaleh, GK 'A diversity scheme for a phase-coherent frequency-hopping spread-spectrum system', *IEEE Trans. Commun.*, vol. 45, pp. 1123–1129.
- Levitt BK 1982 'Use of diversity to improve FH/MFSK performance in worst case partial band noise and multitone jamming', *IEEE Milcomm.*, vol. 3 no. 81, pp. 28.2.1–5.
- Schremmer, SH 2002 'Low density parity check codes in a frequency hopped communication system with partial-band interference', in *Proc. IEEE Military Communications Conference (MILCOM 2002)*, pp. 895–899.
- Simon, MK *et al.* 1985, *Spread spectrum communications*, vol.1. Rockville, MD: Computer Science.
- Simon, MK *et al.* 2002, *Spread spectrum communication handbook*, McGraw Hill, USA.
- Simon, MK & Polydoros, A 1981, 'Coherent detection of frequency-hopped quadrature modulations in the presence of jamming part I: QPSK and QASK modulations', *IEEE Trans. Commun.*, vol. 29, pp.1644–1660.
- Su, CM & Milstein, LB 1990 'Analysis of a coherent frequency-hopped spread-spectrum receiver in the presence of jamming', *IEEE Trans. Commun.*, vol. 38, pp. 715–725.
- Tatsunami, H Ishibashi, K & Ochiai, H 2006 'On the performance of LDPC codes with differential detection over rayleigh fading channels', in *Proceedings IEEE, Vehicular Technology Conference, VTC 2006-Spring*. vol. 5, pp. 2388–2392.

Ionic Conductivity and Morphological Studies of Plasticized Poly(methyl methacrylate) Polymer Electrolyte Films

Z. Osman^{1*}, L. Othman¹, K.B. Md Isa¹, A. Ahmad¹ and N. Kamarulzaman²

In this study polymer electrolytes composed of poly(methyl methacrylate) (PMMA) as a host polymer and ethylene carbonate (EC) as a plasticizer complexed with different lithium salts, i.e. lithium tetrafluoroborate (LiBF₄) and lithium triflate (LiCF₃SO₃) were prepared by the solution casting technique. The conductivities of the films were characterized by impedance spectroscopy. At room temperature, the highest conductivities were $4.07 \times 10^{-7} \text{ S cm}^{-1}$ and $3.40 \times 10^{-5} \text{ S cm}^{-1}$ achieved, respectively from the films containing 30 wt% LiBF₄ in the PMMA-EC-LiBF₄ system and 35 wt% LiCF₃SO₃ in the PMMA-EC-LiCF₃SO₃ system. The conductivity-temperature dependence of the films seemed to obey the Arrhenius equation in which the ion transport in these materials was thermally assisted. Scanning electron microscopy analysis showed that the surface of PMMA-EC-LiCF₃SO₃ film was smooth and homogeneous, hence lithium ions could traverse through the PMMA-EC-LiCF₃SO₃ film more easily compared to the PMMA-EC-LiBF₄ film. X-Ray diffraction studies revealed that complexation had occurred and the complexes formed were amorphous.

Key words: polymer electrolytes; conductivity; plasticizer; lithium salts; SEM; X-Ray diffraction

Solid polymer electrolytes (SPEs) have received increasing attention due to their potential applications in solid state batteries, electrochromic windows supercapacitors and electrochemical sensors (Armand 1986; Sung *et al.* 2005; Qizhen *et al.* 2009). The major advantages of SPEs are favourable mechanical properties, ease of fabrication of thin films, the elimination of leakage possibility and wide electrochemical stability windows over liquid electrolytes (Nan *et al.* 2003; Bhattacharyya *et al.* 2005). The SPE that can conduct ions is formed by dissolving suitable inorganic salts into a polymer matrix.

Numerous approaches have been employed to enhance the ionic conductivity and mechanical stability of polymer electrolytes. These approaches include: synthesizing new polymers (Xu & Wang 1993; Selvaraj *et al.* 1995; Huang *et al.* 1996); blending of two polymers (Baskaran *et al.* 2006) and adding plasticizers to polymer electrolytes to form plasticized polymer electrolytes (Nagasubramanian *et al.* 1994; Tallworth *et al.* 1995; Morales & Acosta 1997; Abbrent *et al.* 1998). Besides reducing the crystalline content and increasing the polymer segmental mobility, the addition of plasticizers such as propylene carbonate (PC) and ethylene carbonate (EC) to polymer electrolytes also can result in greater ion dissociation which allows greater numbers of charge carriers for ionic transport (Song *et al.*

1999). Among the host polymers used for such plasticized electrolytes are poly(methyl methacrylate) (PMMA) (Bohnke *et al.* 1993), poly(acrylonitrile) (PAN) (Hong *et al.* 1992; Peramunage *et al.* 1995) and poly(vinyl chloride) (PVC) (Alamgir & Abraham 1993).

In attempts to look for good lithium ion conducting polymers, plasticized polymer electrolyte systems composed of PMMA as a host polymer and EC as a plasticizer complexed with different lithium salts, i.e. lithium tetrafluoroborate (LiBF₄) and lithium triflate (LiCF₃SO₃) have been prepared. In this work, the ionic conductivity and morphological studies of the PMMA-based polymer electrolytes were analyzed using impedance spectroscopy, scanning electron microscopy (SEM) and X-ray diffraction (XRD) techniques.

MATERIALS AND METHODS

Sample Preparation

PMMA with molecular weight of $9.96 \times 10^5 \text{ g/mol}$ (Aldrich) was dissolved in tetrahydrofuran (THF) solvent. The plasticizer, EC (Fluka) and the lithium salts LiBF₄ and LiCF₃SO₃ (Aldrich) were added accordingly. The

¹Physics Department, University of Malaya, 50603 Kuala Lumpur, Malaysia

²Institute of Science, University Technology of MARA, 40450 Shah Alam, Selangor, Malaysia

*Corresponding author (e-mail: zurinaosman@um.edu.my)

amount of plasticizer was fixed at 35 wt%. The mixtures were continuously stirred with a magnetic stirrer for several hours. After complete dissolution, the solutions were cast in petri dishes and left to dry by solvent evaporation at room temperature to form films. The films were then kept in a desiccator until characterizations were carried out.

Impedance Spectroscopy

A HIOKI 3531 LCR bridge that had been interfaced with a computer was used to perform the impedance measurement for each polymer electrolyte film in the frequency range of 50 Hz to 1 MHz. To measure the impedance of the films, the samples were cut into a round shape that fit the size of the electrodes. The samples were then sandwiched between two stainless steel blocking electrodes with a diameter of 2 cm. From the Cole–Cole plots obtained, the bulk resistance, R_b , of each sample was determined and hence the conductivity (σ) of the samples were then calculated using $\sigma = t/R_b A$; where t is the sample thickness (cm), A the effective contact area of the electrode and the electrolyte (cm²), and R_b is the bulk resistance (Ω). The conductivity-temperature studies were carried out in the range of temperature from 303 K to 373 K.

Scanning Electron Microscopy (SEM)

The films were vacuumed after sputtering with gold at 25 mA for 40 s. The surface morphology of the film was observed by SEM (Stereoscan 420, Leica).

X-Ray Diffraction (XRD)

To study the extent of crystallinity, XRD was carried out with a D5000 diffractometer which employed Cu-K α radiation.

RESULTS AND DISCUSSION

Conductivity Studies

The plots of conductivity versus amount of LiBF₄ and LiCF₃SO₃ in the salted-PMMA systems are shown in Figure 1. It can be observed that the highest room temperature conductivity was obtained from the films containing 40 wt% LiBF₄ in the (PMMA-LiBF₄) system and 40 wt% LiCF₃SO₃ in the (PMMA-LiCF₃SO₃) system with the values 3.66×10^{-7} S cm⁻¹ and 3.97×10^{-6} S cm⁻¹ respectively.

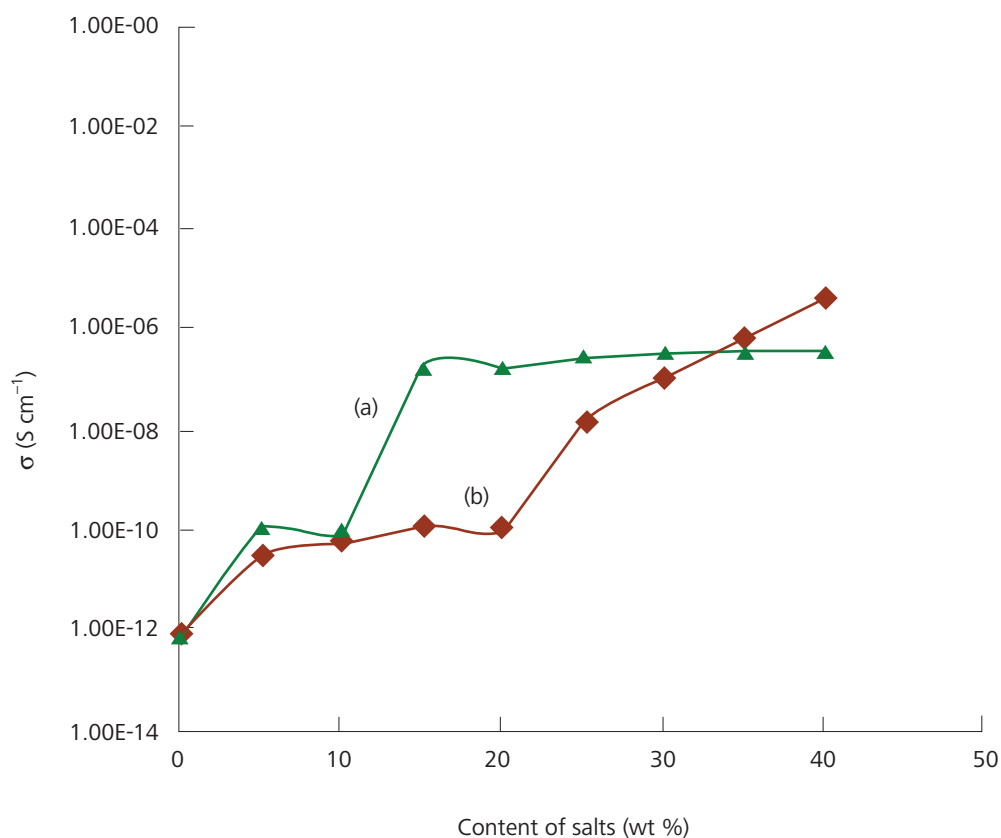


Figure 1. Variation of conductivity with salts content in (a) PMMA-LiBF₄ and (b) PMMA-LiCF₃SO₃ systems.

Figure 2 depicts the plots of conductivity versus salt content for plasticized PMMA containing LiBF_4 and LiCF_3SO_3 . The highest room temperature conductivity was $4.07 \times 10^{-7} \text{ S cm}^{-1}$ and $3.40 \times 10^{-5} \text{ S cm}^{-1}$, achieved respectively from the films containing 30 wt% LiBF_4 in the (PMMA-EC- LiBF_4) system and 35 wt% LiCF_3SO_3 in the (PMMA-EC- LiCF_3SO_3) system. The conductivity of the unplasticized systems was increased upon the addition of plasticizer, EC. This showed that the apparent roles of a plasticizer in a host polymer were to decrease the viscosity of the electrolyte and assist in the dissociation of the salts thereby increasing the number of charge carriers (MacFarlane *et al.* 1995). It could be deduced that EC has dissociated more LiCF_3SO_3 salt compared to LiBF_4 salt, thereby increasing the number of charge carriers in (PMMA-EC- LiCF_3SO_3) film. Higher conductivity in the (PMMA-EC- LiCF_3SO_3) film was due to the higher number of mobile ions it contained. When the salt content was increased, the free ions also increase until it was saturated when more salt was added. This made these ions become closer to one another. Since the ions were so close to one another, the conductivity decreased.

Figure 3 represents the variation of ionic conductivity with the reciprocal temperature for the highest conducting

films from (PMMA-EC- LiBF_4) and (PMMA-EC- LiCF_3SO_3) systems, respectively. The linear variation of $\log \sigma$ versus $1000/T$ plots indicated an Arrhenius type thermally activated process (MacDonald 1987; Hagenmuller & Gool 1978; Julien & Nazri 1994). It was observed that as temperature increased, the conductivity increased and this implied that temperature had increased the degree of salt dissociation into ions. The activation energy, E_a for films of (PMMA-EC- LiBF_4) and (PMMA-EC- LiCF_3SO_3) were 0.29 eV and 0.27 eV, respectively. The low activation energy, E_a for the lithium ion transport was due to the completely amorphous nature of the polymer electrolytes that facilitated the fast Li^+ ion motion in the polymer network. The completely amorphous nature also provided a larger free volume in the polymer electrolyte system upon increase in temperature (Michael *et al.* 1997).

SEM Analysis

A porous surface was discovered in PMMA- LiBF_4 and PMMA-EC- LiBF_4 films as shown in Figure 4. It could be observed that the size of the pores was decreased when the plasticizer EC was added to the PMMA- LiBF_4 film.

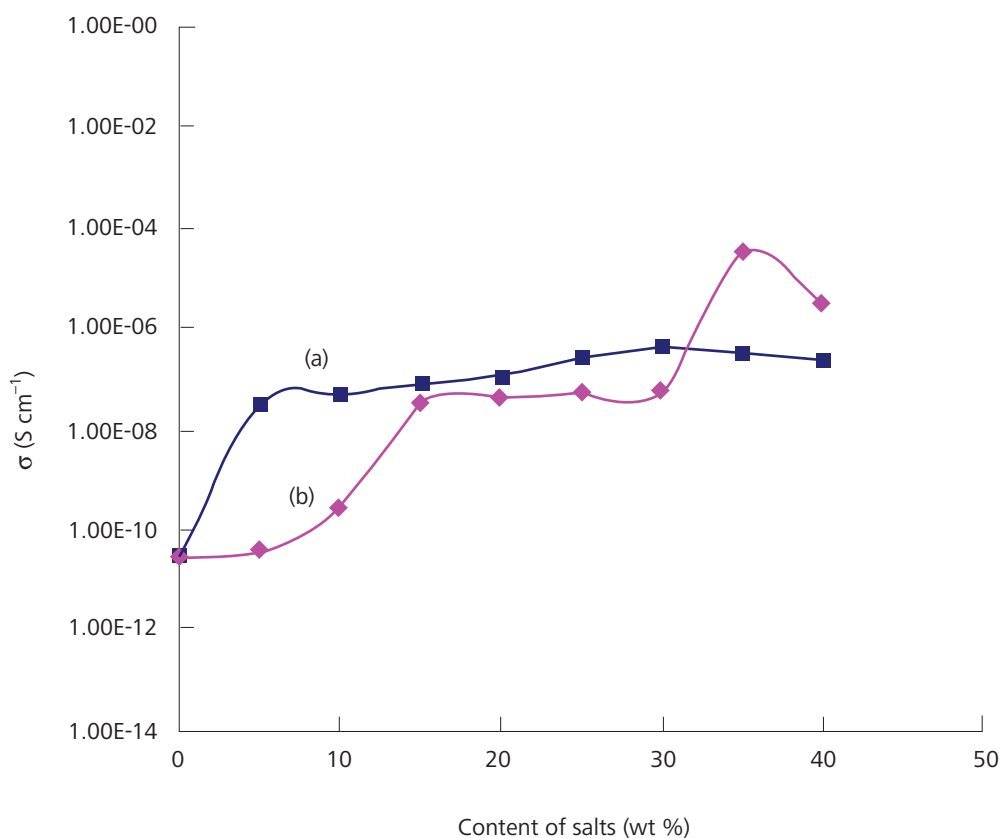


Figure 2. Variation of conductivity with salt content in (a) PMMA-EC- LiBF_4 and (b) PMMA-EC- LiCF_3SO_3 systems.

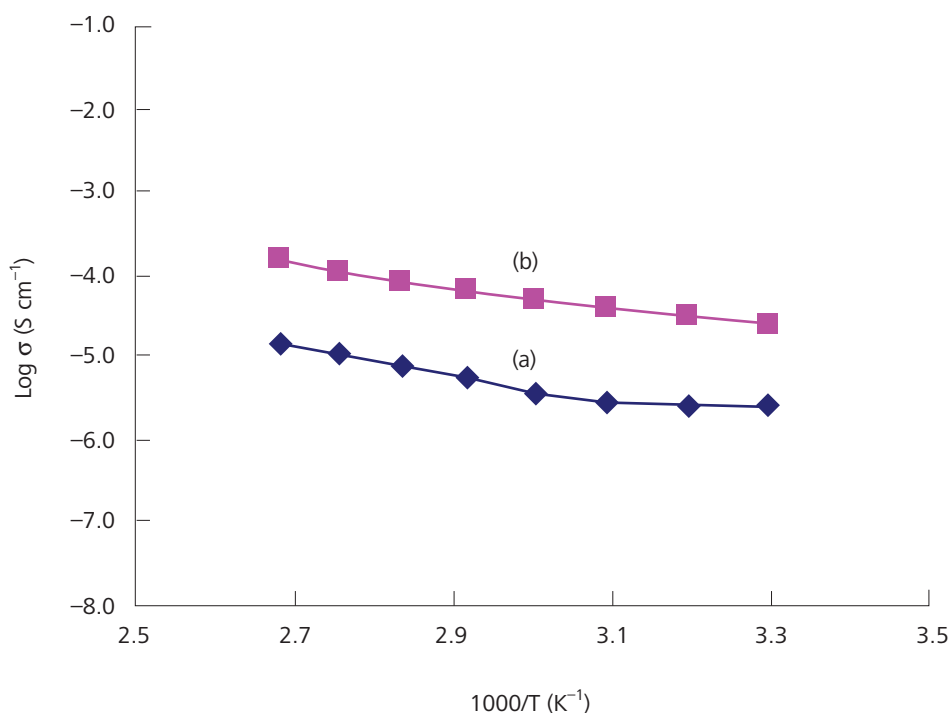
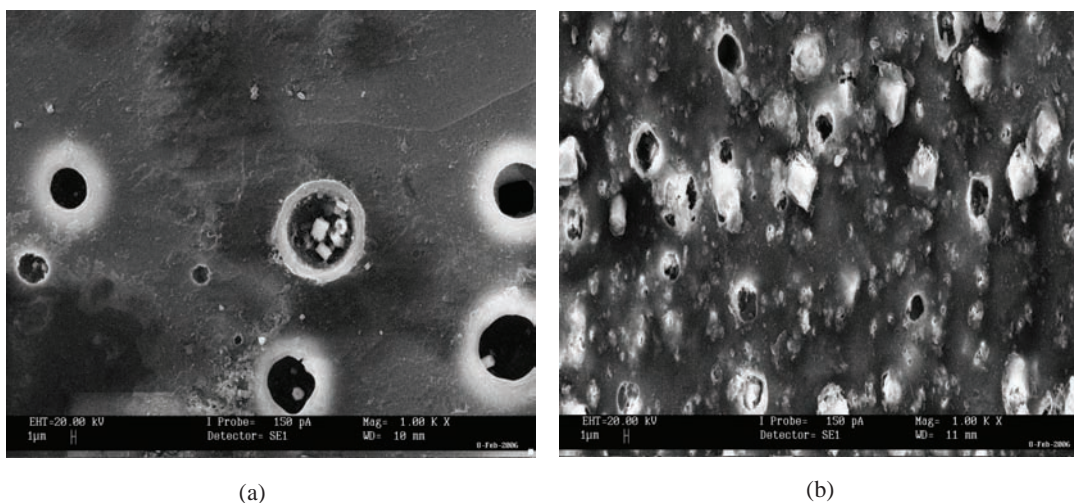


Figure 3. Arrhenius plot for (a) PMMA-EC-LiBF₄ and (b) PMMA-EC-LiCF₃SO₃ films.



(a)

(b)

Figure 4. SEM images of (a) PMMA-LiBF₄ and (b) PMMA-EC-LiBF₄ films.

Figure 5 shows the SEM micrographs of PMMA-LiCF₃SO₃ and PMMA-EC-LiCF₃SO₃ film. The amorphous phase was observed to be prominent in these images. The surface of these film was smooth and homogenous and this was expected to continue in the bulk. Hence, lithium ions could traverse through the triflate film more easily compared to the hexafluoroborate film resulting in the triflate film being more conductive.

XRD Studies

Respective XRD patterns obtained for pure PMMA, LiBF₄, LiCF₃SO₃, PMMA-EC-LiBF₄ and PMMA-EC-LiCF₃SO₃ films are shown in Figure 6. The amorphous and crystalline phase of the polymer and salts were observed. Most of the peaks pertaining to LiBF₄ disappeared in the PMMA-EC-LiBF₄ film and indicated the complete dissolution of the

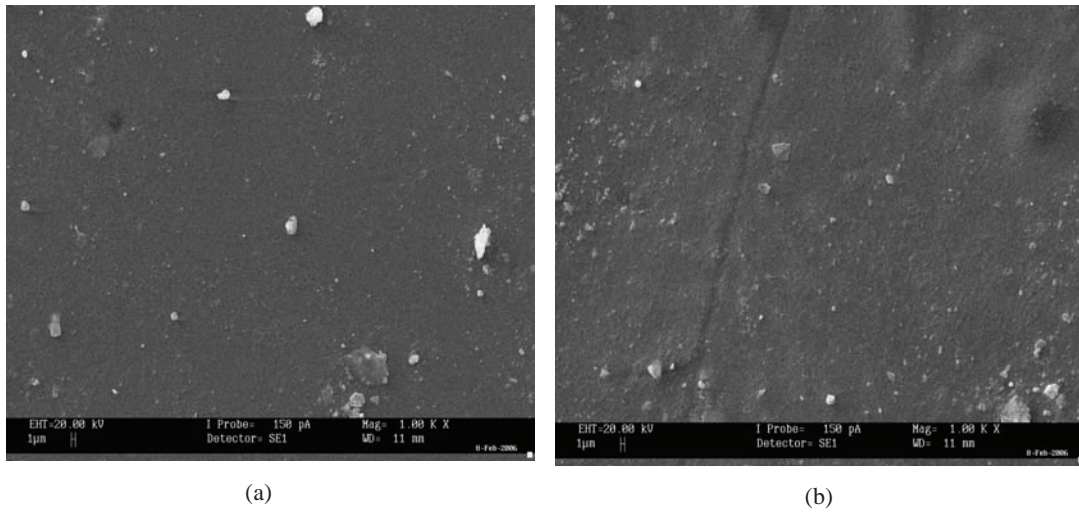


Figure 5. SEM images of (a) PMMA-LiCF₃SO₃ and (b) PMMA-EC LiCF₃SO₃ films.

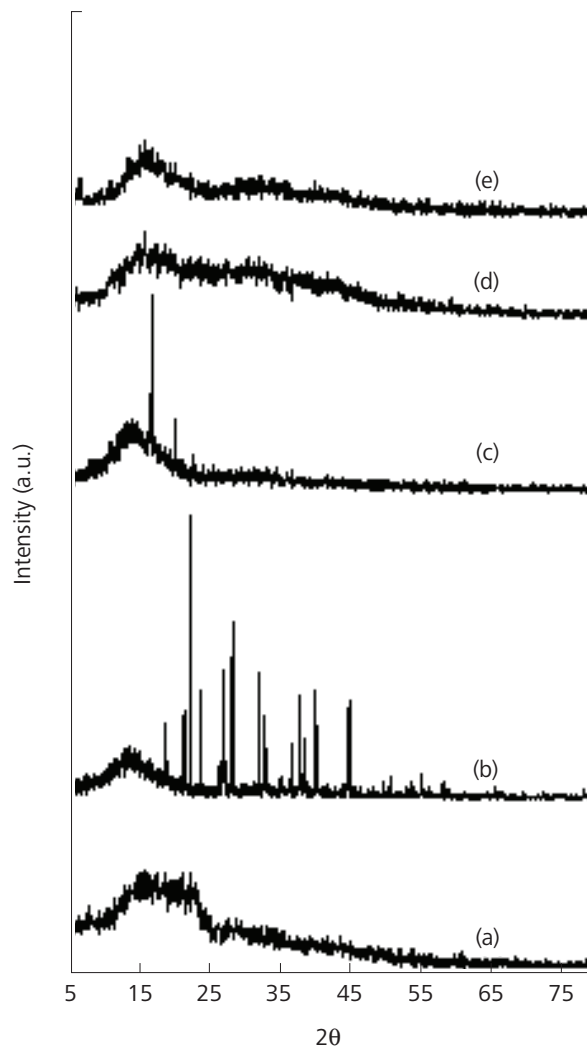


Figure 6. XRD patterns of (a) pure PMMA, (b) LiBF₄, (c) LiCF₃SO₃, (d) PMMA-EC-LiBF₄ and (e) PMMA-EC-LiCF₃SO₃ films.



salt in the plasticized polymer matrix. The sharp peaks at $2\theta = 16.6^\circ$, 19.8° and 22.5° of LiCF_3SO_3 are absent in PMMA-EC- LiCF_3SO_3 film.

These results reveal that complexation had occurred and the complexes formed were amorphous. Berhier *et al.* (1983) established that ionic conductivity in polymer electrolytes is associated with the amorphous phase of the studied films. The higher conductivity observed in the plasticized salted films was believed to result from the lower degree of crystallinity that assisted lithium ion movement in the polymer network, which was confirmed from the XRD patterns.

CONCLUSIONS

The ionic conductivity behaviour of plasticized PMMA films containing the LiBF_4 and LiCF_3SO_3 salts was studied. The room temperature conductivity for the highest conducting film in the (PMMA-EC- LiBF_4) and (PMMA-EC- LiCF_3SO_3) systems were $4.07 \times 10^{-7} \text{ S cm}^{-1}$ and $3.40 \times 10^{-5} \text{ S cm}^{-1}$, respectively. LiCF_3SO_3 was easily dissociated by EC compared to LiBF_4 . The porosity of LiBF_4 film probably hindered lithium ion movement on the surface and in the bulk, resulting in its lower conductivity. XRD studies showed that the conductivity was increased when the crystallinity of the film was reduced.

ACKNOWLEDGEMENTS

The authors would like to thank the University of Malaya and Academy of Sciences Malaysia for the grants awarded.

Date of submission: May 2008

Date of acceptance: April 2010

REFERENCES

- Abbrent, S, Lindgren, J, Tegenfeldt, J & Wendsjo, A 1998, 'Gel electrolytes prepared from oligo(ethylene glycol) dimethacrylate: glass transition, conductivity and Li^+ -coordination', *Electrochim. Acta*, vol. 43, pp. 1185–1191.
- Alamgir, M & Abraham, KM 1993, 'Li ion conductive electrolytes based on poly(vinyl chloride)', *J. Electrochem. Soc.*, vol. 140, no. 6, pp. L96–L97.
- Armand, MB 1986, 'Polymer electrolytes', *Annual Review of Materials Science*, vol. 16, pp. 245–261.
- Baskaran, R *et al.* 2006, 'Conductivity and thermal studies of blend polymer electrolytes based on PVAc-PMMA', *Solid State Ionics*, vol. 177, pp. 2679–2682.
- Bhattacharyya, AJ, Fleig, J, Guo, YG & Maier, J. 2005, 'Local conductivity effects in polymer electrolytes', *Adv. Mater.*, 17, p. 2630.
- Berthier, C *et al.* 1983, 'Microscopic investigation of ionic conductivity in alkali metal salts-poly(ethylene oxide) adducts', *Solid State Ionics*, vol. 11, pp. 91–95.
- Bohnke, O *et al.* 1993, 'Fast ion transport in new lithium electrolytes gelled with PMMA. 1. Influence of polymer concentration', *Solid State Ionics*, vol. 66, pp. 97–104.
- Hagenmuller, P & Gool, WV eds 1978, *Solid electrolytes: general principles, characterization, materials application*, Academic Press, New York.
- Hong, H, Liquan, C, Xuejie, H & Rongjian, X 1992, 'Studies on PAN-based lithium salt complex', *Electrochim Acta*, vol. 37, pp. 1671–1673.
- Huang, B *et al.* 1996, 'The mechanism of lithium ion transport in polyacrylonitrile-based polymer electrolytes', *Solid State Ionics*, vol. 91, nos. 3–4, pp. 279–284.
- Julien, C & Nazri, GA 1994, *Solid state batteries: materials design and optimization*, Kluwer Academic Publishers, London.
- MacDonald, JR 1987, *Impedance spectroscopy*, John Wiley & Sons, New York.
- MacFarlane, DR *et al.* 1995, 'Structure-property relationships in plasticized solid polymer electrolytes', *Electrochimica Acta*, vol. 40, nos.13–14, pp. 2131–2136.
- Michael, MS, Jacob, MME, Prabakaran, SRS & Radhakrishna S 1997, 'Enhanced lithium ion transport in PEO-based solid polymer electrolytes employing a novel class of plasticizers', *Solid State Ionics*, vol. 98 pp. 167–174.
- Morales, E & Acosta, JL 1997, 'Thermal and electrical characterization of plasticized polymer electrolytes based on polyethers and polyphosphazene blends', *Solid State Ionics*, vol. 96, pp. 99–106.
- Nagasubramanian, G, Attia, AI & Halpert, G 1994, 'A polyacrylonitrile-based gelled electrolyte: electrochemical kinetic studies', *J. Appl. Electrochem.*, vol. 24, pp. 298–302.
- Nan, CW, Fan, LZ, Lin, YH & Cai, Q 2003, 'Enhanced ionic conductivity of polymer electrolytes containing nanocomposite SiO_2 particles' *Phys. Rev. Lett.*, 91, p. 266104.
- Peramunage, D, Pasquariello, DM & Abraham, KM 1995, 'Polyacrylonitrile-based electrolytes with ternary solvent mixtures as plasticizers', *J. Electrochem. Soc.*, vol. 142 pp. 1789–1798.
- Qizhen, X, Zhaohui, L, Deshu, G & Hailiang, Z 2009, 'A novel sandwiched membrane as polymer electrolyte for application in lithium-ion battery', *Journal of Membrane Science*, vol. 326, pp. 260–264.
- Selvaraj, II, Chaklanobis, S & Chandrasekhar, V 1995, 'Conductivity Studies on poly(methoxyethoxymethylmethacrylate)-lithium salt complexes', *J. Electrochem. Soc.*, vol. 142, pp. 366–370.

Song, JY, Wang, YY & Wan, CC 1999, 'Review of gel-type polymer electrolytes for lithium-ion batteries', *J. Power Sources*, vol. 77, pp. 183–197.

Sung JP, Young CB & Yang KS 2005, 'Ionic conductivities of solid polymer electrolyte/salt systems for lithium secondary battery', *Polymer*, vol. 46, pp. 3111–3118.

Tallworth, PE *et al.* 1995, 'Lithium-7 NMR and ionic conductivity studies of gel electrolytes based on poly(methylmethacrylate)', *Electrochim. Acta*, vol. 40, pp. 2137–2141.

Xu, QZ & Wang, G 1993, 'Rechargeable Li/LiMn₂O₄ batteries with a polymeric solid electrolyte', *J. Power Sources*, vol. 41, no. 3, pp. 315–320.

Characterization of Skeletons of Simulated Drought and Flood of Water Bodies

S. Dinesh¹

Studies conducted on the various geometric properties of skeletons of water bodies have shown highly promising results. However, these studies were made under the assumption that water bodies were static objects and that they remained constant over time. Water bodies are actually dynamic objects; they go through significant spatio-temporal changes due to drought and flood. In this study, the characterization of skeletons of simulated drought and flood of water bodies was performed. It was observed that as the drought level increased from 1 to 9, the average length of the skeletons decreased due to reduction in the size of the water bodies and increase in the number of water bodies. As the drought level increased from 9 to 15, the average length of the skeletons increased further due to vanishing of small water bodies. Flood caused an increase in the average length of the skeletons due to merging of adjacent water bodies. Power law relationships were observed between the average length of the skeletons of the simulated drought/flood and the level of drought/flood. The scaling exponent of these power laws which was named as a fractal dimension, indicated the rate of change of the average length of the skeletons of simulated drought/flood of water bodies over varying levels of drought/flood. However, errors observed in the goodness of fit of the plots indicated that monofractals were not sufficient to characterise the skeletons of simulated drought and flood of water bodies. Multifractals and lacunarity analysis were required for more accurate characterisation.

Key words: water bodies; simulation; drought; flood; average length; skeletons; fractal dimension; characterization; power law relationship

A skeleton in binary terminology is a one pixel-thick line representation of an object that summarizes the overall shape, size and orientation of the object. Skeletonization is the process of reducing foreground regions in a binary image to a skeleton, while discarding the remaining foreground pixels. The resultant skeleton is used for the computation of length and direction, or for the detection of special topological structures such as end points and triple points (Hilditch 1969; Rosenfeld 1970; Bookstein 1979; Piper 1985; Smith 1987; Meyer 1988, 1989; Jang & Chin 1990; Ji & Piper 1992; Lam *et al.* 1992; Soille 2003; Rémy & Thiel 2005; Palágyi 2008). Skeletons have been extensively applied in several fields such as pattern recognition (Hilditch 1969; Maragos & Schafer 1986; Reinhardt & Higgins 1996; Vasudevan & Cook 1998; Ruberto 2004; Schlei 2008), biological shape description (Blum 1973; Kumasaka & Kashima 1997; Kumasaka *et al.* 2000; Styner 2003; Xie *et al.* 2008), metallography (Lantuéjoul 1978, 1980; Jewell 2003), character recognition (Govindan & Shivaprasad 1990; Trier *et al.* 1996; Zhao 2003; Patil & Sontakke 2007), and hydrological feature extraction (Sagar *et al.* 2000, 2003; Dinesh 2008a) with highly promising results.

Skeletons of water bodies extend to orderings of water bodies for cartographic generalization (Nickerson 1988; McAllister & Snoeyink 2000). A number of studies have been conducted to study the various geometric properties of skeletons of water bodies (Sagar *et al.* 1999; Sagar 2000; Santos *et al.* 2005; Dinesh & Padmanabhan 2007, 2008). Sagar *et al.* (1999) demonstrated that the skeletal networks of water bodies which resemble river networks, follow Horton's laws. The fractal properties of skeletal networks of water bodies are also demonstrated. Sagar (2000) demonstrated the fractal relationship between the length of skeletons and the area of water bodies. Santos *et al.* (2005) employed skeletons of water bodies to perform the categorization of various types of water bodies. Dinesh & Padmanabhan (2007, 2008) performed a comparison of skeletons of water bodies and their corresponding convex hulls. It was observed that convex hull computation reduced the skeleton length of water bodies. However, these studies were made under the assumption that water bodies were static objects and that they remained constant over time. Water bodies are actually dynamic objects; they go through significant spatio-temporal changes due to drought and flood.

¹Science and Technology Research Institute for Defence, Ministry of Defence, Taman Bukit Mewah Fasa 9, 43000 Kajang, Selangor, Malaysia

*Corresponding author (e-mail: dinsat60@hotmail.com)

In this paper, the characterization of skeletons of simulated drought and flood of water bodies is performed. It demonstrated, via power law relationships, the fractal properties of the skeletons of simulated drought and flood of water bodies.

METHODOLOGY

The Data Set

The Godhavary river, which lies in central India, originates near Triambak in the Nasik district of Maharashtra, and flows through the states of Madhya Pradesh, Karnataka, Orissa and Andhra Pradesh. Although its point of origin is just 80 km away from the Arabian Sea, it journeys

1465 km to empty into the Bay of Bengal. Some of its tributaries include the Indravati, Manjira, Bindusara and Sarbari. Some important urban centres on its banks include Nasik, Aurangabad, Nagpur, Nizamabad, Rajahmundry and Balaghat. The Godhavary river is often referred to as the Vriddh (Old) Ganga or the Dakshin (South) Ganga. The Godhavary river has a catchment area of 312 870 km² and receives more than 85% of its annual rainfall during the monsoon season (June–September). Hence, the water resources in this river are largely due to monsoon rainfall and are largely affected by monsoon extremities, resulting in floods during some years and droughts during others.

Figure 1a shows a number of water bodies of varying shapes and sizes situated in a portion of the floodplain region of Godhavary river. The water bodies were traced

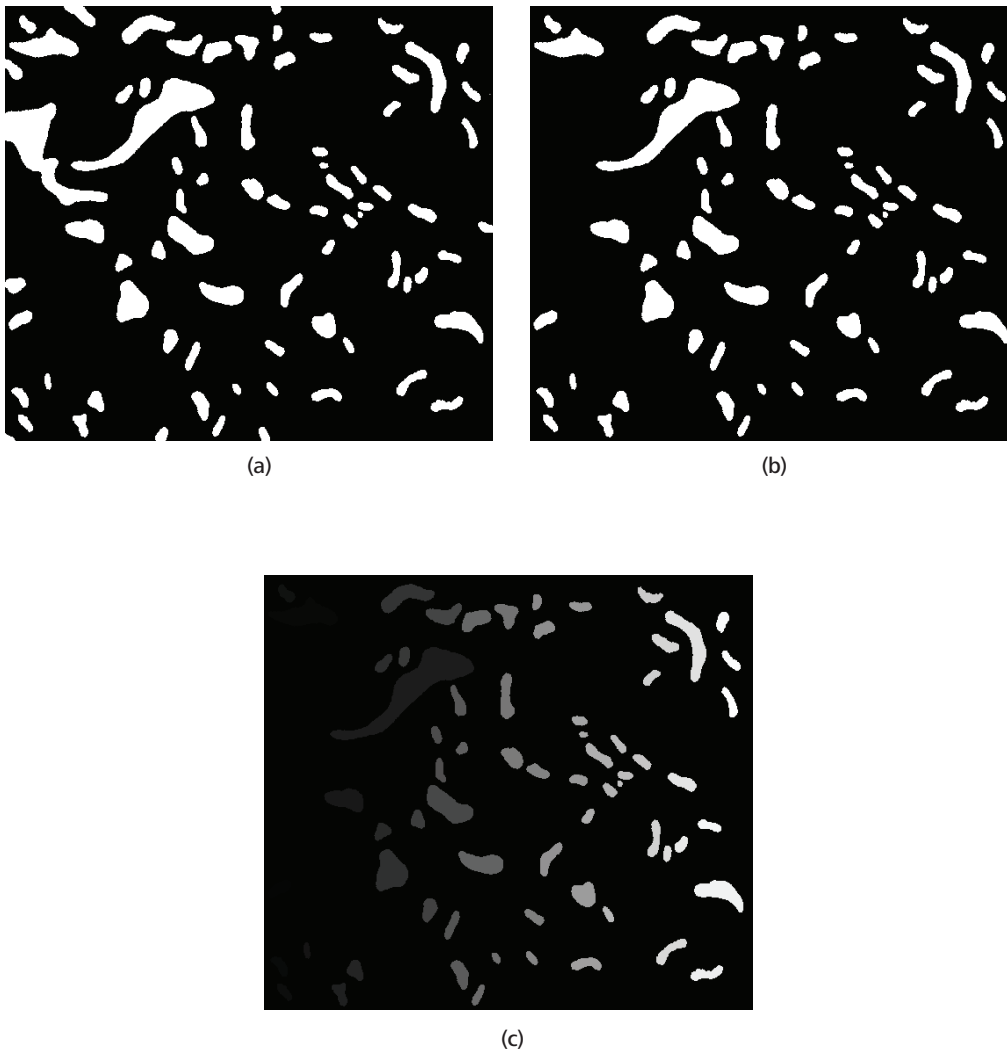


Figure 1. Water bodies of varying shapes and sizes situated in a portion of the flood plain region of Godhavary river: (a) The original water bodies traced from IRS 1D remotely sensed data; (b) The water bodies after removal of incomplete water bodies; (c) Identification of the individual water bodies using connected component labeling. The water body count number was determined by the grey level; the brighter the grey level, the larger the water body count number.

from Indian Remote Sensing Satellite (IRS) 1D remotely sensed data. The IRS-1D was launched on 28 September 1997 by the Indian Space Research Organization (ISRO) operated Polar Satellite Launch Vehicle (PSLV). The data was captured using the multispectral Linear Imaging Self-Scanning Sensor 3 (LISS-3) with spatial resolution of 23.7 m and band range of 520 nm – 590 nm. Due to the impracticalities of dealing with incomplete water bodies, incomplete water body images were removed, and only the complete water body images were considered (Figure 1b). A total of 67 distinct individual water bodies (Figure 1c) were identified using connected component labelling (Pitas 1993).

Generation of Simulated Drought and Flood of Water Bodies

Management of spatial data related to flood analysis largely relies on information derived from geographic information system (GIS) data captures and earth observation (EO) data. In this respect, image processing and pattern recognition techniques have been widely employed for flood analysis applications such as catchment delineation, extraction of surface water, inundated areas and flow measurement computation (Brakenridge 1998; van der Sande *et al.* 2003; Marsalek 2004; Stancalie & Craciunescu 2005; Sanders, 2007; Di Baldassarre 2009).

Mathematical morphology is a branch of image processing that deals with the extraction of image components that are useful for representation and description purposes. Mathematical morphology has a well developed mathematical structure that is based on set theoretic concepts. The effects of the basic morphological operations can be given simple and intuitive interpretations using geometric terms of shape, size and location. The fundamental morphological operators are discussed in Matheron (1975), Serra (1982) and Soille (2003). Morphological operators generally require two input; the input image *A*, which can be in binary or grayscale form, and the kernel *B*, which is used to determine the precise effect of the operator.

Dilation sets the pixel values within the kernel to the maximum value of the pixel neighbourhood. Binary dilation fills the small holes inside particles and gulfs on the boundary of objects, enlarges the size of the particles and may connect neighbouring particles (Duchane & Lewis 1996). The dilation operation is expressed as in Equation 1.

$$A \oplus B = \{a+b: a \in A, b \in B\} \quad \dots 1$$

Erosion sets the pixel values within the kernel to the minimum value of the kernel. Binary erosion removes isolated points and small particles, shrinks other particles,

discards peaks on the boundaries of objects and disconnects some particles (Duchane & Lewis 1996). The erosion operation is expressed as in Equation 2. It should be noted that erosion is the dual operator of dilation (Equation 3):

$$A \ominus B = \{a-b: a \in A, b \in B\} \quad \dots 2$$

$$A \ominus B = (A^c \oplus B)^c \quad \dots 3$$

where,

A^c denotes the complement of *A* and *B* is symmetric with respect to reflection about the origin.

Drought and flood simulation was implemented by performing erosion and dilation respectively, on water bodies using square kernels of increasing size (Dinesh 2007a,b,c, 2008b). Erosion reduced the area of water bodies, mimicking drought, while dilation increased the area of water bodies, mimicking flood. The level of drought/flood was indicated by the kernel size.

Simulated drought (Figure 2) and flood (Figure 3) of the water bodies for levels *r* of 1 to 15 were computed. The areas of the generated drought and flood are shown in Table 1.

Skeletonization of Water Bodies

The skeletons of the generated simulated drought (Figure 4) and flood (Figure 5) were computed using the skeletonization by morphological thinning algorithm proposed in Jang and Chin (1990). Skeletonization by morphological thinning is defined as the successive removal of outer layers of pixels from an object while retaining any pixels whose removal would alter the connectivity or shorten the legs of the skeleton. The process is converged or completed when no further pixels can be removed without altering the connectivity or shortening the skeletal legs.

RESULTS AND DISCUSSION

For each level of drought (Table 2) and flood (Table 3), the total length of the skeletons of water bodies *L* and the number of water bodies *N* were computed. The average lengths of skeletons of the simulated drought and flood of water bodies *AL* were computed using Equation 4. Based on this equation, *AL* increased when *L* increased and/or *N* decreased while *AL* decreased when *L* decreased and/or *N* increased.

$$AL = L / N \quad \dots 4$$

It was observed that as the drought level increased from 1 to 9, the average length of the skeletons of the water bodies

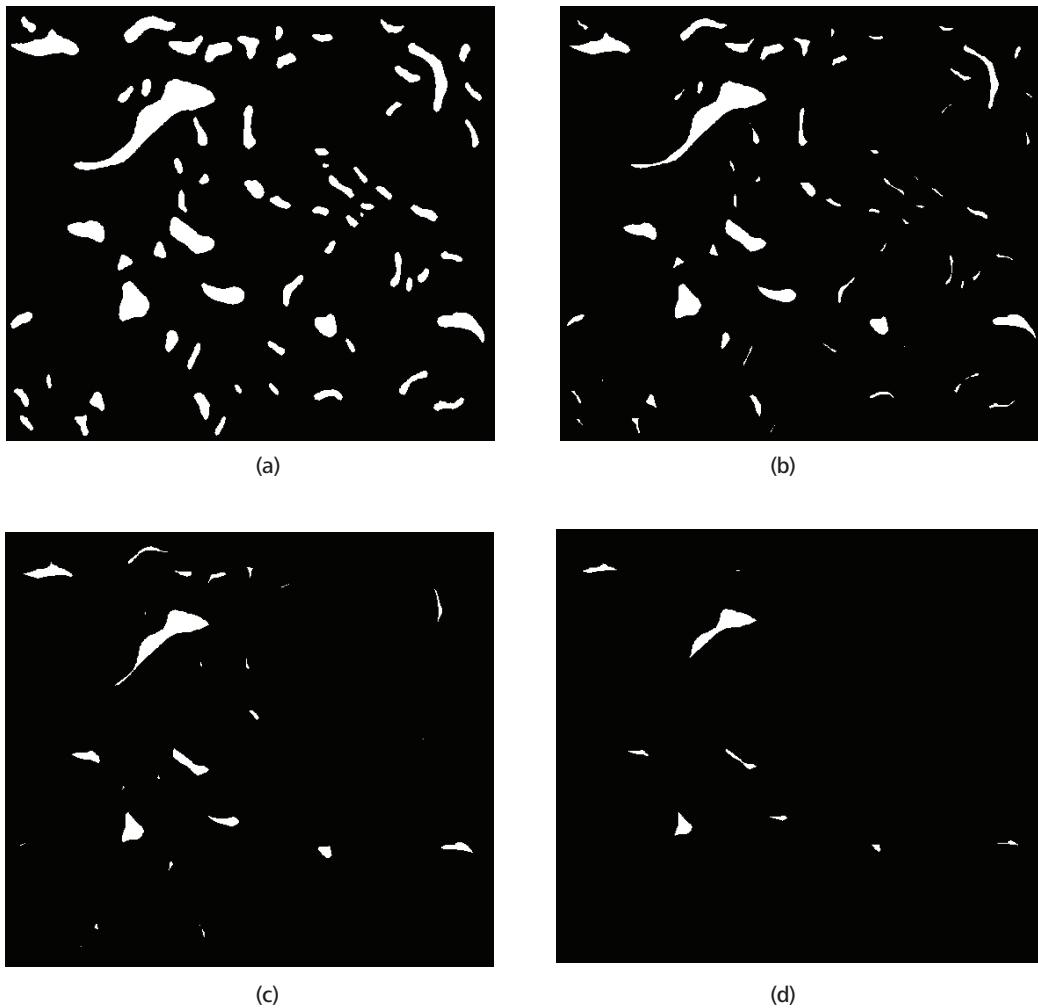


Figure 2. The generated simulated droughts of the water bodies at drought levels of: (a) 3; (b) 7; (c) 11 and (d) 15.

was reduced. This occurred as when the level of drought was increased; the sizes of the water bodies reduced, resulting in a decrease in the total length of the skeletons of the water bodies. Furthermore, drought also caused the breaking up of water bodies into smaller water bodies, resulting in an increase in the number of water bodies.

As the drought level increased from 9 to 15, the average length of the skeletons of the water bodies increased. This occurred as when the level of drought was increased, a number of small water bodies vanished, resulting in a decrease in the number of water bodies, and hence, an increase in the average length of the skeletons.

It was also observed that as the level of flood was increased, the average length of skeletons of water bodies increased. This occurred as when the level of flood was increased, the sizes of water bodies increased, resulting in an increase in the total length of skeletons of the water bodies. Furthermore, the level of merging between adjacent water

bodies increased, resulting in a decrease in the number of water bodies.

A log-log plot of the average length of the skeletons of the simulated floods AL against the level of flooding r was drawn (Figures 6). Two log-log plots of the average length of the skeletons of the simulated drought AL against the level of drought r were drawn, one for drought level of 1 to 9 (Figure 7a), and one for drought level of 9 to 15 (Figure 7b). Power law relationships were observed in all three plots. These power laws took the following form:

$$AL = c * r^D \quad \dots 5$$

These power law relationships arose as a consequence of the fractal properties of the skeletons of simulated drought and flood of water bodies. The term 'fractal' implies that an object or pattern has self-similar or self-affine properties. Self-similar means that parts of an object are identical to the whole, and self-affine means that parts of an object resemble

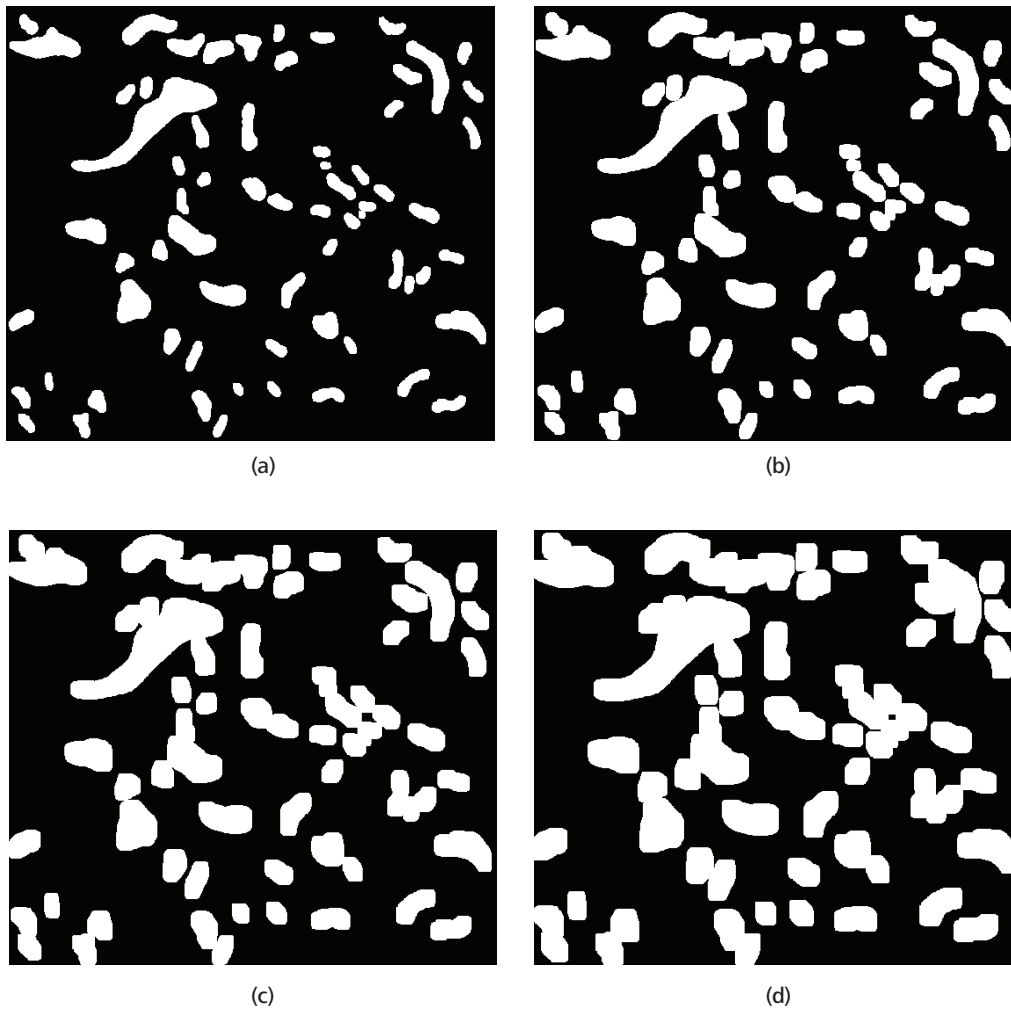


Figure 3. The generated simulated flood of the water bodies at flood levels of: (a) 3; (b) 7; (c) 11 and (d) 15.

Table 1. Areas of the generated simulated drought and flood of water bodies.

Level	Area (pixels)	
	Drought	Flood
1	137837	137837
2	123336	152789
3	109565	167979
4	96328	183647
5	83764	199532
6	71844	215862
7	60839	232283
8	51141	249127
9	42863	265919
10	35980	283048
11	30230	300047
12	25380	317358
13	21220	334503
14	17737	351937
15	14794	369093

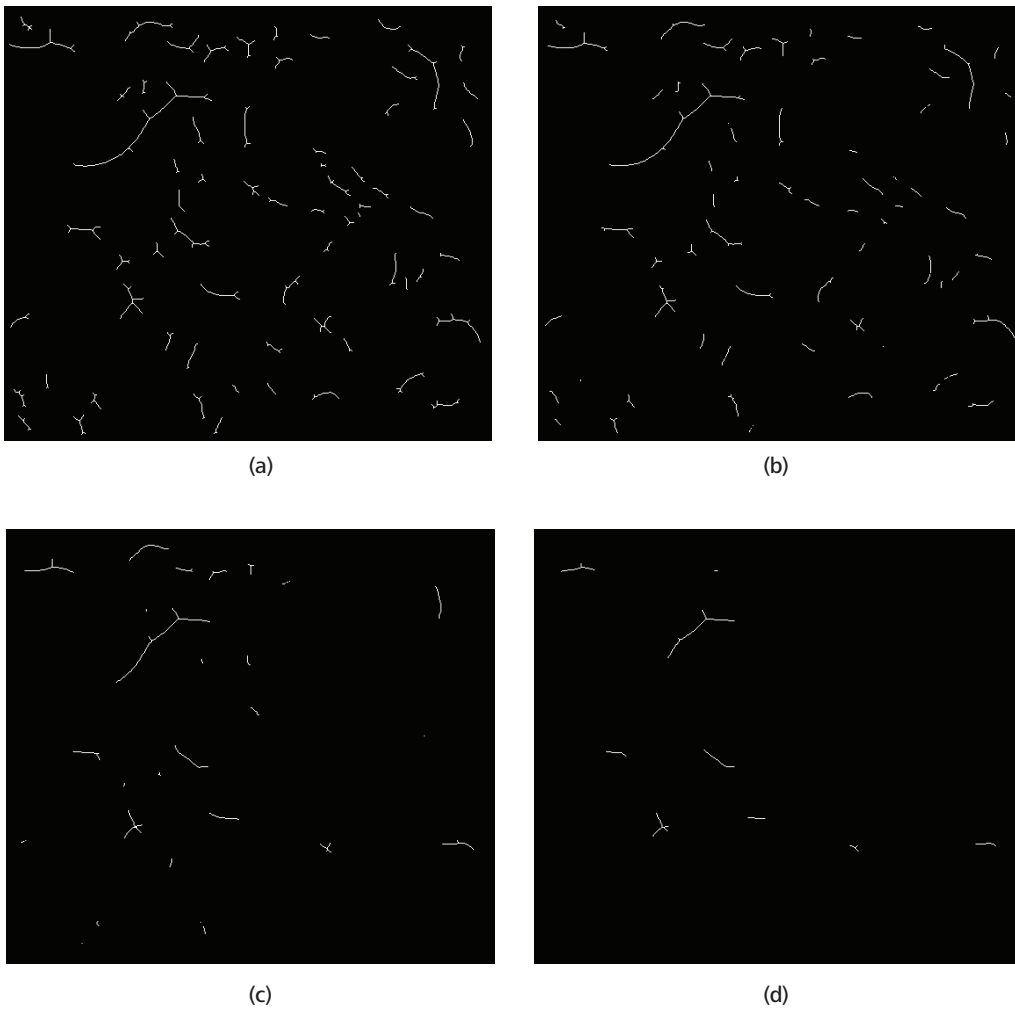


Figure 4. Skeletons of the corresponding simulated drought in Figure 2.

Table 2. Basic measures of the skeletons of the generated simulated drought.

Level	Total length L (pixels)	Number N	Average length AL (pixels)
1	2609	67	38.94
2	2437	67	36.37
3	2277	67	33.99
4	2147	67	32.04
5	2018	67	30.12
6	1866	68	27.44
7	1628	72	22.61
8	1341	72	18.63
9	1039	64	16.23
10	810	39	20.77
11	653	30	21.77
12	524	23	22.78
13	416	17	24.47
14	351	12	29.25
15	295	9	32.78

Table 3. Basic measures of the skeletons of the generated simulated flood.

Level	Total length L (pixels)	Number N	Average length AL (pixels)
1	2609	67	38.94
2	2764	67	41.25
3	2918	66	44.21
4	3092	64	48.31
5	3269	61	53.59
6	3488	57	61.19
7	3674	54	68.04
8	3805	50	76.10
9	3981	45	88.47
10	4118	43	95.77
11	4220	42	100.48
12	4354	41	106.20
13	4524	39	116.00
14	4643	38	122.18
15	4740	37	128.11

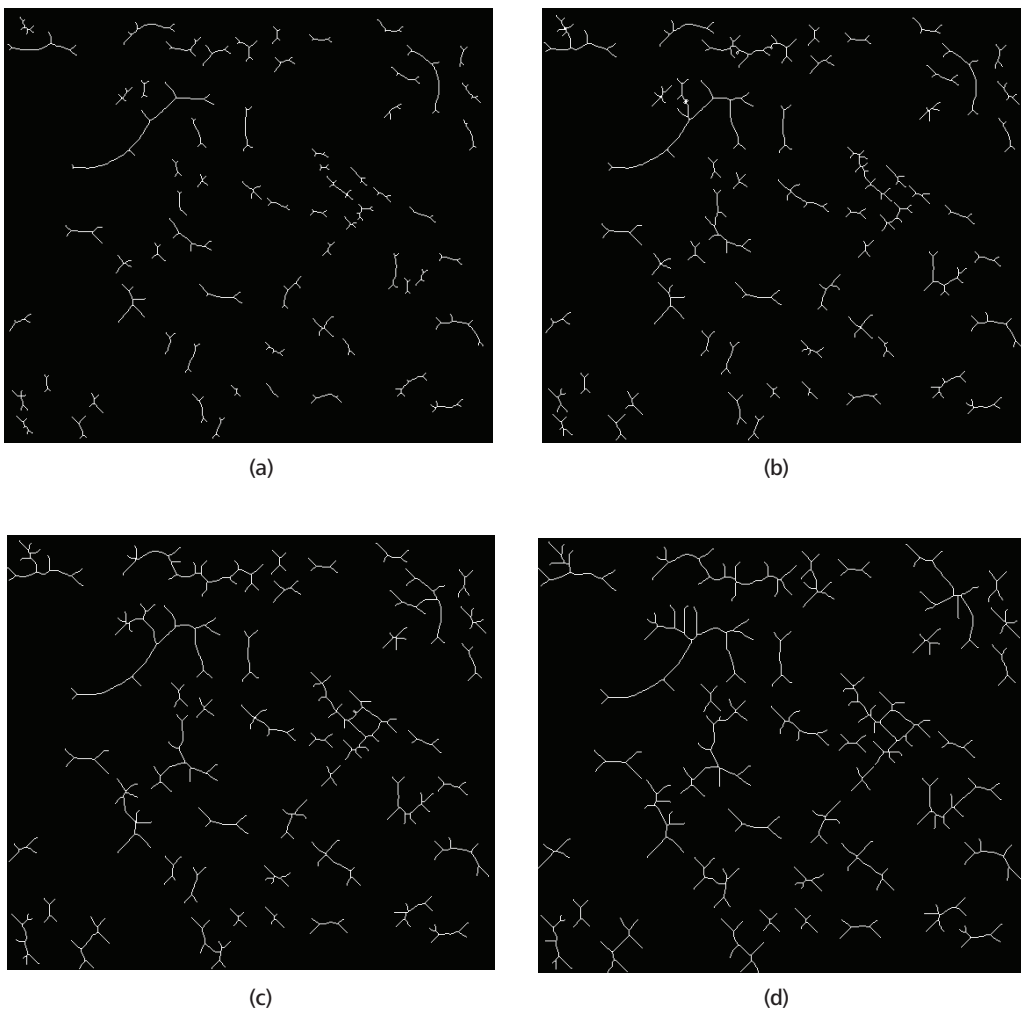


Figure 5. Skeletons of the corresponding simulated flood in Figure 3.

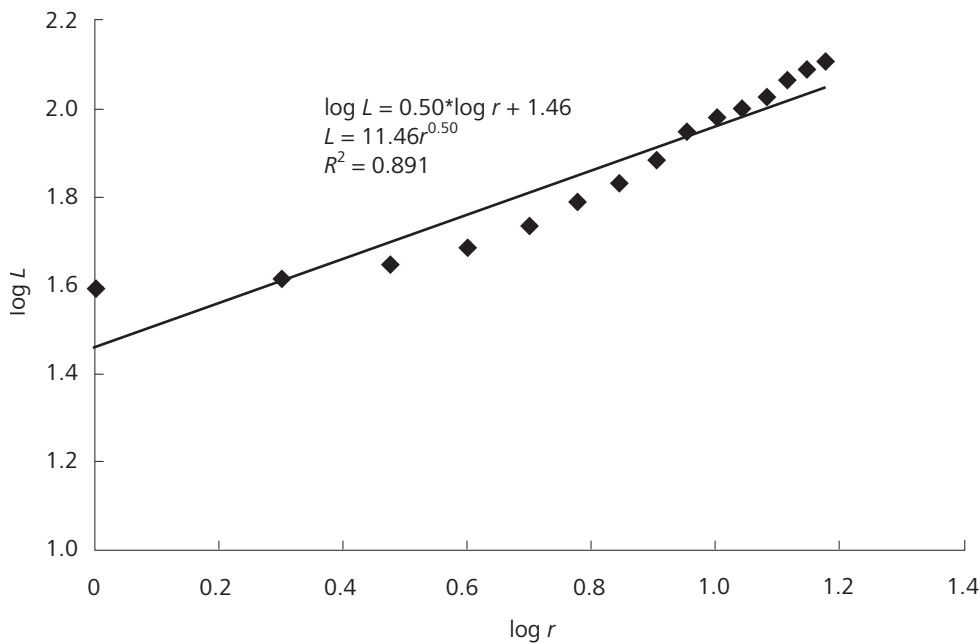


Figure 6. Log-log plot of average length of skeletons of simulated flood AL against flood levels r .

systematically squashed or stretched versions of the whole. Ideal fractals display similarity across an infinite range of scales, which is rarely seen in nature. Consequently, the ranges of fractality could be used to decipher characteristic scales and thresholds at which physical processes operate (Mandelbrot 1967, 1977, 1988).

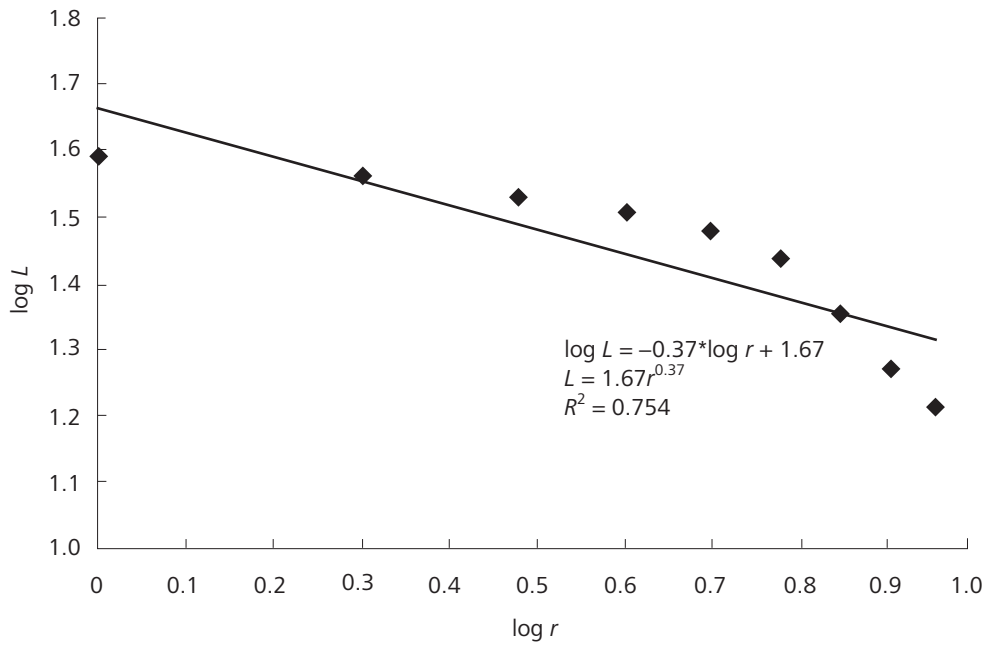
A fundamental characteristic of fractal objects is that their measured metric properties (in this case, the length of skeletons of the water bodies), are a power law function of the scale of measurement (in this case the drought/ flood level). In the case of skeletons of simulated drought and flood of water bodies, the relationship between the length of skeletons of water bodies and the drought/flood level was generalised by the power law in Equation 5. In this equation, c is a constant of proportionality, and D is the fractal dimension of the average length of the skeletons of simulated drought/flood of water bodies, which indicated the rate of change of average lengths of the skeletons over varying levels of drought/flood. Based on the set definition by Mandelbrot (1990), D has a positive value for increasing average lengths of skeletons, and a negative value for decreasing average lengths of skeletons. A positive fractal divergence implies that the water bodies were approaching convergence (self organised criticality), while a negative fractal dimension implies that the water bodies were approaching an empty set (Bak *et al.* 1987, 1998; Bak 1996).

All the plots had power laws with high coefficients of determination R^2 , indicating that the variances of average lengths of skeletons were largely due to the drought/ flood

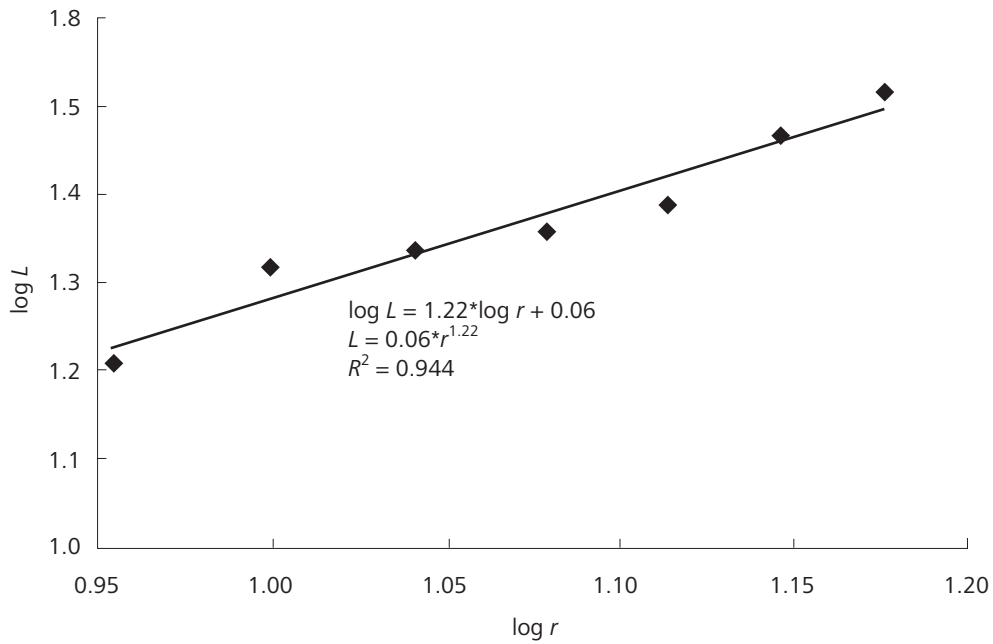
process, rather than from other factors. However, the errors in the goodness of fit of the plots indicated that monofractals which assume that the object under consideration could be characterised by singular fractal dimensions, were not sufficient to characterise the skeletons of simulated drought and flood of water bodies.

Previous studies have shown that various natural processes operating at different scales have properties that deviate from monofractal dimension assumptions (Feder 1988; Mandelbrot 1989; Klinkenberg & Goodchild 1992; Tchiguirinskaia *et al.* 2000; Sun *et al.* 2006). In the case of simulated drought and flood of water bodies, the water bodies at each level had time-dependant fractal dimensions. This indicated that multifractals (Mandelbrot 1989; Harte 2001), characterising multiple fractal power laws, were more suited to water body characterisation. Multifractals has been employed in various applications in geomorphological analysis (Tchiguirinskaia *et al.* 2000; Parrileno & Vaughan 2002; Posadas *et al.* 2005; Abedini & Shaghaghian 2009).

In addition, fractal dimensions only measure the geometric complexity of the shape of skeletons of water bodies. Other factors, such as size and distribution, also affect drought and flood, and hence fractal dimension alone may not be sufficient for the characterisation. Mandelbrot (1982) pointed out that different fractal sets may share the same fractal dimension, but have significantly different appearances, and hence, introduced lacunarity analysis. Lacunarity is related to the distribution of gap sizes; low lacunarity implies homogeneity with similar



(a)



(b)

Figure 7. Log-log plots of average length of skeletons of simulated drought AL against drought levels r : (a) For drought levels of 1 to 9 and (b) For drought levels of 9 to 15.

gap sizes, while high lacunarity implies heterogeneity. It has been demonstrated that object characterisation using a combination of fractal dimensions and lacunarity can provide good results (Keller *et al.* 1989; Dong 2000; Malhi & Román-Cuesta 2005; Chun *et al.* 2008).

CONCLUSION

In this paper, the characterization of skeletons of simulated drought and flood of water bodies were performed. It was observed that as the drought level increased from 1 to 9, the average length of the skeletons was reduced due to reduction in the size of the water bodies and increase in the number of water bodies. As the drought level increased from 9 to 15, the average length of the skeletons increased due to vanishing of small water bodies. Flood caused an increase in the average length of the skeletons due to the merging of adjacent water bodies. Power law relationships were observed between the average length of the skeletons of the simulated drought/flood and the level of drought/flood. The scaling exponent of these power laws, which was named as a fractal dimension, indicated the rate of change of average length of the skeletons of simulated drought/flood of water bodies over varying levels of drought/flood. However, the errors observed in the goodness of fit of the plots indicated that monofractals were not sufficient to characterise the skeletons of simulated droughts and floods of water bodies. Multifractals and lacunarity analysis are required for more accurate characterisation.

It is important to note that in this paper, drought and flood simulations were performed on the assumption that the floodplain regions which had a maximum gradient of less than 2°, approximate isotropic surfaces. However, that assumption does not hold for other areas with gradients higher than 2°. In those cases, drought and flood simulation will need to take into consideration the gradient computed from the corresponding elevation maps. Furthermore, while the study of the Gothavary river floodplain does provide interesting results in regards to a region that underwent significant spatio-temporal changes due to drought and flood, the conclusions drawn from the study of that region did not necessarily apply to all regions. At present, work is being done to study the multifractal and lacunarity of skeletons of simulated drought and flood of water bodies of regions of varying geomorphological topography.

ACKNOWLEDGEMENTS

The author is grateful to the two anonymous reviewers for their constructive suggestions.

Date of submission: October 2008

Date of acceptance: April 2010

REFERENCES

- Abedini, MJ & Shaghaghian, MR 2009, 'Exploring scaling laws in surface topography', *Chaos, Solitons & Fractals*, vol. 42, no. 4, pp. 2373–2383.
- Bak, P, Tang, C & Wiesenfeld, K 1987, 'Self-organized criticality: an explanation of 1/f noise', *Physical Review Letters*, vol. 59, no. 4, pp. 381–384.
- Bak, P, Tang, C & Wiesenfeld, K 1988, 'Self-organized criticality', *Physical Review A*, vol. 38, no. 1, pp. 364–374.
- Bak, P 1996, *How nature works: the science of self-organized criticality*, Copernicus New York.
- Blum, H 1973, 'Biological shape and visual sciences (Part I)', *Journal of Theoretical Biology*, vol. 38, no. 2, pp. 205–287.
- Bookstein, FL 1979, 'The line skeleton', *Computer Graphics and Image Processing*, vol. 11, no. 2, pp. 123–137.
- Brakenridge, RG, Tracy, BT & Know, JC, 1998, 'Orbital SAR remote sensing of river flood wave', *International Journal of Remote Sensing*, vol. 19, no. 7, pp. 1439–1445.
- Cheng, Q 1999, 'Multifractality and spatial statistics', *Computers & Geosciences*, vol. 25, no. 9, pp. 949–961.
- Chun, HY, Giménez, D & Yoon, SW 2008, 'Morphology, lacunarity and entropy of intra-aggregate pores: aggregate size and soil management effects', *Geoderma*, vol. 146, no. 1–2, pp. 83–93.
- Coby, DM, Mason, DC & Davenport, IJ 2001, 'Image processing of airborne scanning laser altimetry data for improved river flood modelling', *ISPRS Journal of Photogrammetry and Remote Sensing*, vol. 56, no. 2, pp. 121–138.
- Di Baldassarre, G, Schumann, G & Bates, PD 2009, 'A technique for the calibration of hydraulic models using uncertain satellite observations of flood extent', *Journal of Hydrology*, vol. 367, no. 3–4, pp. 276–282.
- Dinesh, S 2007a, 'Convex characterization of simulated floods and droughts of water bodies', *Journal of Applied Sciences*, vol. 7, no. 11, pp. 1516–1521.
- Dinesh, S 2007b, 'Characterization of convexity of simulated droughts and floods of water bodies', in *World Engineering Congress 2007 (WEC 2007), 5th–9th August 2007*, Institute of Engineers, Penang.
- Dinesh, S 2007c, 'Analysis of influence zones of simulated droughts and floods of water bodies', in *Joint International Symposium & Exhibition on Geoinformation and GPS/GNSS 2007 (ISG & GPS/GNSS 2007), 5 – 7 November 2007*, Johor Bahru.
- Dinesh, S 2008a, 'Extraction of hydrological features from digital elevation models using morphological thinning', *Asian Journal of Scientific Research*, vol. 1, no. 4, pp. 310–323.
- Dinesh, S 2008b, 'Characterization of influence zones of simulated droughts and floods of water bodies in a floodplain', *Computers & Geosciences*, vol. 34, no. 12, 1791–1797.
- Dinesh, S & Padmanabhan, A 2007, 'Convex characterization of water bodies', in *The 3rd International Conference on Research and Education in Mathematics (ICREM3), 10–12 April 2007*, Kuala Lumpur.

- Dinesh, S & Padmanabhan, A 2008, 'Characterization of the convexity of water bodies', *Malaysian Journal of Mathematical Sciences*, under review.
- Dong, PL 2000, 'Test of a new lacunarity estimation method for image texture analysis', *International Journal of Remote Sensing*, vol. 21, no. 17, pp. 3369–3373.
- Duchene, P & Lewis, D 1996, *Visilog 5 documentation*, Noesis Vision, Quebec.
- Feder, J 1988, *Fractals*, Plenum Press, New York.
- Govindan, VK & Shivaprasad, AP 1990. 'Character recognition: A review', *Pattern Recognition*, vol. 23, no. 7, pp. 671–683.
- Harte, D, 2001, *Multifractals: theory and applications*, Chapman & Hall, Boca Raton.
- Hilditch, J 1969, 'Linear skeletons from square cupboards', in *Machine intelligence*, eds B Meltzer & D Michie, Edinburgh University Press, Edinburgh.
- Jang, BK & Chin, RT 1990, 'Analysis of thinning algorithms using mathematical morphology', *Transactions on Pattern Analysis and Machine Intelligence*, vol. 12, no. 6, pp. 541–550.
- Jewell, MC, Lee, PJ & Larbalestier, DC 2003, 'The influence of Nb3Sn strand geometry on filament breakage under bend strain as revealed by metallography', *Superconductor Science and Technology*, vol. 16, pp. 1005–1011.
- Ji, L & Piper, J 1992, 'Fast homotopy-preserving skeletons using mathematical morphology', *IEEE Transactions on Pattern Analysis and Machine Intelligence*, vol. 14, no. 6, pp. 653–664.
- Keller, JM, Chen, S & Crownover, RM 1988, 'Texture description and segmentation through fractal geometry', *Computer Vision, Graphics and Image Processing*, vol. 45, no. 2, pp. 150–166.
- Klinkenberg, B & Goodchild, MF 1992, 'The fractal properties of topography: A comparison of methods', *Earth Surface Processes and Landforms*, vol. 17, no. 3, 217–234.
- Kumasaka, S & Kashima, I 1997, 'Initial investigation of mathematical morphology for the digital extraction of the skeletal characteristics of trabecular bone', *Dentomaxillofacial Radiology*, vol. 26, no. 3, pp. 161–168.
- Kumasaka, S *et al.* 2000 'Morphologically extracted trabecular skeleton superimposed upon digital radiograph structure', *Journal of Bone and Mineral Metabolism*, vol. 18, no. 4, pp. 208–211.
- Lam, L, Lee, S-W & Suen, C 1992, 'Thinning methodologies: a comprehensive survey', *IEEE Transactions on Pattern Analysis and Machine Intelligence*, vol. 14, no. 9, pp. 869–885.
- Lantuéjoul, C 1978, *La squelettization et son application aux mesures topologiques des mosaïques polycristallines*, PhD thesis, School of Mines, Paris, France.
- Lantuéjoul, C 1980, 'Skeletonization in quantitative metallography', in *Issues of digital image processing*, eds RM Haralick & JC Simon, Sijthoff and Neordhoff, Groningen, The Netherlands.
- Malhi, Y & Román-Cuesta, RM 2005, 'Analysis of lacunarity and scales of spatial homogeneity in IKONOS images of Amazonian tropical forest canopies', *Remote Sensing of Environment*, vol. 112, no. 5, pp. 2074–2087.
- Mandelbrot, BB 1967, 'How long is the coast of Britain? Statistical self-similarity and fractional dimension', *Science*, vol. 156, pp. 636–638.
- Mandelbrot, BB 1977, *Fractals: form, chance and dimension*, Freeman, San Francisco, California, USA.
- Mandelbrot, BB 1982, *The fractal geometry of nature*, Freeman, San Francisco, California, USA.
- Mandelbrot, BB 1989, 'Multifractal measures, especially for geophysicists', *Pageoph*, vol. 131, no. 1–2, 5–42.
- Maragos, P & Schafer, RW 1986, 'Morphological skeleton representation and coding of binary images', *IEEE Transactions on Acoustics, Speech, and Signal Processing*, vol. 34, no. 5, pp. 1228–1244.
- Marsalek, J 2004, *Monitoring of extreme flood events in Romania and Hungary using EO data*, Technical Progress Report No. 3, National Water Research Institute (NWRI), Burlington, Ontario, Canada.
- Matheron, G 1975, *Random sets and integral geometry*, Wiley, New York, USA.
- McAllister, M & Snoeyink, J 2000, 'Medial axis generalization of river networks', *Cartography and Geographic Information Science*, vol. 27, no. 2, pp. 129–138.
- Meyer, F 1988, 'Skeletons in digital spaces', in *Image analysis and mathematical morphology*, vol. 2, ed J Serra, Academic, New York, USA.
- Meyer, F 1989, 'Skeletons and perceptual graphs', *Signal Processing*, vol. 16, pp. 335–363.
- Nickerson, BG 1988, 'Automated cartographic generalization for linear features', *Cartographica*, vol. 25, no. 3, pp. 15–66.
- Palágyi, K 2008, 'A 3D fully parallel surface-thinning algorithm', *Theoretical Computer Science*, vol. 406, no. 1–2, pp. 119–135.
- Parrileno, T and Vaughan, RA, 2002, Multifractal analysis and feature extraction in satellite imagery, *International Journal of Remote Sensing*, vol. 23, no. 9, pp. 1799–1825.
- Patil, PM & Sontakke, TR, 2007, 'Rotation, scale and translation invariant handwritten Devanagari numeral character recognition using general fuzzy neural network', *Pattern Recognition*, vol. 40, no. 7, pp. 2110–2117.
- Piper, J 1985, 'Efficient implementation of skeletonization using interval coding', *Pattern Recognition Letters*, vol. 3, pp. 389–397.
- Pitas, I 1993, *Digital image processing algorithms*, Prentice Hall, London.
- Posadas, *et al.* 2005, Multifractal characterisation of the spatial distribution of elxite on a Bolivian salt flat, *International Journal of Remote Sensing*, vol. 26, no. 3, pp. 615–627.
- Reinhardt, JM & Higgins, WE 1996, 'Comparison between the morphological skeleton and morphological shape decomposition', *IEEE Transactions on Pattern Analysis and Machine Intelligence*, vol. 18, no. 9, pp. 951–957.
- Rémy, E & Thiel, E 2005, 'Exact medial axis with Euclidean distance', *Image and Vision Computing*, vol. 23, no. 2, pp. 167–175.
- Rosenfeld, A 1970, 'Connectivity in digital pictures', *Journal of ACM*, vol. 17, pp. 146–160.

- Ruberto, CD, 2004, 'Recognition of shapes by attributed skeletal graphs', *Pattern Recognition*, vol. 37, no. 1, pp. 21–31.
- Sagar, BSD 2000, 'Fractal relation of medial axis length to the water body area', *Discrete Dynamics in Nature and Society*, vol. 4, no. 2, pp. 97.
- Sagar, BSD, Venu, M & Murthy, KSR 1999, 'Do skeletal networks derived from water bodies follow Horton's laws?', *Mathematical Geology*, vol. 31, no. 2, pp. 143–154.
- Sagar, BSD, Venu, M, & Srivinas, D 2000, Morphological operators to extract channel networks from digital elevation models, *International Journal of Remote Sensing*, vol. 21, no. 1, pp. 21–29.
- Sagar, BSD *et al.* 2003, 'Morphological approach to extract ridge-valley connectivity networks from digital elevation models (DEMs)', *International Journal of Remote Sensing*, vol. 24, no. 3, pp. 573–581.
- Sanders, BF 2007, 'Evaluation of on-line DEMs for flood inundation modelling', *Advances in Water Resources*, vol. 30, no. 8, pp. 1831–1843.
- Santos, P, Bennett, B & Sakellariou, G 2005, 'Supervaluation semantics for an inland water feature ontology', in *Proceedings of the International Joint Conference on Artificial Intelligence (IJCAI-05)*, Edinburgh.
- Schlei, BR 2008, 'A new computational framework for 2D shape-enclosing contours', *Image and Vision Computing*, vol. 27, no. 6, 637–647.
- Serra, J 1982, *Image analysis and mathematical morphology*, Academic Press, London.
- Smith, RW 1987, 'Computer processing of line images: a survey', *Pattern Recognition Letters*, vol. 20, pp. 7–15.
- Soille, P 2003. *Morphological image analysis: principles and applications*, Springer Verlag, Berlin.
- Stancalie, G & Craciunescu, V 2005, 'Contribution of earth observation data supplied by the new satellite sensors to flood disaster assessment and hazard reduction', in *Geo-information for disaster management*, eds P van Oosterom, S Zlatanova & EM Fendel, Springer, Berlin.
- Styner, M *et al.* 2003, Statistical shape analysis of neuroanatomical structures based on medial models', *Medical Image Analysis*, vol. 7, no. 3, pp. 207–220.
- Sun, W, Xu, G, Gong, P & Liang, S 2006, 'Fractal analysis of remotely sensed images: a review of methods and applications', *International Journal of Remote Sensing*, vol. 27, no. 22, pp. 4963–4990.
- Tchiguirinskaia, I *et al.* 2000, 'Multifractal versus monofractal analysis of wetland topography', *Stochastic Environmental Research and Risk Assessment*, vol. 14, no. 1, pp. 8–32.
- Trier, OD, Jain, AK & Taxt, T 1996, 'Feature extraction methods for character recognition—a survey', *Pattern Recognition*, vol. 29, no. 4, pp. 641–662.
- van der Sande, CJ, de Jong, SM and de Roo, APJ 2003, 'A segmentation and classification approach of IKONOS-2 imagery for land cover mapping to assist flood risk and previous flood damage assessment', *International Journal of Applied Earth Observation and Geoinformation*, vol. 4, no. 3, pp. 217–229.
- Vasudevan, K & Cook, FA 1998, 'Skeletons and fractals: A statistical approach to deep crustal seismic data processing and interpretation', *Tectonophysics*, vol. 286, no. 1–4, pp. 93–109.
- Xie, J, Heng, PA & Shah, M 2008, 'Shape matching and modeling using skeletal context', *Pattern Recognition*, vol. 41, no. 5, pp. 1756–1767.
- Zhao, S *et al.* 2003, 'Two-stage segmentation of unconstrained handwritten Chinese characters', *Pattern Recognition*, vol. 36, no. 1, pp. 145–156.

Nomenclature

Symbol	Description
A	Input image
B	Kernel
a	Elements of A
b	Elements of B
x^c	Complement of a variable, in this case of x
L	Total length of skeletons of water bodies
r	Drought/flood level
N	Number of water bodies
AL	Average length of skeletons of water bodies
c	Constant of proportionality
D	Fractal dimension of the average length of the skeletons of simulated drought/flood of water bodies

Effects of Nitrate, Phosphate, Temperature and Light-dark Cycle on Algal Growth Potential of *Chlorococcum* sp. from Reeve Hill, Antarctica

D. Masdialily^{1*}, W.O.W. Maznah¹, M. Faradina¹ and M. Mashhor¹

In this study the effects of phosphorus and nitrogen levels, temperature and light-dark cycle on the algal growth potential (AGP) of an Antarctic *Chlorococcum* isolated from an ephemeral stream at Reeve Hill, Antarctica was investigated. The highest AGP was attained when the cultures were grown at high nitrogen concentration (329.87 mg NO₃-N/l) and low phosphorus concentration (2.6 mg PO₄-P/l) at 4°C on a 12 h:12 h light-dark cycle. The results showed that *Chlorococcum* sp. required a high concentration of nitrogen, low concentration of phosphorus, low temperature with equal lengths of light and dark period (12 h:12 h) for optimum growth.

Key words: algal growth potential; *Chlorococcum* sp.; nitrogen; phosphorus; temperature; light-dark cycle; nutrient levels

Antarctica is the fifth largest continent with unpredictable extreme weather conditions like low temperatures, strong winds, no access to water and long, dark winters. Thus, due to this harsh environment the development of flora in Antarctica is extremely poor and limited. However, environment conditions favour certain plant growth in Antarctica especially phytoplankton.

In general, temperature, light and nutrients are important factors that normally affect algal growth. Nitrogen and phosphorus (plus Si for diatoms) are essential micronutrients that must be taken up from the environment for their growth and are most likely to limit the growth of phytoplankton. Ortho-phosphate is a form of phosphorus normally found in natural water. It plays an important role in most metabolic phases and is involved indirectly in the energy exchange reaction (Stewart 1974) while protein synthesis depends on the availability of nitrogen in the water system.

Within normal limits, temperature also has a direct effect on the development of phytoplankton. Most of the cellular processes of the phytoplankton are temperature dependent and their rates accelerate exponentially with increasing temperature (Robarts & Zohary 1984). The combination of antifreeze and the ability to grow at low temperature indicates that Antarctic algae are adapted to cold. In order to grow in a wide range of temperatures, these algae form zygospores or resistant cells at low temperatures. *Navicula* UMACC 231 and *Chlorella* (UMACC 234 dan UMACC 237) collected from this continent are able to grow in temperatures up to 30°C (Teoh *et al.* 2004).

Light is also one of the essential resources often limiting the growth rate of algae and is also a major factor determining its photosynthetic rate. Kuhl (1968) recorded that the availability of light is important to accelerate the uptake of nutrients in phytoplankton. Microalgae in the Antarctic regions are exposed to very low temperatures throughout the year.

Algal growth potential (AGP) tests have been applied in limnology since the 1960s (Klapwijk *et al.* 1989). Algal assay procedures to determine AGP were used to study the environmental requirements of plankton. It was also used to measure the growth potential as a general water quality parameter, and to determine the limiting nutrient factors (Veenstra 1981; Haan *et al.* 1982; Vries & Klapwijk 1987). Determination of AGP is based on the relationship between maximum production of biomass and uptake of nutrient for algal growth (Travieso *et al.* 1999). The objective of this study was to investigate the effects of nutrient (phosphorus and nitrogen) levels, temperature and light-dark cycle on the growth of Antarctic *Chlorococcum* sp. and to determine the optimum parameters for their maximum growth.

MATERIALS AND METHOD

Culture Conditions

The Antarctic *Chlorococcum* sp. was isolated from upper and middle areas of the ephemeral stream at Reeve Hill, near Casey Station, Antarctica. The stock culture was grown axenically in 1000 ml Erlenmeyer flasks containing

¹School of Biological Sciences, Universiti Sains Malaysia, 11800 Penang, Malaysia

*Corresponding author (e-mail: maslily_dahlan@hotmail.com)

500 ml of Bold Basal Medium (BBM) (Andersen 2005) with continuous illumination (241 Lux) of white fluorescent light, at a constant temperature of 4°C.

Experimental Design

Effects of nitrogen and phosphorus levels. *Chlorococcum* sp. was cultured separately in solutions with different concentrations of nitrogen and phosphorus as shown in Table 1, in which the elements (nitrogen and phosphorus) were varied in increments and fractions of two times the concentration of BBM medium.

Effect of temperature. *Chlorococcum* sp. was cultured in three replicates at 4°C, 15°C and 3°C with the same range of phosphorus and nitrogen concentrations as in the previous experiment. These temperatures had been chosen as 4°C was the summer temperature in Antarctica, 15°C was the spring season in temperate conditions and 32°C was the normal tropical temperature.

Effect of light-dark cycle. Further experiments were done on the light-dark cycle with an equal 12 hour exposure to light and darkness, and total darkness (12 h: 12 h and 0 h: 24 h light-dark cycle).

For each of the experiments, three replicates of each concentration of phosphorus and nitrogen (Table 1), were grown separately in 200 ml Erlenmeyer flasks containing 100 ml cultures using a 10% inoculum and manually agitated (Teoh *et al.* 2004) for 10 days. Preliminary experiments had shown that a stationary phase was reached after 10 days.

Analytical Methods

Growth determination. 200 ml of culture were filtered through cellulose membrane filters (0.45 µm pore size). The chlorophyll pigment was extracted by 90% acetone according to standard methods (APHA 1992). The absorbance value of extracted culture was measured

using a spectrophotometer and calculated according to the following equation:

$$Ca = 11.85 (OD_{664}) - 1.54 (OD_{647}) - 0.08 (OD_{630}) \dots 1$$

where,

Ca = concentration of chlorophyll *a* (mg/l)
 OD₆₆₄, OD₆₄₇ and OD₆₃₀ = corrected optical densities at the respective wavelengths.

Phosphate and nitrate uptake analysis. The concentrations of ortho-phosphate in the samples were determined using the calorimetric method, while the concentration of nitrate was determined with calculated column reduction efficiency and nitrite concentration (APHA 1992). The uptake of nitrate and phosphate was determined by subtracting the amounts of each nutrient concentration at the beginning of the experiment with the concentrations that remained at the end of the experiment.

$$\text{The uptake of phosphate or nitrate} = [A]_i - [A]_f \text{ (mg NO}_3\text{-N/l/mg PO}_4\text{-P/l)} \dots 2$$

where,

[A]_i = Initial concentration of NO₃/PO₄ in each treatment culture
 [A]_f = Final concentration of NO₃/PO₄ in each treatment culture.

Calculation of algal growth potential. AGP can be derived from the reading of mean chlorophyll *a* based on this formula,

$$\text{Algal growth potential} = 1/n (n_f - n_a) \dots 3$$

where,

n = Time set of the experiment [as the time set of this experiment is only 1(10 days)], thus the value of n is 1
 n_f = Final mean reading of chlorophyll *a* (mg/l)
 n_a = Initial mean reading of chlorophyll *a*.

Table 1. Concentrations of nitrogen and phosphorus for each treatment culture.

Concentrations of nitrogen (mg NO ₃ -N/L)	Concentrations of phosphorus (mg PO ₄ -P/L)
2.54	2.60
10.77	13.00
21.06	26.00
41.67 (BBM)	52.00 (BBM)a
82.82	104.00
165.17	208.00
329.87	416.00
659.27	832.00

RESULT

AGP of *Chlorococcum* sp. under Various Concentrations of Phosphorus

Figure 1 represents the AGP of *Chlorococcum* sp. under various concentrations of phosphate at 4°C with 12 h: 12 h light-dark cycles. Maximum AGP (0.487 mg/l of chlorophyll *a*) was recorded at a low concentration of phosphate (2.6 mg PO₄-P/l) and the lowest AGP recorded was 0.191 mg/l of chlorophyll *a* at 104 mg PO₄-P/l. The AGP of this algae grown at 4°C with 12 h: 12 h light-dark cycle and at various concentrations of phosphate were not significantly different ($p > 0.05$).

In the dark experiment, the highest AGP (0.093 mg/l of chlorophyll *a*) was recorded at the same concentration of phosphorus under 12 h: 12 h experiment (Figure 1). The value of AGP decreased to negative at certain concentrations of phosphorus (13, 16, 104 and 832 mg PO₄-P/l). The AGPs attained were significantly ($p < 0.05$) affected by temperature, light-dark cycle and phosphate level. The chlorophyll *a* concentrations and AGPs attained were significantly higher ($p < 0.05$) in cultures grown on 12:12 h light-dark cycle than those grown in the dark.

Further experiments at 15°C showed that growth of *Chlorococcum* sp. was high at the lower concentrations of phosphorus. However, the species were unable to adapt to a higher temperature (32°C) and died (Figure 2). The effects of temperature (4°C, 15°C and 32°C) along with the 12 h exposure to lights and different concentrations of phosphate showed a significant difference to AGP (one-way ANOVA).

AGP of *Chlorococcum* sp. under Various Concentrations of Nitrogen

Experiments were then continued separately with various nitrogen concentrations added to the cultures with 12 h exposure of lights. The results obtained for AGP showed different trends compared to the previous experiment. The maximum AGP was attained by the cultures grown at 329.87 mg NO₃-N/l. Growth of *Chlorococcum* sp. at 32°C was found to be the lowest compared to the growth at 4°C and 15°C. The alga did not grow at nitrogen concentrations of 82.82 mg NO₃-N/l and 659.27 mg NO₃-N/l (Figure 3).

The cultures grown in 24 hour darkness attained the maximum AGP at 82.82 mg/l of chlorophyll *a*. The growth decreased at high nitrogen levels (> 329 mg NO₃-N/l) (Figure 4). In summary, the results showed that the AGP of *Chlorococcum* sp. was significantly affected ($p < 0.05$) by nitrogen level, light-dark cycles and temperature.

DISCUSSIONS

According to Kondol *et al.* (1984), algal assay is a useful method for identifying growth limiting nutrient. Estimation of AGP is of interest to estimate the maximum growth of useful species. It also can predict the maximum biomass of a harmful species (Maestrini *et al.* 1997). For instance, determination of the nutrients limiting AGP helps to focus on the proper mechanisms leading to the situation of interest.

Effect of Concentration of Phosphorus and Nitrogen on the Growth of Antarctic *Chlorococcum* sp.

The concentrations of nitrogen and phosphorus in the growth medium are important for biomass and the growth rate of algae. Metabolism processes in the cell depends on the phosphate and phosphorilate (Batterton & Van Baalen 1967). Thus, the total phosphate available affects the metabolism process as well as the growth of the species. Previous research by Gerloff *et al.* (1950) showed that *Coccochloris peniocyctis* required low concentrations of phosphate for maximum growth.

This finding was related to this experiment as *Chlorococcum* sp. attained the highest AGP at low concentrations of phosphate (2.6 mg/l). However, at 15°C and 4°C experiments, Antarctic *Chlorococcum* sp. recorded a high growth rate and chlorophyll *a* content at the higher concentrations of phosphate. Dash *et al.* (1995) demonstrated that the growth rates and chlorophyll *a* content of both *Chlorococcum* and *Scenedesmus* increased when the cultures were grown in medium with excess of nitrate, phosphate and EDTA. *Chlorococcum* tended to grow better in a medium with high concentrations of phosphate.

Algae however require higher concentrations of nitrogen compared to other elements such as phosphorus and sulphur (Gerloff *et al.* 1950). In order to attain maximum growth, this nutrient needed to be supplied continuously at high concentrations. Low concentrations of nitrate or nitrogen will inhibit algal growth and lead to mortality. In this study, the nitrate content of *Chlorococcum* sp. as recorded was 36.8 mg/l but the concentrations could be different depending on the other environmental factors such as light and temperature.

Effect of Temperature on the Growth of *Chlorococcum* sp.

Ecologically, the average temperature for algal growth is very important as it will show the range of temperatures where the alga can undergo their metabolic process actively (Brock 1974). Reactions that involve enzymes in photosynthesis mostly depend on the temperature (Nielsen & Jørgansen 1968). The maximum activity of RuBP carboxylic limited

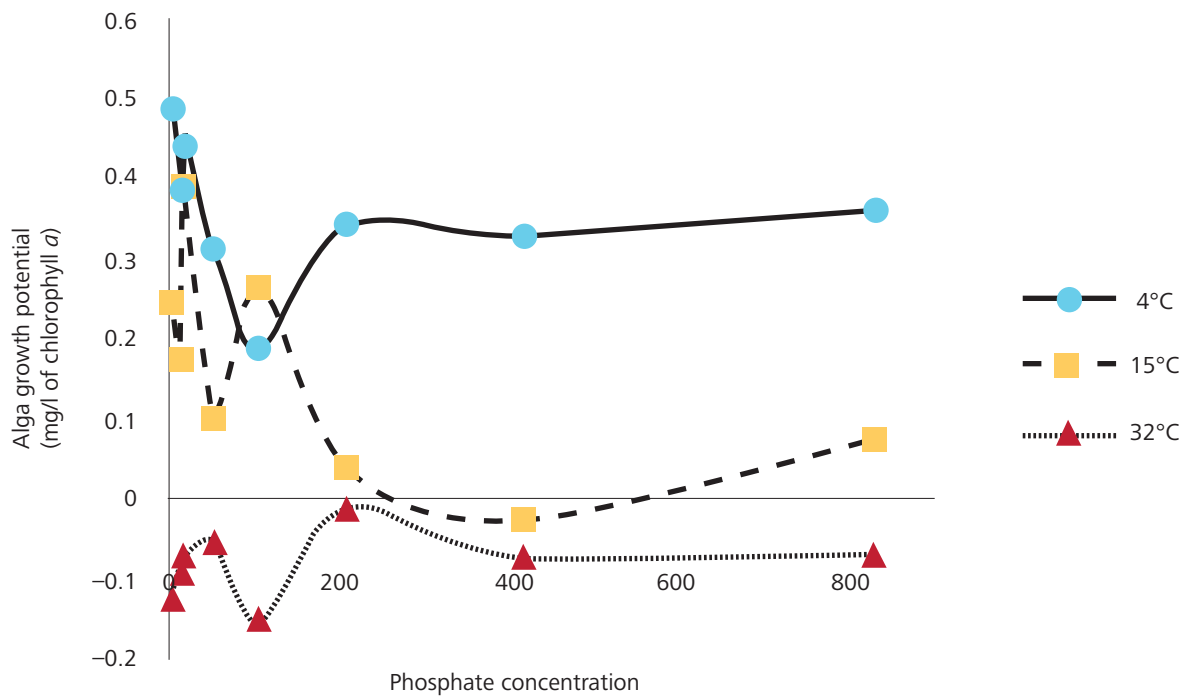


Figure 1. Effect of phosphate concentrations on the AGP of *Chlorococcum* sp. grown at different temperatures.

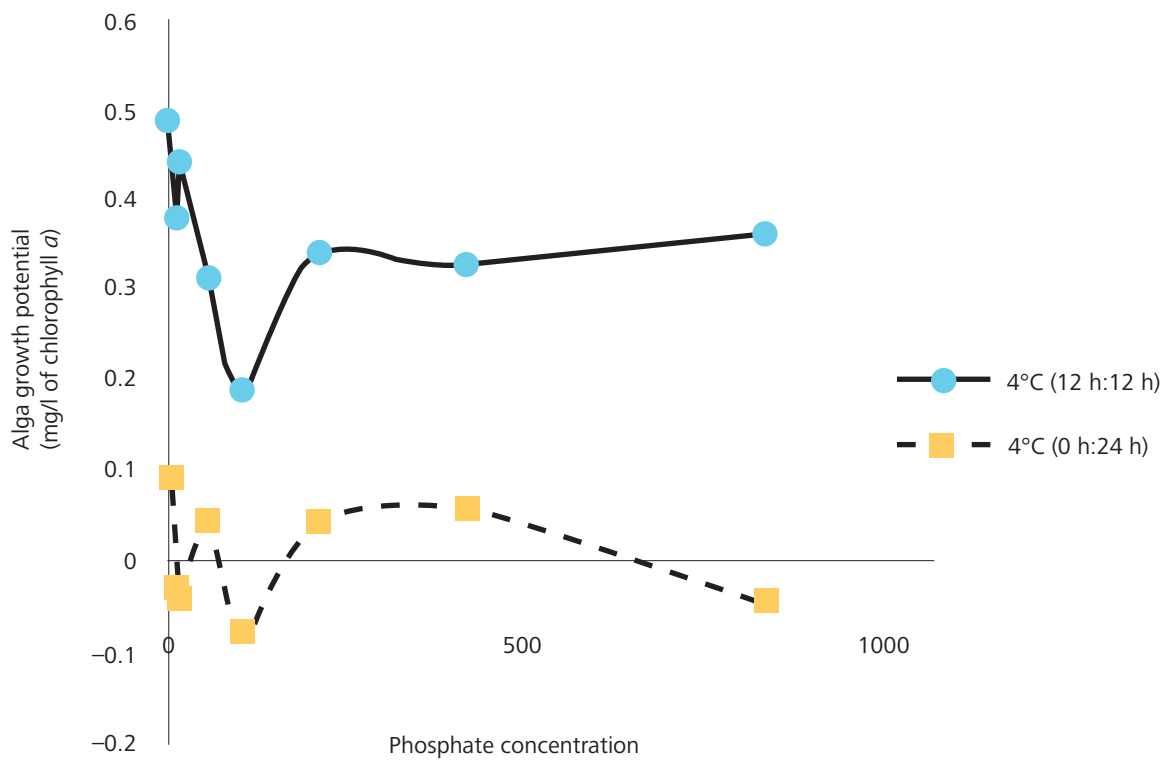


Figure 2. Effect of phosphate concentration on the AGP of *Chlorococcum* sp. grown on different light-dark cycles (12 h: 12 h versus 0 h: 24 h).

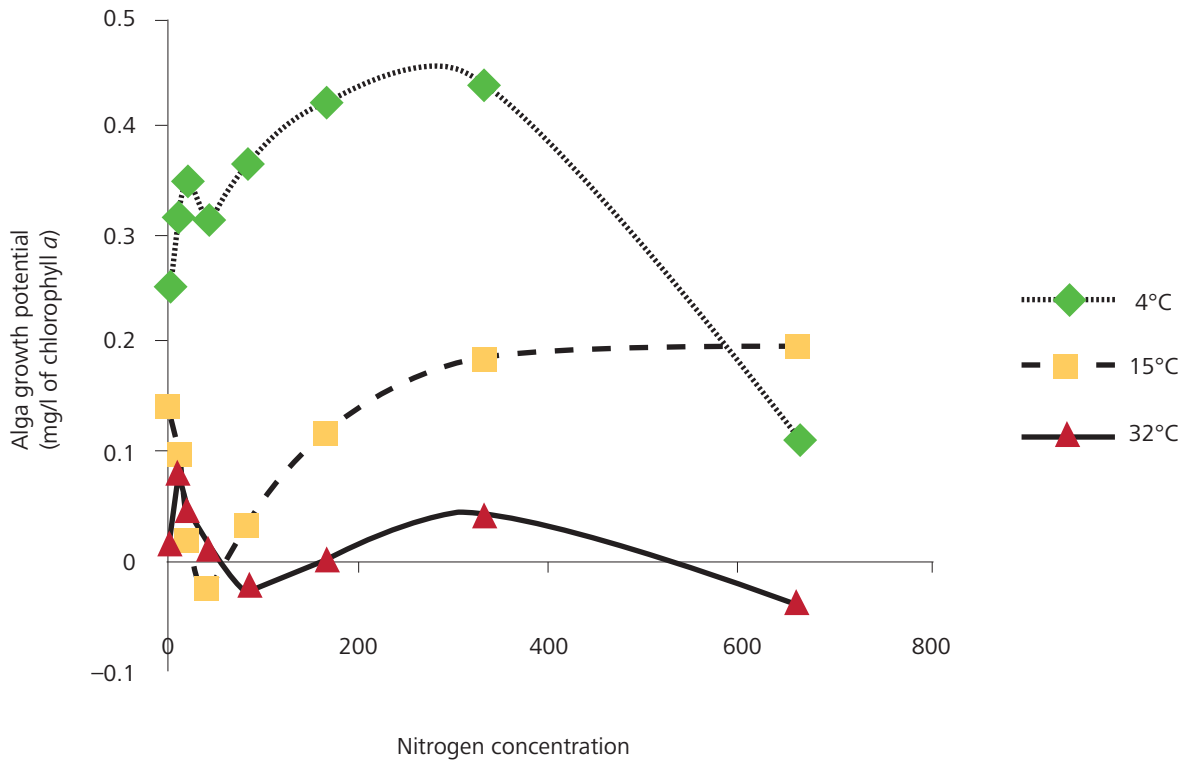


Figure 3. Effect of nitrogen concentrations on the AGP of *Chlorococcum* sp. grown at different temperatures.

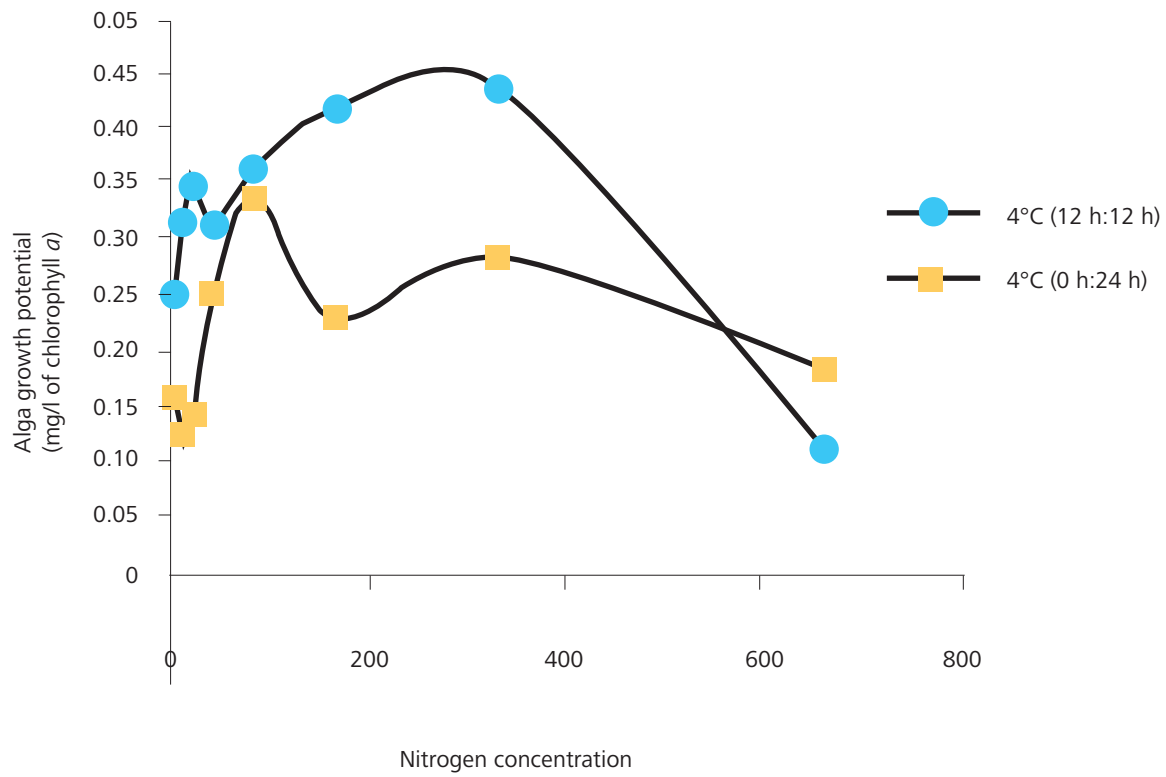


Figure 4. Effect of nitrogen concentration on the AGP of *Chlorococcum* sp. grown on different light-dark cycles 12 h: 12 h versus 0 h: 24 h).

the photosynthetic rate at 4°C for diatoms from Antarctica while temperate species showed maximum activity at 20°C (Descolas-Gros & de Billy 1987). According to Seaburg *et al.* (1981), most of the terrestrial and aquatic habitat in Southern Victoria Land, Antarctica was maintained under the freezing point for at least 9 months every year because of cold weather and high elevation. Order Desmarestiales from Antarctica was able to grow at temperatures as low as 0 – 15°C (Wiencke & Dieck 1989).

In this experiment, Antarctic *Chlorococcum* sp. grew well at low temperatures and a higher temperature (32°C) led to mortality. At 4°C, photosynthetic activities were more energetic and increased chlorophyll *a* contents.

Effect of Light on the Growth of *Chlorococcum* sp.

The experiments indicated that *Chlorococcum* sp. grew better with exposure to light compared to total darkness. The photosynthetic rate of the species was higher with the availability of light, as it increased the chlorophyll *a* and biomass of the species. Based on previous research, Antarctic *Chlorococcum* sp. was able to adapt to total darkness by changing its physiology to grow under extreme weather. Other suggested mechanisms for the growth of algae without light was by lowering their respiration rate and heterotrophic activities (Dehning & Tilzer 1989) as well as preserving their ability for photosynthesis. This algae are able to continue photosynthesizing when there was a good supply of light (Tilzer *et al.* 1977).

The decrease of AGP at a concentration of 36.8 mg/l of nitrate showed that *Chlorococcum* sp. could photosynthesize. According to Dehning & Tilzer (1989), if the alga were left in darkness, the ability to grow will be decreased and the cells will die. Somehow, after being exposed back to light, one third of the alga will start to grow again.

CONCLUSION

This study showed that temperature was the dominant factor in limiting the growth of *Chlorococcum* sp. Maximum growth was attained by this alga when cultured at a high concentration of nitrate (329.87 mg/l) and a low concentration of phosphorus (2.6 mg/l), at 4°C under 12 h:12 h light-dark cycle. The growth of this Antarctic alga was inhibited at 32°C.

ACKNOWLEDGEMENTS

We wish to thank Faradina, Dr Rashidah, Dr Latiffah and all members of Australian Antarctic Division for the collection of samples. We also thank the Malaysian Antarctic Research

Programme for the funding and Universiti Sains Malaysia for their support.

Date of submission: October 2008

Date of acceptance: April 2010

REFERENCES

- Andersen, RA 2005, *Algal culturing techniques*, Elsevier Academic Press.
- APHA 1992, *Standard method for the examination of water and wastewater*, 18th edn, American Public Health Association, American Water Works Association and Water Pollution Control Federation, Washington, DC, USA.
- Batterton, JC & Van Baalen, C 1967, Phosphorus deficiency and phosphate uptake in the blue-green alga *Anacystis nidulans*, *Can. J. Microbiol.*, vol. 22, pp. 341–348.
- Brock, TD 1974, *Biology of microorganism*, New Jersey: Prentice-Hall Inc.
- Dash, RC, Mohapatra, PK & Mohany, RC 1995, 'Salt induced changes in the growth of *Chlorococcum humicola* and *Scenedesmus bijugatus* under nutrient limited culture', *Bull. Environ. Contam. Toxicol.*, vol. 54, pp. 695–720.
- Dehning, I & Tilzer, MM 1989, 'Survival of *Scenedesmus acuminatus* (Chlorophyceae) in darkness', *J. Phycol.*, vol. 25, pp. 509–515.
- Descolas-Gros, C. & de Billy, G 1987, 'Temperature adaptation of RuBP carboxylase: kinetic properties in marine antarctic diatoms', *J. Exp. Mar. Bio. Eco.*, vol. 108, pp. 147–158.
- Gerloff, GC, Fitzgerald, GP & Skoog, F 1950, 'The Mineral Nutrition of *Coccochloris peniocyctis*', *American Journal of Botany*, vol. 37, no. 835, pp. 840.
- Haan, H, de, Wanders, J BW & Moed, JR, 1982, 'Multiple addition bioassay of Tjeukemeer water', *Hydrobiologia*, vol. 88, pp. 233–244.
- Klapwijk, SP, Bolier, G & Van der Does, J 1989, 'The application of algal growth potential tests (AGP) to the canals and lakes of western Netherlands', *Hydrobiologia*, pp. 188–189.
- Kondol, M, Sakai, T, Yamamoto'r, H & Arakawa, Y 1984, 'Algal growth potential and the limiting nutrient in Mikawa Bay', *Journal of the Oceanographical Society of Japan*, vol. 40, pp. 391–396.
- Kuhl, A 1968, *Phosphate metabolism of green algae in algae, man and environment*, New York, Syracuse University Press, pp. 37–47.
- Maestrini, SY *et al.* 1997, 'Nutrients limiting the algal growth potential (AGP) in the PO River plume and an adjacent Northwest Adriatic Sea: enrichment bioassays with the test algae *Nitzschia closterium* and *Thalassiosira pseudonana*', *Estuaries*, vol. 20, pp. 416–429.
- Nielsen, SE & Jørgensen, EG 1968, 'The Adaptation of plankton algae', *Physiologia Pl.*, vol. 21, pp. 401–413.
- Roberts, RD & Zohary, T 1987, 'Temperature effects on photosynthetic capacity, respiration, and growth rates

- of bloom-forming cyanobacteria', *Journal of Marine and Freshwater Research*, vol. 21, pp. 391–399.
- Seaburg, KG *et al.* 1981, 'Temperature-growth response of algal isolates from Antarctic oases', *J. Phycol.*, vol. 17, pp. 353–360.
- Stewart, WDP 1974, *Algal physiology and biochemistry*, Blackwell Scientific Publications.
- Teoh, ML *et al.* 2004, 'Variation of fatty acid profile of six Antarctic microalgae in response to temperature stress', in *Proceeding of the 2nd Malaysian International Seminar on Antarctica, Global Laboratory for Scientific and International Cooperation*, pp. 141–148.
- Tilzer, MM, Paerl, HW & Goldman, CR 1977, 'Sustained viability of aphotic phytoplankton in Lake Tahoe (California-Nevada)', *Limnology and Oceanography*, vol. 22, pp. 84–91.
- Travieso, L, Benitez, F & Dupeyron, R 1999, 'Algae growth potential measurement in distillery wastes', *Bull. Environ. Contam. Toxicol.*, vol. 62, pp. 483–489.
- Veenstra, S 1981, 'De algengroei-potentie-toets. Een nieuw instrument ter beoordeling van het eutrofiërend karakter van een water', LH Wageningen, Vakgroep Waterzuivering, sectie *Hydrobiologie*, Doktoraal verslagen serie nr, vol. 81, pp.1–61. (in Dutch).
- Vries, PJR, de & Klapwijk, SP 1987, 'Bioassays using *Stigeoclonium tenue* Kiitz. and *Scenedesmus quadricauda* (Turp.) Bréb. as testorganisms; a comparative study', *Hydrobiologia*, vol. 153, pp. 149–157.
- Wiencke, C, Dieck, IT 1989, 'Temperature requirements for growth and temperature tolerance of macroalgae endemic to the Antarctic region', *Mar. Eco. Progr. Ser.*, vol. 54, pp. 189–197.

Effects of Temperature on the Photosynthetic Parameters of Antarctic Benthic Microalgal Community

S. Salleh^{1,2*}, A. McMinn¹, M. Mohammad², Z. Yasin³ and S.H.A. Tan³

Elevated temperature affects marine benthic algae by reducing growth and limits the transport of electron or carbon fixation which may reduce the ability of the cell to use light. This resulting excess light energy may cause photoinhibition. In this study, the photosystem II of the benthic microalgal communities from Casey, eastern Antarctic were relatively unaffected by significant changes in temperatures up to 8°C, along with high PAR level (450 $\mu\text{mol photons m}^{-2} \text{s}^{-1}$). Similarly, the community was able to photosynthesize as the temperature was reduced to -5°C. Recovery from saturating and photoinhibiting irradiances was not significantly influenced by temperatures at both -5°C and 8°C. These responses were consistent with those recorded by past experiments on Antarctic benthic diatoms and temperate diatoms which showed that climate change did not have a significant impact on the ability of benthic microalgae to recover from photoinhibitory temperature stress.

Keywords: photoinhibition; recovery; temperature; light; Antarctic; benthic microalgae; photosystem II; Casey;

Elevated temperatures have a significant effect on microalgae, causing photoinhibition before other cell functions are impaired (Harrison & Platt 1986, Davison 1991). Extreme temperatures limit electron transport and carbon fixation by reducing the ability of the algae to use light. This results in excess light energy and causes photoinhibition by damaging the Photosystem II (PSII) apparatus (Levasseur *et al.* 1990; Anning *et al.* 2001). PSII is the most thermo-sensitive component of photosynthesis (Falkowski & Raven 1997). Temperature influences algae photosynthesis by changing the photosynthetic rate, or by inducing phenotypic or genotypic changes among algae species (Davison 1991). In a review by Eppley (1972), the author concluded that phytoplankton cultures grown at low temperature showed low P_{max} and low saturating intensity for photosynthesis. The changes in P_{max} with temperature were caused by effects on the enzymatic complex of inorganic carbon fixation (Davison 1991). Algae show different photosynthetic responses when exposed to temperatures above and below their optimal temperature. High temperatures may cause instability in the structure of the thylakoid membrane, primarily by affecting the composition of membrane lipids (Jensen & Knutsen 1993; Kirk 1994; Falkowski & Raven 1997). Davison (1991) suggested that elevated temperatures were able to modulate the cellular concentrations of RUBISCO and Calvin cycle enzymes that directly decreased the effective quantum yield ($\Delta F/F_m$). Theoretically $\Delta F/F_m$ is the operating quantum

efficiency of PSII; as such, it is a measure of the proportion of light absorbed by PSII that is used for photochemistry rather than being quenched (Maxwell & Johnson 2000). Thus a decrease in the $\Delta F/F_m$ may suggest damage to PSII or increased quenching activity (NPQ) (Ralph *et al.* 2005; Campbell *et al.* 2006). For example, El-Sabaawi & Harrison (2006) observed a decline in $\Delta F/F_m$ of sub-arctic diatoms species when exposed to temperatures from 4°C to 20°C. Microalgae exposed to extreme low temperatures lose flexibility in their membranes which then become crystalline or freeze (Falkowski & Raven 1997). The response of photosynthesis to temperature is also dependent on the available light, with the response at sub-saturating light levels being very different from that at saturating light levels (Davison 1991).

The benthic microalgal communities near Casey Station, eastern Antarctica, experience extreme variations in photoperiod and range of irradiance, ranging from low irradiances under ice cover in winter to high irradiances after the ice melts away or breaks up in spring. Irradiance on the sea floor has been reported to vary from 2 $\mu\text{mol photons m}^{-2} \text{s}^{-1}$ under ice cover to 308 $\mu\text{mol photons m}^{-2} \text{s}^{-1}$ in the absence of ice at depths of approximately 10 m (McMinn *et al.* 2004). Despite experiencing such extreme changes, the microalgal communities were able to adapt to both low and high irradiances. They were able to regulate their irradiance absorption efficiencies in response to the

¹ Institute of Antarctic and Southern Ocean Studies, University of Tasmania, Private Bag 77, Hobart 7001, Tasmania, Australia

² Centre for Marine and Coastal Studies, Universiti Sains Malaysia, 11800, Penang, Malaysia

³ School of Biological Sciences, Universiti Sains Malaysia, 11800, Penang, Malaysia

*Corresponding author (e-mail: sazlinam@utas.edu.au)

amount of irradiance to maximize their photosynthetic capacities (Glud *et al.* 2002; McMinn *et al.* 2004). McMinn *et al.* (2004) for example, found that the photosynthetic efficiencies (α) of benthic microalgae from areas with ice-cover were 50% greater than those from ice free areas at Casey, Antarctica.

The introduction of the pulse-amplitude modulated (PAM) fluorometer, has allowed researchers to study the activity of PSII, based on the direct and non-destructive determination of variable chlorophyll *a* fluorescence indices (Consalvey *et al.* 2005). The technique was originally introduced by Schreiber *et al.* (1986) for the study of terrestrial plant photosynthesis, but since then it has been applied to numerous aquatic autotrophs (McMinn *et al.* 2005a, 2005b; McMinn *et al.* 2003; McMinn *et al.* 2004; McMinn & Hegseth 2004; McMinn *et al.* 2005a, Consalvey *et al.* 2004a, 2004b; Consalvey *et al.* 2005; Ralph & Gademann 2005). Many studies have used rapid light curve (RLC) and this has been found to be a useful tool for the study of photosynthetic activity in benthic microalgae (Perkins *et al.* 2006; McMinn *et al.* 2004b; Serôdio *et al.* 2005; Jordan *et al.* 2008). Although a number of studies have examined the relationship between temperature, algal growth rate and photosynthesis, most of them were carried out on single species cultures. In this study, the effects of temperature and light were conducted on natural, species-rich benthic microalgal communities.

MATERIALS AND METHODS

Experimental Design

Sample collection and laboratory experiments were conducted during the Austral summer 2006. The sediments containing microalgae were collected from Brown Bay, Casey, Antarctica (Figure 1) and exposed to temperatures of -5°C , -1.8°C and 8°C for the duration of four hours. The top 10 mm of the sediment samples were suspended in a beaker and the excess seawater removed. The concentrated sediment samples were then transferred into a transparent 20 ml glass vial. Filtered seawater was added to each vial and the vials were placed in three chambers of different irradiance in a temperature-controlled waterbath (Lauda 20 L, Brinkmann Lauda Inc. Königshoven, Germany). The waterbath was filled with a mixture of methanol:water (1:4) to prevent the water from freezing. Triplicate sample vials were placed in each irradiance chamber. Irradiance intensities that were used in this experiment were $0 \mu\text{mol photons m}^{-2} \text{ s}^{-1}$ and $450 \mu\text{mol photons m}^{-2} \text{ s}^{-1}$, which were provided by a halogen lamp (Thorn 300W, Borehamwood, UK). The irradiance of each chamber was adjusted by the addition of a number of layers of dark plastic filter. These filters also assisted in reducing the heat produced by the halogen lamps. The irradiance in each chamber

was measured with a LI-COR Quantum-Light Metre (Model LI-189). At the end of each incubation temperature, a replicate was transferred into a cuvette for photosynthetic analysis. A PAM fluorometer was used to determine the quantum yield at the end of each temperature treatment. RLCs were run to obtain values for effective quantum yield ($\Delta F/F_m$), relative electron transport rate ($r\text{ETR}_{\text{max}}$), photosynthetic efficiency (α) and photoacclimation index (E_k). Before measurement, the samples were gently shaken to ensure even mixing and to limit settlement, then placed inside the measuring cuvette of the Water PAM fluorometer.

Chlorophyll Fluorescence Measurement

The PAM fluorometer uses a weak measuring light ($0.15 \mu\text{mol photons m}^{-2} \text{ s}^{-1}$) to measure the minimum fluorescence yield (F_o , open PSII reaction centres), while a saturating pulse ($>3000 \mu\text{mol photons m}^{-2} \text{ s}^{-1}$ for 0.8 s) is used to determine maximum fluorescence (F_m in the dark) when all PSII reactions centres are closed. Maximum fluorescence (F_m) is achieved by exposing the dark adapted sample to a pulse of intense irradiance. The maximum quantum yield of PSII is defined as:

$$F_v/F_m = (F_m - F_o) / F_m \quad \dots 1$$

To measure the F_v/F_m , benthic microalgae is dark adapted for approximately 15 minutes. During this period, electron transport stops, thus eliminating the trans-thylakoid pH gradient and allowing the full reduction of the primary electron acceptor Q_A . A fifteen minute dark adaption period has been suggested to be adequate by a number of studies as this is thought to be sufficient to result in a stable level of Q_A oxidation and hence a true measurement of F_o (minimum fluorescence) can be obtained (Kromkamp *et al.* 1998; Consalvey *et al.* 2005; McMinn & Hegseth 2004; McMinn *et al.* 2005a; McMinn *et al.* 2005b; Jordan *et al.* 2008). If a sample is exposed to additional in-situ actinic light, a similar saturating pulse will lead to a lower maximum fluorescence, F_m' , that provides a measure of the effective quantum yield ($\Delta F/F_m'$) and is derived by the following equation:

$$(F_m' - F_o) / F_m' \text{ where } F_m' - F_o = F_v \quad \dots 2$$

(Genty *et al.* 1989).

Under most physiological conditions, $\Delta F/F_m'$ is linearly correlated with the yield of carbon assimilation (Genty *et al.* 1989). Quantum yield of PSII is also a measure of the rate of charge separation in PSII (Bradbury & Baker 1981). Adverse environmental conditions such as high light with extreme temperatures can modulate cellular concentrations of RUBISCO that directly affect PSII. Therefore, a decrease in $\Delta F/F_m'$ values indicates irreversible damage to PSII, which could lead to photoinhibition.

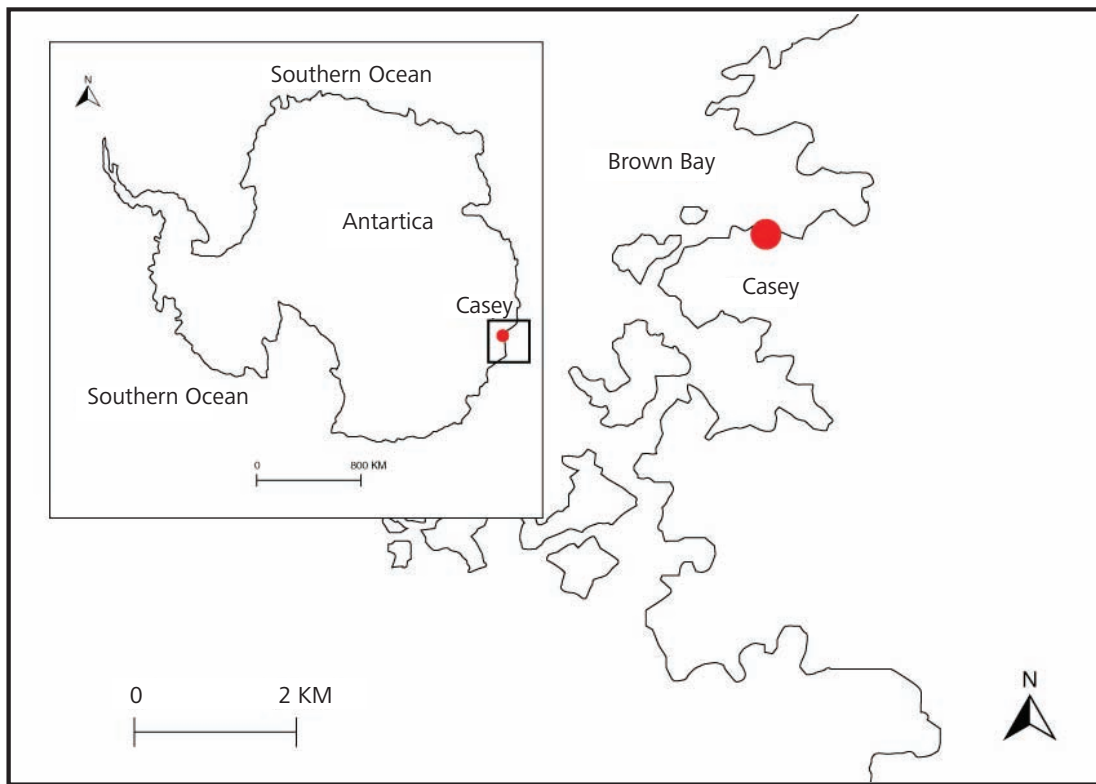


Figure 1. Location of sampling area in Brown Bay, near Casey Station, Antarctica.

RLCs were undertaken on all samples (Schreiber *et al.* 1997). A RLC is light treatment with eight consecutive 10 s intervals of actinic light of increasing intensity with an accompanying yield measurement at the end of each actinic exposure. Light emitting diodes provide the eight step-wise increments of actinic light at 0, 85, 125, 194, 289, 413, 517, 1046 and 1554 $\mu\text{mol photons m}^{-2} \text{s}^{-1}$. Relative electron transport rate (rETR) at a given irradiance is given by:

$$\text{rETR} = \Delta F/F_m \times \text{PAR} \quad \dots 3$$

RLCs provide a snapshot of the physiological state of a plant and its ability to adapt its photosynthetic apparatus to rapid changes in irradiance. Rapid light curves can be described using several characteristic parameters such as α (photosynthetic efficiency), rETR_{max} (relative electron transport rate) and E_k (photoacclimation index), by fitting the rETR and irradiance data to a single exponential decay function (McMinn & Hegseth 2004; McMinn *et al.* 2005b; Ralph & Gademann 2005). In this study, data were exported from WinControl (Walz, Effeltrich, Germany) into SPSS (SPSS 16.0 for Macintosh, SPSS Inc). Empirical data was mathematically fitted to an exponential decay function (Platt *et al.* 1980), using a Marquardt-Levenberg regression algorithm:

$$P = P_m (1 - e^{-(\alpha E_d/P_m)}) \quad \dots 4$$

P_m is a scaling factor defined as the maximum potential rETR (rETR_{max}) in the absence of photoinhibition and represents the photosynthetic capacity at saturating light; α is the initial slope of the RLC before the onset of saturation (light limiting condition efficiency) and E_d is the down-welling irradiance (400 nm – 700 nm). E_k is the photoadaptive index or minimum point of light saturation (Falkowski and Raven 1997) and is described by the following equation:

$$E_k = \text{rETR}_{\text{max}} / \alpha \quad \dots 5$$

NPQ (non-photochemical quenching) is a measurement of the activity of the protective mechanism which is designed to protect against over-reduction of the photosynthetic electron transport chain by dissipation of excess absorbed light energy in the PSII antenna system as heat (Demmig-Adams & Adams 1992). NPQ was determined by the following equation:

$$\text{NPQ} = (F_m - F_m') / F_m' \quad (\text{Schreiber 2004}) \quad \dots 6$$

Analysis of the Rate of Recovery

The method of determining and analyzing the rate of recovery was adapted from McMinn & Hattori (2006).

The measurement of recovery from photoinhibition was made using the pre-installed routine RLC + recovery of the water-PAM (Walz, Effeltrich, Germany). After the last actinic light period of the RLC, the sample was left in the dark while F_v/F_m was determined after 30, 60, 180, 300 and 600 s. The rate of recovery from photoinhibition was calculated following Oliver *et al.* (2003):

$$\Phi_t = \Phi_i + (\Phi_M - \Phi_i)(1 - e^{-rt}) \quad \dots 7$$

where,

Φ_t is the given value of F_v/F_m at time t (s), Φ_i is the initial value of F_v/F_m before recovery measurements have commenced, Φ_M is the fully recovered value and r is an exponential rate constant for the recovery of F_v/F_m from photoinhibition (s^{-1}). This formula assumes that the recovery rate of F_v/F_m is dependent on the degree of damage.

Statistical Analysis

Mean and standard deviations were calculated from three independent replicates. To evaluate the effects of temperature and irradiances (fixed factor) on the photosynthetic parameters ($\Delta F/F_m$, α , $rETR_{max}$ and E_k), NPQ and recovery, a two-way analysis of variance (ANOVA) was used. Differences were accepted as significant at $P < 0.05$ unless otherwise stated.

RESULTS

The effects of temperature and irradiance on all the photosynthetic parameters are presented in Figure 2a to 2f. Decrease in values was observed in a majority of the parameters at temperatures of -5°C and 8°C . These reductions caused by adverse temperature, however, did not enhance photoinhibition. Although significant differences (ANOVA, $P < 0.05$) were observed in $\Delta F/F_m$ values, no photoinhibition occurred as the microalgae were able to recover after each treatment. At temperatures of -5 and -1.8°C , higher values of $\Delta F/F_m$ were observed in the dark adapted samples (Figure 2a). In summary, $\Delta F/F_m$ was more affected by warmer temperatures than colder temperatures. In contrast to the $\Delta F/F_m$, microalgae incubated in ambient temperature (-1.8°C) showed lesser ability to utilise the given irradiance by comparison to -5°C and 8°C . This was seen in the α values in Figure 2b. Effects of temperature were more significant (ANOVA, $P = 0.0178$) by comparison to between irradiances (ANOVA, $P = 0.5771$). Temperatures up to 8°C were found to have a greater effect on $rETR_{max}$ (photosynthetic capacity) by comparison to -5°C (Figure 2c) although, there were significant differences (ANOVA, $P = 0.0016$) between all temperatures. The photoacclimation index (E_k) showed a consistent trend when higher values were obtained in high irradiance

adapted microalgae. Only the microalgae incubated in ambient temperature (-1.8°C) and high irradiance showed the ability to adapt to the given experimental irradiance condition, where E_k values were almost similar to the experimental irradiance (Figure 2d). Significant (ANOVA, $P = 0.0013$) effects between temperatures were observed in the E_k values. Figure 2e shows that the ability to dissipate excess light energy via NPQ was affected by the adverse temperatures (-5°C and -1.8°C). However, in colder and ambient temperatures, microalgae showed a better ability to recover than at warmer temperature (Figure 2f). In summary the data showed that photosynthetic activity was still present at high irradiance and temperature indicating no severe photodamage had occurred.

DISCUSSION AND CONCLUSION

Benthic microalgae in Antarctic shallow areas are naturally exposed to extremes of temperatures and irradiances. However, despite these difficult conditions, *in-situ* photoinhibition was rarely recorded, mostly due to the ability of microalgae to migrate away from irradiance into the sediments and activation of non-photochemical quenching (Longi 2003; McMinn *et al.* 2004). In this current experiment, although the benthic microalgae were exposed to unnaturally low and high temperatures, they were quite resilient to the damaging effects. The PAM analyses showed that photosynthetic activity could be activated and photoinhibition did not occur at either low or high temperatures. Supporting this observation, the effective quantum yield ($\Delta F/F_m$) in the experiments did not indicate any significant effect of temperature stress, thus indicating that these adverse temperatures were unable to enhance photoinhibition. Furthermore, Ralph *et al.* (2005) showed that the $\Delta F/F_m$ of sea ice communities was stable when exposed to temperatures down to -5°C for up to two hours. The decrease in effective quantum yield at high irradiance may also be a mechanism of protection against excessive light absorption (El-Sabaawi & Harrison 2006). This decrease by high irradiance was only observed at temperatures of -5°C and -1.8°C . At a higher temperature (8°C), microalgae were able to utilize the absorbed light energy efficiently for photochemical processes, whose lower values were observed in darkness experiments. This indicated that, although being exposed to high temperature and irradiance, the photosystem II of the Antarctic benthic microalgae not photoinhibited but was able to effectively utilise the absorbed light energy to photochemically fix and store carbon.

Apart from efficiently utilizing absorbed light energy for photosynthesis, the microalgae have the ability to control the amount of light absorption. This process is controlled by the light harvesting pigment complexes that are responsible for the changes in the ratio and quantity of several photosynthetic pigments. In this experiment,

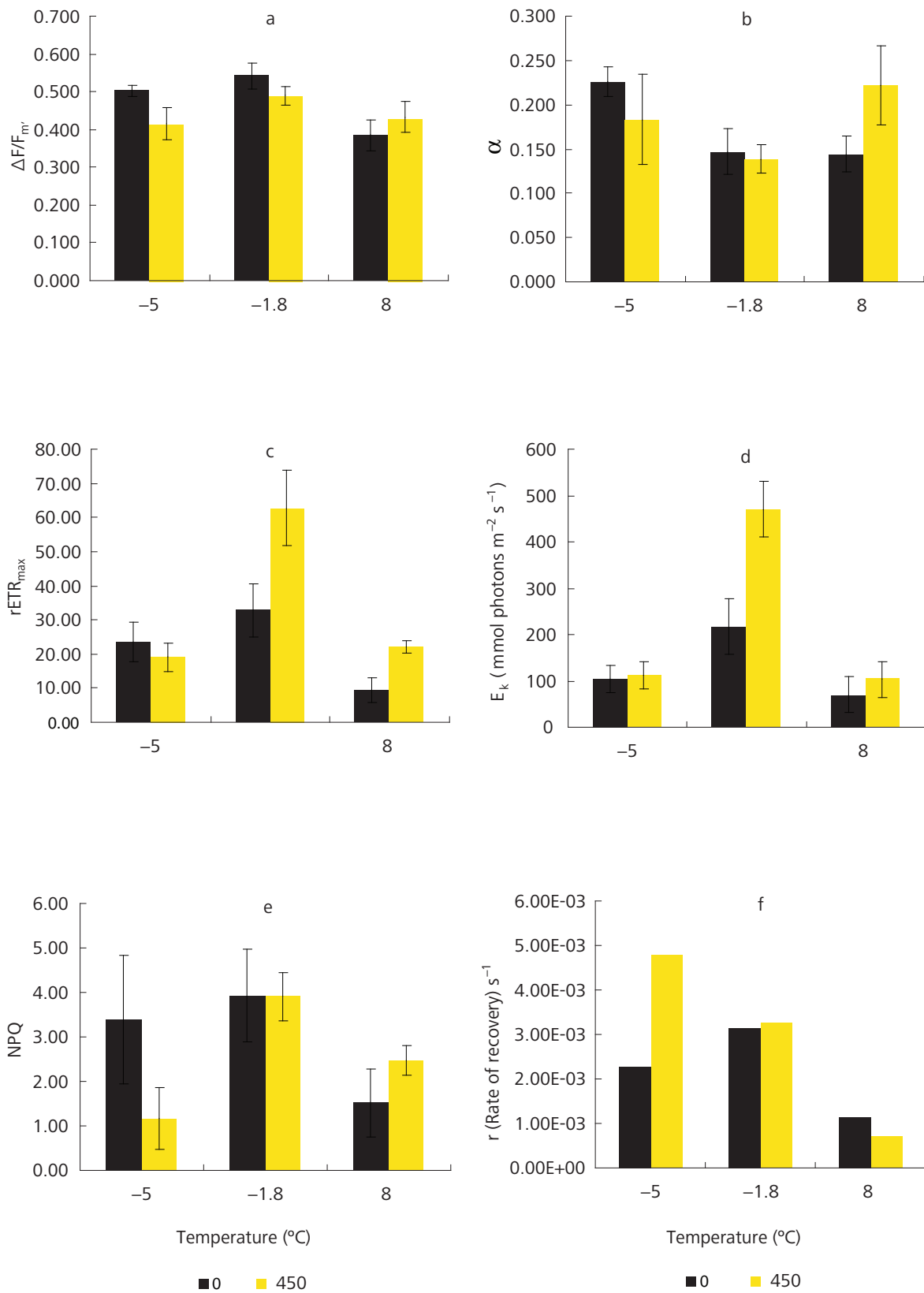


Figure 2. Derived photosynthetic parameters of RLC from temperature experiments. Parameters were plotted against experimental temperatures (-5, -1.8, and 8°C) at irradiances of 450 $\mu\text{mol photons m}^{-2} \text{s}^{-1}$ (yellow bar) and 0 $\mu\text{mol photons m}^{-2} \text{s}^{-1}$ (black bar) (a) Effective quantum yield ($\Delta F/F_m'$), (b) Photosynthetic efficiency (α), (c) Relative electron transport rate ($rETR_{max}$), (d) Photoacclimation index (E_k), (e) Non-photochemical quenching and (f) Rates of recovery (r). Values are means \pm SD (n=3).

although significant differences were observed between temperatures, temperatures up to 8°C, did not affect the microalgae's ability to absorb light for photosynthesis. Supporting this observation, high values (0.222 ± 0.04) were obtained at 8°C and at high irradiances. Past studies have shown that the algae developed specific ways to cope with temperature by inducing change in their energy requirements (Levasseur 1990). Ralph *et al.* (2005) showed that brine microalgae which were exposed to -1.8°C and -5°C showed significant tolerance to high irradiance, as shown by the stable photosynthetic efficiency. Furthermore, the short-term (four hour) incubation may not have been sufficiently extensive to affect the irradiance harvesting efficiency of the cells as was observed by Anning *et al.* (2001) in temperate cultures of *Chaetoceros calcitrans* whose cells were incubated for 4 to 7 days at 6°C and 25°C. If incubated for a longer duration, it is possible that the α value may be affected by temperature thereby giving the cell enough time to acclimatize to a given temperature as observed by other studies (Mock & Hoch 2005; Claquin *et al.* 2008).

The increase in irradiance apparently affected the photosynthetic capability thus reducing the $rETR_{max}$ values especially at temperatures of -1.8°C and 5°C. Adverse temperatures lead to an impairment of membrane functions, thereby limiting the efficiency of electron transport carriers, which affects the photosynthetic rate (Davison 1991; Kirk 1994; Ibelings 1996). These effects were observed in both colder and warmer temperatures as significant decreases were observed. Although the cells were able to absorb and utilise the light energy, adverse temperature had reduced the photosynthetic rate. As it was previously suggested that the maximum rate of photosynthesis was determined by the rate of carbon fixation, which was controlled by RUBISCO activity, thus a decrease in $rETR_{max}$ might have a decrease in the activity of RUBISCO (Davison, 1991). Changes in E_k values were paralleled to the $rETR_{max}$ values, since E_k values were derived from $rETR_{max}/\alpha$. E_k values provide an indication of the irradiance at which energy is diverted from photochemistry to heat dissipation and represents the degree of acclimation to ambient irradiance climate (Schreiber *et al.* 1995). Values are used as an indicator of the photoacclimatization status of microalgae with higher values of E_k indicating acclimatization to higher irradiance (Seradio *et al.* 2004). Most algal communities are able to constantly adjust their metabolism to maximize their response to irradiance. Falkowski and Raven (1997) indicated that the light saturated rate of photosynthesis was strongly affected by temperature, where E_k increased as the temperature increased. That effect was however, absent in this study. Temperatures lower and higher than ambient (-1.8°C) reduced the ability of microalgae to adjust their metabolism to maximize their response to irradiance. At ambient temperature, E_k values were similar to the given experimental irradiance indicating that acclimatization to experimental irradiance had occurred.

The adverse effects of high temperatures and irradiance can be minimized if non-photochemical quenching (NPQ) is activated. NPQ helps to regulate and protect Photosystem II against photoinhibition. When the light energy absorption exceeded the capacity for light utilization, NPQ was activated to dissipate the excess energy (Muller *et al.* 2001). NPQ activity is present in both low and high temperatures. These adverse temperatures, however, had obviously affected NPQ activation as decreases were observed in colder and warmer temperatures. It has been suggested that exposure to direct sunlight under low temperature can be particularly damaging to the photosynthetic apparatus, and this is expected to slow down the photoprotective response under high irradiance (Seródio *et al.* 2005). These effects were seen in microalgae which were exposed to both high irradiance and low temperatures concurrently. In summary, there was no severe photoinhibition in all treatments since the microalgae were able to recover. The lack of recovery of microalgae exposed to adverse temperatures indicates that photosynthetic enzymes may have been de-activated or damaged. However, in this current study, the reduction in the photosynthetic parameters and low rate of recovery at adverse temperatures were both characteristics of reversible photoinhibition. Slower recovery indicated that the community might be experiencing reversible photoinhibition and change in energy distribution in the PSII. Faster recovery indicated that the community was able to acclimatize to the given stress conditions. Samples exposed to $450 \mu\text{mol photons m}^{-2} \text{s}^{-1}$ and -5°C were able to recover the fastest in the temperature treatment. Warmer temperatures (8°C) were seen to have reduced the recovery rates, thus indicating damage to D1 protein in the microalgae caused by high irradiance and temperatures. That indicated high temperatures exacerbated the effects of high irradiance and reduced the ability of the microalgae to recover. It has been indicated that exposure to high irradiance leads to PSII damage and D1 protein degradation, while the repair to D1 protein is temperature dependent, with extreme temperatures decreasing the rate of repair (Campbell *et al.* 2006).

In summary, the benthic microalgal community at Brown Bay, Casey showed the ability to photosynthesize in high stress conditions, such as exposure to extreme irradiance and temperature. Although the community was able to acclimatize and avoid severe photoinhibition, a reduction in the photosynthetic rate could occur and hence, reduce the ability of the cell to adapt to the given irradiance at adverse temperatures. Thus, prolonged exposure might reduce the photosynthetic rate, decrease the growth rate and finally alter the composition of the community.

ACKNOWLEDGEMENTS

This study was supported by Universiti Sains Malaysia, Academy of Sciences Malaysia and University of Tasmania.

We would like to thank the Australian Antarctic Division for the logistic support at Casey Station.

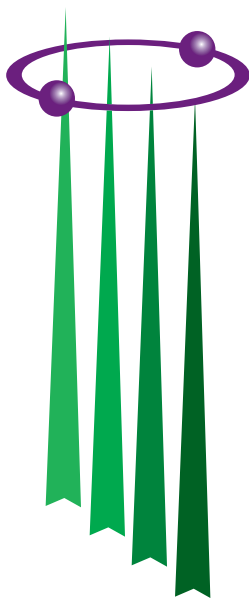
Date of submission: November 2008

Date of acceptance: April 2010

REFERENCES

- Anning, T, Harris, G & Geider, RJ 2001, 'Thermal acclimation in the marine diatom *Chaetoceros calcitrans* (Bacillariophyceae)', *European Journal of Phycology*, vol. 36, pp. 233–241.
- Bradbury N & Baker N 1981, 'Analysis of the slow phase of the *in-vivo* chlorophyll fluorescence induction curve' *Biochimica et Biophysica Acta*, vol. 635, pp. 542–51.
- Campbell, SJ *et al.* 2006, 'Photosynthetic responses of seven tropical seagrasses to elevated seawater temperature', *Journal of Experimental Marine Biology and Ecology*, vol. 330, pp. 455–468.
- Claquin, P *et al.* 2008, 'Effects of temperature on photosynthetic parameters and TEP production in eight species of marine microalgae', *Aquatic Microbiology and Ecology*, vol. 51, pp. 1–11.
- Consalvey, M *et al.* 2004a, 'Monitoring migration and measuring biomass in benthic biofilms: the effects of dark/far-red adaptation and vertical migration on fluorescence measurements', *Photosynthetic Research*, vol. 81 pp. 91–101.
- Consalvey, M *et al.* 2004b, 'The ups and downs of life in a benthic biofilm: migration of benthic diatoms', *Diatom Research*, vol. 19, pp. 181–202.
- Consalvey, M *et al.* 2005, 'PAM fluorescence: A beginner's guide for benthic diatomists', *Diatom Research*, vol. 20, pp. 1–22.
- Davison, IR 1991, 'Environmental effects on algal photosynthesis: temperature', *Journal of Phycology*, vol. 2, pp. 2–8.
- Demmig-Adams, B & Adams, WW 1992, 'Photoprotection and other responses of plants to high light stress', *Annual Review of Plant Biology*, vol. 43, pp. 599–626.
- El-Sabaawi, R & Harrison PJ 2006, 'Interactive effects of irradiance and temperature on the photosynthetic physiology of the pennate diatom *Pseudo-nitzschia granii* (Bacillariophyceae) from the Northeast Subarctic Pacific', *Journal of Phycology*, vol. 42, pp. 778–785.
- Eppley, WR 1972, 'Temperature and phytoplankton growth in the sea', *Fisheries Bulletin of United States*, vol. 70, pp. 1063–1084.
- Falkowski, PG & Raven, JA 1997, *Aquatic photosynthesis*, Blackwell Science, Massachusetts, US.
- Genty B, Briantais JM & Baker NR 1989, 'The relationship between the quantum yield of photosynthetic electron-transport and quenching of chlorophyll fluorescence', *Biochimica et Biophysica Acta*, no. 43, vol. 990, pp. 87–92.
- Glud RN, Kühl M, Wenzhöfer F & Rysgaard S 2002, 'Benthic diatoms of a high Arctic fjord (Young Sound, NE Greenland): importance for ecosystem primary production', *Marine Ecological Progress Series*, vol. 238, pp. 15–29.
- Harrison, WG & Platt, T 1986, 'Photosynthesis-irradiance relationships in polar and temperate phytoplankton populations', *Polar Biology*, vol. 5, pp. 153–64.
- Ibelings, BW 1996, 'Changes in photosynthesis in response to combined irradiance and temperature stress in cyanobacterial surface waterblooms', *Journal of Phycology*, vol. 32, pp. 549–557.
- Jensen, S & Knutsen, G 1993, 'Influence of light and temperature on photoinhibition of photosynthesis in *Spirulina platensis*', *Journal of Applied Phycology*, vol. 5, pp. 495–504.
- Jordan, L, McMinn, A & Wotherspoon S 2008, 'Diurnal and monthly vertical profiles of benthic microalgae within intertidal sediments from two temperate localities', *Marine Freshwater Research*, vol. 59, pp. 931–939.
- Kirk, JTO 1994, *Light and photosynthesis in aquatic ecosystems*, Cambridge University Press.
- Kromkamp, J, Barranguet C & Peene J. 1998, 'Determination of microphytobenthos PSII quantum efficiency and photosynthetic activity by means of variable chlorophyll fluorescence', *Marine Ecological Progress Series*, vol. 162, pp. 45–55.
- Levasseur, ME *et al.* 1990, 'Effects of long term exposure to low temperature on the photosynthetic apparatus of *Dunaliella tertiolecta* (Chlorophyceae)', *Journal of Phycology*, vol. 26, pp. 479–84.
- Longhi ML, Schloss IR & Wiencke C 2003, 'Effect of irradiance and temperature on photosynthesis and growth of two Antarctic benthic diatoms, *Gyrosigma subsalinum* and *Odontella litigiosa*', *Botanica Marina*, vol. 46, pp. 276–284.
- Maxwell, K & Johnson GN, 2000, 'Chlorophyll fluorescence—a practical guide' *Journal of Experimental Botany*, vol. 51, pp. 659–668.
- McMinn, A & Hattori H 2006, 'Effect of time of day on the recovery from light exposure in ice algae from Saroma Ko lagoon, Hokkaido', *Polar Bioscience*, vol. 20, pp. 30–36.
- McMinn, A. & Hegseth EN 2004, 'Quantum yield and photosynthetic parameters of marine microalgae from the Southern Arctic Ocean, Svalbard', *Journal of Marine Biological Association United Kingdom*, vol. 84, pp. 865–871.
- McMinn, A, Runcie, JW & Riddle, M 2004, 'Effect of seasonal sea ice breakout on the photosynthesis of benthic diatom mats at Casey, Antarctica', *Journal of Phycology*, vol. 40, pp. 62–69.
- McMinn, A *et al.* 2005a, 'Contribution of benthic microalgae to ice covered coastal ecosystems in northern Hokkaido, Japan', *Journal of Marine Biological Association United Kingdom*, vol. 85, 283–289.
- McMinn, A *et al.* 2005b, 'Quantum yield of the marine benthic microflora of near-shore coastal Penang, Malaysia', *Marine Freshwater Research*, vol. 56, pp. 1047–1053.
- Mock, T & Hoch, N 2005, 'Long-term temperature acclimation of photosynthesis in steady-state cultures of the polar diatom *Fragilariopsis cylindrus*', *Photosynthesis Research*, vol. 85, pp. 307–317.
- Muller, P, Li, XP and Niyogi, KK 2001, 'Non-photochemical quenching. A response to excess light energy', *American Society of Plant Biology*, vol. 125, pp. 1558–1566.

- Oliver, RL, Whittington, J, Lorenz, Z, & Webster, IT 2003, 'The influence of vertical mixing on the photoinhibition of variable chlorophyll a fluorescence and its inclusion in a model of phytoplankton photosynthesis', *Journal of Plankton Research*, vol. 25, pp. 1107–1129.
- Perkins, RG, Mouget, JL, Lefebvre, S & Lavaud J 2006, 'Light response curve methodology and possible implications in the application of chlorophyll fluorescence to benthic diatoms', *Marine Biology*, vol. 149, pp. 703–712.
- Ralph, PJ & Gademann R, 2005, 'Rapid light curves: A powerful tool to assess photosynthetic activity', *Aquatic Botany*, vol. 82, pp. 222–237.
- Ralph, PJ *et al.* 2005, 'Short-term effect of temperature on the photokinetics of microalgae from the surface layers of Antarctic pack ice', *Journal of Phycology*, vol. 41, pp. 763–769.
- Schreiber, U 2004, 'Pulse-amplitude-modulation (PAM) fluorometry and saturation pulse method, in *Chlorophyll a fluorescence: a signature of photosynthesis, advances in photosynthesis and respiration series*, eds G Papageorgiou, & Govindjee, Kluwer Academic Publishers, Dordrecht, The Netherlands, pp. 279–319.
- Schreiber, U *et al.* 1995, 'Quenching analysis of chlorophyll fluorescence by the saturation pulse method: particular aspects relating to the study of eukaryotic algae and cyanobacteria', *Plant and Cell Physiology*, vol. 36, pp. 873–882.
- Schreiber, U *et al.* 1997, 'Assessment of photosynthetic performance of Prochloron in *Lissoclinum patella* in hospite by chlorophyll fluorescence measurements', *Plant and Cell Physiology*, vol. 38, pp. 945–951.
- Schreiber, U, Schliwa, U & Bilger, W 1986, 'Continuous recording of photochemical and non-photochemical chlorophyll fluorescence quenching with a new type of modulation fluorometer', *Photosynthesis Research*, vol. 10, pp. 51–62.
- Serôdio, J *et al.* 2005, 'Non-photochemical quenching of chlorophyll fluorescence and operation of the xanthophyll cycle in estuarine microphytobenthos', *Journal of Experimental Marine Biology and Ecology*, vol. 326, pp. 157–169.



MAHATHIR SCIENCE AWARD 2011

Invitation for Nominations

The Academy of Sciences Malaysia (ASM) is a body set up with a mission that encompasses pursuit, encouragement and enhancement of excellence in the fields of science, engineering and technology for the development of the nation and the benefit of mankind. The Academy has instituted the Mahathir Science Award (formerly known as ASM Award for Scientific Excellence in honour of Tun Dr Mahathir Mohamad) in recognition of scientists/institutions who have contributed to cutting-edge tropical research that have had an impact on society.

This Award is Malaysia's most prestigious Science Award for tropical research launched in honour of Tun Dr Mahathir Mohamad who promoted and pursued with great spirit and determination his convictions in science and scientific research in advancing the progress of mankind and nations. Tun Dr Mahathir was the major force and the man who put into place much of the enabling mechanisms for a scientific milieu in our country.

This Award will be given to researchers who have made internationally recognised breakthroughs in pioneering tropical research in the fields of Tropical Medicine, Tropical Agriculture, Tropical Architecture and Engineering, and Tropical Natural Resources.

One Award will be conferred in 2011 covering any of the above four fields. The Award carries a cash prize of RM100 000, a gold medal and a certificate.

NOMINATION CRITERIA

- Awards will be given to researchers who have made internationally recognised breakthroughs in pioneering tropical research that have brought greater positive impacts on the well-being of society.
- Nominations can be made by individuals or institutions.
- A recipient could be an individual or an institution.

Nomination forms may be downloaded from the Academy's website:
www.akademisains.gov.my

Closing date: 31 March 2011

For more information, please contact:

Academy of Sciences Malaysia
902-4, Jalan Tun Ismail, 50480 Kuala Lumpur
Tel : 603-2694 9898; Fax : 603-2694 5858
E-mail: seetha@akademisains.gov.my
admin@akademisains.gov.my

22nd Pacific Science Congress

Asia Pacific Science in the New Millennium: Meeting the Challenges of Climate Change and Globalisation

14 –18 June 2011, Kuala Lumpur, Malaysia

The Congress will provide an inter-disciplinary platform for scientists from the region to discuss and review common concerns and priorities; bring together scientists from remote states; and serve as a catalyst for scientific and scholarly collaboration and to announce and establish new research initiatives. The Pacific Science Association (PSA) focuses on countries bordering the Pacific Ocean and the islands of the Pacific basin. PSA is a regional, non-governmental, and a scholarly organization that seeks to advance S&T in support of sustainable development in the Asia Pacific.



Sub-themes will include topics on:

- A Changing Climate: Climate science; Physical impacts; Ecosystem responses; Mitigation and adaptation strategies, Climate policies, Vulnerable human populations
- Global Change & Ecosystems: Biodiversity, Landscape Systems, Ecosystem Services, Coupled Human-Natural Systems, Invasive Species, Museum collections and barcoding
- Oceans: Coral Reefs, Ocean Acidification, Large Marine Ecosystems, Marine Biotechnology; Fisheries, Marine Mammals
- Earth Systems & Risk Management: Earth Science and Geophysics, Meteorology, Natural Hazards, Integrated Disaster Risk Reduction
- Globalization: Human populations, Population movement, Urbanization, Megacities, Gender, Economics and trade, Governance issues, Challenges of small island states, Human security, Poverty alleviation
- Resource Constraints & Sustainability: Millennium Development Goals, Water, Agriculture, Food, Energy, Integrated Coastal Zone Management, Ecological economics
- Health Challenges: Persistent and emerging infectious diseases, HIV/AIDS, Chronic and lifestyle diseases, Microbiology, Medical tourism, Telemedicine
- Science for Policy and the Future: Science communication, Science education, Building science capacity, Science and the media, Traditional knowledge, Data access and management, Intellectual property, Universality of science, Frontiers of science (complexity science, materials science, biotechnology)

Schedule and Programme:

Both plenary and parallel sessions, invited lectures, poster sessions, with at least one session open to the public and an optional post-congress field excursion will be planned. Various symposia will also be organized around the sub-themes.



Announcements

Enquiries:

Congress Secretariat
22nd Pacific Science Congress
c/o Academy of Sciences Malaysia
902-4, Jalan Tun Ismail
50480 Kuala Lumpur
Malaysia

Tel : (603) 2694 9898

Fax : (603) 2694 5858

e-mail: nasa@akademisains.gov.my; fardy@akademisains.gov.my

Website: www.akademisains.gov.my

Important Dates:

15-1-2011: Deadline for Submission of Abstracts
15-3-2011: Notification of Acceptance of Abstracts
31-3-2011: Deadline for Early-bird Registration
18-5-2011: Deadline for Late Registration
18-5-2011: Deadline for Refunds for Cancelled Registrations.
Website: www.22ndpsc.net



MALAYSIAN SCIENCE AND TECHNOLOGY CONGRESS 2010 9–11 NOVEMBER 2010

The Science and Technology Congress (MSTC) is the major event of the Confederation of the Scientific and Technological Association in Malaysia (COSTAM) and has been held for nearly three decades. The Congress is to showcase the scientific and technological research activities in the country, especially under the MOSTI research grants and the Scientific Advancement Fund Allocation for Fundamental Science Research (SAGA), and also related to the Malaysian Development Plan 2005–2010. This year's Congress is unique in that it focuses on the "Emerging and New Innovative Technologies".

MSTC 2010 (organised by COSTAM, MOSTI, ASM and MSSA) will focus on:

- Plenary or keynotes by leading scientists i.e. Fellows from the Academy of Sciences Malaysia (ASM)
- Research papers or reviews by scientists and technologists
- Papers by researchers specially those who have received MOSTI grants and *e*-Science fundings
- Researchers below 40 years of age are encouraged to present their findings. Special recognition will be given to the outstanding papers by this group.

INVITATION TO PRESENT R&D PAPERS

Papers are invited in the following areas:

- Agro and natural resource based sciences
- Applied sciences
- Biology, chemistry, mathematics and physics
- Biomedical sciences
- Earth and space sciences
- Engineering materials, photonics and semi-conductors
- Electronics and bio-sensors
- Emerging and new innovative technologies
- Nano science and technology; and
- Sustainable technologies.

DEADLINE FOR ABSTRACT AND FULL PAPERS

Deadline for Abstract: 31 August 2010

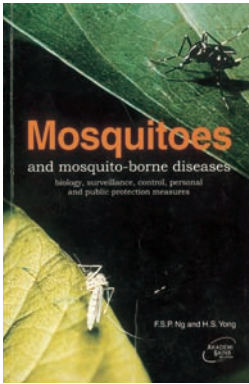
Deadline for Full Papers: 31 September 2010

Please e-mail abstract to: malsci@tm.net.my; abih86@yahoo.com

Registration and other details:

E-mail: malsci@tm.net.my; hamid929@salam.uitm.edu.my; abih86@yahoo.com;

Tel: 03-7955 0576; Fax: 03-7954 6440



Mosquitoes and Mosquito-borne Diseases: Biology, Surveillance, Control, Personal and Public Protection Measures

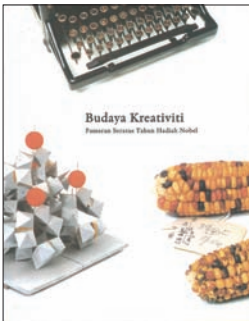
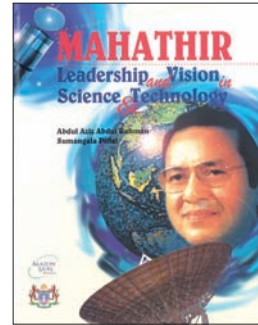
F.S.P. Ng and H.S. Yong (Editors)
(2000)

ISBN 983-9445-05-7
Price: RM60.00 / USD20.00

Mahathir: Leadership and Vision in Science and Technology

Abdul Aziz Abdul Rahman and Sumangala Pillai
(1996)

ISBN 983-9319-09-4
Price: RM100.00 / USD30.00



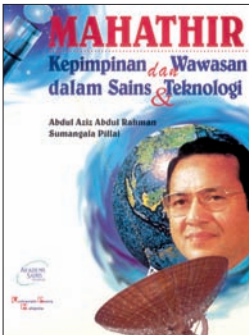
Budaya Kreativiti: Pameran Seratus Tahun Hadiah Nobel

Ulf Larsson (Editor)
(2004)

ISBN 983-9445-09-X
Price: RM50.00 / USD15.00

CD Kompilasi estidotmy

Edisi I – 94, 2002–2009
Price: RM40.00



Mahathir: Kepimpinan dan Wawasan dalam Sains dan Teknologi

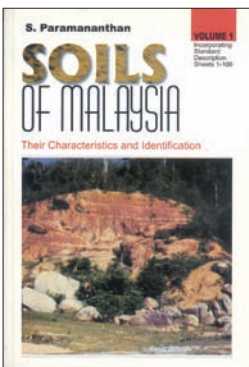
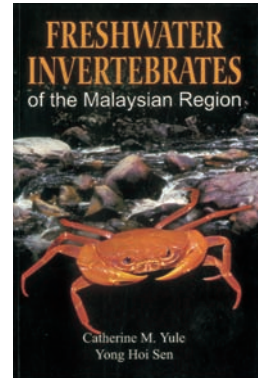
Abdul Aziz Abdul Rahman dan Sumangala Pillai
(1996)

ISBN 983-9319-09-4
Price: RM100.00 / USD30.00

Freshwater Invertebrates of the Malaysian Region

Catherine M. Yule and Yong Hoi Sen
(2004)

ISBN 983-41936-0-2
Price: RM180.00 / USD52.00



Soils of Malaysia: Their Characteristics and Identification (Vol. 1)

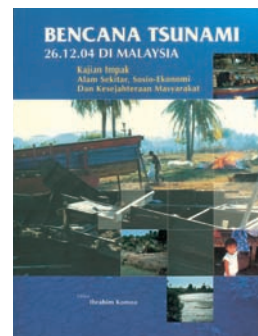
S. Paramanathan
(2000)

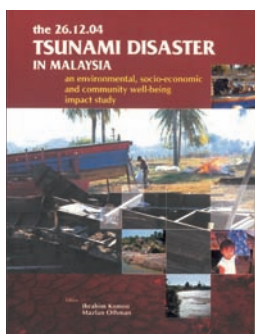
ISBN 983-9445-06-5
Price: RM100.00 / USD30.00

Bencana Tsunami 26.12.04 di Malaysia: Kajian Impak Alam Sekitar, Sosio-Ekonomi dan Kesejahteraan Masyarakat

Ibrahim Komoo (Editor)
(2005)

ISBN 983-9444-62-X
Price: RM100.00 / USD30.00





The 26.12.04 Tsunami Disaster in Malaysia: An Environmental, Socio-Economic and Community Well-being Impact Study

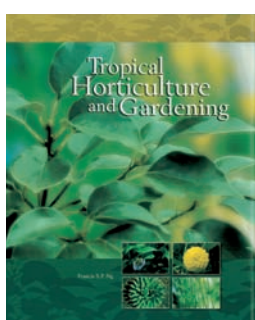
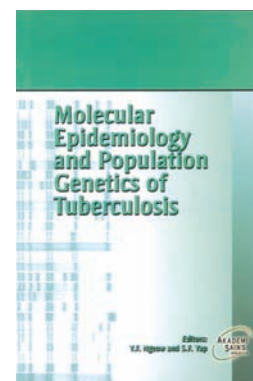
Ibrahim Komoo and Mazlan Othman (Editors)
(2006)

ISBN 983-9444-62-X
Price: RM100.00 / USD30.00

Molecular Epidemiology and Population Genetics of Tuberculosis

Y.F. Ngeow and S.F. Yap (Editors)
(2006)

ISBN 983-9445-14-6
Price: RM40.00 / USD12.00



Tropical Horticulture and Gardening

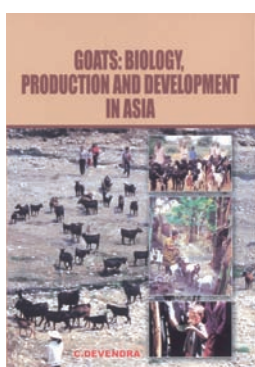
Francis S.P. Ng
(2006)

ISBN 983-9445-15-4
Price: RM260.00 / USD75.00

Kecemerlangan Sains dalam Tamadun Islam: Sains Islam Mendahului Zaman Scientific Excellence in Islamic Civilization: Islamic Science Ahead of its Time

Fuat Sezgin
(2006)

ISBN 983-9445-14-6
Price: RM40.00 / USD12.00



Goats: Biology, Production and Development in Asia

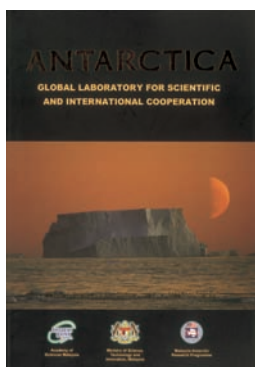
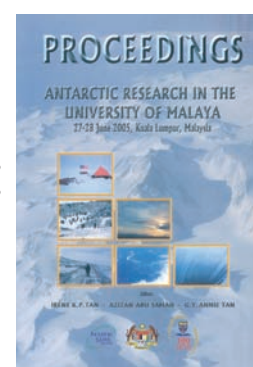
C. Devendra
(2007)

ISBN 978-983-9445-18-3
Price: RM180.00 / USD52.00

Proceedings: Seminar on Antarctic Research, 27-28 June 2005, University of Malaya, Kuala Lumpur, Malaysia

Irene K.P. Tan et al. (Editors)
(2006)

ISBN 978-983-9445-17-6
Price: RM40.00 / USD12.00



Antarctica: Global Laboratory for Scientific and International Cooperation

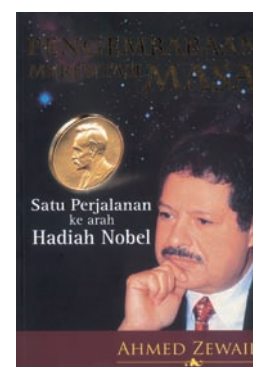
Aileen Tan Shau-Hwai et al. (Editors)
(2005)

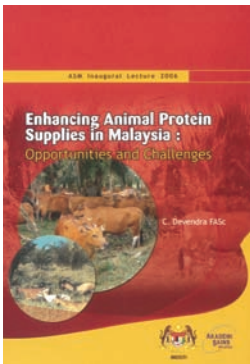
ISBN 983-9445-13-8
Price: RM40.00 / USD12.00

Pengembaraan Merentasi Masa: Satu Perjalanan ke Arah Hadiah Nobel

Ahmed Zewail
(2007)

ISBN 978-9445-20-6
Price: RM40.00 / USD12.00

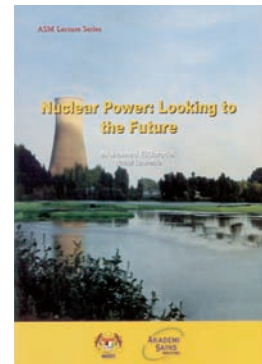




Enhancing Animal Protein Supplies in Malaysia: Opportunities and Challenges

C. Devendra
(2007)

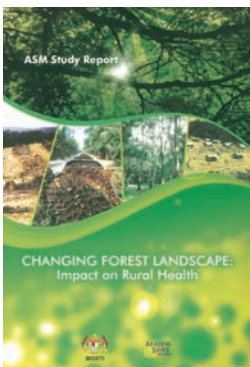
ISBN 983-9444-62-X



Nuclear Power: Looking to the Future

Mohamed ElBaradei
(2008)

ISBN 983-9445-14-6



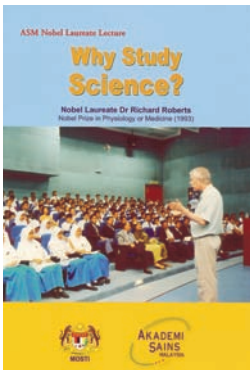
Changing Forest Landscape: Impact on Rural Health
(2007)

ISBN 983-9445-15-4

Dunia Sains
Vol. 5, No. 4, Oktober – Disember 2007
(2008)

A World of Science
Vol. 5, No. 4
October – December 2007

www.akademisains.gov.my/unesco/dunia_sains/okt_dis_2007.pdf



Why Study Science?

Richard Roberts
(2008)

ISBN 978-983-9445-18-3

Dunia Sains
Vol. 6, No. 1, Januari – Mac 2008
(2008)

A World of Science
Vol. 6, No. 1
January – March 2008



ASM Science Journal

Vol. 1, No. 1, June 2007

ISSN : 1823-6782

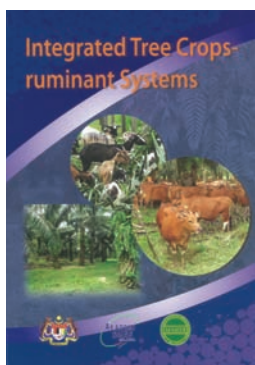
Price: RM100.00 / USD50.00 (Individual)
RM200.00 / USD100.00 (Institution)

ASM Science Journal
Vol. 1, No. 2, December 2007

ISSN : 1823-6782

Price: RM100.00 / USD50.00 (Individual)
RM200.00 / USD100.00 (Institution)



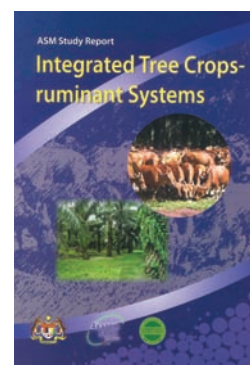


Integrated Tree Crops-ruminant Systems (Proceedings)

C. Devendra, S. Shanmugavelu and Wong Hee Kum (Editors) (2008)

ISSN : 983-9445-24-3

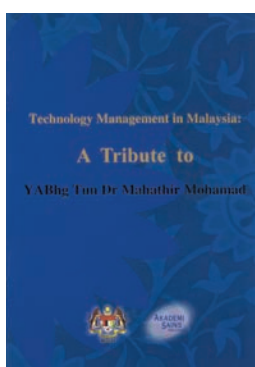
Price: RM40.00 / USD12.00



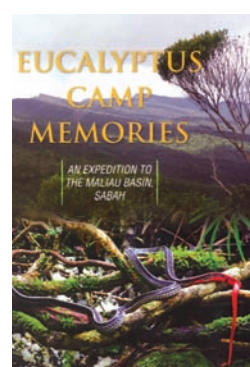
ASM Study Report: Integrated Tree Crops-ruminant Systems (2008)

ISSN : 983-9445-24-4

Price: RM30.00 / USD9.00



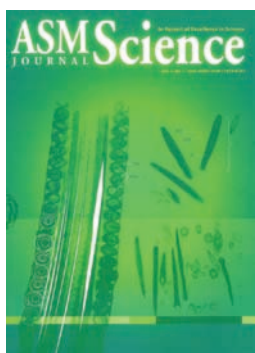
Technology Management in Malaysia: A Tribute to YABhg Tun Dr Mahathir Mohamad (2008)



Eucalyptus Camp Memories: An Expedition to the Maliau Basin, Sabah (2008)

ISSN : 978-983-9445-25-1

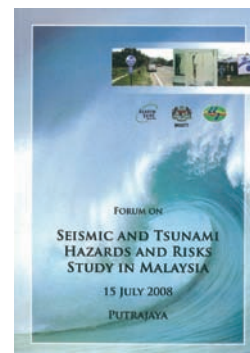
Price: RM220.00 / USD61.00 (Hard cover)
RM160.00 / USD42.00 (Soft cover)



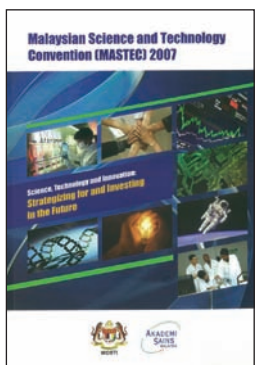
ASM Science Journal Vol. 2, No. 1, December 2008

ISSN : 1823-6782

Price: RM100.00 / USD50.00 (Individual)
RM200.00 / USD100.00 (Institution)



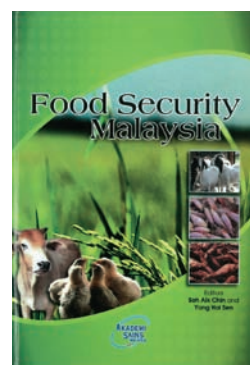
Forum on Seismic and Tsunami Hazards and Risks Study in Malaysia 15 July 2008



Science, Technology and Innovation: Strategizing for and Investing in the Future [Malaysian Science and Technology Convention (MASTEC) 2007] (2009)

ISSN : 978-983-9445-27-5

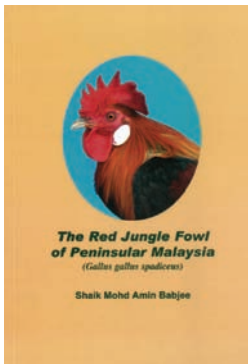
Price: RM51.00 / USD22.00



Food Security Malaysia (Proceedings) Soh Aik Chin and Yong Hoi Sen (Editors) (2009)

ISSN : 978-983-9445-28-2

Price: RM20.00 / USD6.00



The Red Jungle Fowl of Peninsular Malaysia

Shaik Mohd Amin Babjee (2009)

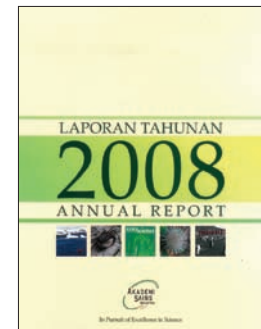
ISBN : 978-983-9445-29-9

Price: RM35.00 / USD12.00

Academy of Science Malaysia

Annual Report 2008

Price: RM50.00 / USD20.00



Journal of Science & Technology in the Tropics

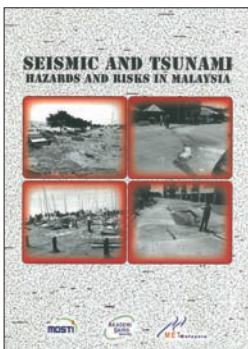
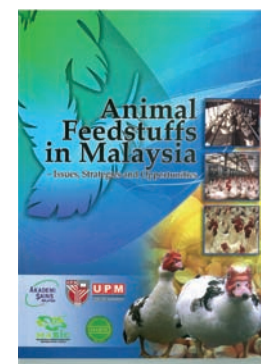
Vol. 4, No. 2, December 2008

ISSN: 1823-5034

Animal Feedstuffs in Malaysia – Issues, Strategies and Opportunities (2009)

ISBN : 978-983-9445-30-5

Price: RM35.00 / USD12.00



Seismic and Tsunami Hazards and Risks in Malaysia (2009)

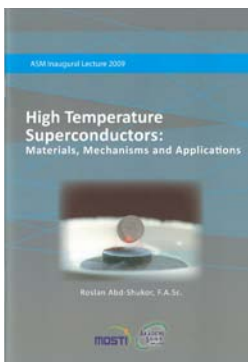
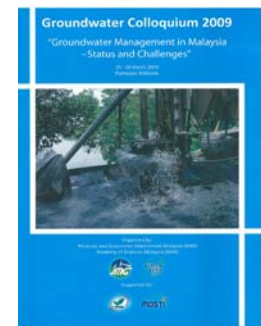
ISBN 978-983-9445-32-9

Price: RM45.00 / USD15.00

Groundwater Colloquium 2009 “Groundwater Management in Malaysia – Status and Challenges”

ISBN : 978-983-9445-30-5

Price: RM100.00 / USD75.00



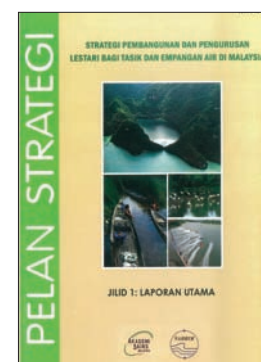
ASM Inaugural Lecture 2009 High Temperature Superconductors: Material, Mechanisms and Applications

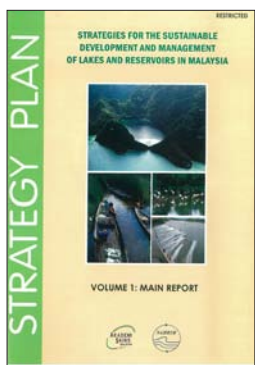
ISBN : 978-983-9445-30-5

Price: RM20.00 / USD8.00

Strategi Pembangunan dan Pengurusan Lestari bagi Tasik dan Empangan Air di Malaysia

Jilid 1: Laporan Utama



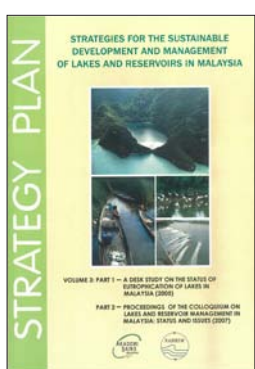
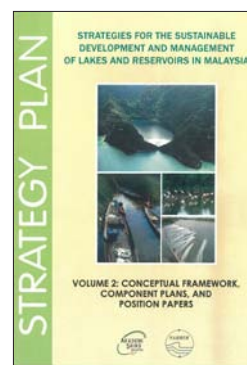


Strategies for the Sustainable Development and Management of Lakes and Reservoirs in Malaysia

Volume 1: Main Report

Strategies for the Sustainable Development and Management of Lakes and Reservoirs in Malaysia

Volume 2: Conceptual Framework, Component Plans, and Position Papers



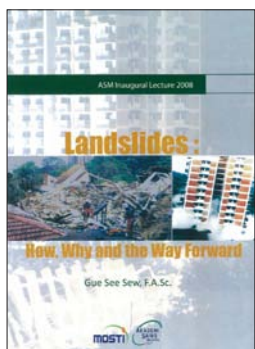
Strategies for the Sustainable Development and Management of Lakes and Reservoirs in Malaysia

Volume 3: Part 1 & Part 2

ASM Science Journal
Vol. 2, No. 2, December 2008

ISSN : 1823-6782

Price: RM100.00 / USD50.00 (Individual)
RM200.00 / USD100.00 (Institution)



ASM Inaugural Lecture 2008 Landslides: How, Why and the Way Forward

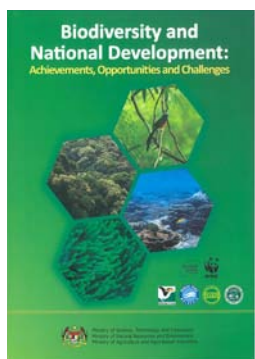
ISBN : 978-983-9445-30-5

Price: RM20.00 / USD8.00

Journal of Science & Technology in the Tropics

Vol. 5, No. 1, June 2009

ISSN:1823-5034



Biodiversity and National Development: Achievements, Opportunities and Challenges

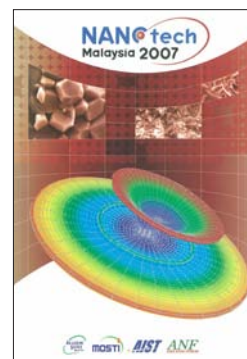
ISBN : 978-983-9445-30-5

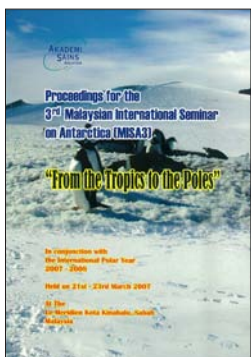
Price: RM40.00 / USD15.00

Nanotech Malaysia 2007

ISBN : 978-983-9445-30-5

Price: RM55.00 / USD20.00





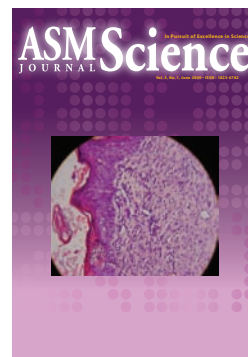
Proceedings for the 3rd Malaysian International Seminar on Antarctica (MISA3) "From the Tropics to the Poles" 2007

ISBN : 978-983-9445-30-5
Price: RM40.00 / USD15.00

ASM Science Journal
Vol. 3, No. 1, December 2009

ISSN : 1823-6782

Price: RM100.00 / USD50.00 (Individual)
RM200.00 / USD100.00 (Institution)



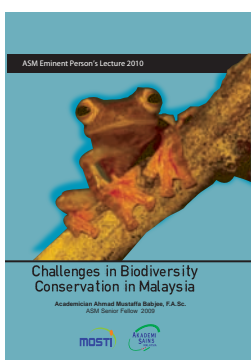
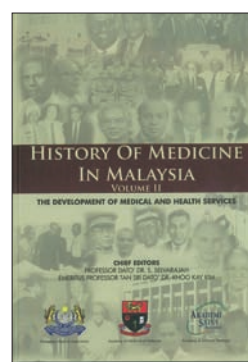
Journal of Science & Technology in the Tropics
Vol. 5, No. 2, December 2009

ISBN : 978-983-9445-30-5
Price: RM40.00 / USD15.00

History of Medicine in Malaysia Volume II
The Development of Medical and Health Services

ISSN : 978-983-42545-1-3

Price: RM100.00 / USD50.00 (Individual)
RM200.00 / USD100.00 (Institution)



ASM Eminent Person's Lecture 2010

Challenges in Biodiversity Conservation in Malaysia

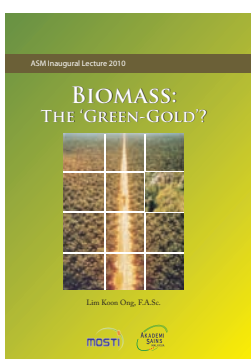
ISBN : 978-983-9445-39-8
Price: RM20.00 / USD8.00

ASM Inaugural Lecture 2010

Single Crystal X-ray Structural Determination:
A Powerful Technique for Natural Products
Research and Drug Discovery

ISBN : 978-983-9445-39-8

Price: RM30.00 / USD12.00



ASM Inaugural Lecture 2010

Biomass: The 'Green-gold'?

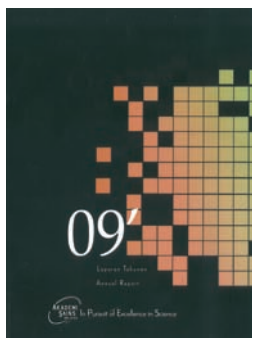
ISBN : 978-983-9445-38-1
Price: RM30.00 / USD12.00

ASM Science Journal
Vol. 3, No. 2, December 2009

ISSN : 1823-6782

Price: RM100.00 / USD50.00 (Individual)
RM200.00 / USD100.00 (Institution)

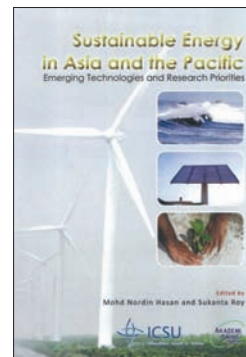




Academy of Science Malaysia

Annual Report 2009

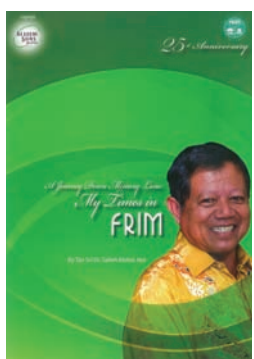
Price: RM50.00 / USD20.00



**Sustainable Energy
in Asia and the Pacific**
Emerging Technologies and Research Priorities
(2010)

ISBN : 978-983-9445-43-5

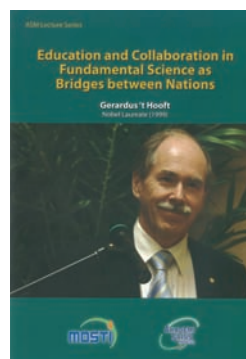
Price: RM100.00 / USD50.00



25th Anniversary

**A Journey Down Memory Lane:
My Times in FRIM**
(2010)

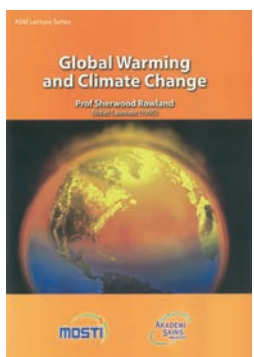
Price: RM40.00 / USD15.00



**Education and Collaboration in
Fundamental Science as Bridges
between Nations**
Gerardus't Hooft
(2010)

ISSN : 978-983-9445-44-2

Price: RM30.00 / USD12.00

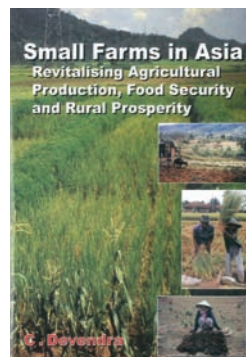


Global Warming and Climate Change

Prof Sherwood Rowland
(2010)

ISBN : 978-983-9445-46-6

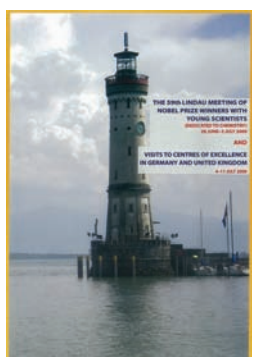
Price: RM40.00 / USD12.00



Small Farms in Asia
Revitalising Agricultural Production,
Food Security and Rural Prosperity

ISBN : 978-983-9445-40-4

Price: RM150.00 / USD50.00



**The 59th Lindau Meeting of Nobel
Prize Winners with Young Scientists**
28 June – 3 July 2009

AND

**Visits to Centres of Excellence in
Germany and United Kingdom**
4-11 July 2009
(2010)



Sustaining Malaysia's Future
The Mega Science Agenda
(2010)



ASM Publications



ASM Science Journal
Vol. 4, No. 1, June 2010

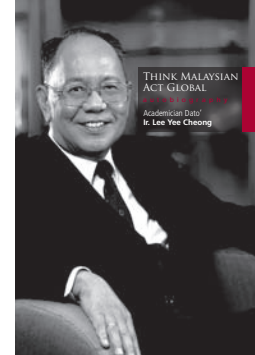
ISSN : 1823-6782

Price: RM100.00 / USD50.00 (Individual)
RM200.00 / USD100.00 (Institution)

Think Malaysian Act Global
(Autobiography)

Academician Dato' Ir. Lee Yee Cheong
(2010)

ISBN : 978-983-9445-47-3



For purchasing, please access:
<http://www.akademisains.gov.my>



About the Journal

Mission Statement

To serve as the forum for the dissemination of significant research, S&T and R&D policy analyses, and research perspectives.

Scope

The *ASM Science Journal* publishes advancements in the broad fields of medical, engineering, earth, mathematical, physical, chemical and agricultural sciences as well as ICT. Scientific articles published will be on the basis of originality, importance and significant contribution to science, scientific research and the public.

Scientific articles published will be on the basis of originality, importance and significant contribution to science, scientific research and the public. Scientists who subscribe to the fields listed above will be the source of papers to the journal. All articles will be reviewed by at least two experts in that particular field. The journal will be published twice in a year.

The following categories of articles will be considered for publication:

Research Articles

Each issue of the journal will contain no more than 10 research articles. These are papers reporting the results of original research in the broad fields of medical, engineering, earth, mathematical, physical, chemical and life sciences as well as ICT. The articles should be limited to 6000 words in length, with not more than 100 cited references.

Short Communications

These are articles that report significant new data within narrow well-defined limits or important findings that warrant publication before broader studies are completed. These articles should be limited to 2000 words and not more than 40 cited references. Five (5) Short Communications will be accepted for publication in each issue of the journal.

Research Perspectives

These are papers that analyse recent research in a particular field, giving views on achievements, research potential, strategic direction etc. A Research Perspective should not exceed 2000 words in length with not more than 40 cited references.

Reviews/Commentaries

Each issue of the journal will also feature Reviews/Commentaries presenting overviews on aspects such as Scientific Publications and Citation Ranking, Education in Science and Technology, Human Resources for Science and Technology, R&D in Science and Technology, Innovation and International Comparisons or Competitiveness of Science and Technology etc. Reviews/Commentaries will encompass analytical views on funding, developments, issues and concerns in relation to these fields and not exceed 5000 words in length and 40 cited references.

Science Forum

Individuals who make the news with breakthrough research or those involved in outstanding scientific endeavours or those

conferred with internationally recognised awards will be featured in this section. Policy promulgations, funding, science education developments, patents from research, commercial products from research, and significant scientific events will be disseminated through this section of the journal. The following will be the categories of news:

- Newsmakers
- Significant Science Events
- Patents from Research
- Commercial Products from Research
- Scientific Conferences/Workshops/Symposia
- Technology Upgrades
- Book Reviews.

Instructions to Authors

The *ASM Science Journal* will follow the Harvard author-date style of referencing examples of which are given below.

In the text, reference to a publication is by the author's name and date of publication and page number if a quote is included, e.g. (Yusoff 2006, p. 89) or Yusoff (2006, p. 89) 'conclude.....' as the case may be. They should be cited in full if less than two names (e.g. Siva & Yusoff 2005) and if more than two authors, the work should be cited with first author followed by *et al.* (e.g. Siva *et al.* 1999).

All works referred to or cited must be listed at the end of the text, providing full details and arranged alphabetically. Where more than one work by the same author is cited, they are arranged by date, starting with the earliest. Works by the same author published in the same year are ordered with the use of letters a, b, c, (e.g. Scutt, 2003a; 2003b) after the publication date to distinguish them in the citations in the text.

General Rules

Authors' names:

- Use only the initials of the authors' given names.
- No full stops and no spaces are used between initials.

Titles of works:

- Use minimal capitalisation for the titles of books, book chapters and journal articles.
- In the titles of journals, magazines and newspapers, capital letters should be used as they appear normally.
- Use italics for the titles of books, journals and newspapers.
- Enclose titles of book chapters and journal articles in single quotation marks.

Page numbering

- Books: page numbers are not usually needed in the reference list. If they are, include them as the final item of the citation, separated from the preceding one by a comma and followed by a full stop.
- Journal articles: page numbers appear as the final item in the citation, separated from the preceding one by a comma and followed by a full stop.

Use the abbreviations p. for a single page, and pp. for a page range, e.g. pp. 11–12.

Whole citation

- The different details, or elements, of each citation are separated by commas.
- The whole citation finishes with a full stop.

Specific Rules

Definite rules for several categories of publications are provided below:

Journal

Kumar, P & Garde, RJ 1989, 'Potentials of water hyacinth for sewage treatment', *Research Journal of Water Pollution Control Federation*, vol. 30, no. 10, pp. 291–294.

Monograph

Hyem, T & Kvale, O (eds) 1977, *Physical, chemical and biological changes in food caused by thermal processing*, 2nd edn, Applied Science Publishers, London, UK.

Chapter in a monograph

Biale, JB 1975, 'Synthetic and degradative processes in fruit ripening', eds NF Hard & DK Salunkhe, in *Post-harvest biology and handling of fruits and vegetables*, AVI, Westport, CT, pp. 5–18.

Conference proceedings

Common, M 2001, 'The role of economics in natural heritage decision making', in *Heritage economics: challenges for heritage conservation and sustainable development in the 21st century: Proceedings of the International Society for Ecological Economics Conference, Canberra, 4th July 2000*, Australian Heritage Commission, Canberra.

Website reference

Thomas, S 1997, *Guide to personal efficiency*, Adelaide University, viewed 6 January 2004, <<http://library.adelaide.edu.au/~stthomas/papers/perseff.html>>.

Report

McColloch, LP, Cook, HT & Wright, WR 1968, *Market diseases of tomatoes, peppers and egg-plants*, Agriculture Handbook no. 28, United States Department of Agriculture, Washington, DC.

Thesis

Cairns, RB 1965, 'Infrared spectroscopic studies of solid oxygen', PhD thesis, University of California, Berkeley, CA.

Footnotes, spelling and measurement units

If footnotes are used, they should be numbered in the text, indicated by superscript numbers and kept as brief as possible. The journal follows the spelling and hyphenation of standard British English. SI units of measurement are to be used at all times.

Submission of Articles

General. Manuscripts should be submitted (electronically) in *MS Word* format. If submitted as hard copy, two copies of the manuscript are required, double-spaced throughout on one side only of A4 (21.0 × 29.5 cm) paper and conform to the style and format of the *ASM Science Journal*. Intending contributors will be given, on request, a copy of the journal specifications for submission of papers.

Title. The title should be concise and descriptive and preferably not exceed fifteen words. Unless absolutely necessary, scientific names and formulae should be excluded in the title.

Address. The author's name, academic or professional affiliation, e-mail address, and full address should be included on the first page. All correspondence will be only with the corresponding author (should be indicated), including any on editorial decisions.

Abstract. The abstract should precede the article and in approximately 150–200 words outline briefly the objectives and main conclusions of the paper.

Introduction. The introduction should describe briefly the area of study and may give an outline of previous studies with supporting references and indicate clearly the objectives of the paper.

Materials and Methods. The materials used, the procedures followed with special reference to experimental design and analysis of data should be included.

Results. Data of significant interest should be included.

Figures. If submitted as a hard copy, line drawings (including graphs) should be in black on white paper. Alternatively sharp photoprints may be provided. The lettering should be clear. Halftone illustrations may be included. They should be submitted as clear black and white prints on glossy paper. The figures should be individually identified lightly in pencil on the back. All legends should be brief and typed on a separate sheet.

Tables. These should have short descriptive titles, be self explanatory and typed on separate sheets. They should be as concise as possible and not larger than a Journal page. Values in tables should include as few digits as possible. In most cases, more than two digits after the decimal point are unnecessary. Units of measurements should be SI units. Unnecessary abbreviations should be avoided. Information given in tables should not be repeated in graphs and vice versa.

Discussion. The contribution of the work to the overall knowledge of the subject could be shown. Relevant conclusions should be drawn, and the potential for further work indicated where appropriate.

Acknowledgements. Appropriate acknowledgements may be included.

Reprints. Twenty copies of reprints will be given free to all the authors. Authors who require more reprints may obtain them at cost provided the Editorial Committee is informed at the time of submission of the manuscript.

Correspondence

All enquiries regarding the *ASM Science Journal*, submission of articles, including subscriptions to it should be addressed to:

The Editor-in-Chief
ASM Science Journal
Academy of Sciences Malaysia
902-4, Jalan Tun Ismail
50480 Kuala Lumpur, Malaysia.
Tel: 603-2694 9898; Fax: 603-2694 5858
E-mail: sciencejournal@akademisains.gov.my



ASM SCIENCE JOURNAL
(ASM Sc. J.)

Subscription (Two issues per year)		
	<u>Malaysia</u>	<u>Other Countries</u>
Individual	RM100	USD50
Institution	RM200	USD100

1. Complete form and return.

Name/Institution:
(Please print)
.....
.....

Street Address:
.....
.....

City, Region:

Country, Postal Code:

2. Payment method: Cheque/Bank Draft/Postal Order/
Money Order No.:
Payable to **“Akademi Sains Malaysia”**
(Please include bank commission, if applicable)
RM/USD:

Date: Signature:

Please send to:
Academy of Sciences Malaysia
902-4, Jalan Tun Ismail
50480 Kuala Lumpur, Malaysia
Tel: 03-2694 9898; Fax: 03-26945858
E-mail: sciencejournal@akademisains.gov.my



In Pursuit of Excellence in Science
ASM Science
JOURNAL

Academy of Sciences Malaysia
902-4, Jalan Tun Ismail
50480 Kuala Lumpur
Malaysia

Afix
stamp
here



RESEARCH ARTICLES

- Characterization of Skeletons of Simulated Drought and Flood of Water Bodies** 62
S. Dinesh
- Effects of Nitrate, Phosphate, Temperature and Light-dark Cycle on Algal Growth Potential of *Chlorococcum* sp. from Reeve Hill, Antarctica** 74
D. Masdialily, W.O.W. Maznah, M. Faradina and M. Mashhor
- Effects of Temperature on the Photosynthetic Parameters of Antarctic Benthic Microalgal Community** 81
S. Salleh, A. McMinn, M. Mohammad, Z. Yasin and S.H.A. Tan

ANNOUNCEMENTS

- Mahathir Science Award 2011 (Invitation for Nomination) 89
- 22nd Pacific Science Congress 90
- Malaysian Science and Technology Congress 2010 92
- ASM Publications 93

